

# **Optoacoustic Characterization of Optical Properties of Human Skin in Vivo in the Ultraviolet Wavelength Range**

**skin phototypes, uv-adaptations and effects of sunscreen**

Von der Naturwissenschaftlichen Fakultät  
der Gottfried Wilhelm Leibniz Universität Hannover  
zur Erlangung des Grades Doktorin der Naturwissenschaften

Dr. rer. nat.

genehmigte Dissertation von  
Dipl.-Phys. Merve Meinhardt  
geboren am 10.11.1976 in Hannover

(2006)

Referentin: Prof. Dr. Angelika Anders-von Ahlften

Institut für Biophysik, Gottfried Wilhelm Leibniz Universität Hannover

Korreferent: PD Dr. Holger Lubatschowski

Laser Zentrum Hannover e.V.

Tag der Promotion: 19.7.2006

## Abstract

The ambition of this dissertation project was the development and application of an experimental setup to determine the optical properties of human skin *in vivo* in the ultraviolet wavelength range.

Optoacoustics was chosen as the appropriate technique allowing non-invasive, depths resolved determination of optical properties. It is a hybrid technique using short pulsed radiation to induce a pressure profile in the skin which carries the information about the light distribution and which is released in an ultrasonic transient unhamperedly traveling back to the pressure sensor above the skin.

Accordingly, the first part of the thesis at hand deals with the development of the necessary experimental and analytical tools for the *in vivo* investigations.

During this dissertation project, a previous first design of the optoacoustic detector was optimized according to the demands of sensitive human skin.

Besides, a tunable UV-laser system was specifically developed for this project in a diploma work. It provides a tunable source of nanosecond pulses covering most of the terrestrial UV: from 300 to 400 nm and up into the visible spectrum. To our knowledge, this is the first time that a nanosecond singly resonant ring oscillator (SRRO) was successfully implemented in the UV-A and parts of the UV-B with a tuning range of more than 100 nm.

As a basis for later data analysis and simulation, the fairly general fundamental expressions of optoacoustic theory were adapted to match the unique conditions of this experimental setup.

In order to plumb the potentials of optoacoustics for the investigation of the optical properties of human skin in the ultraviolet wavelength range, a study on 20 subjects was prepared, designed and carried out in the second part of this dissertation.

Analysis of the obtained subject data showed that the optical properties of human skin *in vivo* can indeed be measured using optoacoustics. The *in vivo* investigations resulted in UV absorption spectra of human skin that are unequaled in the literature: This thesis for the first time provides optoacoustic data on the optical properties of human skin in the ultraviolet wavelength range from 290 nm to 341 nm (UVB and UVA-II) with a spectral resolution of 3 nm. Skin sites with different natural sun exposure (volar and dorsal aspect of forearm), thick horny layer (thenar) or after application of sunscreen lotion were examined. One of the most interesting results crystallizing from the large amount of data obtained in the subject study is a marked influence of keratin on the UVB absorption properties of UV-exposed human skin which even outranks the influence of pigmentation. Besides, the analysis of this large amount of data also pointed at technical and analytical improvements necessary to further improve the significance of the results.

**keywords:** UV-optoacoustics, human skin *in vivo*, optical properties



## Kurzzusammenfassung

Die übergeordnete Zielsetzung dieses Dissertationsprojektes war die Entwicklung und Anwendung einer geeigneten Messmethode zur Bestimmung der optischen Eigenschaften der menschlichen Haut in vivo im ultravioletten Spektralbereich.

Als geeignete Methode wurde die Optoakustik ausgewählt. Sie ermöglicht eine nicht invasive, tiefenaufgelöste Bestimmung optischer Eigenschaften. Bei dieser Hybridmethode wird mittels gepulster Laserstrahlung ein Druckprofil in der Haut induziert, das die Lichtverteilung im beleuchteten Volumen widerspiegelt und das in Form einer Ultraschallwelle ungehindert zurück zum Drucksensor oberhalb der Haut gelangen kann.

Zunächst mussten die notwendigen messtechnischen und analytischen Grundlagen für die spätere Bearbeitung der Messaufgabe geschaffen werden.

Im Rahmen des Dissertationsprojektes wurde ein früheres erstes Design eines optoakustischen Detektors auf die besonderen Anforderungen der menschlichen Haut hin optimiert. Außerdem wurde im Rahmen einer Diplomarbeit ein speziell auf dieses Projekt zugeschnittenes UV-Lasersystem entwickelt. Dieses kann über einen Wellenlängenbereich, der fast den gesamten terrestrischen UV-Bereich umfasst, durchgestimmt werden: Pulse mit einer Pulsdauer von wenigen Nanosekunden im Bereich von 300-400 nm und bis hinein ins sichtbare Spektrum sind damit verfügbar. Unseres Wissens nach ist dies der erste erfolgreiche Versuch einen solchen einfach resonanten Ring Oszillator (singly resonant ring oscillator, SRRO) mit einem vergleichbaren Durchstimmbereich zu realisieren. Als Basis für die spätere Datenauswertung in Form einer Simulation der optoakustischen Signale wurden die grundlegenden theoretischen Ausdrücke den vorliegenden experimentellen Gegebenheiten entsprechend angepasst.

Um das Potential der Optoakustik im Hinblick auf die Untersuchung optischer Eigenschaften von menschlicher Haut im UV auszuloten, wurde schließlich im zweiten Teil des Dissertationsprojektes eine Studie an 20 Probanden erarbeitet und durchgeführt.

Die Auswertung der Probandendaten zeigte, dass Optoakustik zur Bestimmung der optischen Eigenschaften von menschlicher Haut geeignet ist. Es wurden Absorptionsspektren menschlicher Haut im Spektralbereich 290-341 nm (UVB und UVA-II) mit einer Auflösung von 3 nm bestimmt. Derartige Daten sind unseres Wissens nach in der Literatur bisher nicht zu finden. Es wurden Hautbereiche unterschiedlicher natürlicher UV Exposition (Innen- und Außenseite des Unterarmes), mit verdickter Hornschicht (Daumenballen) sowie nach Applikation von Sonnenschutzmittel untersucht. Als eines der interessantesten Ergebnisse kristallisierte sich aus der Vielzahl der Messungen ein starker Einfluss von Keratin auf die UVB Absorptionseigenschaften stärker UV-exponierter Hautareale heraus. Dieser überwog sogar den Einfluss erhöhter Pigmentierung.

Darüberhinaus zeigte die umfangreiche Auswertung der Probandenstudie verschiedene Ansätze auf, um die Aussagekraft der Messungen in Zukunft weiter zu verbessern.

**Schlagwörter:** UV Optoakustik, menschliche Haut in vivo, optische Eigenschaften



# Contents

<b>Abstract</b>	<b>iii</b>
<b>Kurzzusammenfassung</b>	<b>v</b>
<b>1 Introduction</b>	<b>1</b>
<b>2 Optoacoustics – a brief applied theory</b>	<b>5</b>
2.1 Nonstationary thermoelasticity equation . . . . .	6
2.2 Transfer function . . . . .	7
2.3 Inhomogeneous optical properties . . . . .	12
2.4 Evolution of the signal in a dissipative medium . . . . .	14
<b>3 Human skin</b>	<b>17</b>
3.1 Skin physiology . . . . .	17
3.1.1 UV reactions and adaptation . . . . .	17
3.2 Optical properties of human skin in the ultraviolet wavelength range . . .	20
3.2.1 Epidermis . . . . .	21
3.2.2 Dermis . . . . .	26
<b>4 266 nm pumped OPO - the terrestrial UV range in one tunable system</b>	<b>29</b>
4.1 Demands and theoretical limitations . . . . .	30
4.2 Setup . . . . .	33
4.3 Achievements . . . . .	35

<b>5</b>	<b>An experimental setup for UV-optoacoustics on human skin</b>	<b>39</b>
5.1	UVA/B radiation source . . . . .	39
5.2	Capturing optoacoustic transients from human skin . . . . .	42
5.2.1	The optoacoustic detector . . . . .	43
5.2.2	Signal processing and automated operation . . . . .	44
<b>6</b>	<b>Classification and documentation of human skin</b>	<b>51</b>
6.1	UV exposition . . . . .	51
6.2	Documentation of skin physiology . . . . .	51
6.2.1	DigiCam . . . . .	51
6.2.2	SELS . . . . .	52
6.2.3	Fotofinder . . . . .	53
6.2.4	Chromameter . . . . .	53
<b>7</b>	<b>Under investigation - materials</b>	<b>55</b>
7.1	PVA-tissue phantoms - a standard for in vivo measurements . . . . .	55
7.2	Epidermal models . . . . .	56
7.3	Study subjects - human skin in vivo . . . . .	57
7.3.1	Sun protection lotions . . . . .	61
<b>8</b>	<b>Results and Discussion</b>	<b>63</b>
8.1	Tissue phantoms - repeatability of optoacoustic measurements . . . . .	63
8.2	Cell cultures . . . . .	66
8.3	Study subjects - human skin in vivo . . . . .	67
8.3.1	Native pigmentation - volar forearm . . . . .	69
8.3.2	UV-exposed skin . . . . .	90
8.3.3	Intraindividual comparison of skin sites . . . . .	104
8.3.4	wavelength dependent penetration depths . . . . .	119
8.3.5	sunscreens . . . . .	124



---

<b>9</b>	<b>Conclusions and Outlook</b>	<b>127</b>
	<b>Appendix</b>	<b>131</b>
<b>A</b>	<b>Physical properties of relevant materials</b>	<b>132</b>
<b>B</b>	<b>Documentation - study subjects</b>	<b>133</b>
	B.1 Measurement sites at subjects' arms - photographs . . . . .	133
	B.2 SELS pictures . . . . .	140
	B.3 FotoFinder pictures . . . . .	143
	<b>Bibliography</b>	<b>149</b>



# 1 Introduction

According to WHO [66], between 2 and 3 million non-melanoma skin cancers and over 130,000 malignant melanomas occur globally each year. One in every three cancers diagnosed worldwide is a skin cancer. A changing lifestyle, sun-seeking behaviour, and global mobility are responsible for much of the increase in skin cancers. In particular, frequent sun exposure and sunburn in childhood appear to set the stage for high rates of melanoma later in life. Depletion of the ozone layer, which provides a protective filter against UV radiation, may further aggravate the problem. With a sustained 10 % decrease in stratospheric ozone, an additional 300,000 non-melanoma and 4,500 melanoma skin cancers could be expected world-wide according to UNEP estimates. Currently, one in five North Americans and one in two Australians will develop some form of skin cancer in their lifetime. Other chronic skin changes due to UV radiation include injuries to skin cells, blood vessels and fibrous tissue, better known as skin ageing.

These WHO facts should be felt as an intense call and motivation for intensified research into the interaction of ultraviolet radiation and human skin and probably the mystery behind most correlations has been cleared up by now - these were my feelings when I first came across this issue. A closer look to the literature however revealed that this issue is not only far from being thoroughly elucidated, but even some of the most fundamental questions have not been solved yet.

On the one hand, ultraviolet radiation is used more and more and with a lot of success in phototherapy [6, 47]. On the other hand, most photobiologists claim that harmful effects preponderate beneficial effects of UV radiation on human health: for the average population, the daily walk to work or for shopping is sufficient to induce the positive effects such as vitamin D synthesis - any more sun only causes increased health risks. In recent years however, there is a small but growing body of scientific opinion warning against systematic sun abstinence: they call for a higher appreciation of beneficial effects - though not to a rate of excessive sun seeking behaviour [31]. Fortunately, a public consciousness about UV effects has slowly evolved over the last years. The use of tanning booths or a "healthy" tan is discussed more critically. However, thinking and doing are still hugely diverging: a tan is still believed to be beautiful, healthy and sportive, tanning booths are

still well attended and long-haul journeys are still popular among sun-unaccustomed north Europeans.

As far as fundamental research is concerned, some action spectra for photobiological effects such as erythema and pigmentation [4] are already available. Other important effects such as immunosuppression, melanogenesis and vitamin-D synthesis have still to be investigated more thoroughly.

Furthermore, only very little data is available about the optical properties of human skin *in vivo*. Accordingly, cell biologists are bound to guess how much UV radiation in what spectral quality will reach any particular cell type involved in UV interaction. Knowledge of the optical properties of the living tissue is also essential for spotting potentially relevant chromophores, which can then be picked out and examined closely by molecular biologists.

So far, optical properties of human skin in the ultraviolet spectral range have been examined on *ex vivo* tissue for the most part. Transmission, reflection and scattering parameters are measured using integrating spheres or spectrometers. Subsequently, absorption and scattering coefficients are determined from these data [63, 64, 65]. Unfortunately, the results of these measurements differ qualitatively and quantitatively. One of the main reasons is the necessary preservation of the skin tissue. Interestingly, one of the most comprehensive collection of tissue optical properties [33] uses data from *in vitro* neonatal skin and bloodless rat skin as basic references (see also Chap. 3).

The determination of skin optical properties faces several fundamental difficulties. Analysis of reflected, transmitted and scattered light from tissue is done best using integrating spheres or photospectrometers. However, these methods are practically limited to *in vitro* or *ex vivo* tissue samples. Due to preparation of *ex vivo* skin or limited comparability of *in vitro* models, the significance of acquired data still leaves a lot to be desired.

These problems could be overcome by non-invasive *in vivo* methods. However, hitherto existing methods have been facing other difficulties. In reflection spectroscopy for example, the light that is diffusely reflected from the skin is analyzed to determine scattering and absorption properties of the tissue. Unfortunately, application of this technique in the ultraviolet is unattractive since information can only be gathered from the first layers of the skin up to a depth of about 20  $\mu\text{m}$  due to strong absorption. All purely optical methods are subject to similar limitations.

So, recently, hopes have been pinned on hybrid techniques such as optoacoustics, which combine optical signal induction with acoustic signal propagation - i.e. acoustic information transport. Here, samples are illuminated by pulsed laser radiation. The light propagates according to the scattering and absorption properties of the sample and eventually all energy is absorbed. If pulse duration is sufficiently short, the heating due to absorbed energy causes a pressure profile exactly mimicking the light distribution in the sample. This pressure profile is released in an ultrasound pulse from which the initial pressure profile - and thus the light distribution - can be deduced. Of course, the known light dis-

tribution also reveals the optical properties of the sample, i.e. absorption and scattering coefficients.

So far, optoacoustics has been employed in imaging for the most part. For the determination of optical properties, there nearly have been only proofs of principle with occasional use of single UV wavelengths. However, it has been shown that this application of optoacoustics is feasible and promising. In [52], optoacoustic in vitro measurements of tissue were carried out using a frequency-tripled Nd:YAG (355 nm) achieving an accuracy comparable to integrating sphere measurements as certified by the authors. An axial resolution of about 20  $\mu\text{m}$  can be achieved in optoacoustic in vivo measurements [39] and as radiation only has to penetrate into the tissue but not to get out again, information can be gathered from much deeper layers compared to purely optical techniques.

This doctoral thesis shows that optoacoustics is a most valuable tool for analyzing the optical properties of human skin in vivo in the ultraviolet range.

First, a short introduction to the theory of thermo-optical excitation of sound is given focused to the experimental conditions of this work (Chapter 1). The UV-optoacoustic detector setup required some reconsideration of the theoretical description of optoacoustic transients. Several applied theoretical descriptions can be found in the literature (see for example [1, 38, 40]) but the use of an acoustic impedance matched transparent medium - such as ultrasound gel - has not been considered so far. So, the fairly general fundamental expressions of the theory were adapted to match these experimental conditions. Based on the resulting theoretical description, a simulation of optoacoustic transients was developed in a parallel thesis [46].

After a brief description of human skin physiology and UV adaptation mechanisms relevant to this work (Chapter 2), Chapter 3 is dedicated to the presentation of a tunable UV-laser system which was specifically developed for this project in a diploma work. The developed design of a singly resonant ring oscillator (SRRO) finally provides a tunable source of nanosecond pulses covering most of the terrestrial UV: from 300 to 400 nm and up into the visible spectrum. A system with a comparable setup was reportedly in use within the visual part of the spectrum [30]. To our knowledge, this is the first time that a nanosecond SRRO was successfully implemented in the UV-A and parts of the UV-B with a tuning range of more than 100 nm.

Starting with my diploma work in 2001, an optoacoustic setup was developed for the investigation of optical properties of human skin in vivo using ultraviolet radiation (see also [8, 44, 45, 46, 48]). During this dissertation project, the detector design was optimized for use with sensitive human skin, while a synchronized fiber energy monitor and data acquisition system was parallelly developed in another dissertation [46] (see Chapter 5). Measurements on Poly(vinyl alcohol) (PVA)-tissue models and in vitro epidermal models paved the way for a study on twenty human subjects which was prepared, designed and carried out in this dissertation project in order to plumb the potential of UV optoacoustics for measurements on human skin. A wide spectrum of applications was to be tested here in order to enable us to judge which applications are promising enough to focus on in

future research. So, the subject study investigates native and induced pigment, and the influence of horny layer as well as of sun screen on the optical properties of human skin in vivo. To validate and make comparable the results of optoacoustic measurements on human subjects, several dermatologic standard methods were applied during the study as presented in Chapter 6. The study was carried out at the Institut für experimentelle Dermatologie/DermaTronnier of the Universität Witten/Herdecke who also kindly provided the dermatologic reference measurements and the subject group. The optoacoustic investigations are described in Chapter 7 and their results are presented in Chapter 8.

Final comprehensive conclusions, a reflection of this dissertation and an outlook on future work are finally given in Chapter 9.

## 2 Optoacoustics – a brief applied theory

The mechanism behind optoacoustics is the absorption of radiation energy in matter, its transfer to heat and pressure and the release of a resulting transient stress wave - thermo-optical excitation of ultrasound. This process is illustrated in Fig. 2.1.

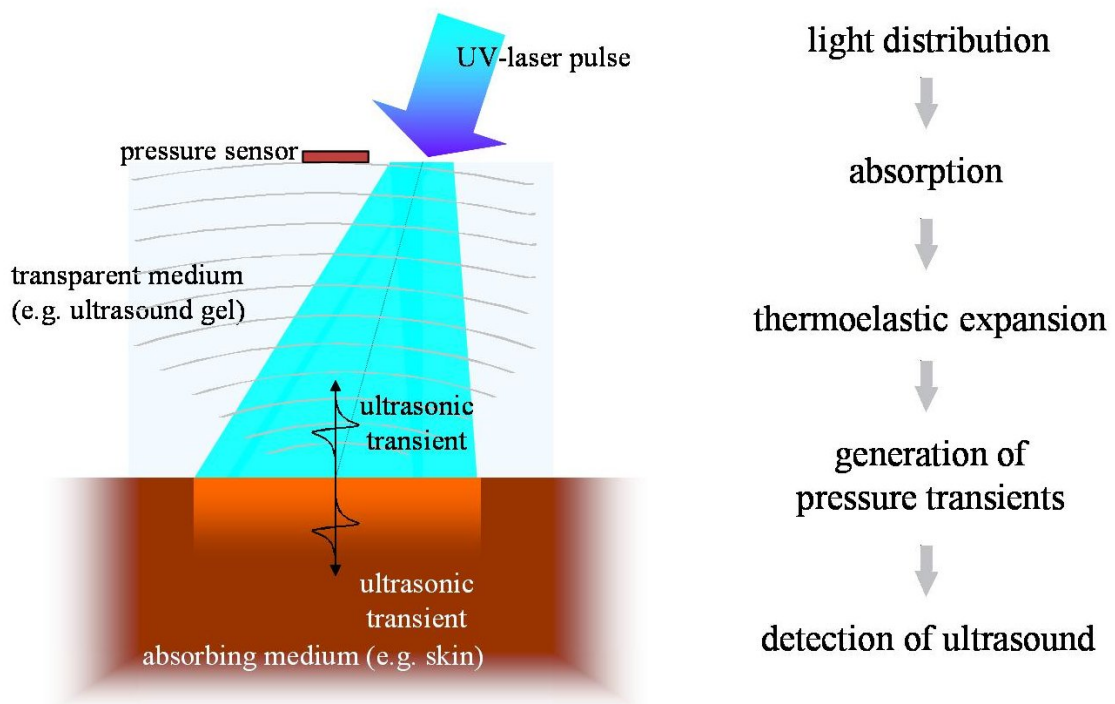


**Figure 2.1:** Principle of optoacoustics: the process of thermo-optical excitation of ultrasound

For theoretical considerations, the process can be separated into two fairly independent stages: the formation of the initial pressure distribution and the transformation of the traveling wave on its way to the detector.

First, radiation propagates in a sample according to its optical properties. Finally, all the radiation energy is absorbed and transferred to heat - ideally instantaneously and with radiationless transitions. This leads to a location dependent pressure rise in the sample, which is released in an ultrasonic transient. If the incident light pulses are sufficiently short - typically in the low nanosecond range - the profile of the stress transient reproduces the distribution of heat sources in the sample and consequently, the light distribution in the sample can be deduced.

The traveling pressure transient then is subject to a variety of acoustic influences. Dissipation, nonlinearity effects and diffraction may alter the profile of the initial stress wave depending on the acoustic properties of the propagation medium as well as geometry of the sources, the detector and their relative position.

In the following sections, a theory of thermo-optical excitation of sound is sketched based on the comprehensive theoretical description of optoacoustics in a liquid as presented in [27]. Skin rather resembles a liquid than a solid in the optoacoustic sense. The high water content dominates over solid and elastic effects. Condensed overviews providing some additional insights into the mechanisms of optoacoustics are set out in [1, 14, 37, 38] and [40]. Here, the treatment of practical considerations and experimental setup is dealt with more explicitly.

The following theoretical description is adapted to the experimental demands and prerequisites of optoacoustics on living skin using ultraviolet radiation. Relevant physical properties of skin layers, ultrasound gel, etc. are arranged in Table A in the Appendix. Due to the acoustically well matched transparent medium, the experimental setup presented in this thesis is unlike those found in the literature. Diffraction of the acoustic wave on its way to the rigid PVDF (polyvinylidene fluoride) detector and boundary conditions at the interface between the absorbing and the transparent interface cannot be considered under extreme acoustic boundary conditions which are often applied to simplify pleasantly the theoretical descriptions of optoacoustics. Thus, a close look at and adaptation of the theory was necessary from the start and the following sections will be confined to describing mainly the present case.

## 2.1 Nonstationary thermoelasticity equation

A comprehensive description of the expected optoacoustic transient requires solving a nonstationary thermoelasticity problem. Because of the high water content, skin can be assumed to show the characteristics of a viscous liquid rather than a solid. This implies for example that only longitudinal acoustic waves are expected in both the sample medium (skin) and the transparent medium between the sample and the ultrasound detector.

The first aim of the theoretical description is to deduce a basic expression to describe pulsed thermo-optical sound excitation in liquids from rather fundamental equations. This



is achieved by taking the continuity equation, the Navier-Stokes equation and the heat conduction equation and completing and simplifying them by the equations of state of the medium near the equilibrium values. Only minor deviations from equilibrium values are assumed. Since sound absorption is low at distances of the order of the wavelength, acoustic dissipation in the sound excitation zone can be neglected. Moreover, when ultrasonic frequencies are produced, heat conduction is not significant in liquids. Taking all of this into account, the following equation can be derived:

$$\frac{\partial^2 \varphi}{\partial t^2} - c_0^2 \Delta \varphi = \left( \frac{c_0^2 \beta}{\rho_0 c_p} \right) \text{div} \langle \mathbf{S} \rangle \quad (2.1)$$

with  $\varphi$ : the scalar potential of the velocity field (vibrational velocity of the particles),  $c_0$ : (adiabatic, longitudinal) sound velocity in the sample,  $\beta$ : thermal coefficient of volume expansion of the sample,  $\rho_0$ : average density of the sample,  $c_p$ : specific heat at constant pressure.

In order to analyze optoacoustic signals, its solution for the experimental conditions has to be found. The appropriate approach to all solutions of this equation is the transfer function method.

## 2.2 Transfer function

The optoacoustic wave form is determined by the characteristics of the medium as well as of the parameters of the laser irradiation. With the aid of the transfer function method, it is possible to differentiate between both. This method is employed to find the spectrum of an optoacoustic signal to a depth of a few (3-5) absorption lengths  $\mu_a^{-1}$  of light - accordingly, more than 95 % of the incident light is contained within these limitations.

It is reasonable first to consider the one-dimensional problem and to expand the solutions to the three dimensional case where necessary subsequently.

Besides, considerations will first be limited to the case of homogeneous optical properties to allow easier access to the theory of thermo-optical excitation of sound. There are two ways of dealing with the inhomogeneous optical properties of skin. A rough approximation may be achieved assuming several layers (at least epidermis and dermis) each displaying different but homogeneous properties. A more rigorous approach is to assume an arbitrary distribution of heat sources in the sample. Both approaches will be considered in Section 2.3.

A plane light wave from a transparent medium is incident perpendicularly, in z direction, to an absorbing medium - the skin. As we are dealing with a light pulse, its wave intensity is given by  $I = I_s f(t)$ .  $I_s$  is the incident radiation intensity and  $f(t)$  describes the time

dependence. Some of the light may be specularly reflected at the boundary or scattered back from inside the medium. So, the Poynting vector is given by

$$\langle \mathbf{S} \rangle = I_0 f(t) e^{-\mu_{eff} z} \mathbf{n}_z \quad (2.2)$$

$\mathbf{n}_z$  is the unit vector on the z axis.

$\mu_{eff}$  is the effective attenuation coefficient of light, which is composed of the absorption and scattering coefficients  $\mu_a$  and  $\mu_s$ .

$I_0 = TI_s$  is the light intensity at the boundary of the absorbing medium. The transmission  $T$  is wavelength dependent. Reflection on the skin surface increases towards lower wavelengths. It is as high as 20% for 400 nm and falls below 1% at 280 nm. In the UVB (280 to 315 nm), it is only about 2.5% on average [16]. In the experimental setup,  $I_s$  is determined by photodiode measurements (see Section 5.2.2). In the range from 290 nm to 340 nm, UV reflection is quite low. It rises from about 2 % to about 5 % and will be neglected in the analysis. Variations within skin types and for different pigmentation are fairly high and would have to be measured individually for each subject.

Some thoughts concerning the influence of scattering on the optoacoustic signal profile: For the ultraviolet wavelength range, absorption dominates the optical properties (see [20] and Chap. 3). Besides, all skin layers are strongly forward scattering in the range of wavelengths from 240 nm to 633 nm. A predictive equation for the mean scatter cosine  $g$  in this range is [26]:

$$g \approx 0.62 + 0.29 \times 10^{-3} \lambda \quad (2.3)$$

This strong forward directed nature makes scattering again less important for the light distribution with respect to thermo-optical excitation of sound. According to [13], 100% of light are transmitted through a thin layer of epidermis within an angle of  $62.5^\circ$  with the normal and more than 45 % are transmitted even within an angle of  $22.5^\circ$  with the normal throughout the ultraviolet - corresponding to the illumination cone of the fiber. For the stratum corneum, values are even higher. This indicates that the incident radiation is only subject to small deflection angles and there is hardly any backscattering towards the surface. Besides, the sample is illuminated by a wide laser beam:  $\mu_a a \gg 1$  -  $a$  is the radius of the incident light beam and as the scattering probability (coefficient) is usually lower than the absorption probability, multiple scattering events for one photon are not common. So, most of the light is contained in the same volume and in a similar depths distribution as it were if scattering was completely neglected. Hence description of  $\mu_{eff}$  according to diffusion theory is not indicated in this case.

Of course, light propagation is retarded by scattering causing a concentration of light in the subsurface layers of the skin and less light in the deeper layers - compared to the light distribution without scattering. Depending on the internal reflection coefficient  $R_{int}$  of the skin - ultrasound gel boundary, maximal fluence may even occur not at the skin surface but at a depth  $z_{max}$  in the skin (see e.g. [38]). As scattering coefficients of skin are usually

lower than absorption coefficients in the UV however, this effect is not to be expected investigating human skin in vivo.

Recapitulating, it seems even more appropriate to use  $\mu_{eff} \approx \mu_a$  than the Lambert-Beer description  $\mu_{eff} = \mu_a + \mu_s$  especially in the UVB as the incorporation of scattering would introduce a kind of leakage in the description of available radiation intensity, which should not be assumed following the previous argumentation. So, scattering will be neglected in the analysis of the subject data as a first approximation.

If scattering should still be accounted for, then light intensity  $I(z,t)$  has to be split up in a ballistic term  $I_{bal}(z,t) = I_0 e^{-(\mu_a + \mu_s)z}$  and a diffuse component  $I_{diff}(z,t)$  which acts as an additional source refeeding the thermo-optical excitation with scattered photons. This effect might also be simulated by increasing the apparent laser pulse duration depending on the assumed scattering coefficient.

In the one-dimensional case, applying (2.2), and assuming  $\mu_{eff} \approx \mu_a$ , the thermo-optical sound excitation can thus be described by

$$\frac{\partial^2 \varphi}{\partial t^2} - c_0^2 \frac{\partial^2 \varphi}{\partial z^2} = \left( \frac{\mu_a c_0^2 \beta}{\rho_0 c_p} \right) I_0 e^{-\mu_a z} f(t), \quad (2.4)$$

which can be solved by the spectral method.

$$\varphi = (2\pi)^{-1} \int_{-\infty}^{\infty} e^{-i\omega t} \tilde{\varphi}(\omega, z) d\omega \quad (2.5)$$

$$\Rightarrow \frac{d^2}{dz^2} \tilde{\varphi} + \frac{\omega^2}{c_0^2} \tilde{\varphi} = \frac{\mu_a \beta}{\rho_0 c_p} I_0 e^{-\mu_a z} \tilde{f}(\omega) \quad (2.6)$$

$$\text{with} \quad \tilde{f}(\omega) = \int_{-\infty}^{\infty} e^{i\omega t} f(t) dt \quad (2.7)$$

The latter is the spectrum of the laser radiation intensity (i.e. the spectrum of the laser pulse envelope). The solution of the differential equation consists of two complex components corresponding to the acoustic waves traveling into the medium and exiting the medium towards the boundary as well as a real term describing the perturbations localized near the surface.

$$\tilde{\varphi} = C_+ e^{i \frac{\omega}{c_0} z} + C_- e^{-i \frac{\omega}{c_0} z} + \frac{\beta I_0}{\rho_0 c_p} \frac{\mu_a}{\mu_a^2 + \frac{\omega^2}{c_0^2}} \tilde{f}(\omega) e^{-\mu_a z} \quad (2.8)$$

Outside the heating zone ( $\mu_a z \geq 3-5$ ), only an acoustic traveling wave will be present. The wave spectrum of this wave can be determined using auxiliary boundary conditions on the surface. Ordinarily, a rigid or a free boundary of the absorbing medium is assumed.

At a rigid boundary, the relation between the acoustic impedances of the absorptive and transparent media  $N = \frac{\rho_0 c_0}{\rho_{tr} c_{tr}}$  is much smaller than 1. Consequently, the particle velocity at the boundary is 0. For a free boundary,  $N \gg 1$ , the pressure  $p$  vanishes at the boundary.

Using  $\mathbf{v} = \text{grad } \phi$ , rigid boundary conditions and

$$\frac{v}{c_0} = \frac{p'}{\rho_0 c_0^2} = \frac{\rho'}{\rho_0} \quad (2.9)$$

for a planar acoustic wave,

$$v = (2\pi)^{-1} \frac{\beta I_0}{\rho_0 c_p} \int_{-\infty}^{\infty} \frac{\mu_a^2}{\mu_a^2 + \frac{\omega^2}{c_0^2}} \tilde{f}(\omega) e^{-i\omega\tau} d\omega \quad (2.10)$$

with the reference time  $\tau = t + \frac{z}{c_0}$  indicating the readout time of the pressure-wave profile at the piezoelectric detector. This is valid for any pulse duration. It can be seen, that the optoacoustic signal spectrum is a product of the laser intensity  $I_0 \tilde{f}(\omega)$  and a transfer function  $K_r(\omega)$ , which is determined only by the properties of the medium.

$$K_r(\omega) = \frac{\beta}{\rho_0 c_p} \frac{\mu_a^2}{\mu_a^2 + \frac{\omega^2}{c_0^2}} \quad (2.11)$$

Of course, the transfer function for a free boundary can be found applying analogous calculations.

Transfer functions can be used to show frequency dependence of the efficiency of optoacoustic sound generation (see Fig. 2.2). At  $\omega_a = \mu_a c_0$ , the acoustic wave vector is equal to the absorption coefficient of light -  $\omega_a$  is called the characteristic frequency of the optoacoustic signal. This is valid for any boundary condition. Thus, the efficiency of optoacoustic sound generation is equal for free and rigid boundaries at this frequency. For rigid boundaries, the efficiency increases to lower frequencies reaching twice the efficiency of  $\omega_a$  at  $\omega=0$ . Free boundaries show most efficient sound generation at  $\omega_a$ . In the range  $\omega > \mu_a c_0$  sound generation is more efficient for free than for rigid boundaries. As can be seen, too, the frequency band for effective sound generation is wider for free than for rigid boundaries.

Some useful results appear when limiting the consideration to the case of short laser pulses. Here, the spectral range of light intensity is significantly broader than the range of the transfer function. So, light intensity can be treated as constant across the entire frequency range of efficient sound excitation  $I_0 \tilde{f}(\omega) = I_0 \tilde{f}(\omega = 0) = E_0$ ,  $E_0 = I_0 \int_{-\infty}^{\infty} f(t) dt$  being the radiation energy flow density. Applying this to (2.10)

$$v_r(\tau) = \frac{\mu_a c_0 \beta I_0}{2\rho_0 c_p} \int_{-\infty}^{\infty} f(t) e^{-\mu_a c_0 |\tau - t|} dt \quad (2.12)$$

The initial optoacoustic signal thus is a symmetric compressional pulse with exponential leading and trailing edges and an amplitude proportional to the absorbed energy density  $\mu_a E_0$ .

The condition of a short laser pulse is expressed by  $\mu_a c_0 \tau_L \ll 1$  ( $\tau_L :=$  laser pulse duration). The physical meaning of this relation is that energy will not be lost due to stress

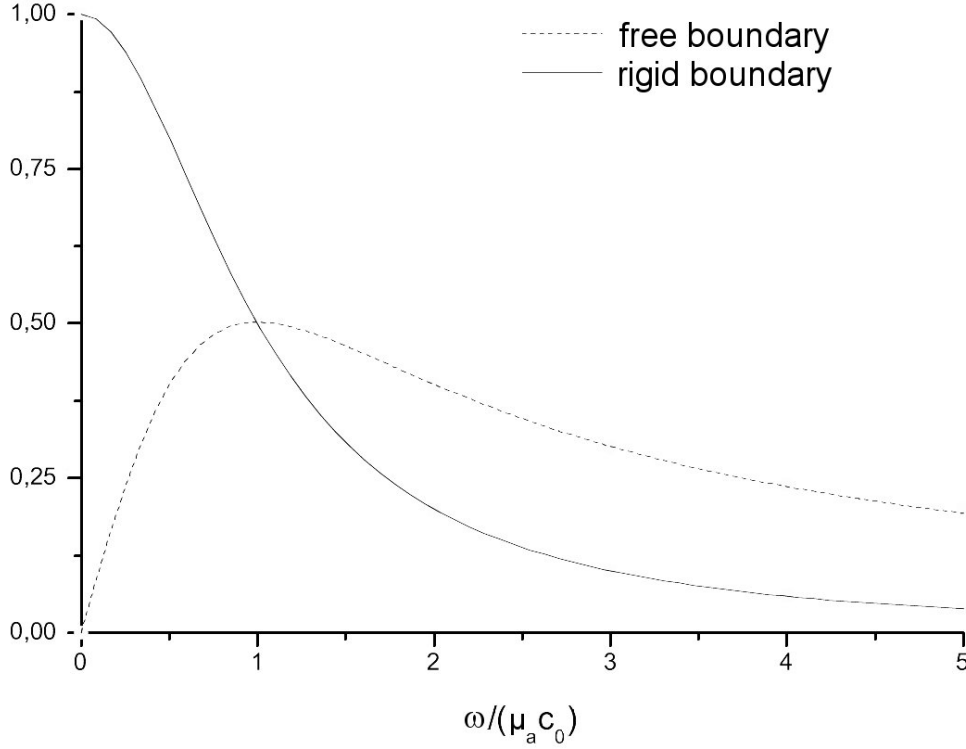


**Figure 2.2:** Relative efficiency of optoacoustic sound generation according to the transfer functions for rigid and free boundaries

dissipation but only by the stress relaxation in the ultrasonic transient. Thus, it is also called stress confinement. If this condition is not fulfilled, the pressure transient follows the temporal profile of the laser pulse. So, for optoacoustic investigations on human skin, one criterion for the choice of the appropriate laser system is a pulse duration convenient for the expected absorption coefficients. As can be seen, higher absorption coefficients call for shorter laser pulses. Assuming typical values (see Chap. 3.2.1) for  $\mu_a$  in skin and approximately 4 ns pulse duration for the UV pulses leads to a good fulfillment of the stress confinement condition.

The short but finite nature of the laser pulse shows most prominently at the signal peak amplitude which is smoothed and lowered. Assuming a Gaussian laser pulse  $f(t) = \pi^{-\frac{1}{2}} e^{-\left(\frac{t}{\tau_L}\right)^2}$ , stress confinement, and keeping in mind that sound is only excited in the absorbing medium ( $z > 0$  resp.  $t < \tau$ ), the integral in (2.12) is expressed analytically by the error function  $\Phi$

$$v_r = \frac{c_0 \mu_a \beta E_0}{2 \rho_0 c_p} e^{\frac{\mu_a^2 c_0^2 \tau_L^2}{4}} e^{-\mu_a c_0 \tau} \left[ 1 + \Phi \left( \frac{\tau}{\tau_L} - \frac{\mu_a c_0 \tau_L}{2} \right) \right] \quad (2.13)$$

As mentioned before, (2.13) describes the initial velocity (and corresponding stress) dis-

tribution in a homogeneous absorber excited by a temporally Gaussian laser pulse. Unfortunately, such an analytic expression is not available for the case of inhomogeneous optical properties.

In the following two sections, expressions will be generalized to account for real experimental conditions. First, two approaches of how to deal with an arbitrary distribution of heat sources will be presented. Subsequently, deformation of the transient on its way to the detector will be discussed.

### 2.3 Inhomogeneous optical properties

If a rigorous consideration of the optical properties of skin is desired, the wave equation for a scalar potential of the type

$$\frac{\partial^2 \phi}{\partial t^2} - c_0^2 \frac{\partial^2 \phi}{\partial z^2} = -\rho_0^{-1} \frac{\partial G(t, z)}{\partial t} \quad (2.14)$$

is to be solved (compare (2.1)).  $G(t, z)$  is the potential of the force field  $\mathbf{f}$  initiating motion of the medium:

$$f_z(t, z) = -\frac{\partial G(t, z)}{\partial z}$$

This expression is equivalent to (2.1) with

$$\text{div} \mathbf{S} = -I_0 f(t) g(z),$$

and  $g(z)$  designating the spatial distribution of heat sources. This distribution may be expressed by

$$g(z) = \mu_a(z) e^{-\int_0^z \mu_a(\xi) d\xi} \quad (2.15)$$

The solution to (2.14) can again be found by the spectral method (for details see [27]). Finally, the following relation between the acoustic wave profile and the space-time distribution of sound sources is found:

$$v_r(\tau) = (2\rho_0 c_0^2)^{-1} \int_0^\infty \frac{\partial G}{\partial \tau} \left( \tau - \frac{z'}{c_0}, z' \right) dz' \quad (2.16)$$

The acoustic wave sources for coordinate dependent absorption coefficients  $\mu_a = \mu_a(z)$  can be represented as

$$\frac{\partial G(t, z)}{\partial t} = -\frac{c_0^2 \beta}{c_p} I_0 f(t) \frac{d}{dz} \left[ e^{-\int_0^z \mu_a(\xi) d\xi} \right] \quad (2.17)$$

Applying this to a traveling acoustic wave (2.16) in the rigid boundary case, continuing the source function  $g(z)$  evenly into the domain  $z < 0$  and assuming a weakly scattering medium ( $\mu_{eff} \approx \mu_a$ ) yields

$$v_r(z = c_0\tau) = \frac{\beta I_0}{2\rho_0 c_p} \mu_a(c_0\tau) c_0 e^{-\int_0^{c_0\tau} \mu_a(\xi) d\xi} \int_{-\infty}^{\infty} f(\tau) d\tau. \quad (2.18)$$

From any expression for  $v$ , the pressure profile according to changes from the equilibrium value is found using (2.9) and accordingly

$$p(c_0\tau) = \frac{\beta c_0^2}{2c_p} \mu_a(c_0\tau) I_0 e^{-\int_0^{c_0\tau} \mu_a(\xi) d\xi} \int_{-\infty}^{\infty} f(\tau) d\tau. \quad (2.19)$$

In the experiments, ultrasound gel (USG) is used as the transparent, sound conducting medium between the skin and the PVDF detector. The boundary between skin and the USG is neither rigid nor free but rather acoustically well matched. For an arbitrary impedance boundary,

$$v(c_0\tau) = \frac{v_r(c_0\tau)}{1+N} \quad (2.20)$$

is to be used.  $N = \frac{\rho_0 c_0}{\rho_{tr} c_{tr}}$  is the relation between the acoustic impedances of the absorptive and the transparent medium.  $N \gg 1$  determines a free,  $N \ll 1$  a rigid boundary (cf section 2.2). For skin as the absorptive and USG as the transparent medium  $N \approx 1.03$  (see Table A, and [59]).

Additionally, because of the impedance mismatch between USG and the PVDF detector, not all the acoustic wave energy is transmitted to the detector. In a rigorous approach, (2.20) would have to be applied again. As this boundary may be considered to be fairly rigid, transformation of the pressure profile can be simply described by a loss due to reflection at the boundary. The reflection coefficient  $R_{ac} = \frac{1-N}{1+N}$  at the USG-PVDF boundary is approximately 0.43. Thus, the signal amplitude at the detector is only 57% of the actually incident.

Expressions (2.18) and (2.19) make it possible to find the distribution of the light absorption coefficient from the shape of the initial optoacoustic signal without the need for absolute pressure measurements.

$$\mu_a(z = c_0\tau) = \frac{p(c_0\tau)}{\int_{c_0\tau}^{\infty} p(\xi) d\xi}, \tau > 0 \quad (2.21)$$

(2.21) is of course still valid in the case of (2.20). Unfortunately this straightforward analysis of the depth dependent absorption coefficient is only possible if the initial pressure distribution is known. As will be shown in the next section, diffraction has concealed this information to a certain extent at the distance where the signal is measured.

The optoacoustic signal spectrum reveals to be the product of the laser radiation density spectrum and the Fourier spectrum of the spatial distribution of absorption. This is again the fundamental result from the transfer function method. So, if the laser pulse wave form is known, the spatial distribution of the optoacoustic sources can be recovered from the measured spectrum of the transient.

Applying this rigorous description to the analysis of optoacoustic transients salves the consciences to the cost of a massive amount of computational effort. If the sample can be approximately described as consistent of several layers with different optical properties but homogeneous within themselves, it may be more convenient to use a succession of (2.13) for the different layers.

Applying the one or the other approach, if the initial pressure profile is known, the effective attenuation can be deduced from its shape using (2.21). Unfortunately, it is practically impossible to measure this initial pressure profile directly. Under normal experimental circumstances, the optoacoustic transient is recorded at a certain distance from the absorbing sample - 3 mm in the setup used in this dissertation project. On its way from the sample surface to the detector, the pressure wave is subject to acoustic deformations. Important effects on the signal will be discussed in the following section.

## 2.4 Evolution of the signal in a dissipative medium

As shown in the previous sections, the spectrum of the optoacoustic signal can be found by the transfer function method in the generation zone. However, the transient is usually recorded at distances far greater than a few absorption lengths of light. In skin, absorption lengths of only some tenths to a few hundredths of a millimeter are expected for ultraviolet radiation while the ultrasound wave has to travel 3 mm to the detector. There are basically three effects which can alter the signal profile outside the generation zone: dissipation, nonlinearity and diffraction.

The evolution of an acoustic wave of finite amplitude in a dissipative medium is described by

$$\frac{\partial}{\partial \tau} \left( \frac{\partial v}{\partial z} - \frac{\varepsilon}{c_0^2} v \frac{\partial v}{\partial \tau} - \frac{b}{2\rho_0 c_0^3} \frac{\partial^2 v}{\partial \tau^2} \right) = \frac{c_0}{2} \Delta_{\perp} v. \quad (2.22)$$

$v$  in this case represents the  $z$ -component of the vibrational particle velocity,  $\varepsilon$  is the nonlinear acoustic parameter of the medium, and  $b$  is the dissipation coefficient. This general equation (Khokhlov-Zabolotskaya) can only be solved numerically. For analytic results, it is necessary to try and separate the scales of the individual effects.

**Dissipation** only begins to dominate in optoacoustic experiments in the hypersonic frequency range (GHz). For UV-skin measurements, characteristic frequencies are in the two digit MHz region. Thus, dissipation can be neglected here.



The Reynold's number  $Re$  indicates if **nonlinear effects** are to be expected in the behaviour of the acoustic wave.

$$Re \sim \frac{2\rho_0 c_0 \epsilon}{b\omega} v_a,$$

where  $v_a$  is the amplitude of the particle (vibrational) velocity. At high Reynold's numbers ( $Re \gg 1$ ), a shock wave front is formed and dissipation will have a significant effect in its neighborhood. If  $Re \ll 1$ , nonlinear effects are only weakly manifested. The latter is expected under the conditions of UV-optoacoustics on human skin.

The primary competition in optoacoustics is between nonlinear and diffraction effects. **Diffraction** is important even at distances  $z \sim 0.1L_D$ ,  $L_D = \mu_a a^2$  being the diffraction length ( $a$  is again the radius of the illuminating laser beam). In the present case, nonlinear effects may become noticeable only in the wave far field. In the crossover zone, the transformation of the transient is given by

$$\frac{\partial}{\partial \tau} \left( \frac{\partial v}{\partial z} \right) = \frac{c_0}{2} \Delta_{\perp} v. \quad (2.23)$$

If - as in this case - a Gaussian intensity distribution in the cross section of the laser beam

$$I(t, \mathbf{r}_{\perp}) = I_0 f(t) H(\mathbf{r}_{\perp}) = I_0 f(t) e^{-\frac{x^2+y^2}{a^2}} \quad (2.24)$$

can be assumed ( $\mathbf{r}_{\perp}$  is the radius vector perpendicular to the laser beam axis), the optoacoustic velocity spectrum can be represented as

$$\tilde{v}(\omega, z, \mathbf{r}_{\perp}) = \frac{\pi a^2 K(\omega) I_0 \tilde{f}(\omega)}{(2\pi)^2} \iint_{-\infty}^{\infty} e^{i(\mathbf{k}_{\perp} \mathbf{r}_{\perp}) - i \frac{k_{\perp}^2 z}{2\omega/c_0} - \frac{k_{\perp}^2 a^2}{4}} d\mathbf{k}_{\perp} \quad (2.25)$$

$$= K(\omega) I_0 \tilde{f}(\omega) \frac{1}{1 + i \frac{z}{L_{DF}}} e^{-\frac{r_{\perp}^2}{a^2 \left(1 + i \frac{z}{L_{DF}}\right)}}. \quad (2.26)$$

$L_{DF} = \frac{\omega a^2}{2c_0}$  is the diffraction length of frequency  $\omega$ . As the detector geometry is designed to detect the ultrasound centrally above the source, the behaviour on this axis ( $\mathbf{r}_{\perp} = 0$ ) is most significant for the measured signal. Here, the spectrum of the diffraction wave is the initial spectrum multiplied by the diffraction factor.

The corresponding expression for the pressure transient in the time domain shows that when the pulse propagates, the transverse light-intensity distribution remains Gaussian for every harmonic component and may be written in the form

$$p(z, \tau, \mathbf{r}_{\perp}) = \int_{-\infty}^{\infty} p_0(t) dt \left( \frac{1}{2\pi} \int_{-\infty}^{\infty} e^{-i\omega(\tau-t) - \frac{r_{\perp}^2}{a^2} \frac{\omega}{\omega + i \frac{2c_0 z}{a^2}}} (\omega + i \frac{2c_0 z}{a^2})^{-1} \omega d\omega \right) \quad (2.27)$$

$p_0(\tau)$  is the wave profile at the boundary of the light-absorbing medium. On the beam axis,  $\mathbf{r}_\perp=0$ , this expression can again be simplified:

$$p(z, \tau, \mathbf{r}_\perp = 0) = p_0(\tau) - \int_{-\infty}^{\tau} \omega_D e^{-\omega_D(\tau-t)} p_0(t) dt \quad (2.28)$$

$\omega_D = \frac{2zc_{lr}}{a^2}$  ( $= z\omega/L_{DF}$ ) is the characteristic diffraction frequency. If - as in this case - only the pressure profile at the detector is known, the initial pressure distribution  $p_0(\tau)$  may be found by:

$$p(z = 0, \tau, r_\perp = 0) = p(z, \tau, r_\perp = 0) + \int_{-\infty}^{\tau} \omega_D p(z, t, r_\perp = 0) dt \quad (2.29)$$

So, recapitulating, equations (2.18), (2.20), (2.27), and (2.29) are the fundamental theoretical expressions describing thermo-optical sound excitation by UV light in skin under the geometric conditions of the experimental setup. Keeping in mind the wave reflection at the boundary ultrasound gel - PVDF-detector, using again relation  $p' = \nu\rho_0c_0$  (2.9) and applying Fourier transformation where necessary, a comprehensive expression for the pressure transient is thus given by

$$p(z, \tau, \mathbf{r}_\perp = 0) = 0.57 \left( p_0(\tau) - \int_{-\infty}^{\tau} \omega_D e^{-\omega_D(\tau-t)} p_0(t) dt \right) \quad (2.30)$$

$$p(z = 0, \tau, r_\perp = 0) = \rho_0 c_0 \frac{1}{1+N} \nu_r(\tau) \quad (2.31)$$

$$\nu_r(z = c_0\tau) = \frac{\beta I_0}{2\rho_0 c_p} \mu_a(c_0\tau) c_0 e^{-\int_0^{c_0\tau} \mu_a(\xi) d\xi} \int_{-\infty}^{\infty} f(\tau) d\tau \quad (2.32)$$

These expressions are used in the simulation and analysis of the optoacoustic data assuming a temporally Gaussian laser pulse with duration 5 ns.

## **3 Human skin**

The human skin is the largest organ of the human body. It serves a variety of functions - from the regulation of the body temperature over protection from pathogens and detrimental environmental influences to perception of temperature, touch or pain. In order to meet all of these demands, skin has developed into a fairly complex organ. It consists of three major layers - epidermis, dermis, and subcutis - which serve different functions.

### **3.1 Skin physiology**

The deepest layer of the skin is called the subcutis. Built from a network of collagen and fat cells, it conserves heat and has a shock-absorbing effect that helps protect the body's organs from injury. The middle layer of the skin, the dermis, contains hair follicles, sweat glands, blood vessels, and nerves. Fibroblasts are the main cell type of the dermis. They produce elastin and collagen fibers, which provide the skin's resilience and strength. The top layer is called the epidermis. It is the thinnest layer of the skin with only a tenth of a millimeter in some skin regions. Being directly exposed to environmental influences, its main task is to serve as a barrier to germs, prevention of water loss and adaptation in order to minimize harmful effects of UV radiation.

#### **3.1.1 UV reactions and adaptation**

Being the outer layer of the skin, it is naturally the epidermis which has developed potent protection and adaptation mechanisms towards excessive and changing UV doses.

Keratinocytes (also called squamous cells) are the main cell type of the epidermis. In the lowest part of the epidermis, the basal layer, basal cells continually divide to form new keratinocytes. These newly formed cells push the older cells towards the surface of the skin. On their way to the surface, the keratinocytes mature. They form keratin and lose viability so that the outermost layer of the epidermis, the stratum corneum or horny layer, is composed of dead cells completely filled with keratin. This protein is very important

e.g. for the barrier function of the skin. The so-called keratin matrix proteins or filaggrin - necessary in giving the correct formation and macrostructure of the keratin microfibrils in the stratum corneum - are identical with the natural moisturising factor (NMF) which is essential for the protection from loss of body fluids [56]. The dead cells are continually shed from the skin's surface and replaced by younger ones so that the epidermis completely renews itself in about one month. The constant regeneration of the epidermis by the replacement of keratinocytes is one of the most important mechanisms avoiding carcinogenesis. Most keratinocytes with damaged and unrepaired DNA are simply gone within a month by this natural turnover.

UV induced damage appears in a variety of direct and indirect processes, different cell types, different target molecules, and may be acute or chronic. DNA damage for example may be directly induced by UVB radiation causing photoproducts or dimerization most of which will quickly be repaired by the potent repair mechanisms of the nucleus. UVA and UVB may cause immunosuppression and thus hamper the self-healing ability of the skin. At normal doses, UVA has mostly indirect yet important effects such as oxidative stress.

The keratin also plays an important role in UV protection. As a reaction to stronger UV radiation, the epidermis and especially the stratum corneum gets thicker (UV-induced epidermal thickening and hyperkeratosis). Consequently, the light has to pass more cell layers and more attenuating keratin to get to the viable cells.

However, it is the melanocytes, located in the basal layer of the epidermis, that normally provide the most - and the most popular - UV protection [15]. They produce the pigment melanin in elongated, membrane-bound organelles known as melanosomes. Melanin is packaged into granules which are moved down dendritic processes and transferred by phagocytosis to adjacent keratinocytes. In the inner layers of the epidermis, melanin granules form a protective cap over the outer part of keratinocyte nuclei. In the stratum corneum, melanin granules are uniformly distributed to form a UV-absorbing blanket which reduces the amount of radiation penetrating the skin.

UV radiation triggers two different melanin reactions in the skin. Within minutes after UV exposure, preformed melanin is darkened by photo-oxidation. This immediate pigment darkening may last only some hours or turn to persistent darkening with UVA doses  $> 1\text{mJ}/\text{cm}^2$ . It is primarily induced by UVA. Different from native pigment, it cannot serve as a long-term protection against UV radiation as its UV protection capacity is much poorer in the UVB than in the UVA range and its protection factor is rather limited due to a limited amount of available melanin precursors [53]. In a second mechanism, melanocytes are stimulated to produce new melanin. This delayed or persistent pigment darkening (PPD) can only be seen within days after exposure and provides long-term protection. The maximum of pigmentation is reached 72 h after exposure [35, 50].

One other very prominent skin reaction to excessive UV exposure is erythema (sunburn). Unfortunately, this inflammation reaction appears only 8h to 24h after exposure. So, this rather unpleasant reaction is incapable of serving as a warning at the right time. In Fig. 3.1 action spectra for both erythema and melanogenesis are shown. Both were evalu-

ated within the same project using a dye-laser system [2, 3, 4]. In contrast to the current CIE (commission internationale d'éclairage) standard spectrum, these spectra reveal more details on the spectral dependencies.

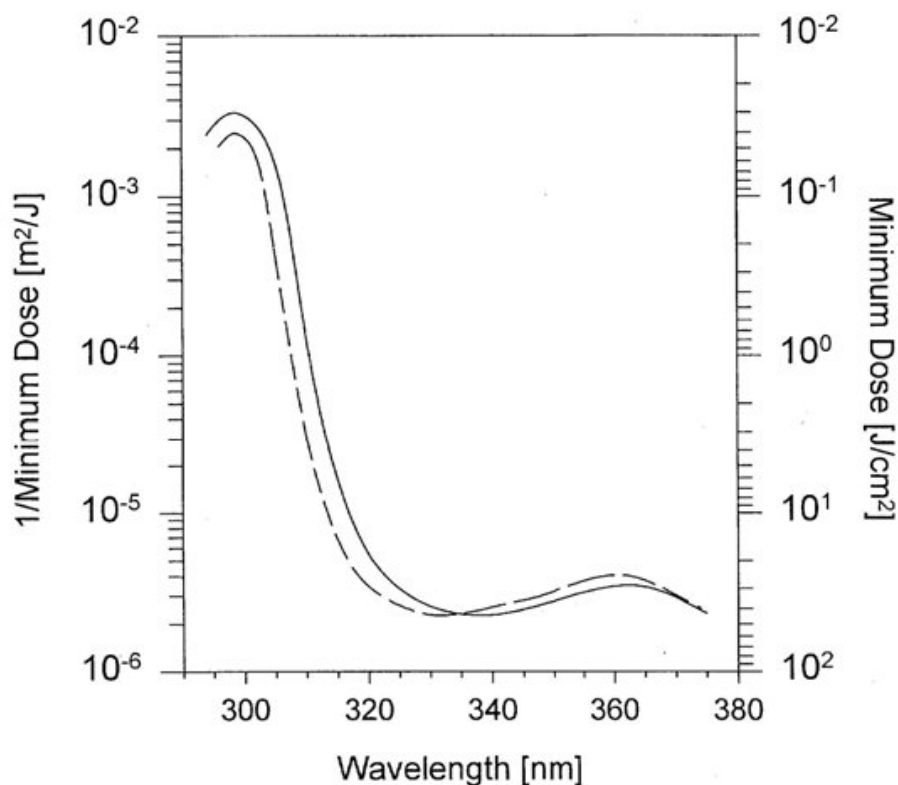


**Figure 3.1:** Action spectra for minimal erythema dose MED (solid line) and minimal melanogenic dose MMD (dashed)[4].

As can be seen, the skin is much more susceptible to both reactions in the UVB. Apart from that, the minimal dose for pigmentation is only lower than the MED in the UVA. Accordingly, a tan without reddening is possible only with 'pure' UVA irradiation. However, a constant exposure to suberythemal doses of sunlight will also induce a tan - but very slowly. Any newly formed melanin stays in the epidermal cells until their desquamation at the surface. Thus, cumulative production of small amounts of melanin below the MMD plus a light hyperkeratosis is perceived as a mild tan.

Melanin itself is a rather complex molecule most of whose secrets are yet to be solved (see e.g. [11, 18, 32]). Amongst other competences, melanin is a free radical quencher [54]. There are basically two kinds of melanin: eumelanin and pheomelanin. Eumelanin is a brown to black, photostable pigment that is packed in rather oblong melanosomes whereas pheomelanin may form phototoxic derivatives [21, 35] under the influence of ultraviolet radiation and is packed in spherical melanosomes. The red to yellow colour of the pheomelanin shows for example in red hair and feathers. Recent findings point in

the direction that it is the ratio between the two melanins that determine their protective properties and skin colour [21].

### **3.2 Optical properties of human skin in the ultraviolet wavelength range**

The optical properties of human skin in the ultraviolet wavelength range are of great interest for both fundamental research and application. The optical properties may provide some crucial hint to elucidate photobiological mechanisms, for example to finding a key chromophore for erythema. Reliable estimation of light absorption and attenuation are needed in therapy and diagnosis in order to choose the right dosis for each individual patient.

Choosing the appropriate theoretical description for this tissue at a certain wavelength range is not trivial, and *in vivo* data of optical properties are still scarce (see [20, 33]). Light transport calculations in living skin are difficult for a variety of reasons. First of all, skin is a rather inhomogeneous material. The three major layers of the skin show different optical properties and vary in thickness not only at different parts of the body. Pores, hair follicles and vessels represent additional inhomogeneities and the skin's surface is far from being even but rather furrowed. The ultraviolet range again provides some extra challenges. Not only is the human skin capable of adapting to UV exposure by changing its optical properties - the main chromophores being melanin for absorption and keratin for scattering - but native and adapted optical properties are highly individual. Native and adapted pigmentation and hyperkeratosis differ not only from person to person but also from area to area within the same individuum. Biophysical and biochemical differences add to the individual sun or UV sensitivity of each person.

As a result of the various adversaries towards a comprehensive light transport theory, different theoretical approximations are used according to the expected penetration depth. For the different wavelength components of UV radiation, penetration depths or optical properties are usually estimated from *ex vivo* measurements or analysis of UV effects at different depths in the skin. Generally, it is assumed that UVC radiation is completely blocked at the horny layer of the epidermis (at normal doses). UVB radiation penetrates the epidermis so that an efficient amount may reach the melanocytes in the basal layer and trigger melanogenesis. UVA radiation even penetrates the dermis where it can lead to photoageing, etc. For a theoretical approach, the major layers of the skin (epidermis, dermis, subcutis) are assumed to be optically homogeneous and physically isotropic. Absorption and scattering are introduced by random but homogeneous distribution of absorbing (e.g. melanin, hemoglobin) and scattering particles (e.g. keratin, elastin and collagen). Such a simplification has proven to be reasonable and practical at least for penetration depths in

the order of the epidermal thickness. For smaller penetration depths, the sublayers of the epidermis must be considered separately.

As far as skin reaction - especially erythema and tanning - is concerned these individual differences were accounted for by Fitzpatrick, who developed a phototype classification. Using a survey, people would be classified into six types. Caucasians are classified in four groups; from type I which does not tan and burns easily to type IV who does not burn and tans well. Type V classifies people of Asian descent and Africans are subsumed in phototype VI. The skin typing is used to predict individual MED in therapy for example. Unfortunately, this skin type evaluation is not very reliable. A low reproducibility is shown for example by Henriksen et. al. [29] reporting that only two of three persons were classified in the same class by repeated questioning by the same physician. As this evaluation method gives only a starting point rather than a reliable result, much effort has been made in order to develop some technical equipment able to predict UV sensitivity. However, none of the presented systems has provided a satisfactory result so far. One of them is assessment of pigmentation and skin lightness by chromameter measurements which was used as a reference for the optoacoustic experiments and will be presented in some detail in Section 6.2.4.

### 3.2.1 Epidermis

Fairly little is known about the optical properties of the epidermis especially in the UV. Searching the literature reveals only a few publications dealing with this topic - all of them calling for better experimental methods and especially for in vivo investigations. A quite comprehensive overview on the (optical) properties of human tissue was given by Francis A. Duck [20] in 1990. However, even this extensive work only shows a few entries for human skin and ultraviolet radiation and most of these data come from ex vivo skin.

Two fundamental and exemplary publications are [23] and [26]. Here, experimental results are compared with simulations or extrapolated values for the epidermal properties and single layers. Everett [23] determines the transmission of ex vivo samples - extensively discussing the adverse influence of tissue preparation methods. Gemert [26] reviews the data available at that time and (re)analyzes the optical properties in terms of absorption and scattering coefficients (see Fig. 3.2).

A more recent summary of skin optical properties is given by Jacques [33]. His approach towards a description of skin optics is not only to look at scattering and absorption coefficients separately but to divide absorption effects into baseline (skin background) and a dominant chromophore absorption.

The epidermal background absorption ( $\mu_{a,\text{skinbaseline}}$ ) was deduced from integrating sphere measurements on rat skin in a wavelength range from 350 nm to 1100 nm.

$$\mu_{a,\text{skinbaseline}} = 0.244 + 85.3e^{-\frac{\lambda-154}{66.2}} \quad (3.1)$$

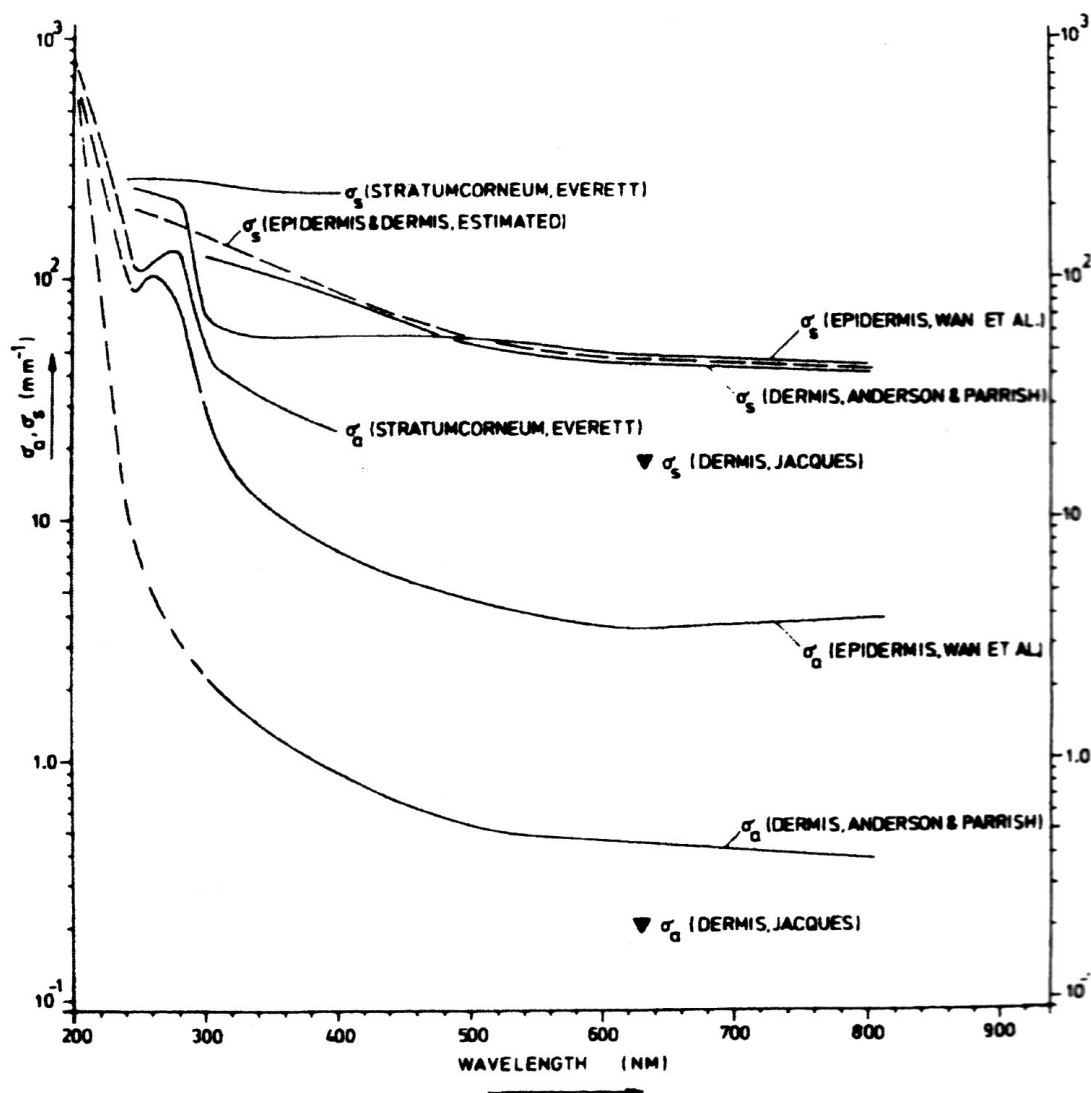


**Figure 3.2:** Experimental absorption ( $\sigma_a$ ) and scattering ( $\sigma_s$ ) coefficients for stratum corneum, epidermis and dermis. Dashed lines are estimates. [26]

Extrapolation over the whole terrestrial UV range yields fairly low background absorption from  $2.32 \text{ cm}^{-1}$  at  $400 \text{ nm}$  to  $12.96 \text{ cm}^{-1}$  at  $280 \text{ nm}$ .

Melanin concentration is assumed to be the dominant factor of skin absorption. Jacques deduces the absorption coefficient of single melanosomes ( $\text{mua.mel}$ ) from threshold exposure for explosive vaporization of melanosomes by pulsed lasers at various wavelengths.

$$\text{mua.mel} = (6.6 * 10^{11}) \lambda^{-3.33} \quad [\text{cm}^{-1}] \quad (3.2)$$

Of course, the melanin content varies amongst melanosomes so this is only a first approximation. In order to find an expression for the absorption due to melanin throughout the epidermis, it is necessary to know the volume fraction ( $f.\text{mel}$ ) of melanosomes within the total volume of the epidermis. This fraction varies due to native skin colour and tanning.



Values for orientation are for light-skinned caucasians  $f.mel = 1.3-6.3\%$  to  $f.mel = 18-43\%$  for darkly pigmented Africans.

The total absorption of the epidermis ( $mua.epi$ ) is then given by

$$mua.epi = (f.mel)(mua.mel) + (1 - f.mel)(mua.skinbaseline) \quad (3.3)$$

The resulting absorption coefficient for light to well pigmented caucasian skin is included in Figure 3.7 which is shown in Sec. 3.2.2.

Due to the thinness of the epidermis, the epidermal background scattering ( $musp.epi$ ) is assumed to be the same as in the dermis as a first approximation (see Sec. 3.2.2).

Another approach towards an estimation of the optical properties focuses on the pure chromophores expected to dominate in a special wavelength range. As mentioned before, the optical properties of the epidermis in the UV are mainly determined by the chromophore melanin. Fig. 3.3 shows the melanin absorption spectrum of synthetic melanin species. Both types of melanin show increasing absorption towards shorter wavelengths. However, absorption spectra of 'pure' melanin are a tempting yet potentially misleading

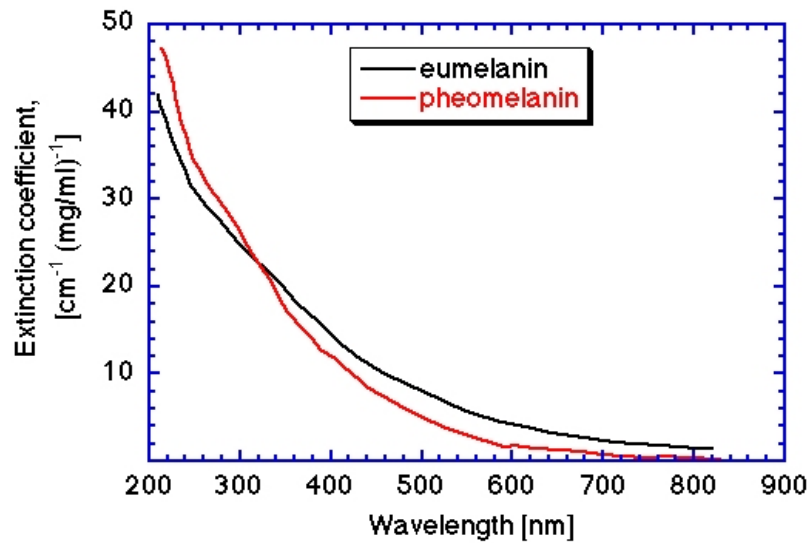


**Figure 3.3:** Absorption spectra of eumelanin and pheomelanin [34].

guide. This warning should be kept in mind for both, the chromophore approach as well as the semi-empiric approach by Jacques. Melanin is a highly heterogeneous, hardly soluble material. Natural melanin is rather a complex heteropolymer made up of both eumelanin and pheomelanin building blocks than its 'pure' synthetic relative often used in *in vitro* investigations [18, 32]. Apart from that, native pigmentation is formed by melanin packed in melanosomes and not uniform or 'pure'. The very poor solubility of eumelanin hampers spectroscopic investigations - especially as increasing solubility is discussed as

a form of melanin degradation. So, *in vitro* and *in vivo* spectroscopic data is bound to differ and results must be handled with adequate care.

Interestingly, the apparent pigmentation spectrum of constitutive epidermal melanin pigmentation obtained by comparing normal skin to vitiligo involved skin looks different (see Fig. 3.4 (a)). Here, absorption shows a pronounced maximum at 335 nm decreasing quickly towards shorter wavelengths.

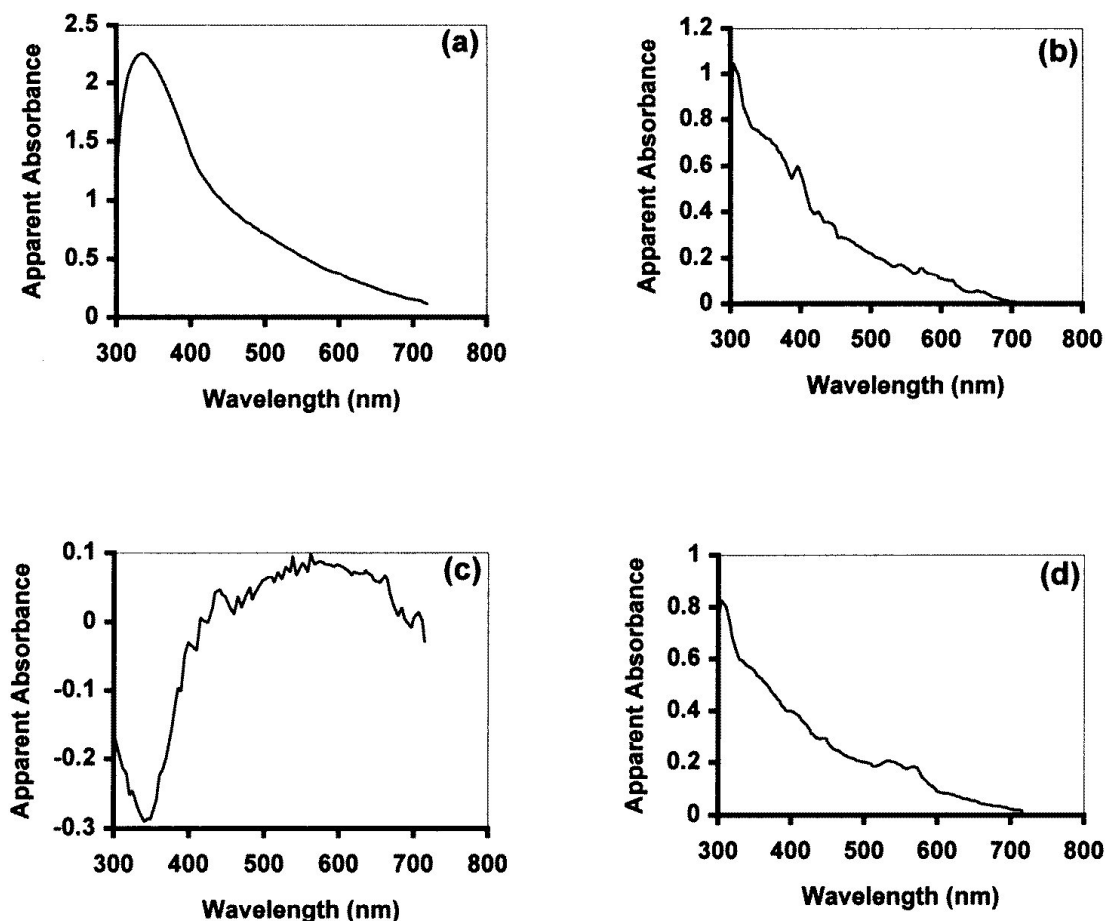


**Figure 3.4:** Apparent absorbance spectra of melanin in human skin *in vivo* determined by reflectance spectroscopy: (a) constitutive melanin; (b) UVB-induced pigmentation; (c) UVA-induced pigmentation; (d) PUVA-induced pigmentation. [43, 69]

Figs. 3.4 b) and c) show the UVB- and UVA-induced pigmentation respectively. Whilst the UVB-induced pigment has a constantly rising spectrum similar to that of *in vitro* melanin, UVA-induced melanin shows a reduced ability to absorb UV(B) radiation. The marked differences seen in these three spectra of 'melanin absorption' can be taken as a reminder that optical properties of chromophores may be brought to a further dimension *in vivo*.

In the stratum corneum, lipids and keratin play an additional important role for the optical properties. Here, keratin accounts for up to 85% of the cellular protein, which itself is

the major constituent of this skin layer with 75-80% [36, 55]. Keratin is usually only included as a scattering molecule in considerations about the optical properties of skin as its absorption is negligible for most wavelengths whereas its fibrous structure makes it an important Rayleigh scatterer. However, these general assumptions must be reconsidered for the ultraviolet range. Still, keratin is a potent Rayleigh scatterer as the fibrils have diameters of about 70-100 Å but besides, keratin is also a strong absorber in the UVB (see Fig. 3.5).

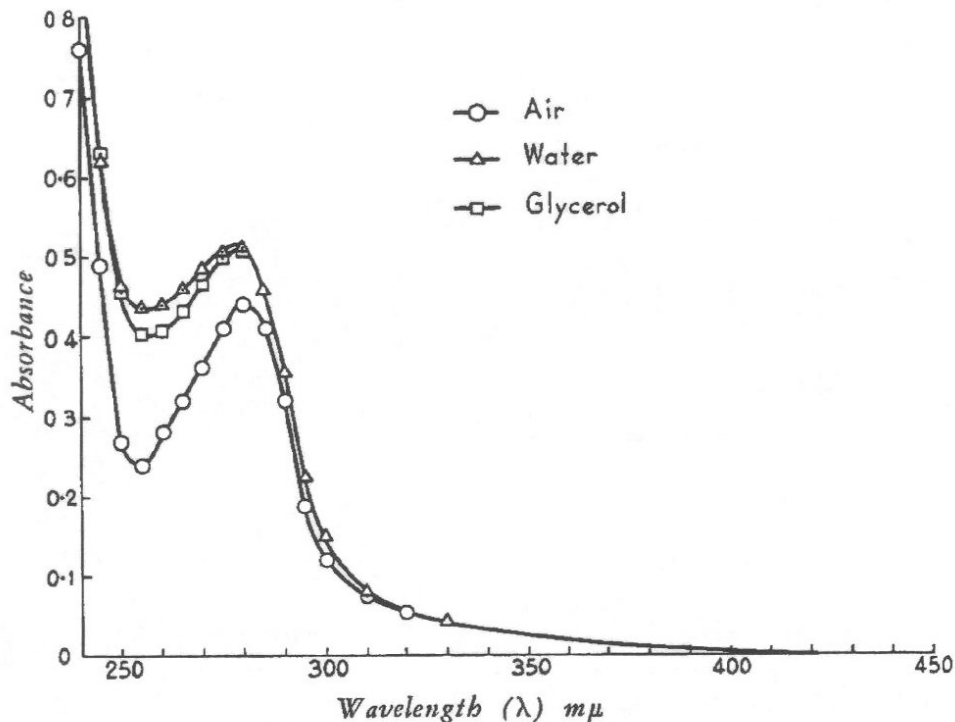


**Figure 3.5:** Absorbance spectra of solid keratin section in different immersion media which have to be used to reduce surface scatter [10].

Comparing epidermal skin absorption and scattering (compare Sec. 3.2.2) in the UV range shows that absorption plays the dominant role in average pigmented skin (see Fig. 3.6). Additionally, taking the strong forward scattering nature of epidermis and especially of the stratum corneum into account (compare Sec. 2.2), scattering might even be neglected for well pigmented epidermis in the context of optoacoustic measurements. However the optical properties of the stratum corneum might have to be considered separately from the rest of the epidermis at least for skin sites with thick horny layer. Melanin concentration is relatively low in the stratum corneum whereas keratin concentration is very high. If keratin is dominating the optical properties of the stratum corneum, scattering might not be neglected. On the other hand, keratin absorption probably dominates over scattering in the short wavelength range down to at least 300 nm and thus may reestablish the dominance of absorption in this range.

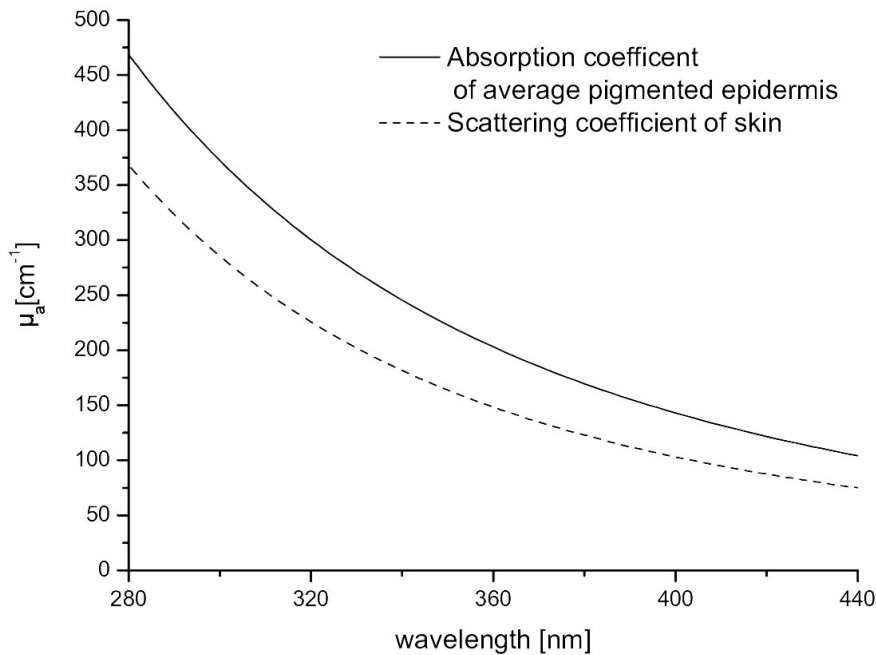


**Figure 3.6:** Comparison of epidermal absorption and scattering coefficients for average pigmented epidermis

### 3.2.2 Dermis

The cutaneous blood perfusion is the dominant variable for the absorption properties of the dermis. The related dominant chromophore is thus hemoglobin in its oxygenated or deoxygenated form. Of course, the blood is not distributed uniformly in this skin layer and blood perfusion may vary due to temperature regulation mechanisms. The cutaneous blood content is concentrated in a venous plexus about 100-200  $\mu\text{m}$  from the surface and the volume fraction ( $f.\text{blood}$ ) in this region is likely to be about 2-5%, which is a common blood volume fraction in other well-perfused tissues. In the surrounding tissue, the absorption coefficient is approximately equal to the general background absorption of skin ( $\text{mua.skinbaseline}$ ). When looking at only a small area of skin - like in optoacoustic measurements - it seems to be appropriate to take both extremes into consideration. For most applications however, it is sufficient to work with an average blood content of 0.2% throughout the dermis.

Hemoglobin absorption differs for the oxy and deoxy variety of the molecule and thus for venous and arterial blood (see Fig. 3.7, curves are representative for a well-perfused dermal layer). In order to calculate the total absorption of the dermis, an approach equivalent to that for the epidermis can be used (compare Eq. (3.3) in Sec. 3.2.1):

$$\text{mua.derm} = (f.\text{blood})(\text{mua.blood}) + (1 - f.\text{blood})(\text{mua.skinbaseline}) \quad (3.4)$$

Absorption coefficients for the average dermal absorption are shown in Fig. 3.7 and compared to absorption of a well pigmented epidermis. Obviously, attenuation of ultraviolet radiation primarily takes place in the epidermis with its special UV pigments.

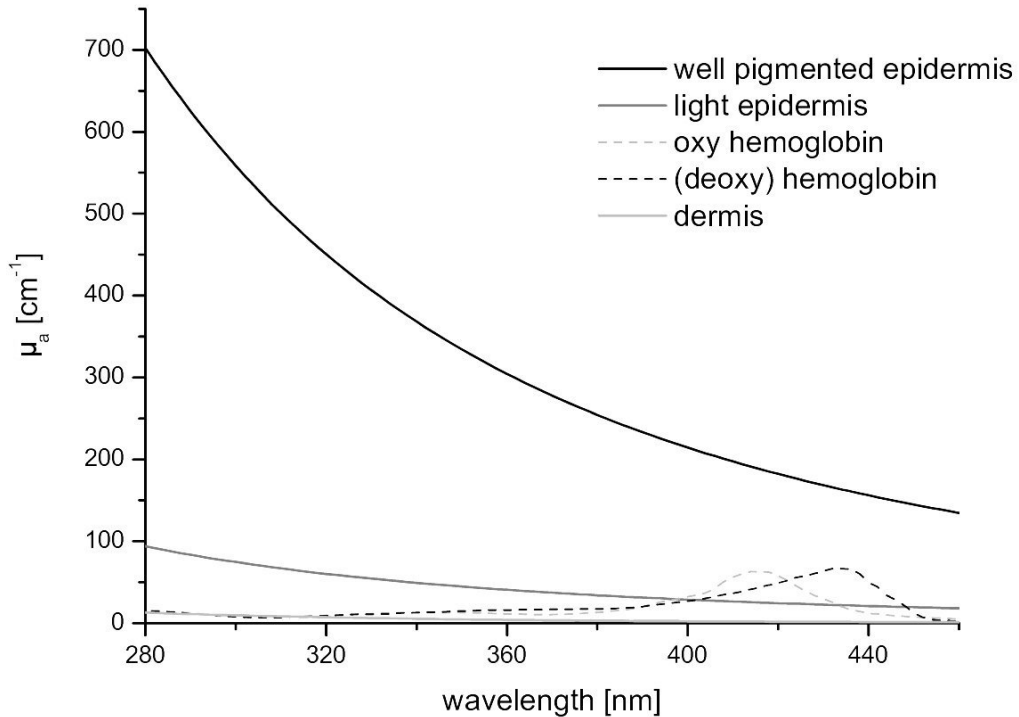


**Figure 3.7:** Absorption coefficients of the epidermis in light (f.mel=2%) and well pigmented (f.mel=15%) caucasian skin, the dermal absorption spectrum in well-perfused parts of the tissue (f.blood=5%, 45% hematocrit, for oxy and deoxy hemoglobin) and average dermal absorption coefficients (f.blood=0.2%)

The reduced scattering coefficient of the dermis ( $musp$ ) is combined of Mie-scattering ( $musp.Mie.fibers$ ) due to the rather large collagen fibres and Rayleigh-scattering ( $musp.Rayleigh$ ) due to smaller structures.

$$musp(\lambda) = musp.Rayleigh(\lambda) + musp.Mie(\lambda) \quad (3.5)$$

With  $musp.Rayleigh(\lambda) = 2 * 10^{12} \lambda^{-4}$  and  $musp.Mie.fibers(\lambda) = 2 * 10^5 \lambda^{-1.5}$  this equals

$$musp(\lambda) = 2 * 10^{12} \lambda^{-4} + 2 * 10^5 \lambda^{-1.5} \quad (3.6)$$

The keratin fibers of the epidermis are very similar to the collagen fibers of the dermis regarding their scattering properties. Thus, the reduced scattering coefficient of the epidermis and dermis can be considered equal in a first approximation.

Obviously, a lot of information and spectra relevant to the UV optical properties can be found in the literature as collected and shown on the previous pages. However, it must be pointed out again, that only Figs. 3.1 and 3.4 are based on in vivo data. Still, the ex vivo or in vitro spectra of course prove very useful in the analysis of the in vivo data that is gathered in the course of this dissertation project.

## **4 266 nm pumped OPO - the terrestrial UV range in one tunable system**

One of the aims of this dissertation project was to show that the optical properties of human skin *in vivo* can be measured using optoacoustics. As stated in the introduction, all parts of the terrestrial UV spectrum are of great interest in photobiology even though or precisely because their effects and sites of action may be different. Consequently, there was a need for an appropriate light source accounting for the demands of optoacoustics and suitable for subject measurements (see also Chap. 5).

In general, there are two laser types capable of providing tunable UV radiation: dye lasers and optical parametric oscillators (OPOs). A system suitable for subject studies should allow for fast wavelengths tuning over the whole terrestrial UV range. To cover the whole UVA/UVB range, several different dyes would be needed, which would have to be exchanged from one wavelength range to the other, making this system disadvantageous for the application (for more information on dye lasers see e.g. [12]). OPOs on the other hand achieve wavelength tunability simply by rotating a nonlinear crystal. However, there is no commercial OPO system providing tunability over the whole UV range with one module. Oportek Inc. offer for example the Vibrant system for UV applications. In this case, a system composed of a 355 nm pumped OPO with frequency doubler (235-300 nm) and mixer (300-380 nm) and a frequency doubled 532 nm pumped OPO (350-475 nm) would be needed [51].

Consequently, a tunable UV source optimized for the demands of the dissertation project was developed in the course of a diploma thesis [42]. For first optoacoustic measurements (see esp. [46] and [48]) a 355 nm pumped frequency doubled OPO courtesy of the Laser Zentrum Hannover e.V. had been used for UVB measurements. It was later replaced by a new 355-OPO by Ekspla (see Sec. 5.1) making 210-345 nm available. So, the new light source should meet the following demands:

- wavelength tunability from ca. 320-400 nm (shorter wavelengths desired)
- pulse duration: low (single-digit) ns-range

- high pulse energies sufficient to induce clear optoacoustic transients

The solution of choice was a 266 nm pumped OPO.

## 4.1 Demands and theoretical limitations

As stated in the previous section, basic requirements for the new system were wavelength tunability over the whole UVA range at least, pulse duration in the low ns range to ensure stress confinement even in the case of strong absorption, and comparatively high pulse energies to allow for good signal to noise ratios in the optoacoustic transients.

Nanosecond pulses in the UV are usually generated by frequency-doubling the output of an OPO in the visible range. The disadvantage of this setup is that the output of the OPO undergoes a second nonlinear process, and thus the pulse-to-pulse instability is increased while the output intensities are severely decreased. In recent years, considerable work was put into the development of optical parametric oscillators overcoming the predicaments of low output energy and low conversion efficiency. The discovery of beta-bariumborate (BBO) [17] finally paved the way for OPO systems working as light sources between the visible and the UVC. BBO with its broad transparency window from 193 nm down to 3.5  $\mu\text{m}$  allows using a pump source of 266 nm wavelength to obtain UV nanosecond pulses directly from the OPO. In the nonlinear crystal of an OPO, pump photons (p) are split up into a signal (s) and an idler (i) photon following the laws of energy and impulse conservation. So, by pumping with 266 nm, signal wavelengths from close to 532 nm down to the UV are supplied as well as idler wavelengths longer than 532 nm. However, such a UV-OPO system faces a few obstacles. At wavelengths below 350 nm, the nonlinearity of the diffraction indices of BBO become more and more pronounced (see Fig.4.1). In addition, the loss by two-photon absorption (TPA) in BBO is increasing rapidly with shorter wavelengths and higher intensities. At intensities needed to evoke parametric oscillation, losses of 10 per cent or more are to be expected (see Fig. 4.2).

These effects have prohibited effective nanosecond pulse generation between 300 and 400 nm when using a 266 nm pump source in the past. A singly resonant ring oscillator (SRRO) was designed to overcome these issues and provide a tunable source of nanosecond pulses covering most of the terrestrial UV from 300 to 400 nm and up into the visible spectrum.

A detailed theoretical description of this OPO is given in [42]. Here, I would like to focus on the fundamental and characteristic qualities of the system and point to interesting theoretical results.

The characteristic quantities of an OPO are the steady-state threshold pump power, the conversion efficiency and the generated output power. For pulsed systems, the steady-state threshold is replaced by the threshold fluence, the rise time, and the minimal peak



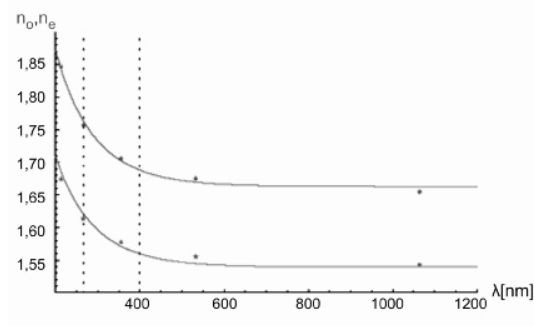


**Figure 4.1:** Ordinary (top) and extraordinary (bottom) diffraction indices for BBO ([5, 42] and references therein).

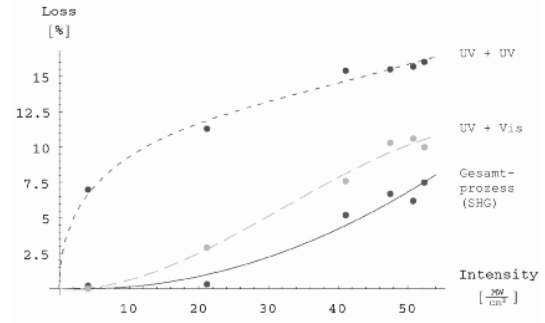


**Figure 4.2:** Right: Two photon absorption (TPA) in BBO [67, 42].

power for oscillation. For the range between 300 and 400 nm with BBO as the nonlinear optical material, the most important parameter is the threshold at which oscillation is initiated. A wavelength dependent conversion efficiency of 50 per cent and more for the parametric process is given in the literature allowing for a rapid increase in the output once the pump power exceeds the threshold [61]. With pulse durations of a few nanoseconds, the presented system should be considered as a pulsed pumped system. However, the condition for a continuously pumped system is not too far away: "quasi-continuous waves" (cw) means the duration of the pump pulse is long compared to the time of a resonator round trip and the resonator size of the developed system was minimized in order to maximize the number of resonator round trips of the signal wave during one pump pulse. For comparison, the system was evaluated theoretically under both assumptions: as a quasi-continuously pumped cw-system and as a pulsed system.

The case of a **quasi-continuous pump** wave can be treated by an analytical approach. In the limit of low loss, the steady-state pump threshold power is

$$P_{p,th} = \frac{\epsilon n_s n_i n_p c_0 \lambda_p^2}{2\pi^2 d_{eff}^2 L^2} A R_{es}(R, \alpha) \quad (4.1)$$

with P being the radiation power,  $c_0$  the velocity of light in vacuum,  $n_{s,i,p}$  the refraction indices of the nonlinear optical material for the respective wavelengths,  $\lambda_p$  the pump wavelength,  $d_{eff}$  the effective coefficient of the nonlinear optical d-tensor, L the length of the medium, A the effective beam area, and  $R_{es}$  the resonator function depending on total reflectivity R and total loss  $\alpha$ . Eq. (4.1) is based on formulas given in [61], which were rewritten to separate effects due to the properties of the medium and the resonator properties from those due to the beam profile to allow adaptation to different resonator layouts and beam profiles. The resonator function of the presented system was calculated to be

$$R_{es}^{SRRO} \cong 2(1 - R_s e^{-\alpha_s L}) \quad (4.2)$$

The effective beam area was approximated with Gaussian (or Super-Gaussian theory respectively) as

$$A = \frac{\pi}{8M^2} \quad (4.3)$$

$$M = \frac{w_s w_i w_p}{w_s^2 w_i^2 + w_s^2 w_p^2 + w_i^2 w_p^2} \quad (4.4)$$

with  $w$  being the  $e^{-1}$ -radii of the involved signal-, idler- and pump beams.

Calculated results for a hattop (Super-Gaussian) and a Gaussian pump beam profile dependent on the signal wavelength are shown in Figure 4.3. It can be seen that especially

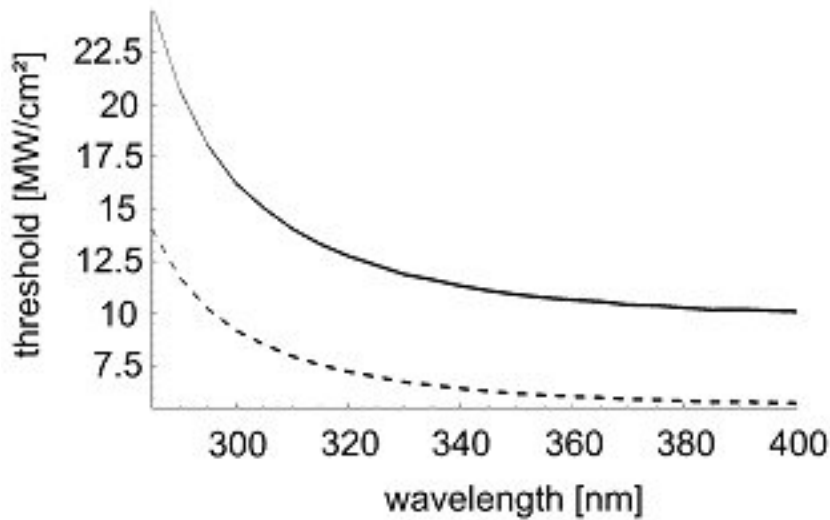


**Figure 4.3:** Steady state pump threshold for a hattop (dotted) and a Gaussian (solid) beam profile

for the shorter wavelengths the steady state pump threshold is increasing rapidly. This is due to a stronger absorption of the corresponding idler in the infrared and the increasingly nonlinear form of the refractive indices below 350 nm. As expected, a Gaussian beam profile leads to a higher threshold than a hattop profile because the intensity in the wings of the profile is too low to pump parametric oscillation.

Assuming a **pulse pumped system** requires a numerical approach. The behaviour of a pulsed OPO can be calculated numerically by integrating the wave equations of the signal-, idler-, and pump waves through the crystal with appropriate boundary conditions for modeling resonator layout and mirrors. This was done using the SNLO software by A. V. Smith [58]. Since there is no routine directly giving the threshold fluence, the numerical modeling was done in steps of 5 mJ for the pump energy until the generated signal exceeded  $1 \mu\text{J}/\text{cm}^2$  on the outcoupling mirror. The behavior of the steady state

threshold curve in Figure 4.3 indicated that for wavelengths below 315 nm the damage threshold of BBO at  $13 \text{ J/cm}^2$  [5] was exceeded. At 315 nm the threshold intensity was found to be  $1.115 \pm 0.0025 \text{ J/cm}^2$  using a Gaussian pump beam with a pulse duration of 4.4 ns.

So, theoretically, the threshold pump intensity of a pulsed OPO of  $1.115 \pm 0.0025 \text{ J/cm}^2$  was found to be approximately two orders of magnitude larger than the corresponding steady state threshold for a similar cw pumped system at  $0.0130 \pm 0.0025 \text{ J/cm}^2$ . This difference in the results is not explicable within the analytical or numerical theories currently given in the literature [61] and does not allow for a justified prediction whether or not the system behaves more like a pulsed or like a cw pumped system. However, both theoretical frameworks predict the threshold to lower rapidly for longer wavelengths, so that even in case the system behaved purely like a pulsed system, the OPO could be operated at longer wavelengths towards the visible spectrum range. If the system behaves closer to a cw pumped OPO, then even shorter wavelengths below 315 nm are expected.

## 4.2 Setup

On this basis, a 266 nm pumped OPO was developed and constructed as a singly resonant ring oscillator. In practice, the design was governed by the attempt to find the most suitable compromise between a number of demands and restrictions:

- the wide tuning range asks for a wide crystal and broadband reflection coatings at the resonator mirrors. Those broadband reflection coatings display particularly low damage thresholds.
- the resonator path length has to be minimized to allow as many signal round trips as possible during one pump pulse in order to achieve the necessary amplification.
- the predicted pump threshold for oscillation is close to the damage threshold of the nonlinear crystal and exceeds the damage threshold of most optical coatings.

The last item provided the greatest challenge for the construction of the system and even made the introduction of additional pump coupling mirrors unavoidable in order to protect the resonator mirrors from the aggressive pump power even though this action considerably increased the resonator dimensions.

The experimental setup finally decided for is shown in Fig. 4.4.

A commercial frequency-quadrupled Nd:YAG laser (NL303G, Ekspla ltd., Lithuania) with a 266 nm output power of 60 mJ in 4.4 ns pulses of Gaussian beam profile serves

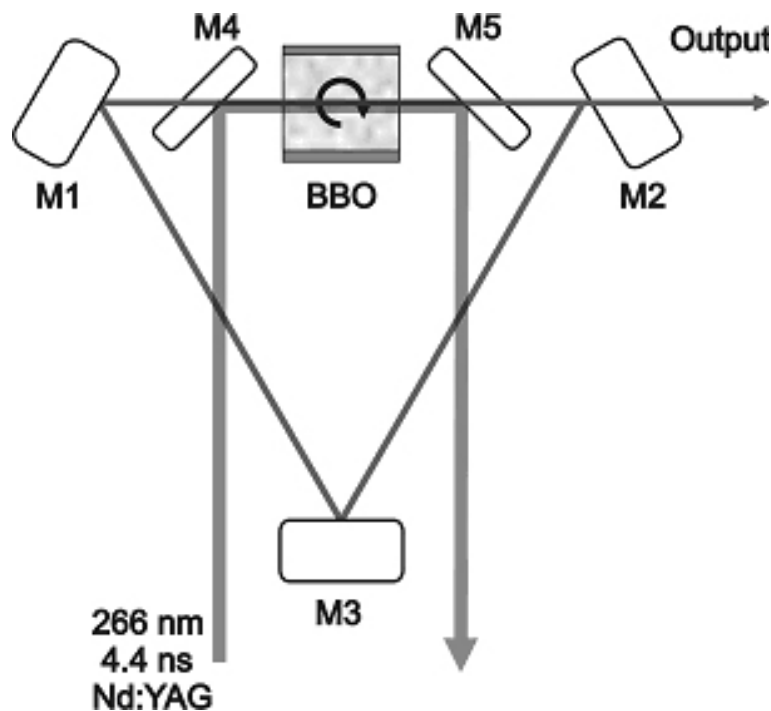


**Figure 4.4:** Schematic diagram of the OPO. Mirrors M1-M3 form the resonator (HR for the signal); mirrors M4 and M5 direct the pump beam through the BBO crystal (HR for 266 nm, HT for the signal wavelengths).

as the pump source. Its beam diameter of 8 mm was reduced to 4 mm by means of a Galilean telescope, achieving a energy density of  $120 \text{ mJ/cm}^2$  on the surface of the non-linear optical medium. The nonlinear optical medium is a  $10 \times 12 \times 6 \text{ mm}$  type-I cut beta-bariumborate crystal (BBO) with protection coating from Eksma UAB, Lithuania. Tuning was achieved by rotating the crystal in the beam path. Two rectangular mirrors (M4 and M5) of fused silica lead the pump beam through the crystal. Both mirrors measure  $8 \times 10 \text{ mm}$  with a thickness of 1.5 mm. They have an oxidic coating for 78 per cent transmission between 300 and 430 nm and 95 % reflection of 266 nm at an angle of incidence of 45 degrees. Their alignment in the experimental setup is chosen to minimize overall resonator length and thus maximize the number of resonator round trips during a pump pulse. The damage threshold of M4 and M5 was measured to be  $1.1 \pm 0.2 \text{ J/cm}^2$ . These pump coupling mirrors are necessary as the damage threshold for the wideband coatings of the resonator mirrors was much too low to directly expose them to the pump beam. The resonator itself consists of three mirrors (M1 - M3) in an equilateral triangle. They all measure 12.7 mm in diameter and are transmissive for the infrared wavelengths of the idler. Aside from that, all mirrors have different specifications: M1 is made of fused silica and has an oxidic coating for maximum reflectivity between 300 and 430 nm at 30 degrees angle of incidence; M2 is equally made of fused silica and has an oxidic coating for 50 % transmission between 300 and 430 nm at 30 degrees angle of incidence; M3 is made of BK-7 glass and coated like M1. All mirrors were custom made by Laseroptik GmbH, Germany. The SRRO has a resonator length of 10 cm in an equal angle geometry.

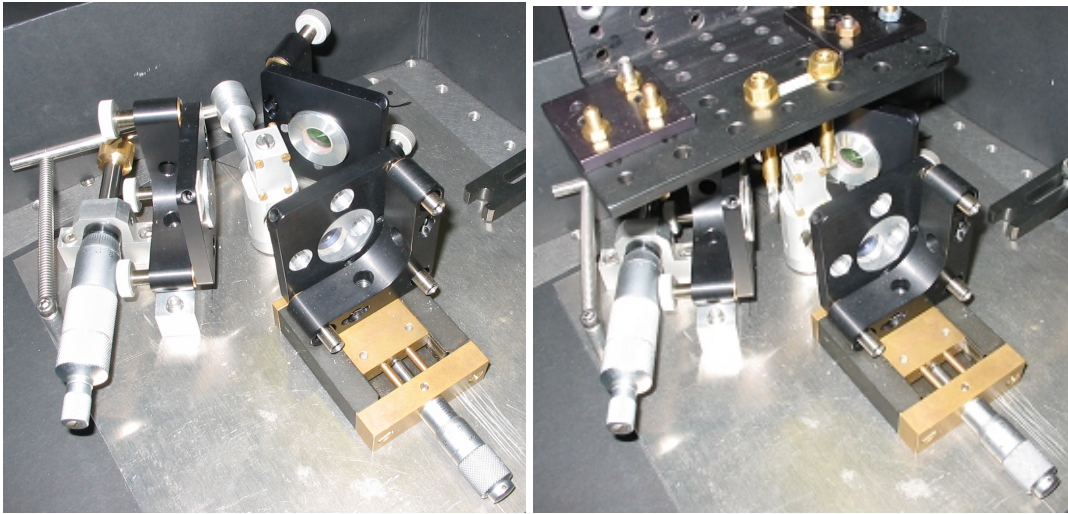


**Figure 4.5:** Pictures of the 266-OPO: The resonator mirrors (black mounts) form a triangle around the OPO-crystal (centrally, silver mount), which can be rotated by a micrometerscrew (left). Pump radiation enters and leaves the resonator through the holes on both sides of the front resonator mirror and is directed through the crystal by the suspended mirrors (see right picture). The signal wave circulates the resonator triangle and is uncoupled at the back/right resonator mirror.

The three mirrors M1-M3 lead the generated signal wave unidirectional through the crystal so that there are no material passes without amplification. At any given moment there is only the radiation involved in the optical parametric amplification within the medium: the signal radiation generated in all consecutive passes, the remaining pump radiation, and the idler radiation of only the current pass of the pump pulse through the medium. Therefore, the occurrence of two-photon-absorption and the recombination of signal photons with idler photons to photons of the pump wavelength have been minimized.

Pictures of the real OPO are shown in Fig. 4.5. Still, the damage thresholds of the pump coupling mirrors and the BBO-crystal are close to the working threshold of the OPO. As it is the coating which normally decreases the damage threshold, the first BBO-crystal was replaced by a new wider crystal without protection coating in a first upgrade of the system. To avoid humidity damages, a heater was installed keeping the BBO crystal at a temperature of more than 50 °C.

### 4.3 Achievements

Actual operation of the designed OPO system showed that its characteristic quantities, especially its pump threshold and the spectral form of its output pulses are between the calculated values for pulsed resp. steady state systems.

The SRRO was found to be continuously tunable from 300 to 410 nm with a pump threshold of 120 mJ/cm<sup>2</sup> at 300 nm. Figure 4.6 shows the measured intensities of the SRRO

depending on the wavelength in 5 nm steps. The three-dimensional plot allows easy

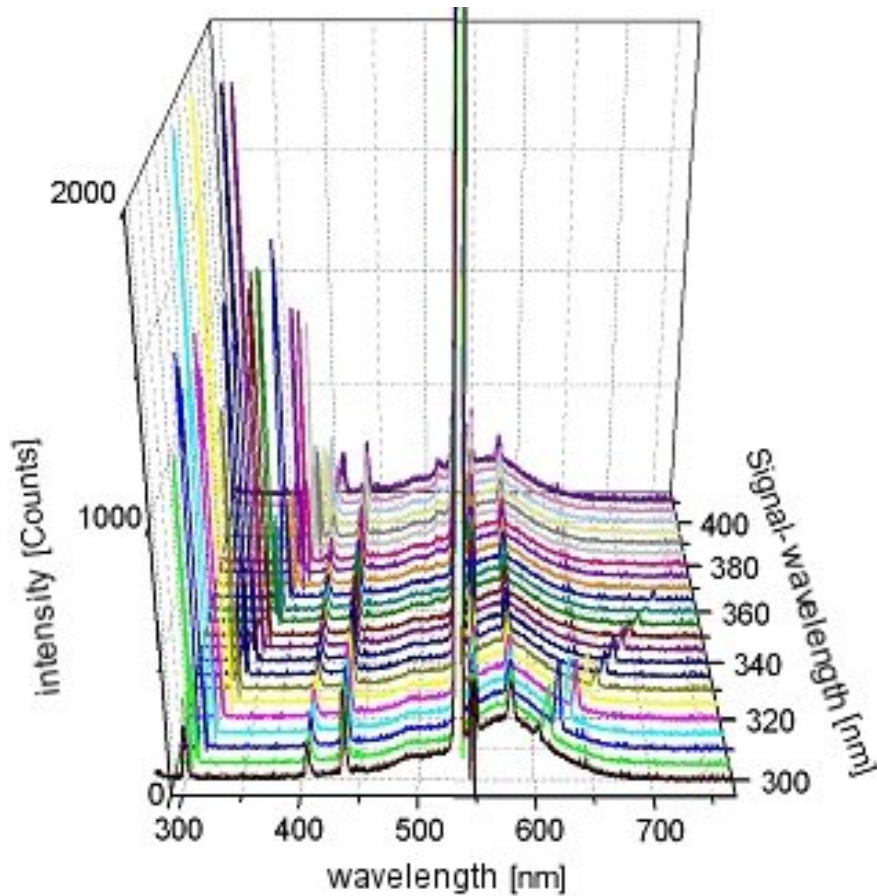


**Figure 4.6:** Output spectrum of the 266-OPO at different signal wavelengths.

differentiation between signal output and background. The background consists of the remaining pump radiation at 266 nm (not shown), the 532 nm radiation contained in the pump laser output, and a broad low intensity spectrum overlaid with several lines between 400 and 675 nm, which originates from the laboratory illumination. Aside from statistical variations, this background is constant throughout all measurements. The intensity of the signal pulses range from 100  $\mu$ J (at the long wavelength edge of the tuning range) to 3.5 mJ at 325 nm - measured behind the outcoupling mirror filtered by a DUG11x UV-bandpass filter (Schott, Germany). The visible end of the tuning range at 410 nm is determined by the width of the BBO crystal in use. The signal intensities drop sharply below 300 nm corresponding with the increased absorption of the related idler wavelengths in the BBO crystal and decreasing reflectivity of the resonator mirrors. The shortest wavelength measured was 298 nm. Below that the signal vanishes in the increasing background.

A system with a comparable setup was reportedly in use within the visual part of the spectrum [30]. To our knowledge, this is the first time however that a nanosecond SRRO was successfully implemented in the UV-A and parts of the UV-B with a tuning range of

more than 100 nm.

As the system was constructed not only for laboratory use but for application in subject studies, a high level of robustness was another important criterion. The constructed system is very compact, taking up a space of less than 20 cm<sup>2</sup> (pump source and beam collimation excluded), and it is highly insensitive regarding vibrations and other mechanical disturbances making it highly suitable for in situ conditions.





# **5 An experimental setup for UV-optoacoustics on human skin**

Optoacoustics is - as the name implies - composed of an optical and an acoustic part. First of all, a pulsed laser light source is needed to induce thermo-optical stress in the sample. For the dissertation project, the light source had to fulfill several requirements. It had to provide nanosecond pulses short enough to ensure stress confinement (see Chap. 2). The ultraviolet radiation should be tunable over the whole terrestrial UV range (290 nm - 400 nm) and fast wavelength selection should be possible to minimize expenditure of time for subjects. The light pulses have to be coupled into a fiber and be lead to the sample in a way that the fluence on the sample surface is high enough to induce detectable thermo-optical stress transients in combination with a homogeneous illumination area.

The optoacoustic sensor head has the function of coupling the optical and the acoustic part. Alignment of the fiber light source and the stress detector is implemented to allow optimal stress induction and detection. The stress detector is located centrally above the illuminated spot and its dimensions have to be small compared to those of the illuminated area. The sensor head also includes an electronic amplifier for the optoacoustic signals. These signals then must be read out and processed to achieve the status of raw data for the analysis by simulation of the optoacoustic transients.

A comprehensive and reliable analysis of the data requires knowledge of the illumination conditions and of all subsequent acoustic and electronic influences on the optoacoustic signal. So, the intensity of each UV pulse must be measured and assigned to the appropriate optoacoustic transient. For this purpose, pulse intensities were measured online by a photodiode using stray light from the fiber.

## **5.1 Tunable pulsed UVA/B radiation - a combination of two OPOs pumped by the same Nd:YAG source**

The ultraviolet laser system consists of two different OPO units sharing the same pump source (see Figs. 5.1 and 5.2). A commercial frequency doubled 355nm-OPO provides

UVB and UVA-II radiation (290 nm - 340 nm) while the remaining UVA-I plus a sufficient UVA-II overlap is made available by the constructed 266nm-OPO. As pointed out in Sec. 4.3 already, great emphasis was laid on the robustness of the system. As can be seen in Fig. 5.2 the whole system is mounted on an aluminium plate. For the subject study, the system was transported on this plate by car and could be operated the next day after only minor readjustments.

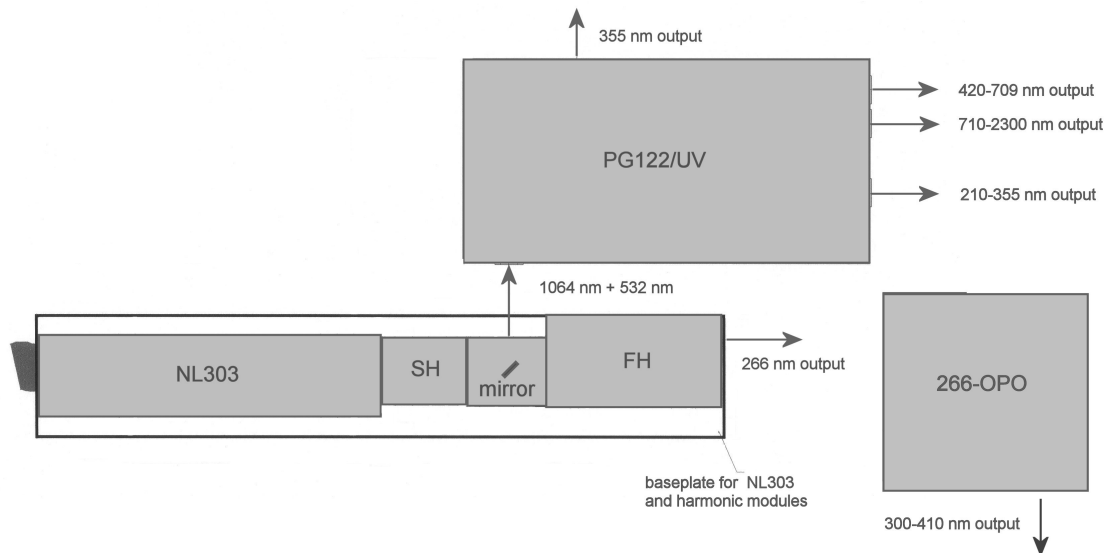


**Figure 5.1:** Arrangement of complete tunable UV laser system: Nd:YAG pump (NL303), second harmonic unit (SH), switch mirror to fourth harmonic unit (FH) and 266 nm pumped OPO or to the 355 nm pumped OPO (PG122/UV) with internal third harmonic unit and UV module.

The common pump source NL303G, Ekspla, Lithuania, for the two units is a Nd:YAG laser with a Gaussian beam profile working at 1 to 10 Hz. For use with the constructed 266nm-OPO (see Chap. 4), it is equipped with a second (SHG) and fourth (FHG) harmonic unit. Optimized for maximal fourth harmonic output power, up to 160 mJ per 4.4 nm pulse are delivered at 266 nm. Optional pumping of the 355nm-OPO is achieved by a switching unit situated between the SHG and FHG module (second and fourth harmonic generation module). An adjustable fold-away mirror (HR532+1064 nm) allows redirection of the second harmonic beam into the commercial 355nm-OPO (PG122/UV, Ekspla, Lithuania), which is equipped with internal third harmonic frequency conversion. The visible signal output of this OPO is then again converted to ultraviolet radiation by second harmonic generation. The optical layout of the 355nm-OPO unit is shown in Fig. 5.3. All participating wavelengths are accessible for experiments as the system provides separate exits for 355 nm, OPO signal (VIS), OPO idler (IR) and frequency doubled OPO signal beams. Wavelength selection is motorized and remote-controlled. The signal is filtered from remaining visible light by a 0.5 mm thin UG11 filter (Schott, Germany) and focused on a fiber using a  $f=60$  mm fused silica plano-convex lens.

For pumping of the 266nm-OPO, the 8 mm diameter beam is condensed to about 4 mm

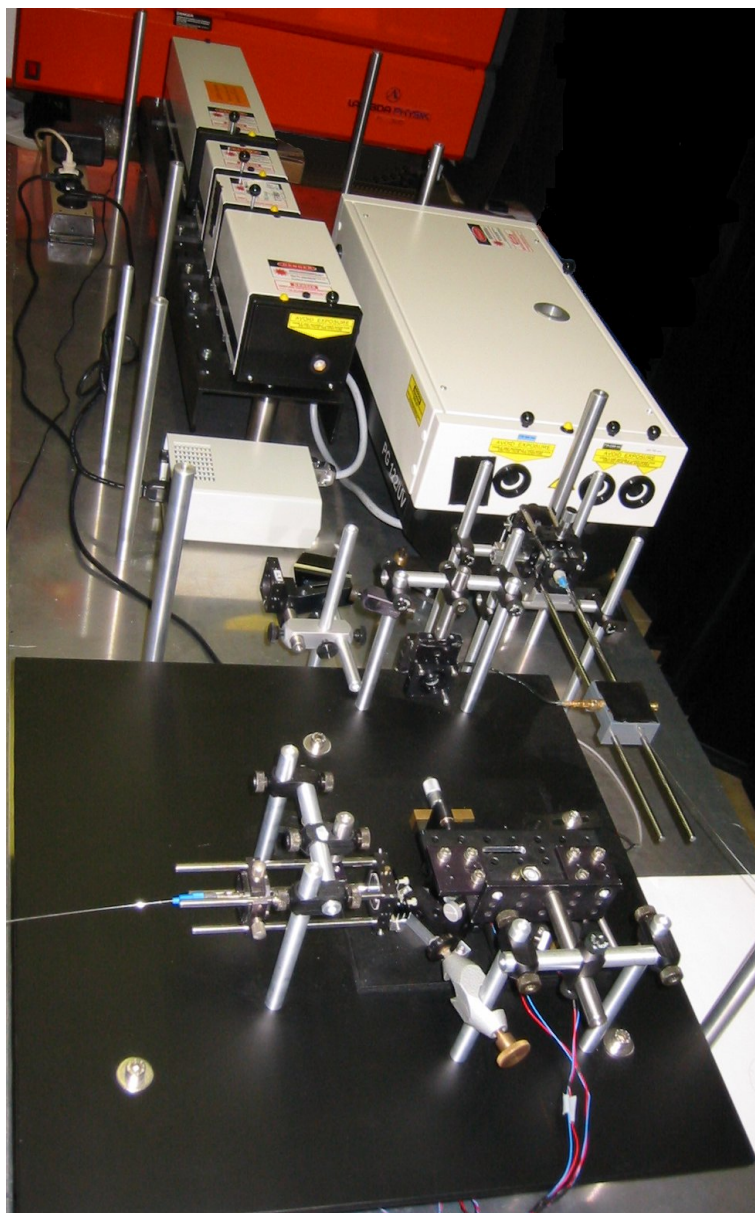


**Figure 5.2:** Picture of the complete UV laser system including fiber couplings and energy monitor (see Sec. 5.2.2). The white four component system at the back is the pump source (NL303G; long, back) and the units for SHG, redirection, and FHG (front). The larger box to the right is the 355nm-OPO (PG122/UV) and the black open structure at the front is the 266nm-OPO.

diameter by a Galilean telescope. Pump source and 266nm-OPO are in linear alignment. The tunable OPO signal leaves the resonator rectangular to the 266 nm pump beam. Remaining UVC pump radiation is filtered by DUG-11(x), a UV-bandpass filter by Schott, Germany. The signal beam is smoothly focused into the fiber by a plano convex lens ( $f=100$  mm) (see Fig. 5.2 and Chap. 4).

So, optoacoustic measurements over the whole terrestrial ultraviolet range are possible with this system. As minor readjustment of the switch mirror is necessary after turning it

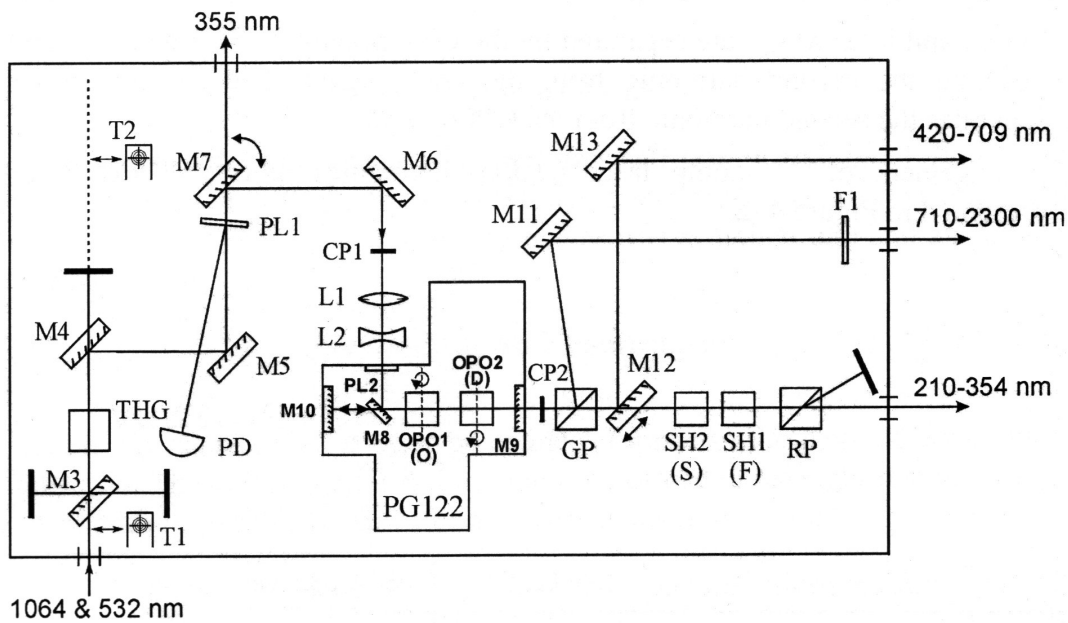


**Figure 5.3:** Optical layout of the 355 nm pumped commercial OPO system [22].

up for redirection into the 355-OPO unit, it is tempting to split measurements accordingly. Such a procedure also ensures comparability between results from different subjects. As the two UV units have different outputs, the optical fiber leading the UV light to the sample has also to be switched from the output fiber coupling of one unit to the other. Both small changes in the experimental setup might entail minor deviations in the experimental conditions from one subject to the other as the initial state of the experiment might not be exactly reestablished from switch to switch. However, if favored, a full terrestrial UV scan is of course possible with only a few extra minutes of adjustment time.

Signal radiation is coupled into a UV enhanced fiber (FVA8008801100, Optronis, Germany) with  $NA=0.22$  and  $800 \mu\text{m}$  core diameter.

The pulse energy of each single pulse is monitored by a photodiode measuring the stray light from the fiber (for details see Sec. 5.2.2 and [46]). In Fig. 5.2, it can be seen as the grey box through which the fiber from the PG122/UV is lead.

## 5.2 Capturing optoacoustic transients from human skin

Apart from a convenient light source, the coordination of the optical and the acoustic part of the experimental setup is a central aspect in optoacoustics. This includes the optoacoustic sensor head itself as well as the signal processing and collection of all relevant data for each single measurement such as assignment of the actual pulse energy.

### 5.2.1 The optoacoustic detector

A basic design of an optoacoustic sensor head for UV optoacoustics on human skin was already presented in [48]. During the dissertation project, the design was optimized for study subjects.

The optoacoustic detector is composed of a Polyvinylidene fluoride (PVDF) block guiding the optical fiber, a PVDF-pressure sensor glued to the block by methanol-diluted two-component adhesive and shielded by customary tinfoil, and a 3 mm thick PVDF spacer disk. As the optical fiber illuminates the sample not normally but at a tilt angle of  $18^\circ$ , the pressure sensor can be placed directly next to the fiber outlet to be situated centrally above the illuminated area. The spacer disk has an about 4 mm long oval hole, which is filled with UV transparent ultrasound gel to allow unhampered transmission of both ultraviolet light and the ultrasound transient. The principle of this design is illustrated in Fig. 5.4.

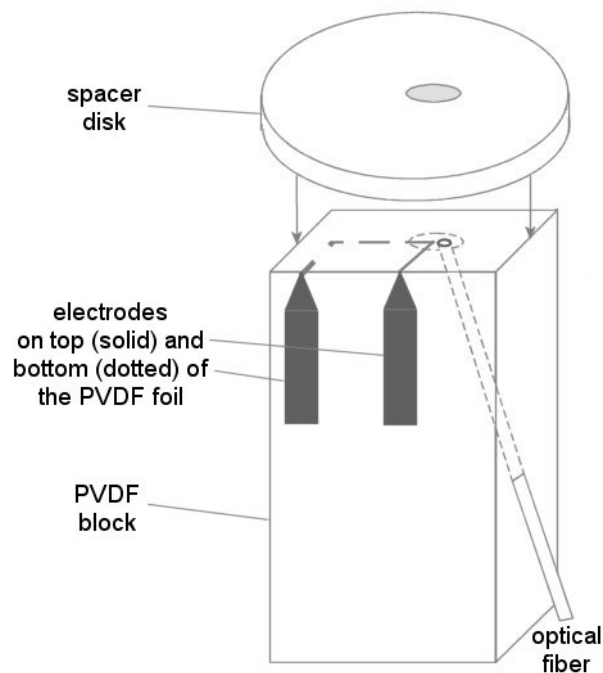


**Figure 5.4:** Sketch of the optoacoustic detector. The optical fiber is guided through the PVDF block. The active area of the detector (crossing of electrodes) is placed close to the outlet of the optical fiber. The dotted electrode is at the bottom side of the (not shown) PVDF foil - the solid line marks the electrode on top. The tinfoil shielding is left out in this sketch for clarity reasons. For better insight, the spacer disk normally directly glued on the tinfoil shielding is shown separated from the detector block here. The dotted ellipse at the top of the detector marks the area where the hole in the spacer is placed.

The ultrasound gel has to meet quite a lot of essential requirements: it has to be UV transparent and stable; it must not contain air bubbles which would severely perturb not only

the acoustic wave but also distort illumination; and its viscosity should allow injection into the ultrasound chamber. The latter is especially important in application. USG is directly injected to the bottom of the USG chamber through a duct omitted at the underside of the spacer disk. In this way, bubbles or contamination can be pressed out of the chamber and removed at the surface. Sonoglide UP (Ultra Pure) Grade 20 (Sonotech Inc., Bellingham, USA) was found to meet these requirements best, even though this gel caused some inconvenience because of its stickiness. Originally designed for non-destructive material testing, it has very good UV transparency, produced to contain no microbubbles and still is acoustically well matched to the properties of skin: the longitudinal velocity of sound is  $1530 \frac{m}{s}$  at an impedance of 0.155 [59].

As the spacer disk is in direct contact with the sample, it was designed with a rather large area of about  $3 \text{ cm}^2$  and smooth edges to avoid irritation of the subject's skin. To minimize impression of soft tissue or samples, the hole was designed as an oval just large enough not to constrict illumination or cause boundary effects to the ultrasonic transient. The actual pressure sensor is a  $9 \mu\text{m}$  thin PVDF film. This thickness was chosen not to limit the depths resolution of the optoacoustic measurements. The Al-coating of this piezoelectric material was etched to form contact electrodes overlapping in only a very small ( $< 0.25 \text{ mm}^2$ ) rectangular area. This small capacitor forms the active area for pressure transient detection. Etching masks of the detector films were drawn by hand. Thus, small differences might occur from film to film. These should however not affect the recorded signal significantly as long as the active area is small compared to the illuminated area on the sample and consequently to the plane area of the incident pressure transient. Connection between film and transducer was achieved by small clamps. Theoretically, the resistance of these contacts could also differ due to surface conditions of the clamps for example. To minimize this effect, clamps were gilded and polished.

Requirements for the transducer include wide-band (2-200 MHz) sensitivity and good linearity for the amplification throughout this wide frequency band. Details on the transducer setup are given in [46].

To definitively ensure comparability of the subjects' data, the same detector was used throughout the subject study.

### 5.2.2 Signal processing and automated operation

Signal processing includes synchronized record of all available data as well as their analysis by simulation. The necessary programs and energy monitor, which will be briefly presented in this section, were developed by Ronald Krebs and are described in detail in his doctoral thesis [46]. His simulation program for optoacoustic transients in this special experimental environment is based on the theoretical expressions developed in Chap. 2 of the thesis at hand.

### **energy monitor**

To analyze optoacoustic transients, the energy of the pulse inducing the pressure has to be known. As the output power of the UV laser system would be close to the limit of clear transient induction at some wavelengths, an intensity sparing approach towards pulse energy measurement was to be followed. A small device was developed recording the energy of each pulse by the stray light from the fiber. Close to the input, the fiber was lead through a light shielded box, where it was bent lightly and well-defined towards a sensitive photodiode. Before optoacoustic measurements, this energy monitor was calibrated by the synchronized recording of photodiode peak voltage and pulse energy at the fiber end. Pulse energy was measured with DUO energy monitor (Gentec-EO Inc. with ED-100AUV V5 sensor head) at the normal sample location, i.e. at the spacer disk and through the ultrasound gel. This calibration was then applied during measurements to calculate the correct pulse energy for each single measurement and assign it to the respective optoacoustic transient.

### **automated measurement protocol**

A fast data acquisition card (Acqiris AP 240) was used for recording of the optoacoustic signal. The energy monitor readout was done by Acquitek DAC card (CH 3140). Both cards were synchronized for reliable pulse energy assignment to each optoacoustic transient.

For the subjects' convenience, UV dosis and experimental time was to be minimized as much as possible. On the other hand, the data obtained from the subject study should allow a reasonable evaluation of the potential of optoacoustics for UV investigations of human skin. As a compromise between these two demands, a large amount of data was to be accumulated in a short time and be coped with appropriately. A short anticipation of the design of the subject study (see also Secs. 7.3 and 8.3) can illustrate the expected amount of data: 20 subjects were measured at 9 different sites/times (volar/dorsal aspect of forearm, thenar, two sunscreens, volar aspect 72h after irradiation with 1 MED, and the respective controls). For each of these 9 investigations, 3 spectra (wavelength scans) were measured optoacoustically covering the range from 290-341 nm in 3 nm steps (18 single measurements). Accordingly ca. 500 single optoacoustic measurements had to be recorded and analyzed accumulating to a total of almost 10,000. Obviously, the amount of time needed for both the measurement and the analysis had to be kept within a reasonable limit by extensive automatization.

The greatest potential for optimization of measurement time was in connection with wavelength selection and pulse release within one wavelength scan. So, a control program was developed allowing choice of overall scan wavelength range, scan stepsize, number of repetitions, as well as partly automated file naming and storage in a customizable database.

Following this experimental input, the program signals the desired wavelength of the first measurement to the motorized OPO system, releases one radiation pulse, reads out and stores the pressure and energy data, controls measurement quality and repeats single measurements if necessary, and then moves on to the next step of the experimental schedule. Measurements are repeated for example if the background offset at the diode could not be determined properly [N.B.] (i.e. peak voltage appeared too early and there was not a sufficient amount of data points for background determination in the stored file), or if the applied energy was too low for an acceptable signal to noise ratio [L.P.]. Finally, quality assessment and pulse energy of the complete wavelength scan are documented in a corresponding log file. Together with the corresponding optoacoustic data files, this log file is called a dataset and this is later utilized in the simulation program for analysis of the data.

### **signal simulation - analysis procedure**

Our first idea for analysis/simulation of the optoacoustic data was to take the theoretical curves as developed in Chap. 2, include the frequency response of the transducer and smooth the data to exclude high frequency noise components. Unfortunately, this simple approach could not be followed in this case, as the setup most sensitive to the optoacoustic signals displayed an unwanted, system inherent, interfering signal with a central frequency just in the range of the optoacoustic signal frequencies. So, an alternative approach had to be followed. To analyze the optoacoustic data and to extract the absorption coefficients, a two step analysis procedure was developed: finding a general noise/corruption function from the data of samples with known optical properties and then applying it to analyze unknown datasets.

First, reference samples of known homogeneous optical properties were analyzed. These reference samples (see also Sec. 7.1 and Sec. 8.1) were measured before and after the subject's optoacoustic measurements. The simulation program is given the theoretical spectrum of the absorption coefficients of the reference samples. For each measurement, a Fourier transformation is applied to signal data and theoretical curve, a deconvolution of the theoretical optoacoustic signal of the sample from the measured signal is carried out in order to separate optoacoustic information from noise and corruption. The remaining 'foil-function' should represent the influence of the setup in the frequency domain and should be free from information about the optical properties. Ideally, all foil functions generated in this way should be very similar. Differences can arise from mistakes in the 'facts' that were set as preconditions for the theoretical optoacoustic signal (energy per pulse, absorption coefficient of the sample, etc.) or from varying acoustic contact between sample and detector - a detrimental influence which may again occur in the subject measurements.

To extract the optical properties from the optoacoustic data of the subjects, a 'master' foil function and a theoretical optoacoustic signal are recombined by convolution in the



frequency domain. Such a master foil function usually is an average function of a certain set of foil functions - e.g. all foil functions derived from measurements before and after a certain subject or all foil functions of a certain day, etc. The absorption coefficient for the theoretical curve is adjusted until the combined simulated curve fits the (smoothed) measured data as well as possible.

Analysis of several datasets in this way showed that the process could be automated. The first negative peak of a measured optoacoustic signal is a pure noise peak and does not contain any optoacoustic information. The most important feature of the optoacoustic signal is the main positive peak. It generally shows a relatively good signal to noise ratio and is hardly corrupted. The second negative peak is a combination of signal diffraction and noise. The influence of the noise is stronger in this negative peak as compared to the central positive peak. Besides, manual analysis and comparison of the data from optically homogeneous reference samples and the subject data showed that assuming one optically homogeneous absorbing layer for the subject measurements allowed finding simulated transients matching the measured data within the noise level at the significant data sections. So, it was decided to assume one layer with homogeneous optical properties for the automated simulation routine for saving computing time. For manual analysis, three layers can be varied in optical properties and thickness. It should be pointed out however, that the simulation program is capable of using any distribution for the absorption coefficient.

Apart from that, in some measurements, a low frequency background noise or offset appeared which also had to be included in data analysis.

So, the following automated analysis procedure was chosen:

- The log-file of a chosen dataset and a master foil function is loaded. The master foil function is derived from the foil functions available for the respective day.
- The first measured optoacoustic signal of the dataset is loaded, actual pulse energy is transferred to the simulation programme, low frequency background noise or offset of the measured signal are removed by filtering of components with frequencies below 150 kHz, and the signal is smoothed over 20 datapoints.
- A simulated optoacoustic curve is calculated and compared to the measured data by the peak values of their positive maxima yielding a difference value in per cent. The initial default value for the absorption coefficient is  $100 \text{ cm}^{-1}$ . Later iteration is done using the value used in the previous simulation.
- The absorption coefficient is adjusted according to the difference value. If the difference is greater than 100 %, the coefficient is doubled or halved respectively to avoid negative absorption coefficients. If the absolute value of the difference percentage does not halve from step to step, the absorption coefficient is adjusted by twice the difference percentage. An adjusted simulation is calculated and compared with the data again.

- This procedure is iterated until the absolute difference percentage is less than 1 % or until 10 iterations are accomplished. In either case, the final absorption coefficient as well as the final difference percentage for the measurement is documented in a results (.rsl) file
- The program proceeds to the next data file in the data set or loads a new log-file if a wavelength scan has been analyzed successfully. A list of data sets (log-files) to be processed can be given to the program.

Figs. 5.5-5.7 show a series of snapshots of the simulation process computed with the TranSim (v1.3.1) software. Here, a mel100 reference sample is simulated using an average of all foil-functions calculated with this data set. This set consists of a 1 nm stepsize scan with 3 measurements at each wavelength (156 valid data files).

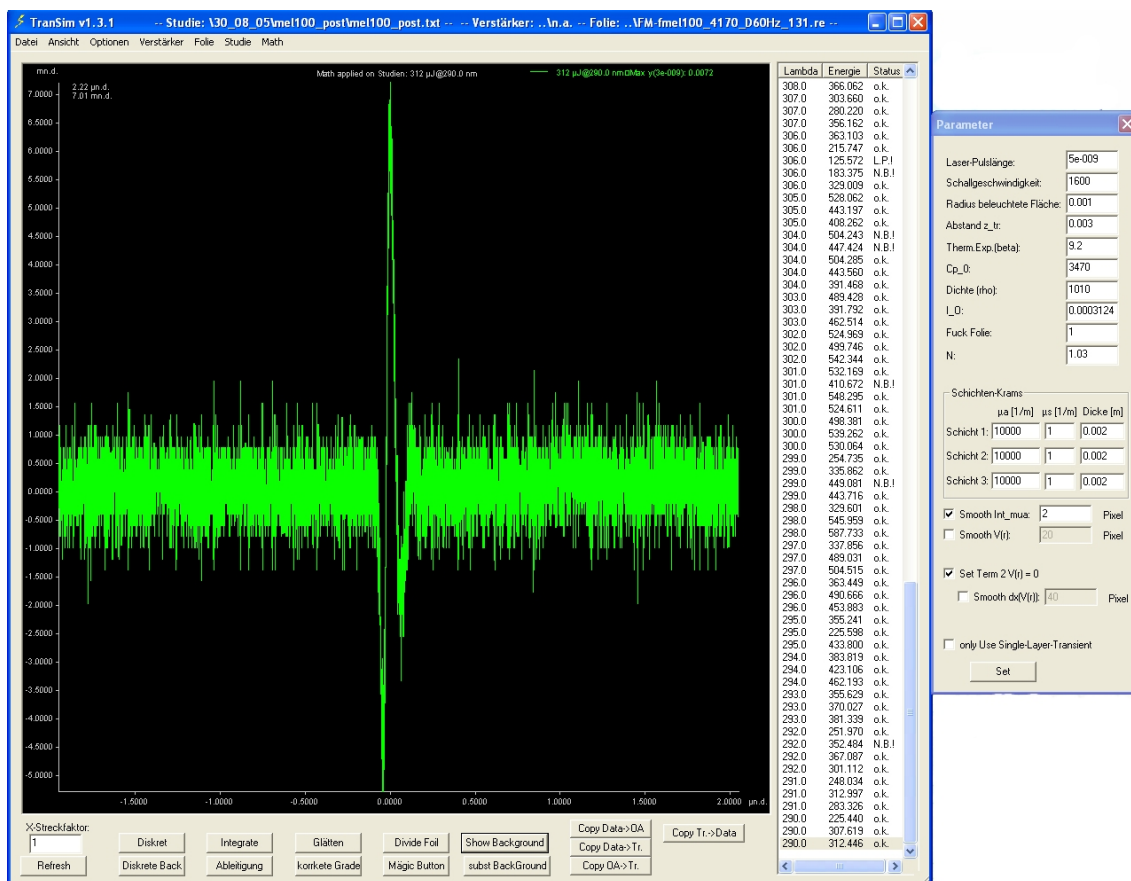


**Figure 5.5:** A (raw) data file is loaded. The column on the right hand side of the simulation window displays the log-file information of this data set. The loaded data file is marked. The 'Parameter' window shows the values of each significant optoacoustic parameter. Note that the actual pulse energy ( $I_0$ ) of this measurement is adopted from the log file.

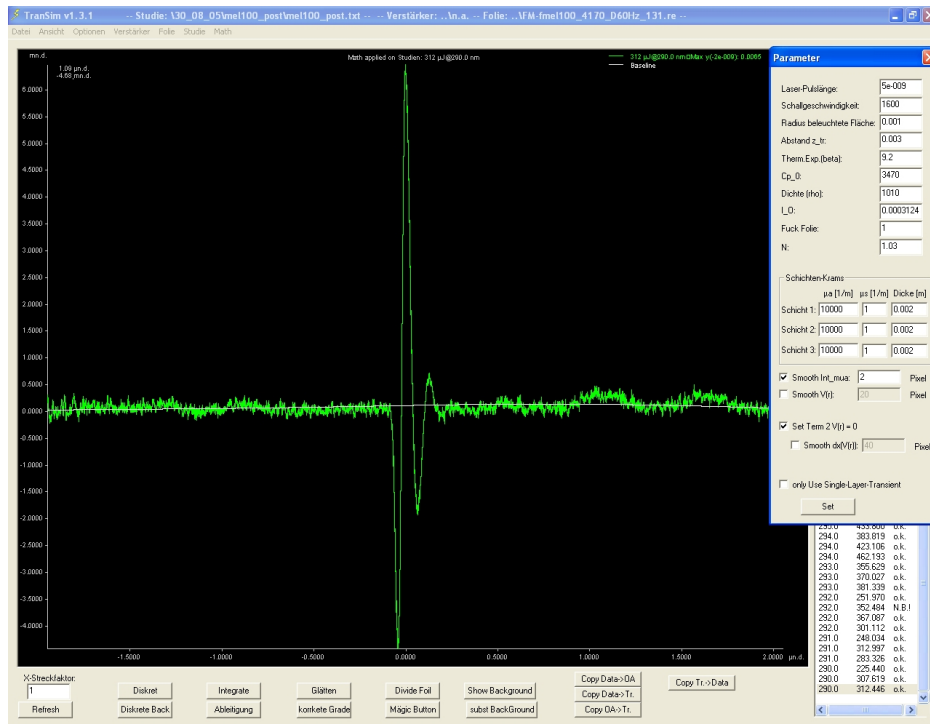


**Figure 5.6:** The optoacoustic data is smoothed over 20 points. A background function is determined using frequencies below 150 kHz and shown as a white line.

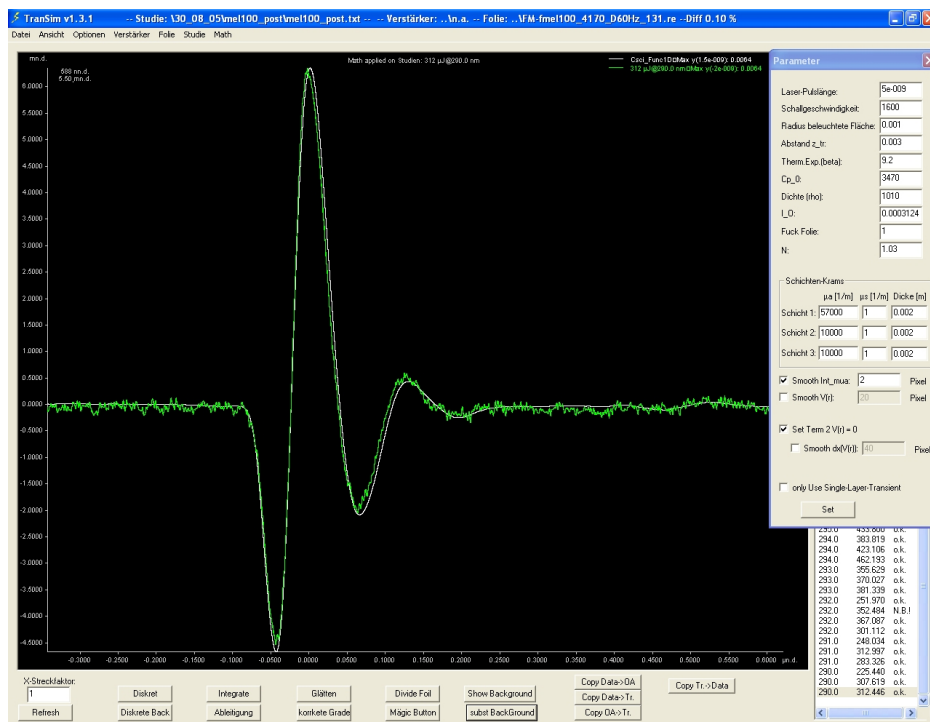


**Figure 5.7:** Scaled up section of the original data and its corresponding simulated transient (white) at the final iteration of the simulation process. Note the actual absorption coefficient of this sample - as found by the simulation - in the Parameter panel and that the difference percentage between the two is displayed in the right corner of the header.



# **6 Classification and documentation of human skin**

Skin types of subjects were classified by the cooperation partner DermaTronnier/Institut für experimentelle Dermatologie of the Universität Witten/Herdecke. UV irradiation to induce minimal erythema as well as documentation of skin physiology and skin color were carried out with standard systems available at DermaTronnier which are briefly described in the following sections.

## **6.1 UV exposition**

For the subject study, individual minimal erythema dose (MED) was determined by irradiation with a solar simulator (M.U.T. GmbH, Germany) according to the COLIPA/CIE norm for sunscreen testing (see Fig. 6.1). The system irradiates spots of 8 mm diameter. For the experiments, two starting doses were chosen by DermaTronnier according to their experience with the subjects. MED was determined by chromameter measurements (see Sec. 6.2.4). If necessary, irradiation was repeated at lower or higher doses.

## **6.2 Documentation of skin physiology**

### **6.2.1 DigiCam**

In order to record the subjects' phototype impression as revealed by a first look as well as to document the optoacoustic measurement sites, the arms of all subjects were photographed by a Canon digital IXUS V2 (2 Megapixels). These pictures are documented in B.1.



**Figure 6.1:** Solar simulator by M.U.T. as used in the experiments [49].

## 6.2.2 SELS

SELS (surface evaluation of living skin) is a special skin camera developed by Derma-Tronnier for assessment of skin structure, roughness, etc.. In the subject study, this system was used especially to document the erythema and pigmentation spots induced by the optoacoustic measurements. The size of the UV irradiated spot can be read from the pictures in those cases, where a defined pigmentation spot develops. Figs. 6.2 and 6.3 illustrate the system. SELS pictures are documented in B.2.



**Figure 6.2:** Evaluating a coffee mug.

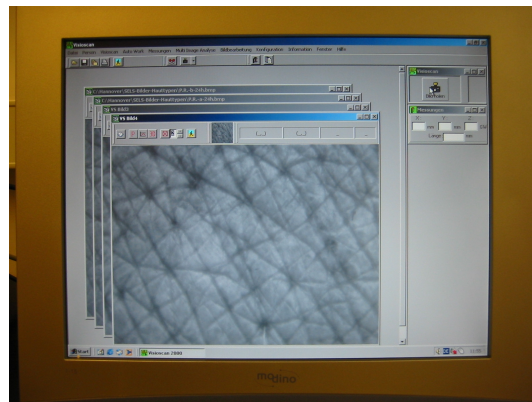


**Figure 6.3:** Evaluating a skin's surface.

### 6.2.3 Fotofinder

The FotoFinder MediCam by Techscreen, Germany is an imaging system optimized for dermatologic investigations. Colour pictures of a subject's skin can be taken with different standard lighting conditions and an up to 50x magnification. Overview and magnified pictures of optoacoustic (erythema) spots were taken from each subject. Documentation can be found in B.3.



**Figure 6.4:** The FotoFinder MediCam with microscope attachment.

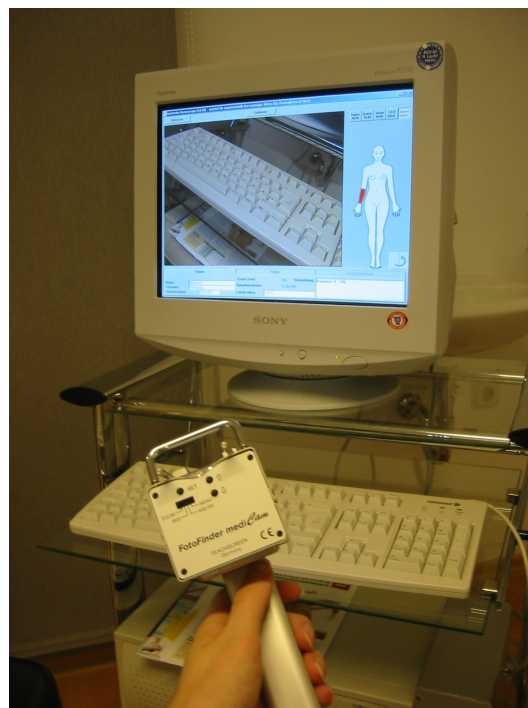


**Figure 6.5:** Picturing a keyboard with the FotoFinder skin camera.

### 6.2.4 Chromameter

Skin colour was assessed by measuring  $L^*$ -,  $a^*$ - and  $b^*$ - values with a Minolta Chromameter CR200.  $L^*$  indicates light intensity and is related to the luminous reflectance (quantity of reflected light weighted with the spectral response of the human eye) and takes values from 0 (black) to 100 (white).  $a^*$  indicates the color of the object on a scale that goes from green (negative values) to red (positive values) and  $b^*$  indicates the color of the object on a scale that goes from blue (negative values) to yellow (positive values). Axes  $a^*$  and  $b^*$  cross the  $L^*$  axis at their zero values. In the study of skin color only the positive sides of the  $a^*$  and  $b^*$  parameters are considered (i.e. red and yellow).

MED determination was done according to the COLIPA recommendation as an increase of the redness parameter  $\Delta a^* = 2.5$ .  $L^*$ - (lightness) and  $b^*$ - (yellow) values were



**Figure 6.6:** Minolta Chromameter.

additionally used for documentation of skin pigmentation. The individual typology angle (ITA) or alpha characteristic angle has been proposed for this purpose.

$$ITA = \arctg \left( \frac{L^* - 50}{b^*} \right) * \frac{180^\circ}{\pi}.$$

ITA<sup>°</sup> values are inversely related to skin pigmentation, i.e. UV induced pigmentation decreases the measured ITA<sup>°</sup> values [60]. It is even proposed that ITA<sup>°</sup> values can serve to predict MED values under certain conditions (see e.g. [28]).



## **7 Under investigation - tissue phantoms, in vitro skin and human skin in vivo**

Various samples were investigated during the UV optoacoustic project covering the whole spectrum from inanimate tissue phantoms over in vitro models to real in vivo human skin. Tissue phantoms were primarily needed to validate the feasibility of the method. They also acquired a more practical use as reference samples for the in vivo measurements.

Epidermal models were studied in preparation for in vivo investigations. Being comparable to in vivo human epidermis but lacking the dermal substratum, the optoacoustic signals of these samples provided material for first estimations of UV penetration depths in vivo and consequently a vague idea of the depths from which optoacoustic signals were to be expected at an outmost estimate.

Finally, in vivo human skin of various UV sensitivities, pigmentations, or thickness of the stratum corneum was investigated in a subject study on 20 volunteers as well as the influence of sunscreen.

### **7.1 PVA-tissue phantoms - a standard for in vivo measurements**

For validation of the method, it is necessary to find some kind of standard sample with known properties simulating the relevant properties of the target sample. Soft tissue phantoms can be created from a lot of different materials such as silicone or gelatine, depending on which properties are desired. For use as an optoacoustic skin phantom for UV investigations, it should not only resemble the acoustic properties of skin but also show as little UV absorption and scattering of its own as possible. The latter is important in order to allow rather free manipulation of the optical properties of the sample - e.g. for creating a purely absorbing/non-scattering tissue phantom. Besides, the tissue material should keep its properties for some time to allow comparative measurements.

In [41] Poly(vinyl alcohol) (PVA) hydrogel is suggested as an appropriate phantom material for optoacoustics. Freezing and defreezing of an aqueous solution of PVA results in physical cross-linking by hydrogen bonding between the hydroxyl groups on the PVA chains of this polymer. The mechanical strength progressively increases with the number of freezing-thawing cycles. However, this rigidification is accompanied by increasing turbidity. When refrigerated, large pores are formed due to the accompanying large volume expansion of the water. This results in refractive index fluctuations causing the turbidity. This effect can be avoided by mixing the aqueous PVA solution with a freezing inhibitor. Optical properties can be adjusted by addition of scattering or absorbing particles. According to [41], such clear samples display relevant acoustic properties close to those of skin (see Table 7.1).

sample	density $\rho$ [ $10^3 \text{ kg m}^{-3}$ ]	sound velocity $c_s$ [ $\text{m s}^{-1}$ ]	impedance $z$ [ $10^6 \text{ kg m}^{-2} \text{ s}^{-1}$ ]	attenuation $\alpha$ [ $\text{dB cm}^{-1}$ ]
PVA	$1.07 \pm 0.02$	$1.58 \pm 0.03$	$1.712 \pm 0.064$	$0.62 \pm 0.03$
skin <sup>(1)</sup> /tissue	$1.01^{(1)}$	$1.58^{(1)}$	1.425-1.685	0.5-1.1

**Table 7.1:** Average acoustic properties of clear PVA samples [41] compared to data for human skin or soft tissue collected in [20]

Thus, partly following the procedure described in [41], skin phantoms were prepared dissolving PVA (Poly(vinyl alcohol) 99+% hydrolyzed, Sigma) in a 80:20 mixture of Dimethylsulfoxide (DMSO) and demineralized water to obtain a PVA solution of 15% concentration by weight. To imitate the optical properties of human skin in the ultraviolet range, melanin was added to the solution, resulting in a highly absorbing and weakly scattering sample. Gently stirred, the mixture was heated and maintained in a boiling water bath for 2 h. The solution is poured in appropriate containers and allowed to stand for a while, to allow the air bubbles that may have been trapped to migrate to the surface. Then, the gel is refrigerated at  $-20 \text{ }^\circ\text{C}$  for 24 h. The resulting rigid gel samples are then immersed in water to remove the organic solvent and to yield the PVA hydrogels. Some amount of the dye is usually washed out during immersion. Optical properties of thin slices ( $75\text{-}400 \mu\text{m}$ ) of the samples - cut in a Leica VT 1000S vibratome - are determined in a photospectrometer.

## 7.2 Epidermal models

In the context of the biological diploma work by Myriam Bartels [9], commercial in vitro epidermal models were studied. These reconstituted human (tanned) epidermis are a keratinocyte matrix into which melanocytes of different photo types are embedded. Models with melanocytes of type IV and VI as well as without any melanocytes were purchased from SkinEthic (SkinEthic Tissue Culture Laboratories, Nice, France). The

structure of these air lifted models is histologically similar to in vivo human epidermis and features a functional permeability barrier after an incubation time of less than three weeks (see Fig. 7.1). After this time, melanocyte seeded epidermis has also gained the phototype specific native tan.

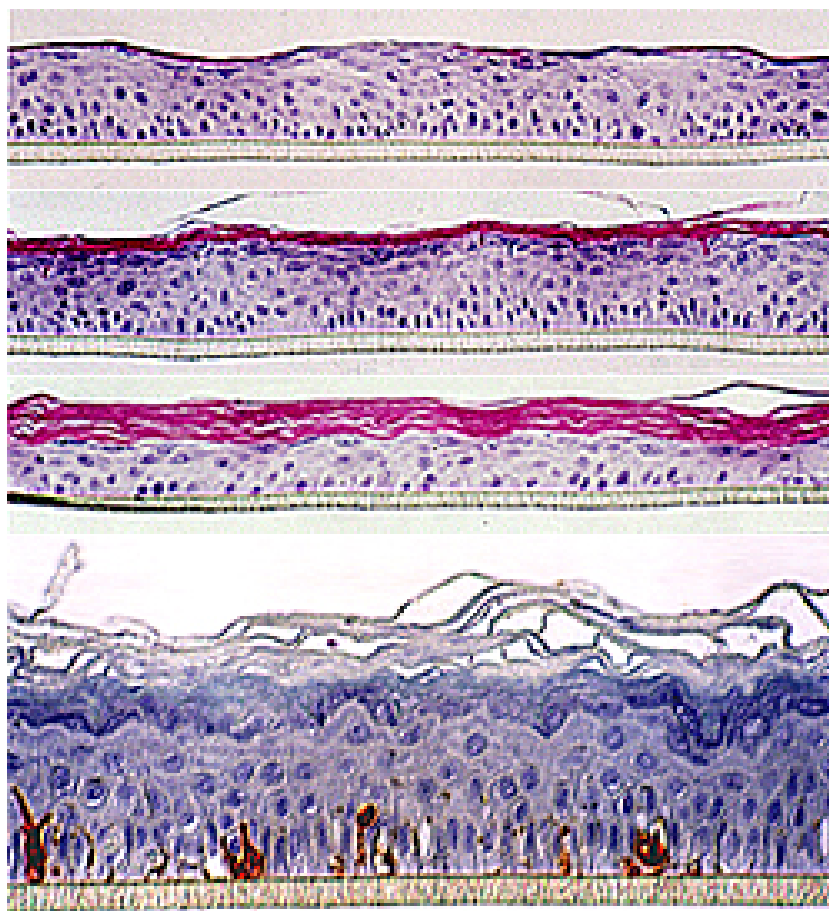


**Figure 7.1:** Growth kinetics of SkinEthic epidermal models during regular incubation time. Top to bottom: histology on day 6, 12, 20 and HMB5 staining revealing the melanocytes in the basal layer. [57]

### 7.3 Study subjects - human skin in vivo

To test and prove the applicability of optoacoustics to illuminate questions concerning the interaction of ultraviolet radiation and human skin in vivo was the aim of all endeavors. Fundamental questions such as in vivo measurement of absorption coefficients in the UV were concerned as well as application oriented questions such as sunscreen testing in vivo. A study on twenty subjects was conducted to allow reasonable assessment.

For UV sensitivity and phototype assessment, twenty subjects were chosen by DermaTronnier to cover the whole range of Caucasian photo types (I-IV). There are several methods to classify subjects according to their (predicted) UV-sensitivity: Fitzgerald suggested a survey-based classification into six phototypes (see e.g. [24], [7] and references therein) which is widely followed in dermatology. The individual typological angle (ITA) from luminance  $L^*$ - and yellow  $b^*$ -values of chromameter measurements should predict the phototype based on experimental data [28].  $ITA^\circ$  is calculated as

$$ITA^\circ = \text{ArcTan} \left( \frac{L^* - 50}{b^*} \right) \frac{180^\circ}{\pi}$$

The calculated  $ITA^\circ$  relates to the Fitzpatrick skin type classifications by categorizing the resulting angles into Type I (Very Light)  $56^\circ - 90^\circ$ , II (Light)  $42^\circ - 55^\circ$ , III (Intermediate)  $29^\circ - 41^\circ$ , IV (Tan)  $11^\circ - 28^\circ$ . As the study was conducted during summer months, a change of phototype from their native/winter type towards the less susceptible end of the scale was expected for some of the subjects.

However, in practice, it is the actual MED value of a particular subject at the particular experimental skin site that is the criterion to which any other assessment method must be geared.

All three approaches were applied in the study to allow comparison. Native and actual skin phototype were assigned by DermaTronnier.  $L^*$  and  $b^*$  values from the volar side of the forearm were charted and evaluated as an additional reference. Last but not least, MED values were determined at the volar side of the forearm. Erythema was induced by an international standard solar simulator and the minimal dose was assessed by an increase of the chromameter  $a^*$ -values (redness) by 2.5 24 h after irradiation. The ultra-violet radiation doses for MED were estimated and chosen according to the experience of DermaTronnier. Two sites at the right volar forearm were irradiated with two different doses on Day 1 of the study. If MED had not been achieved by exposure on Day 1, irradiation was repeated on Day 2 and the remaining schedule was adjourned accordingly. Table 7.3 shows the subject's native and actually adapted phototype, MED values and  $ITA^\circ$ . Obviously, ITA does not allow a good prediction of MED as all applied doses lie in a range of  $200-400 \frac{mJ}{cm^2}$  and the same ITA ( $53^\circ$ ) is measured for a subject with MED of  $200 \frac{mJ}{cm^2}$  (G.O.) as well as for a subject with MED of  $300 \frac{mJ}{cm^2}$  (P.R.). Furthermore, according to ITA values there would be 1 phototype I, 15 type II, 2 type III, and 2 type IV which matches neither the UVR sensitivity as determined by MED measurements nor as evaluated by DermaTronnier according to the Fitzpatrick scale.

For evaluation of native optical properties of human skin of different photo types, optoacoustic measurements were carried out at the volar forearm in vicinity of the irradiated spots, i.e. at a skin site similar in skin physiology and pigmentation.

All subjects displayed a perceivable tan on the dorsal side of the forearm. Pigmentation differences were documented by chromameter  $L^*$ -values (see Table 7.3). Some of the

subject	initials	native/winter phototype	actual summer phototype	MED ( $\frac{mJ}{cm^2}$ )	ITA-phototype
6	G.O.	I	I	200	II (53°)
18	M.M.	I	I	220	I (63°)
9	M.H.	II	II	230	II (47°)
1	L.K.	I	I	240	II (47°)
2	W.K.	I	II	250	II (53°)
7	K.K.	II	II	250	II (46°)
10	Kr.G.	III	II	250	III (41°)
12	E.R.	II	II	250	II (46°)
15	H.M.	II	II	250	II (55°)
19	K.H.	II	II	250	II (53°)
3	K.I.	II	III	250	II (45°)
13	D.C.	I	III	260	II (44°)
14	F.M.	III	III	260	II (55°)
8	S.R.	II	III	270	III (38°)
20	W.M.	III	III	280	II (42°)
11	B.I.	III	IV	300	II (50°)
4	P.R.	IV	IV	300	II (53°)
16	Kn.G.	IV	IV	300	II (45°)
5	L.U.	IV	IV	320	IV (19°)
17	K.B.	IV	IV	400	IV (26°)

**Table 7.2:** Native/winter and actual summer phototypes of the subjects, approximate MED, phototype prediction according to chromameter (ITA°); sorted according to MED

subjects had spent considerable time in the summer sun - be it on a recent holiday or in their garden. These subjects showed a particularly high contrast in pigmentation between the volar and dorsal side of the forearm (see Table 7.3). To investigate signal differences due to pigmentation contrast within the same subject, optoacoustic measurements were carried out on the dorsal side of the forearm. For some male subjects, it was necessary to carefully shave the respective skin site. In all optoacoustic measurements special care was taken not to illuminate and measure hair or hair follicles.

Besides, pigmentation effects were investigated at the one MED sites three days (72 h) after irradiation, i.e. at the peak time of persistent pigment darkening. As MED exceeds MPD in most subjects, the newly formed pigmentation was hardly perceivable in most subjects (see Table 7.3).

The dorsal and volar side of the forearm should differ not only in pigmentation but also in the thickness of the horny layer. On the volar side, skin and stratum corneum are relatively thin. The horny layer differs from the viable part of the epidermis due to a higher concentration of keratin. However, it is improbable that UV optoacoustics is capable of

subject	initials	L*-value, volar, before exposure to 1 MED	L*-value, volar, 72h after 1 MED	L*-value, dorsal side
1	L.K.	65.76	64.04	55.68
2	W.K.	65.78	64.94	53.65
3	K.I.	63.91	60.29	57.84
4	P.R.	68.08	68.06	66.14
5	L.U.	57.15	56.20	50.48
6	G.O.	66.82	64.10	67.59
7	K.K.	62.77	63.70	63.46
8	S.R.	62.48	61.34	63.80
9	M.H.	66.06	60.84	55.99
10	Kr.G.	64.10	61.46	57.55
11	B.I.	65.96	62.96	57.93
12	E.R.	64.62	63.71	59.28
13	D.C.	64.72	64.37	59.24
14	F.M.	66.95	63.94	56.71
15	H.M.	67.54	65.92	60.36
16	Kn.G.	63.31	62.83	55.53
17	K.B.	58.86	56.17	52.29
18	M.M.	70.11	66.73	68.04
19	K.H.	64.65	64.71	59.69
20	W.M.	65.30	61.08	57.16

**Table 7.3:** L\*-values of subjects: native pigmentation and pigmentation induced by 1 MED at volar aspect of the forearm and at the dorsal aspect. High L\*-values indicate light skin /low pigmentation.

differentiating between the stratum corneum and the viable epidermis in this case as the stratum corneum should be approximately ten to thirty  $\mu\text{m}$  thick at these sites while the resolution of optoacoustics is expected to be approximately 20  $\mu\text{m}$  at considerable optical contrast. If the high keratin concentration caused considerably stronger scattering in the surface layer of the epidermis, this could result in a higher fluence in this layer appearing as higher absorption in optoacoustic measurements despite an unchanged absorption coefficient. Recapitulating Secs. 2.2 and 3.2.1 which are dealing with the expected scattering and absorption properties of stratum corneum and its keratin, the optical properties of the stratum corneum will probably still be dominated by absorption - even though it is keratin absorption rather than the melanin absorption dominant in the viable part of the epidermis. At the resolution limit of in vivo optoacoustics however, it is impossible to discriminate between higher absorption caused by a higher subsurface fluence due to (back)scattering and higher absorption caused by a higher absorption coefficient of the subsurface layer.

Therefore, the thenar was chosen as another site for optoacoustic measurements. Here,

at the palm of the hand, the horny layer can be expected to be several hundred  $\mu\text{m}$  thick allowing measurements on 'pure' stratum corneum.

Figure 7.2 illustrates the arrangement of relevant skin sites marked for measurements on Day 1. Labels were placed in comparable positions for all subjects.

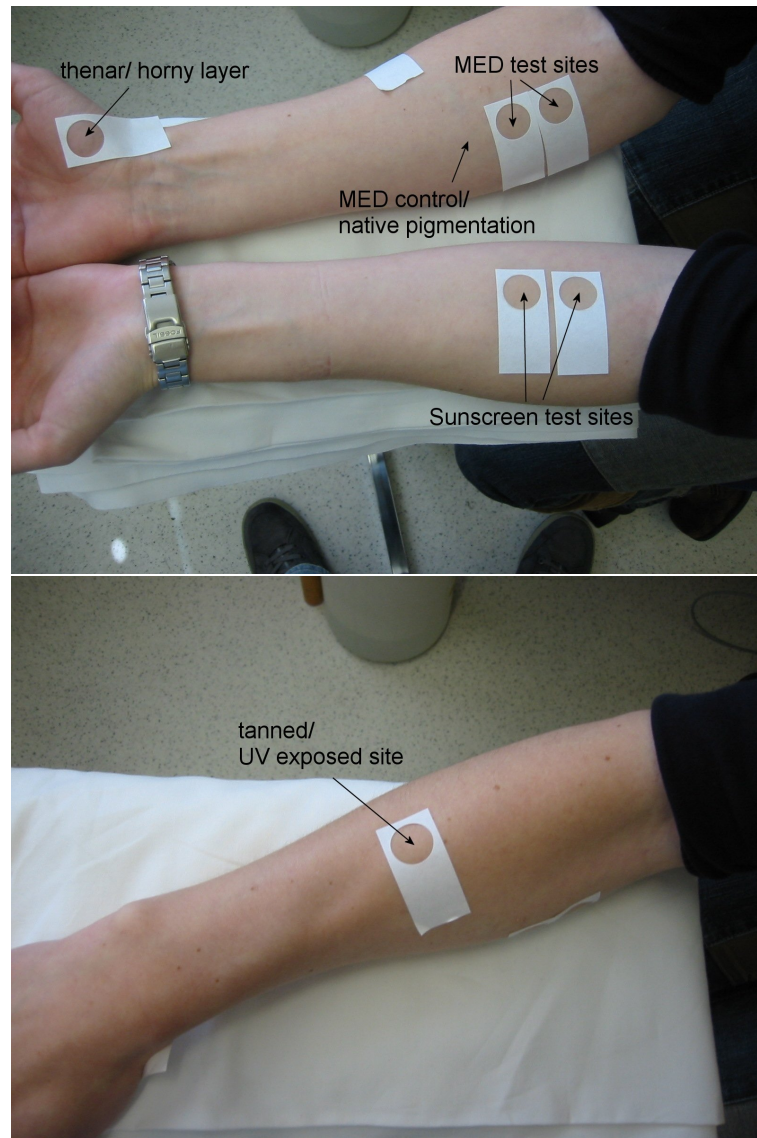


**Figure 7.2:** Skin sites marked for measurements

### 7.3.1 Sun protection lotions

To evaluate optoacoustics as a possible sun screen in vivo testing method, two sun protection lotions were chosen both of which had been tested for their sun protection factor

(SPF) by DermaTronnier in vitro and in vivo.

Sun Gel with SPF 30 by Bio Gen Milchserum Marketing GmbH, Bad Ems, Germany, was rated SPF 32 by in vivo testing in a group of 12 subjects.

Sun Lotion denoted SPF 10 by Börlind, Gesellschaft für kosmetische Erzeugnisse mbH, Calw, Germany, was rated only SPF 7 by in vivo testing in a group of 12 subjects and SPF 7.46 by in vitro testing.

According to COLIPA and FDA recommendations  $2 \frac{\text{mg}}{\text{cm}^2}$  or  $2 \frac{\mu\text{l}}{\text{cm}^2}$  are to be applied to the skin for SPF testing. As the round test fields used in this subject study had a radius of 9 mm, 5.1 mg had to be pipetted on the skin and were evenly spread by a saturated fingerstall.



## 8 Results and Discussion

In this chapter, the results of optoacoustic investigations of optical properties in the ultra-violet range are presented and discussed.

The first section deals with *in vitro* phantoms dyed with melanin. As the optical properties of these reference samples are known, they are used for two purposes: to assess repeatability of the optoacoustic method and to serve as standard samples from which reliable foil functions (necessary to discriminate noise from information, compare Sec. 5.2.2) for the simulation of the *in vivo* data can be deduced.

The second section shows one example of *in vitro* epidermis culture measurements which were investigated more thoroughly in a diploma thesis [9].

The third and largest section deals with the results of the study on 20 subjects conducted in cooperation with the Institut für experimentelle Dermatologie of the Universität Witten/Herdecke (DermaTronnier). It is divided into several subsections each focusing on one aspect in the context of the assessment of UV optoacoustics on human skin *in vivo*.

### 8.1 Tissue phantoms - repeatability of optoacoustic measurements

Poly(vinyl alcohol) (PVA) tissue phantoms (see Sec. 7.1) dyed with melanin served as reference samples for the *in vivo* measurements.

Three samples containing 25 mg/ml (mel25), 53 mg/ml (mel53) and 100 mg/ml (mel100) respectively were used. Absorption coefficients were determined by photospectrometric measurements (see Fig. 8.1). Deviations in the absorption spectra of different slices of the same reference sample probably arise from the cutting procedure. Due to the soft but elastic and tough nature of the tissue phantoms even the vibratome could only cut slices whose thickness might differ a few microns from the setpoint value. As darker samples were cut into thinner slices, this mistake most prominently appears in mel100. Since variations may appear in both directions - pushing back of the sample causing thinner slices and sucking up resulting in thicker slices - choosing an average spectrum is most appropriate.

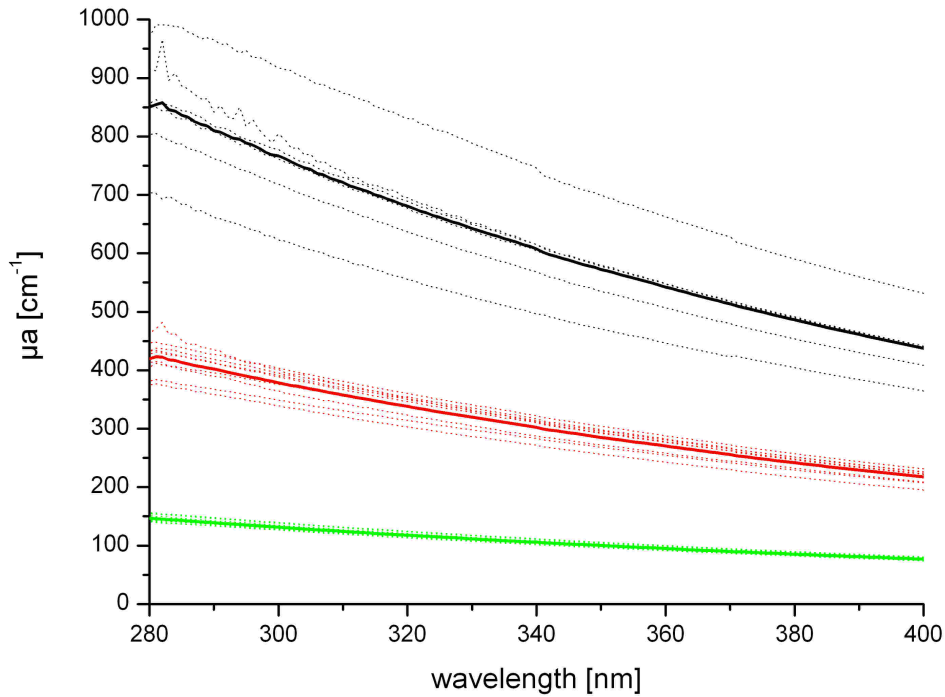


**Figure 8.1:** Absorption spectra of the three reference samples mel25 (bottom/green), mel53 (middle/red), and mel100 (top/black). Single slices: dotted; average spectrum: solid.

An analytic expression for the wavelength dependent absorption properties of each reference type was approximated to their respective average absorption spectrum. According to Jacques [33] (and compare Sec. 3.2.1), the general shape of the melanosome absorption spectrum ( $mua.mel$ ) is approximated as

$$mua.mel = 6.6 * 10^{11} nm^{-3.33} [cm^{-1}].$$

Melanosome absorption as well as the absorption of the PVA samples should be dominated by the chromophore melanin. Using the same mathematical approach, approximations for the three reference samples are

- $mua.mel25 [cm^{-1}] = 4 * 10^6 nm^{-1.82}$
- $mua.mel53 [cm^{-1}] = 2 * 10^7 nm^{-1.89}$
- $mua.mel100 [cm^{-1}] = 4 * 10^7 nm^{-1.91}$

with  $R^2 > 0.998$ . For use in the simulation program, an exponential description of the wavelength dependency of the absorption coefficient was chosen as these expressions fit the experimental data even a little better ( $R^2 > 0.999$ ) and were easier to integrate into the program.

- $\mu_{a,mel25}[cm^{-1}] = 664 * e^{-0,0054\lambda[nm]}$
- $\mu_{a,mel53}[cm^{-1}] = 2035 * e^{-0,0056\lambda[nm]}$
- $\mu_{a,mel100}[cm^{-1}] = 4170 * e^{-0,0057\lambda[nm]}$

The same three PVA samples were measured as references before and/or after the subject's measurements. On the one hand, this should provide quality assessment and assurance - on the other hand, these data were used to separate the optoacoustic signal from noise and corruption due to effects of the experimental setup. The procedure is presented in Sec. 5.2.2 and described in more detail in [46]. In brief, the simulation program is given the theoretical values of the absorption coefficients of the reference samples. For each measurement, the program compares (deconvolutes) the theoretical optoacoustic signal of the sample at the actual wavelength and pulse energy with (from) the measured signal to separate optoacoustic information from noise and corruption. The remaining 'foil-function' should represent the setup influence and should be free of information about the optical properties.

For the reference measurements on the PVA samples, an optoacoustic wavelength scan was carried out with a stepsize of 1-3 nm and 2-3 consecutive measurements at each wavelength. These measurements can be used to assess the **repeatability** of the results for absorption coefficients measured by optoacoustics.

For each measurand, the absolute value of the difference between each pair of measurements was divided by the mean value obtained for the measurand. This ratio  $q_{range}$  shows the range of contributing measurement results with respect to their mean value.

Interestingly, there was a significant difference in  $q_{range}$  between the three samples which is probably due to the different absorption coefficient ranges covered by them:  $q_{range} = (8.7 \pm 3,4)\%$  for mel25,  $q_{range} = (14.0 \pm 4.0)\%$  for mel53, and  $q_{range} = (17.6 \pm 4.1)\%$  for mel100.

One possible explanation is provided by the degree to which stress confinement (see Sec. 2.2) is obeyed. The higher the absorption coefficient of the sample, the worse stress confinement is fulfilled and the less good the theory describes the actual ultrasonic transients as the pulse more and more becomes less dependent on the optical properties but rather following the temporal shape of the laser pulse. For mel25, the stress confinement parameter  $\mu_a c_0 \tau_L$  - which should be  $\ll 1$  - is smaller than 0.1, for mel53 it is smaller than 0.3, and for mel100 it is smaller than 0.6. The poorer the stress confinement, the smaller the changes in the amplitude and slope of the optoacoustic signal become for the same relative change of the absorption coefficient. Consequently, the 1% confidence mark that was set as a stop mark for the iteration process (see again Sec. 5.2.2) fitting the simulated transient to the measured signal allows deviations in the calculated  $\mu_a$  of less than 1% for low absorption coefficients and larger relative deviations for high absorption coefficients. However, as this mark - which refers to the peak voltage amplitude of the signal - was

chosen according to error and signal-to-noise ratio estimations, this effect is probably inevitable. Possibly, the accuracy of the simulation results could be enhanced by setting the value of the confidence mark dynamically according to the actual voltage amplitude and noise as well as to the simulated absorption coefficient. For example, the signal-to-noise ratio is usually better for high peak voltage signals as induced by strongly absorbing samples and/or by high laser pulse energies. However, looking at other error sources such as the energy monitor, which may include deviations of up to 8 %, there might not be enough benefit to compensate for the extra calculation time and effort.

To summarize, the repeatability of the optoacoustic measurements is not yet as satisfactory as desired. Future work should concentrate on minimizing error sources (pulse energy, simulation accuracy, acoustic mismatch e.g. due to bubbles in ultrasound gel, etc.) as well as on even better characterization of the experimental conditions to finetune the theoretical description (determination of the actual energy distribution over the illuminated area, actual temporal shape of the laser pulse etc.) and consequently enhance the simulation quality.

## 8.2 Cell cultures

Epidermal models were investigated applying different spectroscopic techniques in the course of a diploma work [9]. On epidermal models with different or no melanocytes measurements including attenuation spectra, fluorescence measurements and optoacoustic structure characterization were carried out and the effects of repeated UVA irradiation were investigated.

Optoacoustic structure characterization indicated that stratum corneum and the viable part of the epidermis can be differentiated by this method.

Fig. 8.2 shows the optoacoustic signal of an unpigmented epidermal model induced by a 295 nm laser pulse. Three peaks can be identified reaching the detector after about 2, 2.2 and 2.8  $\mu\text{s}$  respectively. The first peak of every optoacoustic signal is induced at the sample surface - accordingly, the peak at 2.2  $\mu\text{s}$  marks the surface of the epidermis, i.e. the horny layer. Each peak corresponds to the beginning of a layer with different optical properties. The thickness of these layers can be calculated from the runtime differences between two peaks. Accordingly, the surface layer is about 20  $\mu\text{m}$  thick and the main layer 90  $\mu\text{m}$ . The last peak is induced at a depth of 110  $\mu\text{m}$  - indicating that it marks the tissue culture dish as 110  $\mu\text{m}$  matches well with the expected thickness of the whole epidermal model.

Optical or acoustic contrast for the optoacoustic measurements on this model may only be induced by water content and keratin concentration as no melanocytes are contained in this model. Both changes from the viable to the dead part of the epidermis. In the absence of melanin absorption, optical contrast in the ultraviolet range is probably mainly

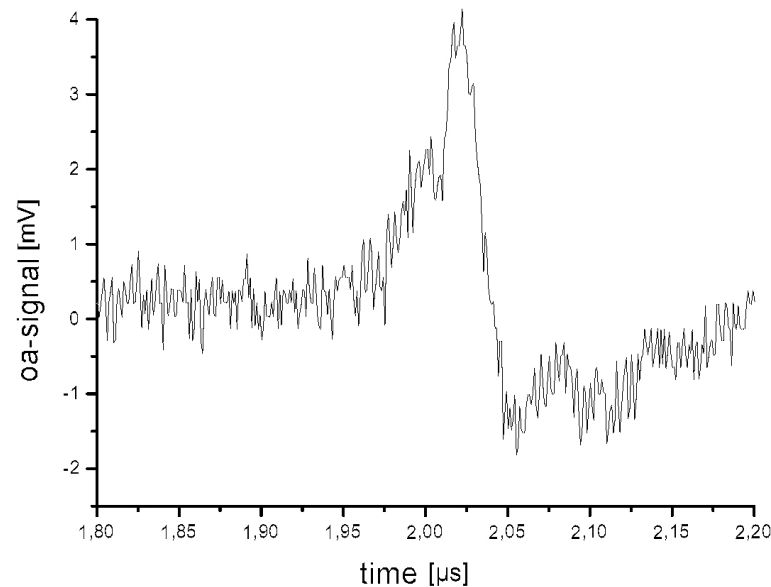


**Figure 8.2:** Optoacoustic signal of an epidermal model without melanocytes. Three peaks can be distinguished, referring to the stratum corneum surface layer, the viable epidermis and the polystyrol tissue culture dish.

due to keratin. Higher keratin concentration is able to increase the peak amplitude of optoacoustic signals by both, a higher fluence due to scattering as well as by an increased absorption coefficient. Apart from that, water concentration is much lower in the stratum corneum than in the viable part of the epidermis. This might lead to a different sound velocity in this layer underscoring the effect of the keratin scattering.

### 8.3 Study subjects - human skin in vivo

As mentioned before, a subject study was prepared, designed, and conducted in the context of this doctoral thesis to allow a first reasonable assessment of the potentials of UV optoacoustics for the investigations of human skin in vivo. From preliminary measurements, it was already clear that due to the lateral inhomogeneity of skin combined with the relatively small area covered by the optoacoustic detector, several optoacoustic measurements in close vicinity had to be averaged to describe one skin site. To minimize strain for the subjects and to optimize reliability of the data, it was thus decided to concentrate measurements on the UVB/UVA-II range.

The subject study was designed to allow answers to the following questions:

- What are the wavelength dependent optical properties of human skin in vivo in the ultraviolet range?
- What is optoacoustics able to tell about the UV sensitivity of individual skin?

- What differences can be found between native/low exposure sites and highly pigmented sites within one individual?
- How does the horny layer affect the optoacoustic signal?
- Is optoacoustics a potential method to assess sun protection factor of sunscreens in vivo?

Additionally, the effect of the optoacoustic measurements on the skin should be documented. For this purpose, SELS and FotoFinder pictures were taken from the erythema spots induced by optoacoustic measurements (refer to Chap. 6 for additional information on the methods and to the Appendix B.2 and B.3 for documentation).

So, in agreement with DermaTronnier, the study was designed as follows (for details and additional information see also Sec. 7.3).

Twenty healthy subjects (14 female, 6 male) were chosen by DermaTronnier covering all Caucasian photo types - Type I: 3 subjects, Type II: 7 subjects, Type III: 5 subjects, Type IV: 5 subjects.

Day 1:	forearm, volar side	- UV irradiation (for MED determination)
	"-", "-"	- optoacoustic measurement (control site)
	"-", dorsal side	- optoacoustic measurement (tanned area)
	thenar	- optoacoustic measurement (thick horny layer)
	forearm, volar side	- sunscreen products (SPF 10 and 30)
	"-", "-"	- oa-measurements: sunscreen test sites and control
	all sites	- chromameter measurements: irradiation/oa-measurement sites (pre-exposure)
Day 2	volar side	- MED determination by chromameter
(24 h later):	"-"	- SELS, Fotofinder: oa-irradiation site (control MED)
Day 3	volar side	- optoacoustic measurement on 1 MED spot
(72 h later):	"-"	- SELS, Fotofinder: oa-irradiation site (control MED)

At least three optoacoustic wavelength scans were carried out at each target area to allow averaging. The detector was displaced some millimeters between scans. Every scan characterizes the respective skin spot in the wavelength range from 290-341 nm, normally in 3 nm steps with one measurement at each wavelength.

The following subsections address the various questions (see above) connected with the assessment of UV optoacoustics for the investigation of human skin.

In the first subsection, the obtained spectra from a low UV exposure site - the volar side of the forearm - are discussed with respect to their reproducibility as well as their correlation to the individual minimal erythema dose (MED) at this site.

The following section is concerned with the differences between the absorption spectra of low and high UV exposure skin sites.

In the third section, the mean absorption spectra obtained at different skin sites of the same person are compared.

This leads to a reevaluation of the absorption spectra in terms of penetration depths which is shown in the fourth section.

The final fifth section is dedicated to the optoacoustic investigations on sunscreen lotions applied to the subject's skin.

### 8.3.1 Native pigmentation - volar forearm

On the volar aspect of the forearm, natural pigmentation is fairly low throughout the year due to relatively low UV exposure. So, this site can be considered to represent the native, i.e. non UV-induced, pigmentation of each subject.

As a major reference, individual MED was determined in this area on the right arm.

For each subject this area was optoacoustically measured on the first day of the study on both arms (control for the solar simulator (MUT) irradiation with 1 MED and control for the sunscreen measurements) and on the right arm it was measured again three days later as a control for the pigmentation 72h after irradiation with one MED (compare Fig. 7.2 for an illustration of the measurement sites).

Additionally, skin colour was documented by chromameter measurements for this site on both arms on Day 1 of the study.

In this section, the optoacoustic results obtained from these low pigmentation control sites are shown, analyzed, and discussed.

First, Figs. 8.3 to 8.22 show the spectra of the optoacoustically measured absorption coefficients and their standard deviation as primary reference for the subsequent analysis. The different sites are denoted as follows: control for one MED irradiation by a solar simulator (MUT) on the right arm on Day1: "control\_MUT\_mean"; control for sunscreen test sites on the left arm: "control\_SunScreen\_mean"; control for the pigmentation 72h after irradiation with one MED: "control\_MUT\_72h\_mean". Subjects are sorted according to their individual MED at the volar aspect of the forearm. Chromameter L\*-values and phototype are given as additional information ("cMUT": right arm, "cSunScreen": left arm) as well as extra information about notable pigmentation or complexion characteristics if applicable. Figs. B.1 to B.19 in Appendix B.1 may be consulted as further reference.

In a first step, these data are then analyzed to assess the reproducibility of the optoacoustic measurements. Subsequently, the spectral characteristics revealed by the individual absorption spectra are analyzed in an interindividual comparison especially with respect to the individual MED values and to the documented L\*-values indicating the individual skin lightness.

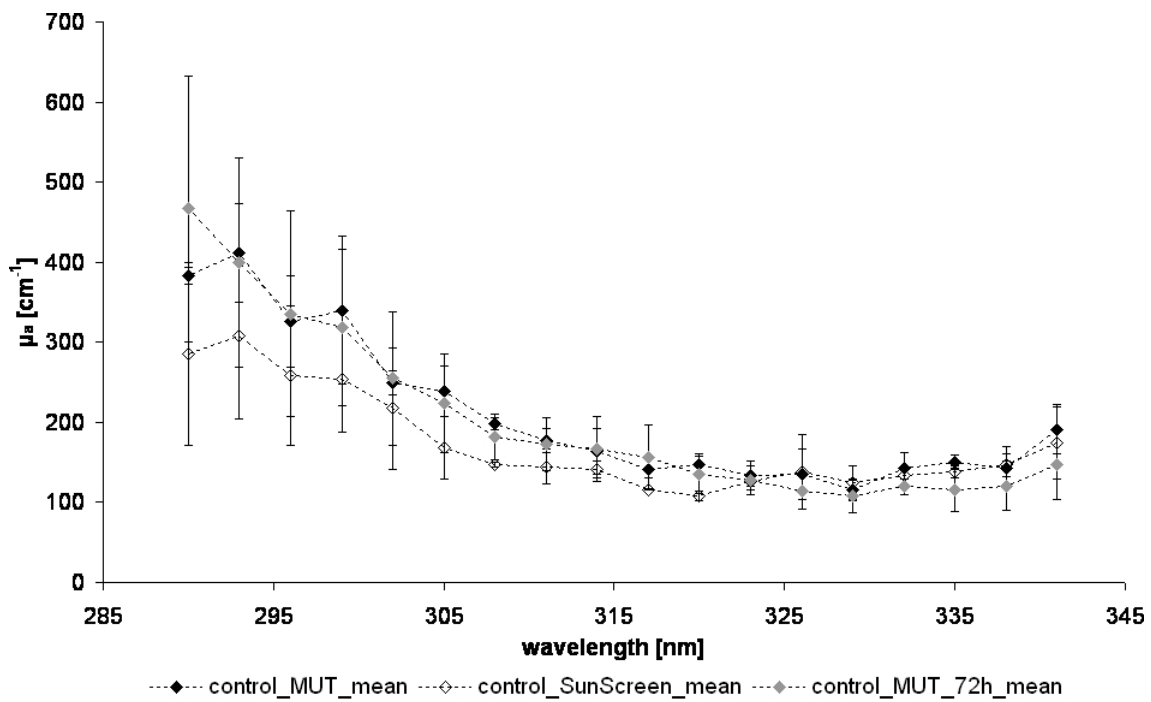


**Figure 8.3:** Spectrum of the absorption coefficient  $\mu_a$  on the volar aspect of the forearm. Subject G.O.: even (light) pigmentation. MED: 200  $\text{mJ}/\text{cm}^2$ . Phototype: I. L\*: 66.82 (cMUT), 66.21 (cSunScreen)

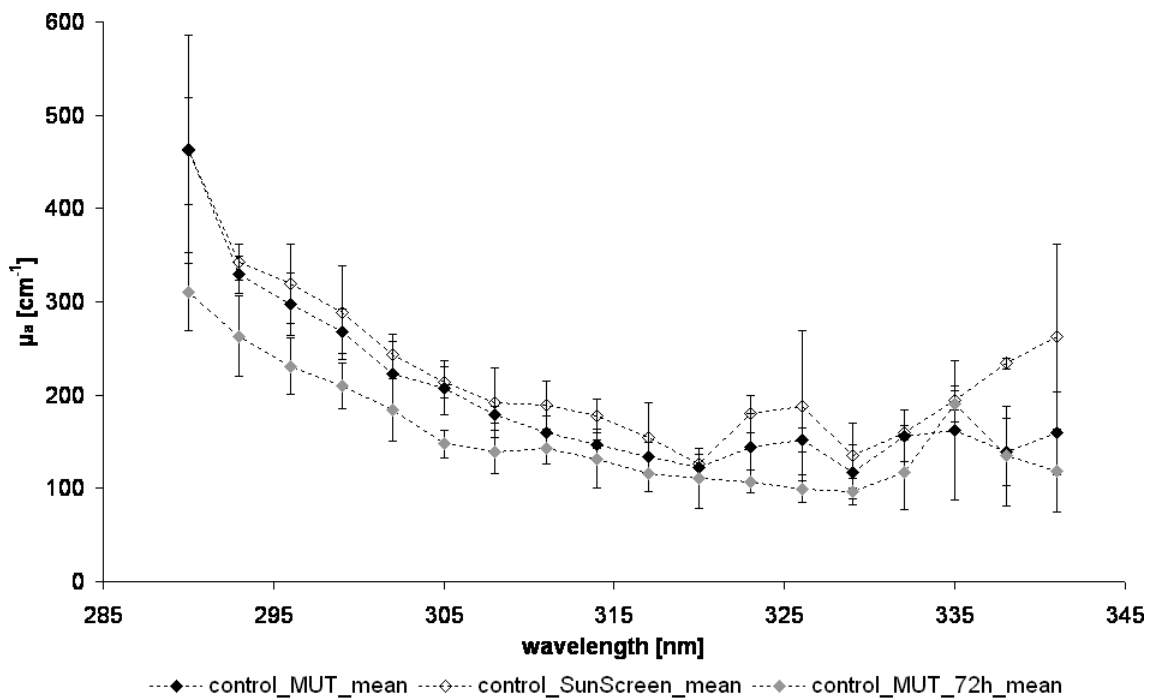


**Figure 8.4:** Spectrum of the absorption coefficient  $\mu_a$  on the volar aspect of the forearm. Subject M.M.: even (very light) pigmentation. MED: 220  $\text{mJ}/\text{cm}^2$ . Phototype I. L\*: 70.11 (cMUT), 70.14 (cSunScreen)



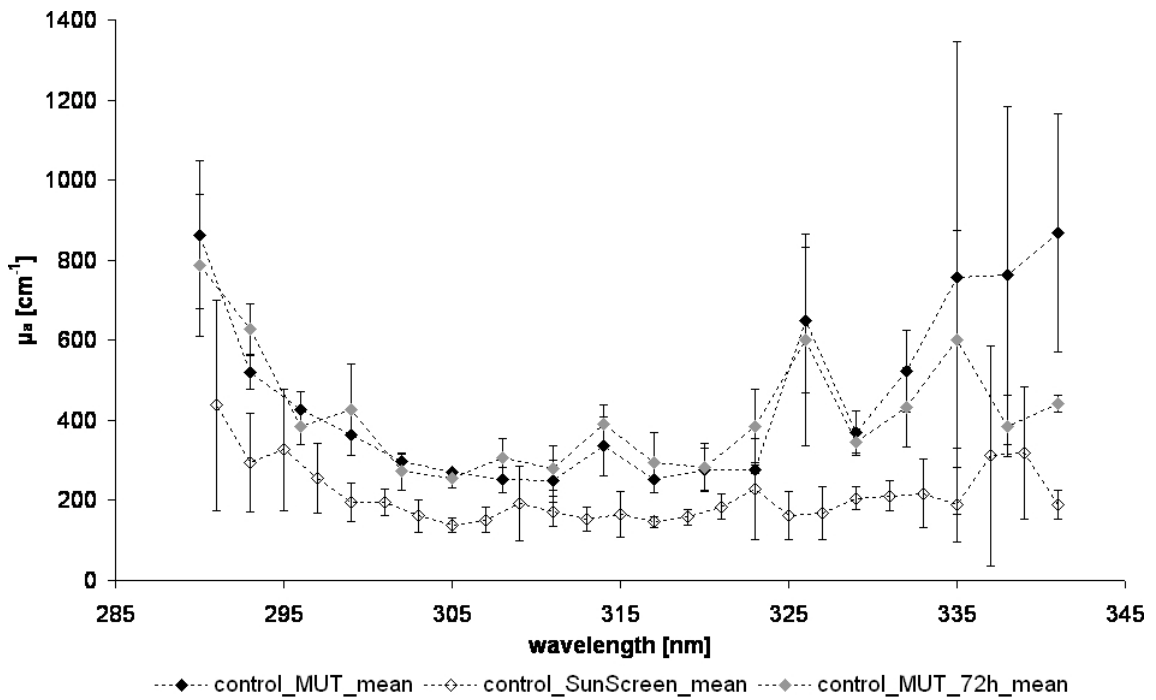


**Figure 8.5:** Spectrum of the absorption coefficient  $\mu_a$  on the volar aspect of the forearm. Subject M.H. MED: 230  $\text{mJ}/\text{cm}^2$ . Phototype II.  $L^*$ : 66.06 (cMUT), 67.44 (cSunScreen)

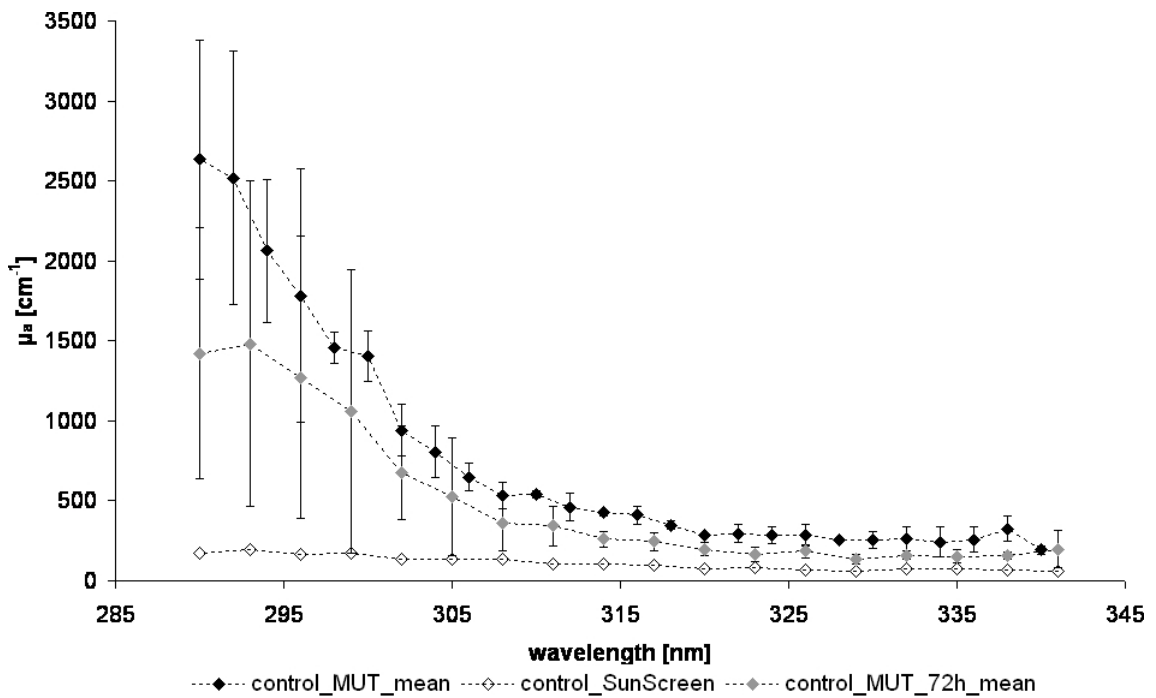


**Figure 8.6:** Spectrum of the absorption coefficient  $\mu_a$  on the volar aspect of the forearm. Subject L.K.: solarium user (weekly). MED: 240  $\text{mJ}/\text{cm}^2$ . Phototype I.  $L^*$ : 66.06 (cMUT), 67.44 (cSunScreen)

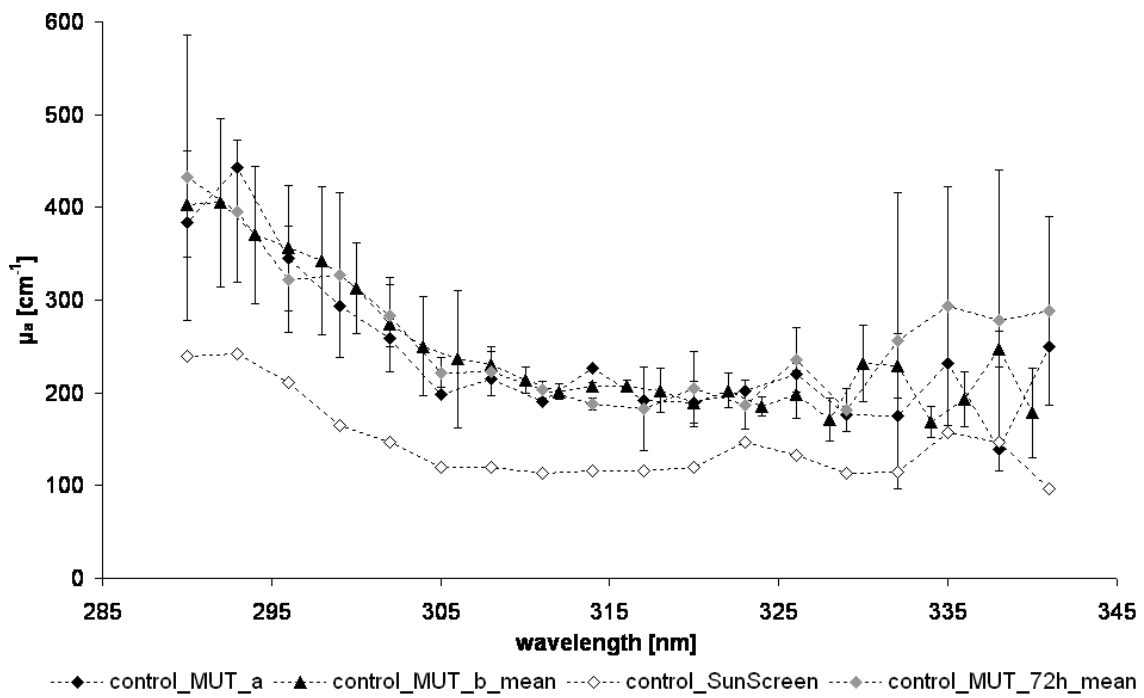


**Figure 8.7:** Spectrum of the absorption coefficient  $\mu_a$  on the volar aspect of the forearm. Subject W.K.: very dark hair. MED: 250  $\text{mJ}/\text{cm}^2$ . Phototype: II.  $L^*$ : 65.78 (cMUT), 67.27 (cSunScreen)

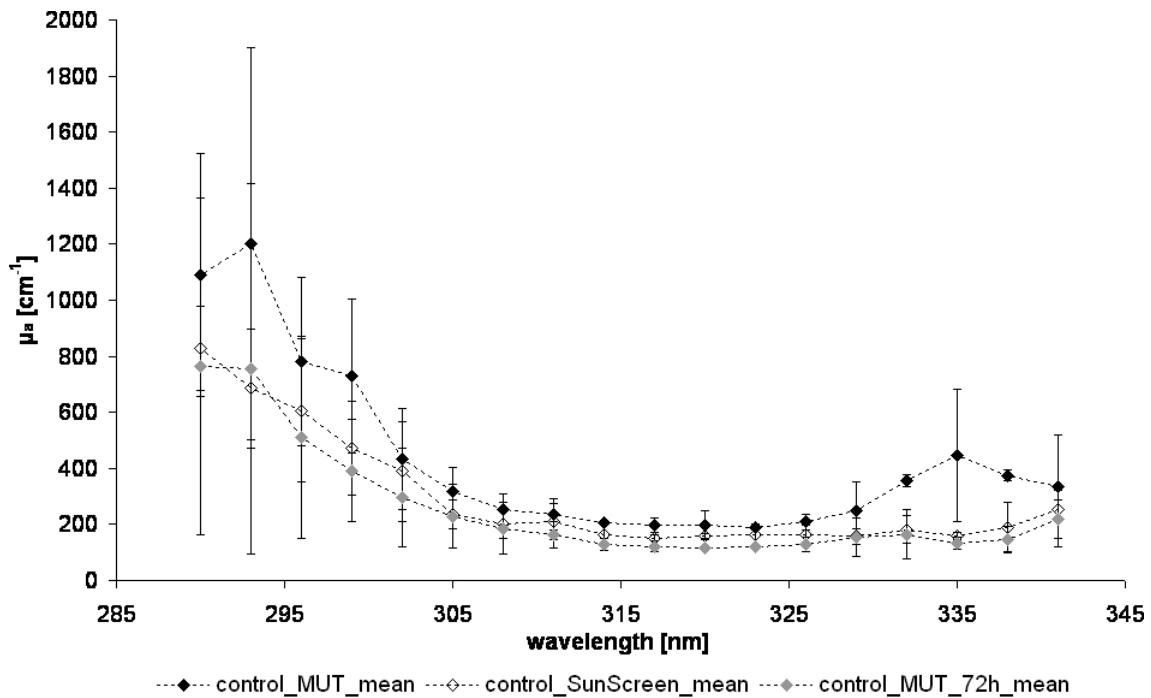


**Figure 8.8:** Spectrum of the absorption coefficient  $\mu_a$  on the volar aspect of the forearm. Subject K.K. MED: 250  $\text{mJ}/\text{cm}^2$ . Phototype: II.  $L^*$ : 62.77 (cMUT), 64.78 (cSunScreen)

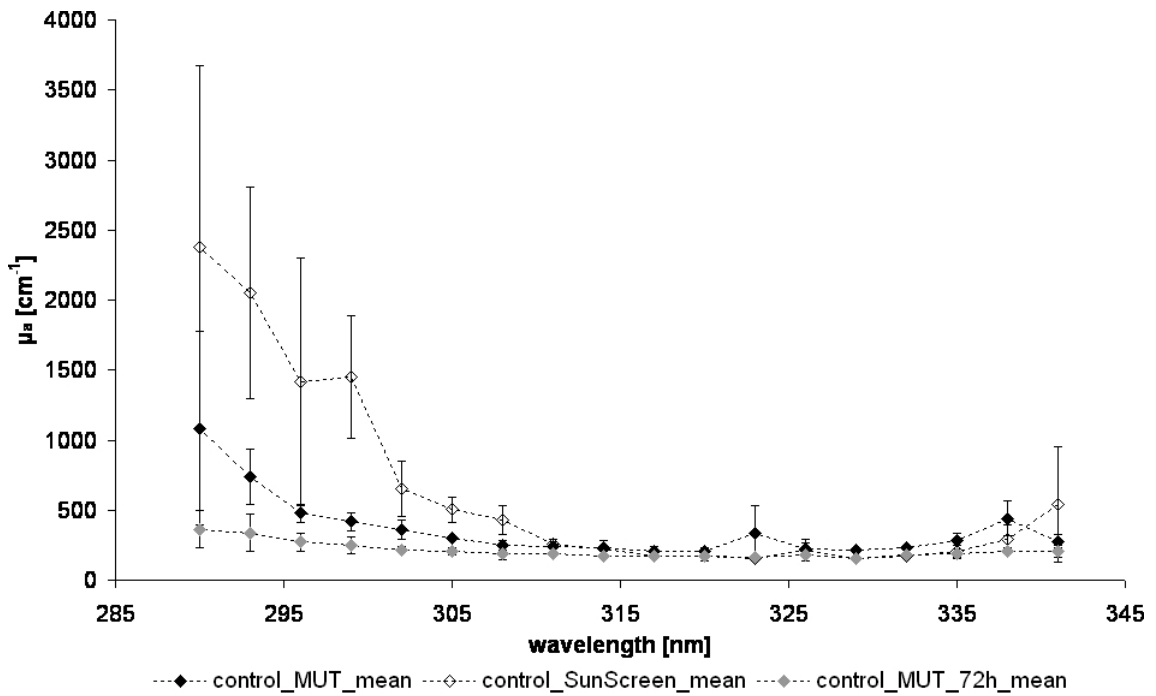


**Figure 8.9:** Spectrum of the absorption coefficient  $\mu_a$  on the volar aspect of the forearm. Subject Kr.G.: fairly inelastic skin. MED: 250 mJ/cm<sup>2</sup>. Phototype: II. L\*: 64.1 (cMUT), 66.03 (cSunScreen)

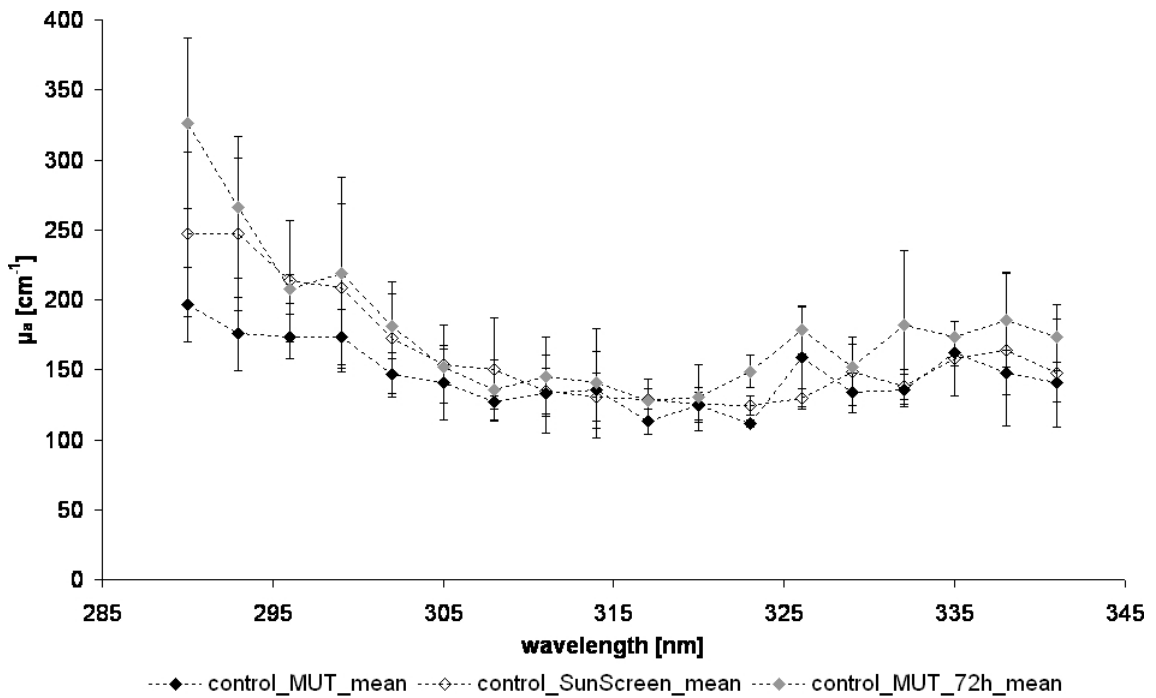


**Figure 8.10:** Spectrum of the absorption coefficient  $\mu_a$  on the volar aspect of the forearm. Subject E.R.: very soft, sensitive skin. MED: 250 mJ/cm<sup>2</sup>. Phototype: II. L\*: 64.62 (cMUT), 64.80 (cSunScreen)

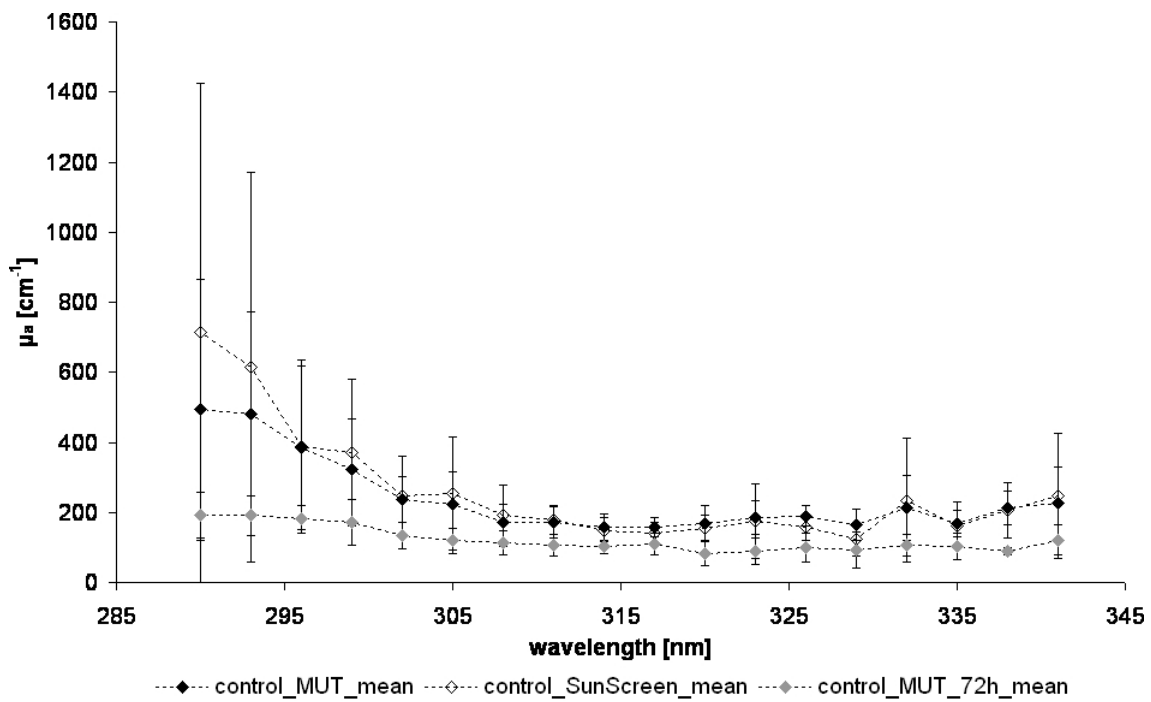


**Figure 8.11:** Spectrum of the absorption coefficient  $\mu_a$  on the volar aspect of the forearm. Subject H.M.: recent holiday/sun bathing. MED: 250  $\text{mJ}/\text{cm}^2$ . Phototype: II. L\*: 67.54 (cMUT), 65.08 (cSunScreen)

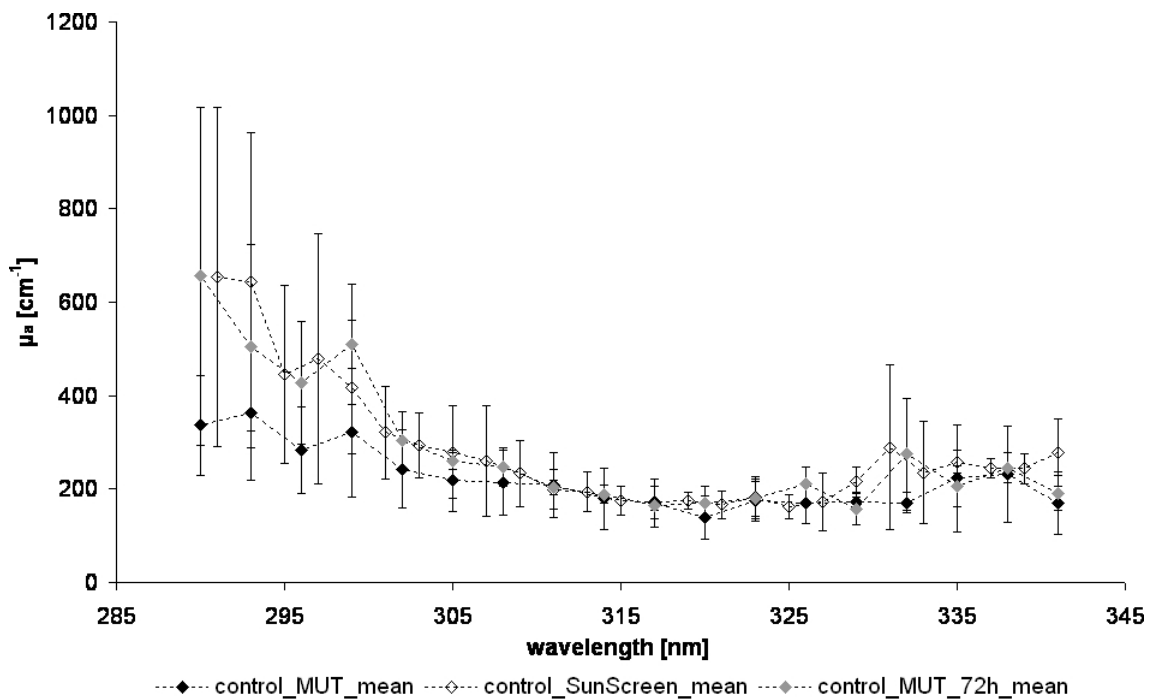


**Figure 8.12:** Spectrum of the absorption coefficient  $\mu_a$  on the volar aspect of the forearm. Subject K.H. MED: 250  $\text{mJ}/\text{cm}^2$ . Phototype: II. L\*: 64.65 (cMUT), 65.32 (cSunScreen)

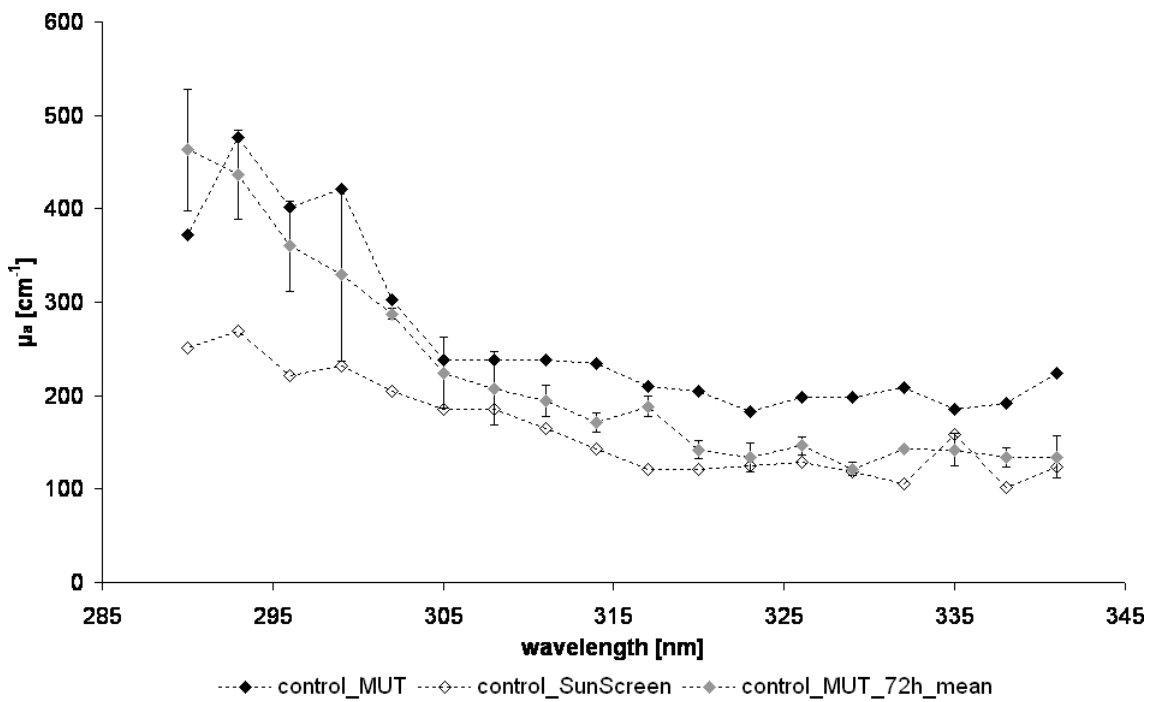


**Figure 8.13:** Spectrum of the absorption coefficient  $\mu_a$  on the volar aspect of the forearm. Subject K.I.: recent biking holiday. MED: 250 mJ/cm<sup>2</sup>. Phototype: III. L\*: 63.91 (cMUT), 60.57 (cSunScreen)

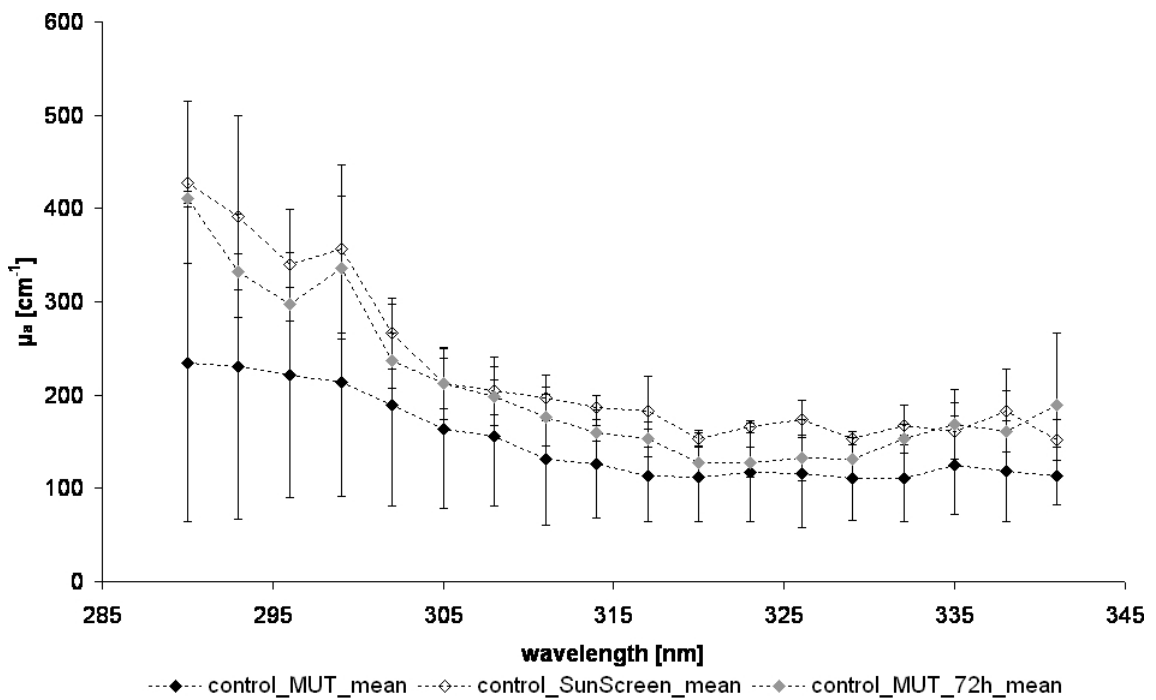


**Figure 8.14:** Spectrum of the absorption coefficient  $\mu_a$  on the volar aspect of the forearm. Subject D.C.: recent holiday, even mild tan. MED: 260 mJ/cm<sup>2</sup>. Phototype: III. L\*: 64.72 (cMUT), 66.92 (cSunScreen)

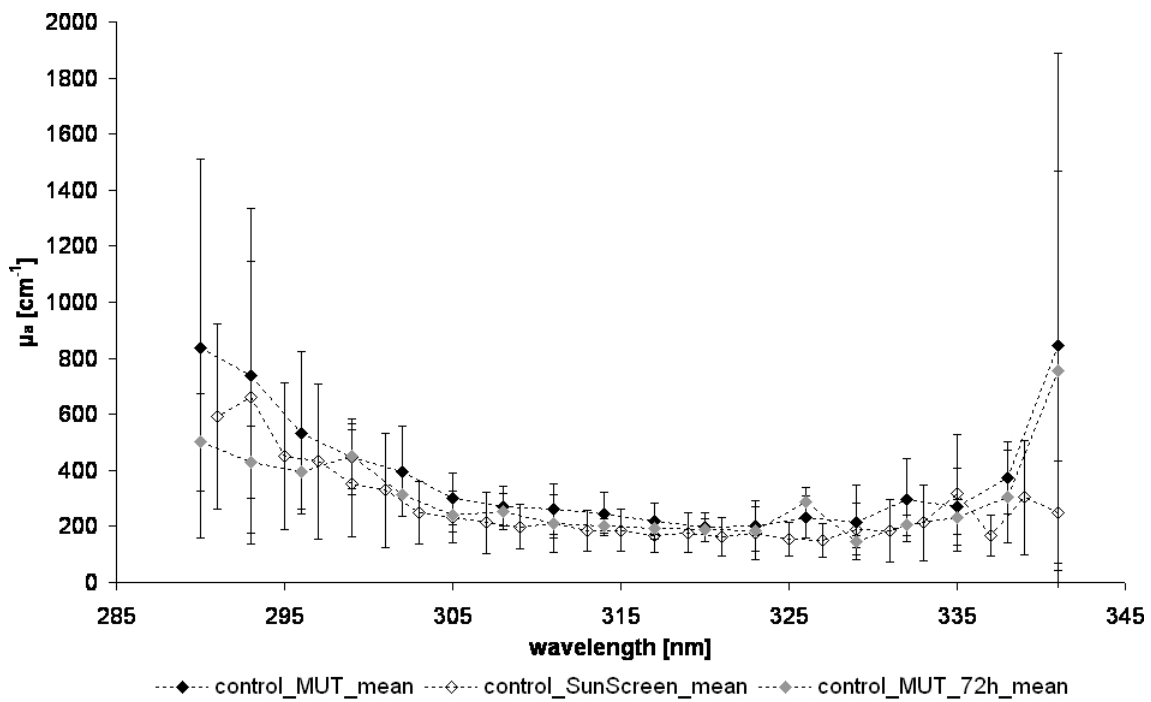


**Figure 8.15:** Spectrum of the absorption coefficient  $\mu_a$  on the volar aspect of the forearm. Subject F.M.: very densely freckled skin. MED: 260  $\text{mJ}/\text{cm}^2$ . Phototype: III.  $L^*$ : 67.54 (cMUT), 65.08 (cSunScreen)

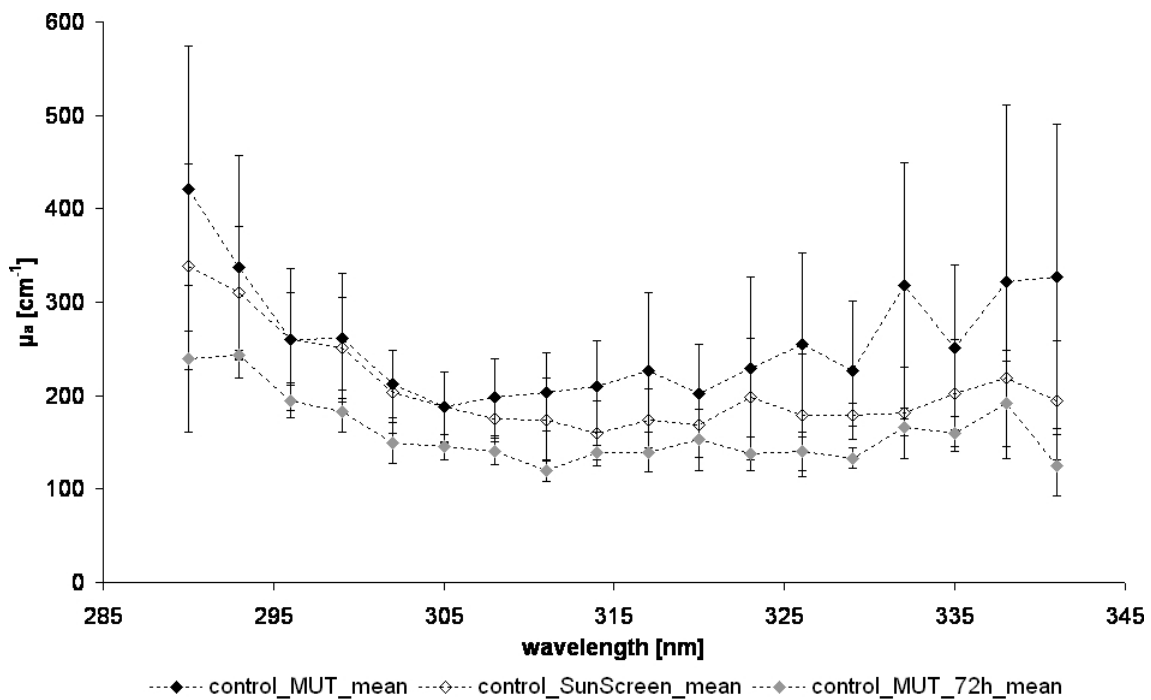


**Figure 8.16:** Spectrum of the absorption coefficient  $\mu_a$  on the volar aspect of the forearm. Subject S.R. MED: 270  $\text{mJ}/\text{cm}^2$ . Phototype: III.  $L^*$ : 62.48 (cMUT), 63.32 (cSunScreen)

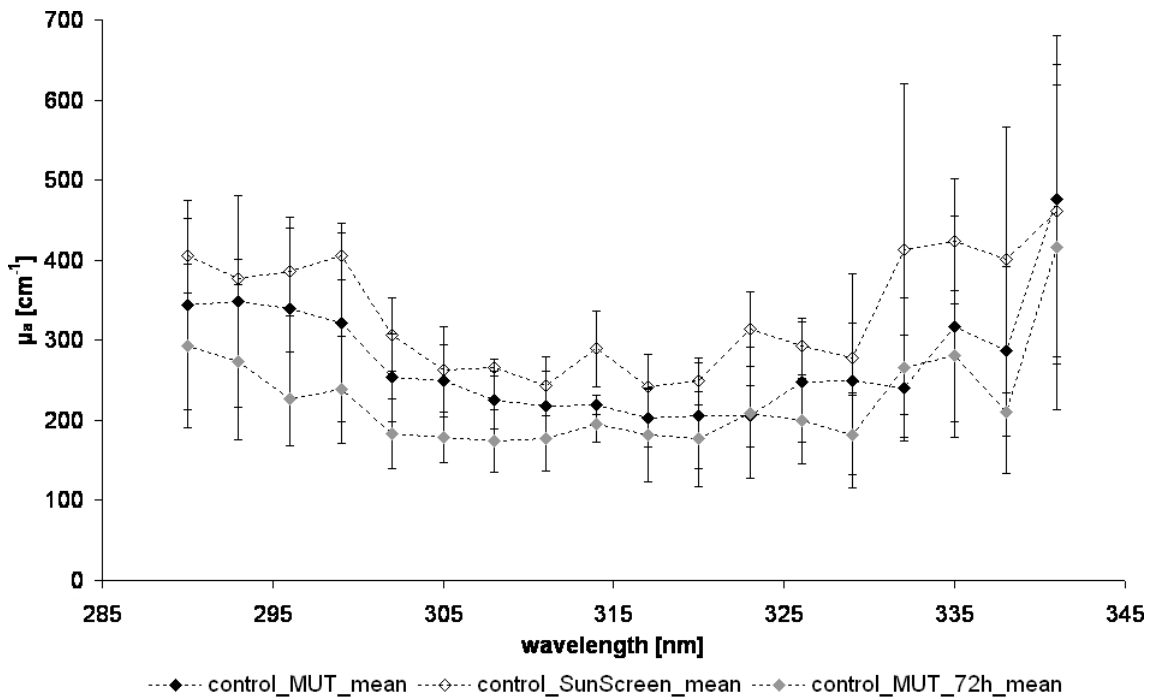


**Figure 8.17:** Spectrum of the absorption coefficient  $\mu_a$  on the volar aspect of the forearm. Subject W.M.: garden-worker, i.e. strong, even tan. MED: 280  $\text{mJ}/\text{cm}^2$ . Phototype: III.  $L^*$ : 65.3 (cMUT), 62.37 (cSunScreen)

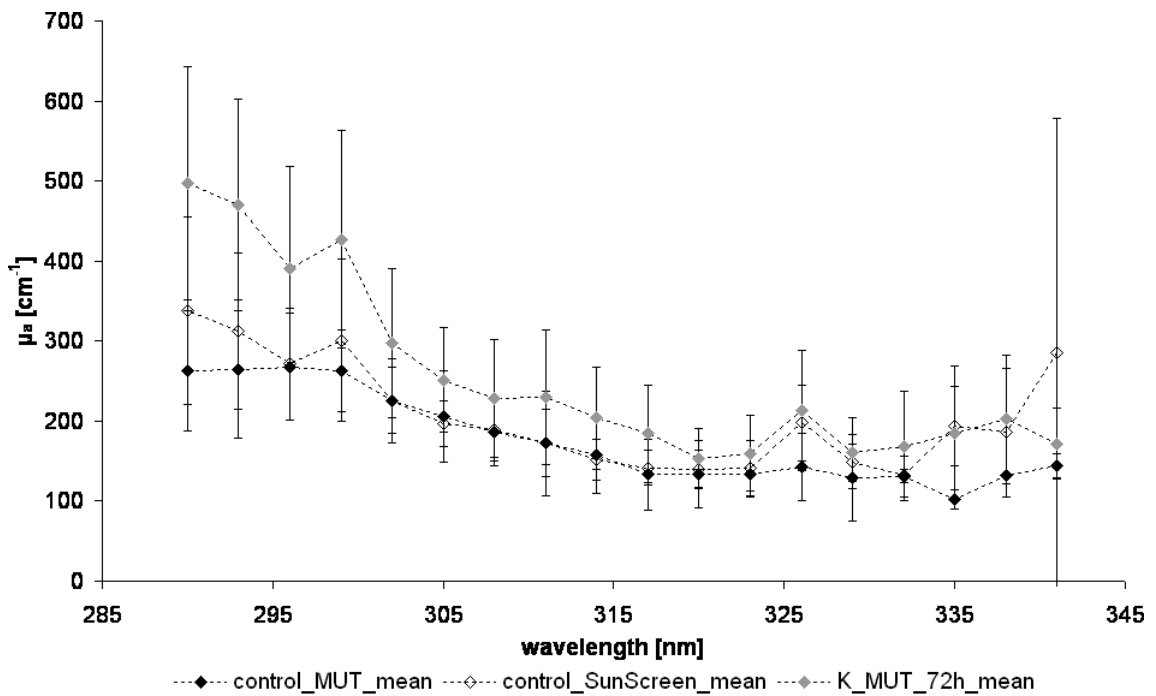


**Figure 8.18:** Spectrum of the absorption coefficient  $\mu_a$  on the volar aspect of the forearm. Subject B.I.: garden-worker, freckly, blotchy tan. MED: 300  $\text{mJ}/\text{cm}^2$ . Phototype: IV.  $L^*$ : 65.96 (cMUT), 67.06 (cSunScreen)

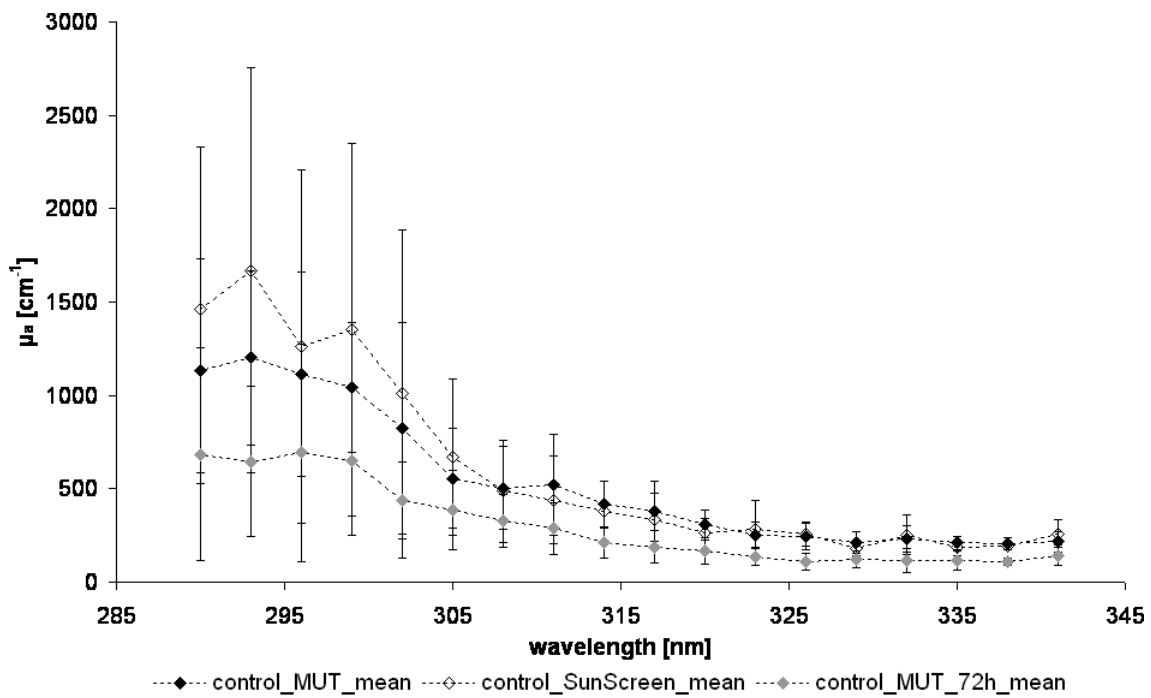


**Figure 8.19:** Spectrum of the absorption coefficient  $\mu_a$  on the volar aspect of the forearm. Subject P.R.: very light, ashen complexion. MED: 300  $\text{mJ}/\text{cm}^2$ . Phototype: IV.  $L^*$ : 68.08 (cMUT), 69.17 (cSunScreen)

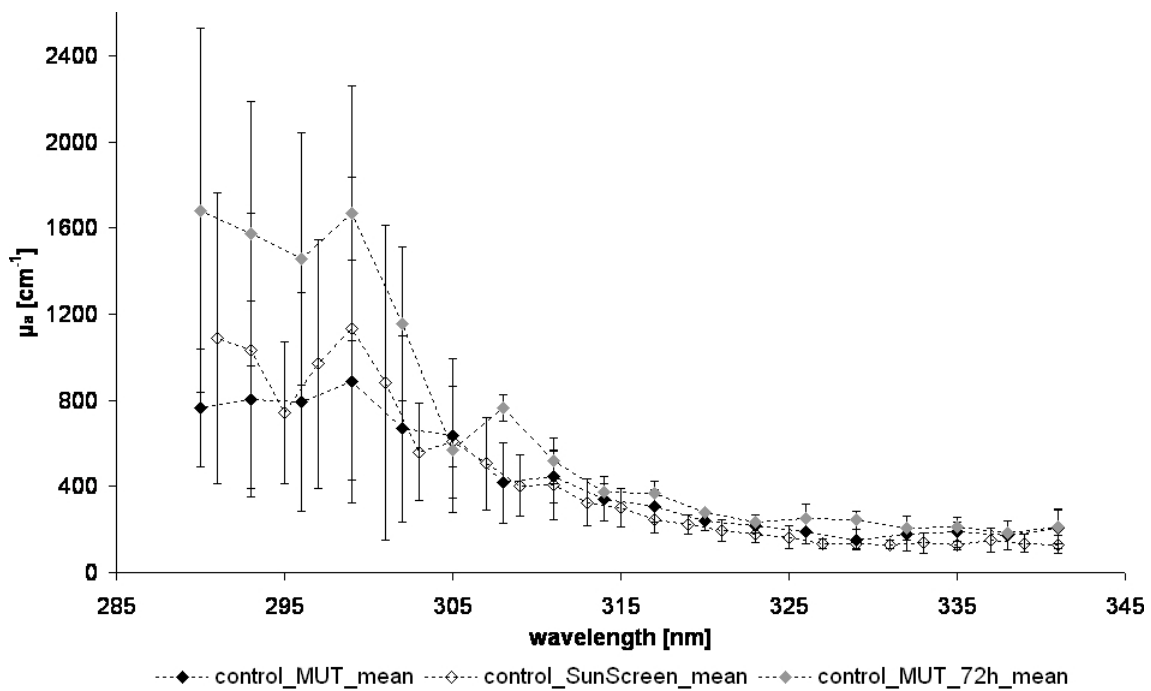


**Figure 8.20:** Spectrum of the absorption coefficient  $\mu_a$  on the volar aspect of the forearm. Subject Kn.G.: very dense freckled pigmentation. MED: 300  $\text{mJ}/\text{cm}^2$ . Phototype: IV.  $L^*$ : 63.31 (cMUT), 64.74 (cSunScreen)



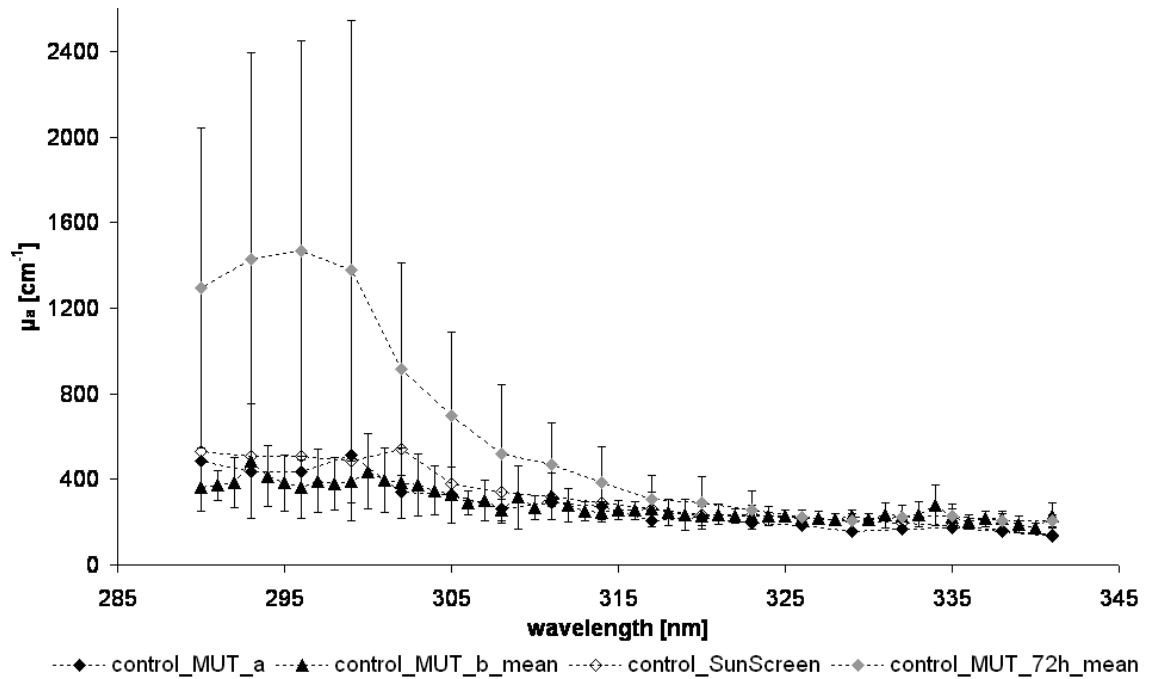


**Figure 8.21:** Spectrum of the absorption coefficient  $\mu_a$  on the volar aspect of the forearm. Subject L.U.: fairly inelastic skin, solarium user (very high weekly doses). MED: 320 mJ/cm<sup>2</sup>. Phototype: IV. L\*: 57.15 (cMUT), 56.43 (cSunScreen)

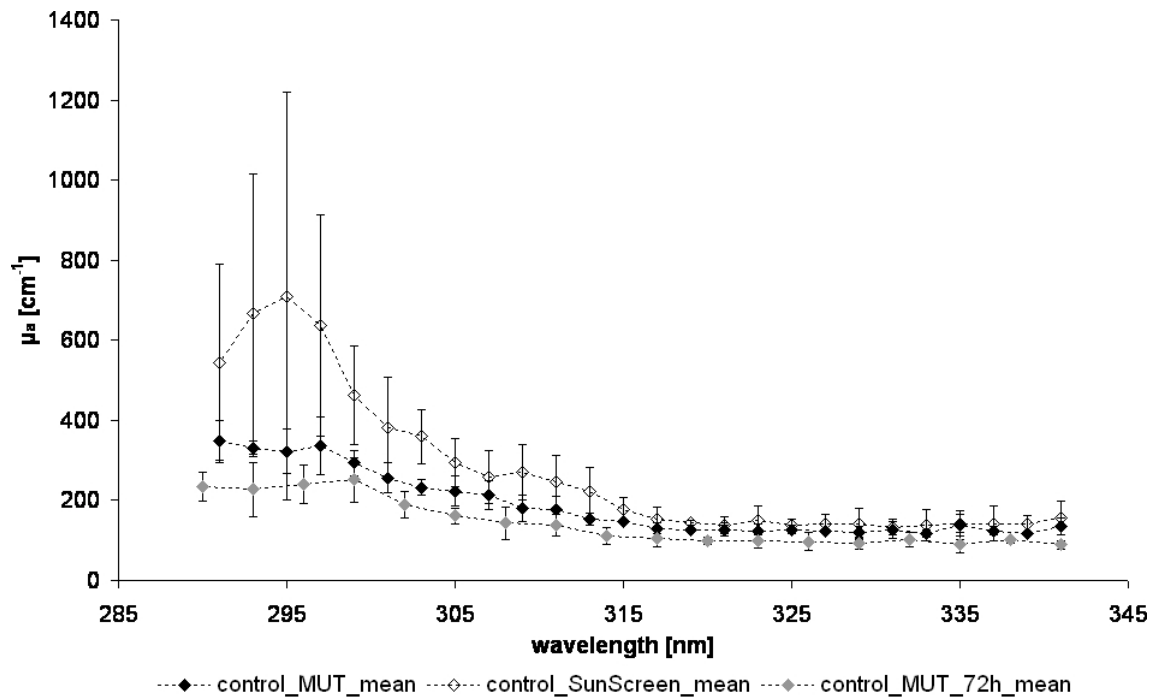


**Figure 8.22:** Spectrum of the absorption coefficient  $\mu_a$  on the volar aspect of the forearm. Subject K.B. MED: 400 mJ/cm<sup>2</sup>. Phototype: IV. L\*: 58.86 (cMUT), 61.81 (cSunScreen)

## reproducibility

At a first unquantified glance, the measurement results at the volar aspect of the arm (Figs. 8.3-8.22) appear to be similar for both arms as well as on different days. For most subjects, the three scans are fairly close together and they show similar characteristics in their wavelength dependency - this is best seen comparing the scan triplets of different subjects while keeping in mind that the scale of  $\mu_a$  differs from picture to picture.

However, this 'similarity' has to be quantified in order to be valuable. In this section data obtained at the same site but on different days are compared to see whether measurements are reproducible. The following subsection will deal with spectral characteristics and interindividual signal differences to see for example whether the three measurements on the volar aspect of the arm show different features for different subjects.

The optoacoustic data measured at the MUT irradiation control site on Day 1 and Day 3 of the study are used to assess reproducibility of the optoacoustic measurements. In contrast to the repeatability as discussed in Sec. 8.1, almost all experimental conditions are slightly changed between these two compared measurements - from the exchange of the ultrasound gel in the detector over daily energy calibration to new reference spectra from the Poly(vinyl alcohol) standards for the simulations. Most importantly, it is impossible to measure at exactly the same spots once and then again three days later. Consequently, the following paragraphs will deal with a comparison of the results from the in vivo measurements at several spots within the same skin area which were obtained at different days and thus under changed experimental conditions rather than giving a true reproducibility estimation.

In order to minimize strain for the subjects only about three measurements were taken to be averaged for the mean values on each day for each site. Consequently, an elaborate statistical analysis of the reproducibility is not reasonable. Due to the inhomogeneous structure and pigmentation of the skin, these three measurements could vary quite considerably around their mean resulting in fairly high standard deviations.

Hence, three measures are calculated to be able to estimate reproducibility of the measurands instead: number of overlapping standard deviations of the mean values (normally max. 18 per wavelength scan), number of mean values within the range of the standard deviation of the compared mean value (normally max. 36 per wavelength scan), and the ratio  $q_{range}$  of the difference between the two corresponding mean values and their average. If there are no two datapoints at the same wavelength due to different wavelength scan stepsize, neighboring wavelengths (wavelength difference = 1 nm) were compared for the first two assessments.

The wavelength scans of 19 subjects were used to calculate the **number of overlapping standard deviations** and the number of mean values within the standard deviation of the result from the other data set. One subject (K.I., Fig. 8.13) had to be excluded from

this assessment as there was only one valid scan for each area and day. Out of these 19 subjects, 9 had overlapping standard deviations for more than 90 % of the wavelengths in the scan, 13 had an overlap for more than 75 % and 18 for more than 50 %.

Looking at how many **mean values** of each measurand lay **within the standard deviation of the measurements from the other day**, it was found that there was no subject where more than 90 % of the results fulfilled this criterion, in 3 subjects this was achieved for more than 75 % of the measurands and 10 out of 19 had more than 50 % results fitting within the standard deviation of the other measurement of this measurand.

The average **ratio  $q_{range}$**  of the difference between the respective average values from the compared measurements and their mean is  $(30.9 \pm 15.8) \%$ . A minimal relative range of the two measurements is found in subject K.B. (see Fig. 8.22) with 8.5 % on average, maximal ranges are found in the measurements of subject H.M. (see Fig. 8.11) with 61.4 % on average.

At first sight, these results do not seem to be a brilliant advertisement for the accuracy and reproducibility of optoacoustic data in vivo. However, it should be pointed out again, that the human skin is structurally highly inhomogeneous. The grid like, very low scale wrinkled structure of the skin, which is easily seen on the SELS and Fotofinder pictures (compare Appendix B.2 and B.3), can strongly influence the light propagation and distribution. As the optoacoustic detector integrates over only less than  $1 \text{ mm}^2$ , it can be expected that this influence causes quite a large difference in the optoacoustic signals of measurements at sites which may be even very closely located. Even more so of course, if the skin is unevenly pigmented or if the subject has fairly dark hair.

Furthermore, these results have to be compared with the repeatability results for the PVA-samples (see Sec. 8.1) as well as with the ratio  $q_{stddev}$  of standard deviation and mean value for the two results for one measurand.

Looking at the repeatability assessment,  $q_{range}$  was as high as ca. 9-18 % depending on the absorption coefficient. So, more than halve of the deviations in the in vivo measurements could be assigned to a deficiency in repeatability, i.e. accuracy, which is capable of improvement.

$q_{stddev}$  shows how strong single measurements deviate from their mean. As it is calculated separately for each mean value it does not compare between Day1 and Day3 results but shows variability of measurements in the same area on the same day. A mean  $q_{stddev}$  of ca. 26 % is found for measurements on these two days. Hence, single measurements on the same day in the same area cover a range comparable to the difference between mean values from two different days. This underscores again the effect of the skin's inhomogeneity.

In conclusion, the deviation among two mean absorption coefficients measured at approximately the same area but on different days is relatively high. However, the major reason for this deviation is probably to be found in the high, small-scale inhomogeneity of human skin in vivo. Despite of this, the accuracy of the optoacoustic measurements still has to

be enhanced in the future reducing errors from technical components as outlined in detail in Sec. 8.1.

Taking all of this into consideration, the development of an optoacoustic detector integrating over a much larger area would be a reasonable approach to improve the quality of optoacoustic in vivo measurements. In combination with an improved accuracy (see Sec. 8.1), a second large scale sensor head could be an excellent complement for the existing ca. 1 mm<sup>2</sup>-detector. However, such a design would have to cope with a couple of new challenges of technical as well as analytical considerations. e.g.: How can a larger area be homogeneously illuminated? This cannot be achieved by simply using a larger distance between fiber and sample as this would significantly reduce the fluence at the sample surface - and thus lead to much weaker optoacoustic signals with a much worse signal-to-noise ratio. In principle, a fiber array could be used of course, but their arrangement to produce a relatively homogeneous energy density over a large area will be difficult. Besides, this homogeneously illuminated area must be large compared to the sound detector area as this is one of the basic conditions for a reasonably simplified theoretical approach to the analysis of the optoacoustic transients. So, realizing a setup with an enlarged pressure sensor with an area 20 mm<sup>2</sup> for example will be quite a challenge. Apart from that, skin features like hair, hair follicles, moles, etc. which can be avoided with the small detector will then contribute to the optoacoustic signals. Not only are these unwanted contributions hardly identifiable and separable from the main skin signal but exposing moles to very strong and high dose UV radiation poses a considerable risk on the subjects. More measurement spots for better averaging are another alternative. However, this would increase measurement times and thus imposes additional strain on the subjects.

Probably, both approaches should be followed in the future. Then, both could be considered and decided upon individually for each subject depending on the skin characteristics.

### **interindividual comparison**

There are some similar spectral characteristics in the absorption coefficients for most subjects as judged by the spectra given in Figs. 8.3 to 8.22:

- A fairly flat course of  $\mu_a$  in UVA-II is followed by a steeper rise in UVB towards shorter wavelengths.
- Maximal values for the absorption coefficient are usually found at the short wavelength end.
- The absolute values of the absorption coefficients may differ a lot from subject to subject as well as between the UVA ( $\lambda > 315$  nm) and UVB ( $\lambda < 315$  nm) region.

The last item of this list is particularly obvious looking ahead at Fig. 8.23, which allows an overview about all individual spectra.

**Correlation between UV absorption spectra and minimal erythema doses (MED)**

will be the focus of the next paragraphs. Fig. 8.23 shows the mean spectra of all measurements on the volar aspect of the forearm for each subject with reference to the subject's individual MED at this site. The standard deviation is omitted for clarity reasons.

No pronounced dependency of the absorption spectra on the individual erythema doses of the subjects can be deduced from this collection of individual spectra. This is interesting with regard to the literature where the importance of pigmentation and skin colour as well as their ability to indicate individual UV sensitivity is widely discussed (see e.g. [19] and [29]). As optoacoustics measures the individual optical properties, the lack of a pronounced phototype dependent difference in these spectra supports the view that it is the individual biochemistry rather than the UV optical properties that determine the UV sensitivity of human skin in vivo.

If stepping back from the individual spectra and looking at the mean spectra of the four phototype (or MED range) groups instead, a certain trend can be seen. These four spectra are shown in Fig. 8.24. The two subjects regularly tanning in a solarium (L.U and L.K.) were not included in these average spectra as their skin optical properties might be too strongly affected by the artificial UV exposure to be considered representative for natural low UV exposure. Apart from that, only the means at the standard 3 nm spacing are shown as they represent average values of a maximal number of measurements. Judging by the spectra in Fig. 8.24 there seem to be certain trends in the characteristics of the spectra for more or less UV-sensitive skin:

- The optical properties of all four phototypes are very similar at the UVA/UVB border - here  $\mu_a \approx 190 \text{ cm}^{-1}$ .
- In the UVA, UV insensitive skin (esp. phototype IV) absorbs less ultraviolet radiation compared to very UV sensitive skin like that of phototype I.
- In contrast to this, absorption is lower in UV sensitive skin in the UVB compared to the absorption in less sensitive skin (esp. phototype IV).
- For phototype IV  $\mu_a$  is increasing towards shorter wavelengths. The slope is also increasing towards shorter wavelength.
- In phototype I  $\mu_a$  first decreases in the UVA till near the UVA/UVB border, then stays almost constant up to 305 nm and then rises again to its maximum at 290 nm.
- The ratio of short to long wavelength absorption coefficient(s) is higher for UV insensitive skin than for UV sensitive skin.

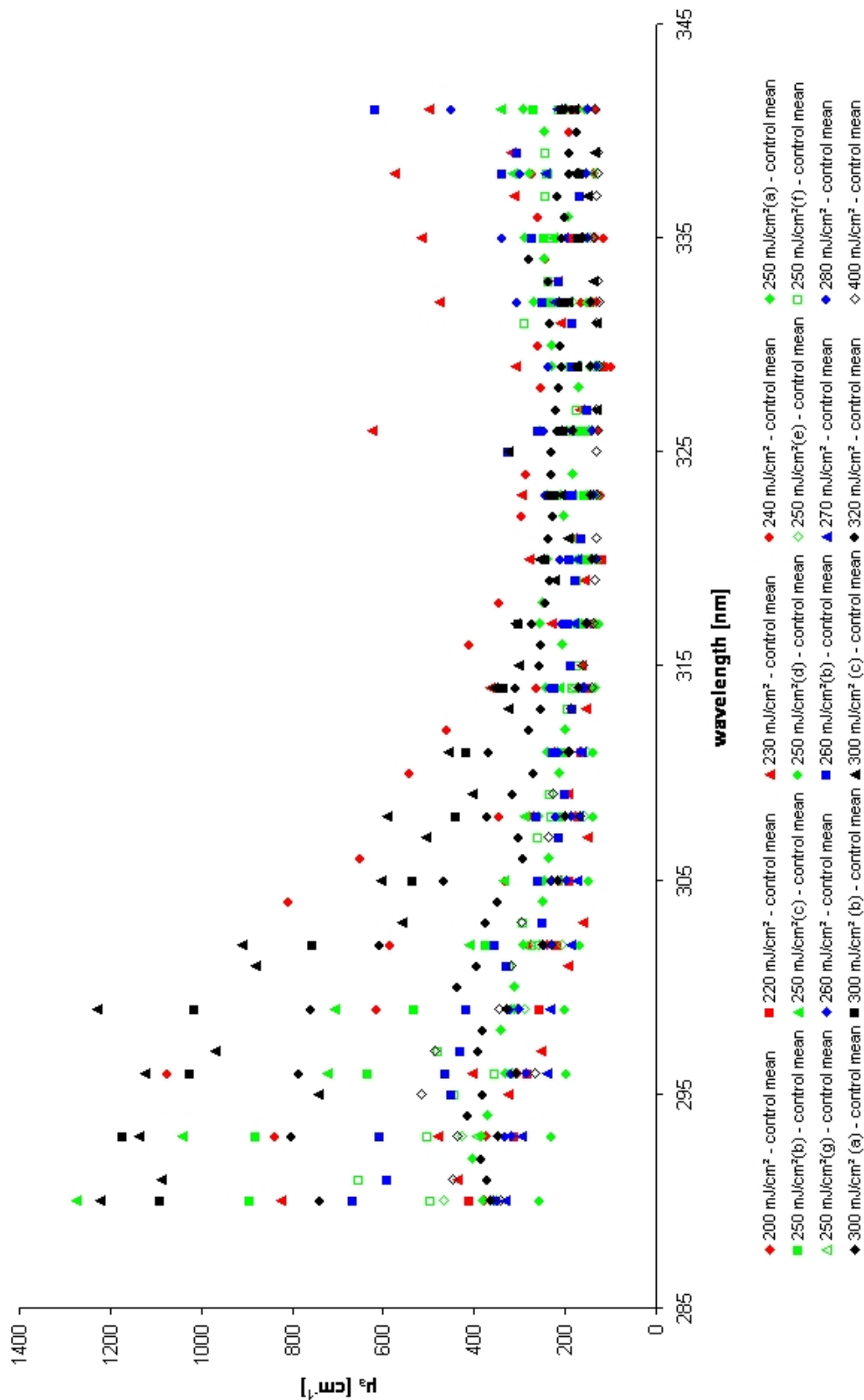


**Figure 8.23:** Mean spectra of the absorption coefficient  $\mu_a$  at the volar aspect of the forearm for all 20 subjects. MED values are given and MED/phototype groups are colour-marked. red: MED 200-240  $\text{mJ/cm}^2 \approx$  phototype I, green: MED 250  $\text{mJ/cm}^2 \approx$  phototype II, blue: MED 260-280  $\text{mJ/cm}^2 \approx$  phototype III, black: MED 300-400  $\text{mJ/cm}^2 \approx$  phototype IV.

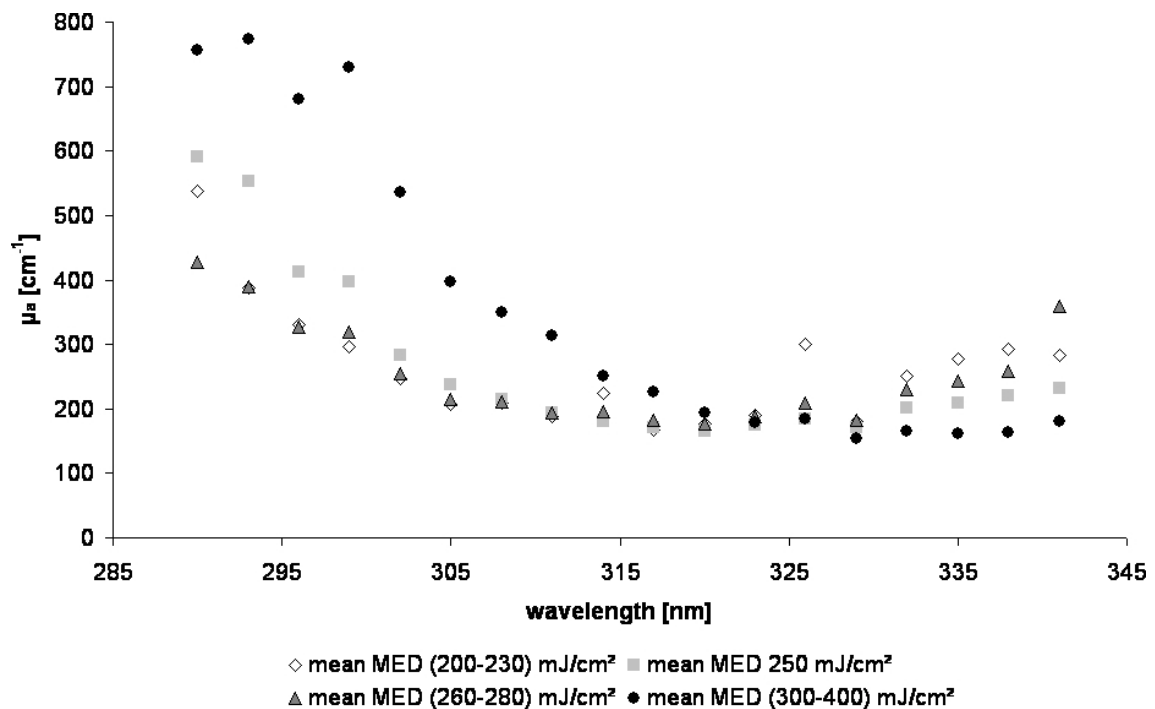


**Figure 8.24:** Mean spectra of the absorption coefficient  $\mu_a$  at the volar aspect of the forearm for the four phototypes/MED ranges: type I (200-230 mJ/cm<sup>2</sup>), type II (250 mJ/cm<sup>2</sup>), type III (260-280 mJ/cm<sup>2</sup>) and type IV (300-400 mJ/cm<sup>2</sup>).

However, it must be pointed out, that these observations are indeed only trends. Fig. 8.25 shows the same data as Fig. 8.24 again, but here the standard deviation of the means is given as additional information. The large standard deviation of the measurements of course weakens the significance of the mentioned spectral features characteristic for the different phototypes. Possibly, these trends will prove to be significant, if repeatability and reproducibility are enhanced in the future. Unfortunately, these elaborate and time-consuming improvements have to be left for future works.

The next paragraphs are dedicated to the investigation of a **correlation between UV absorption spectra and Chromameter L\*-values (skin lightness)**. The colour value L\* describes the skin brightness and is thus a first reference for skin pigmentation (see also Sec. 6.2.4 and 7.3 as well as [62]). Higher L\*-values indicate light, i.e. weakly pigmented skin and thus low melanin concentration.

Fig. 8.26 shows the individual  $\mu_a$  spectra again but this time with reference not to the individual MED but to the L\*-value of the skin site. Judging by Fig. 8.26, there is no obvious relation between L\*-values and optoacoustic spectra.

Parallel to the approach used for the MED data before, it was tried to group the subject data according to their L\*-ranges to find a trend in the resulting mean spectra. Again, the subject data was divided into four groups starting with L\*-values larger than 67 (n=3) for very light skin, over L\*=67-64 (n=11), and L\*=64-61 (n=4), to the darkest group with

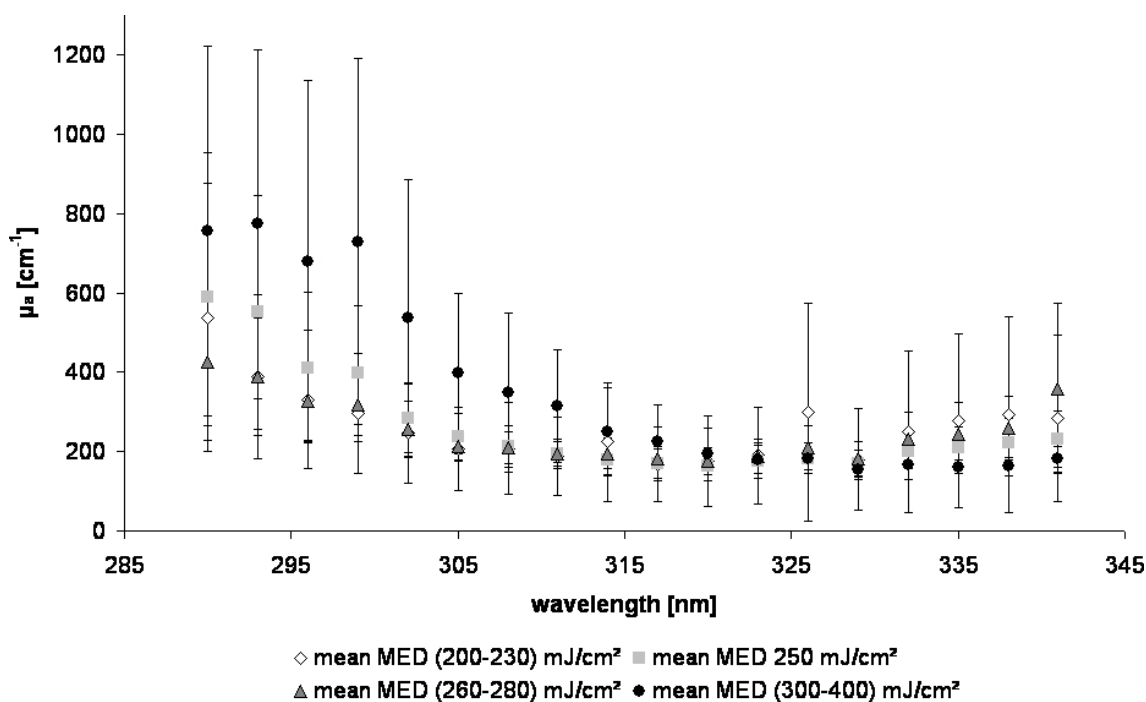


**Figure 8.25:** Mean spectra of the absorption coefficient  $\mu_a$  at the volar aspect of the forearm for the four phototypes/MED ranges as in Fig. 8.24. Error bars show the standard deviation.

$L^*$  smaller than 61 ( $n=2$ ). The distribution according to even  $L^*$ -ranges is arbitrary but should still be capable of showing a trend. The result is shown in Fig. 8.27.

In contrast to the results averaged according to individual MED, not even a trend can be seen in these spectra. Of course, the general characteristics are still prevalent in the spectra, e.g. the rise of  $\mu_a$  values from UVA to UVB which is starting fairly flat and then increases in the UVB.

The reasons for the apparent independency of the spectra on skin brightness probably are primarily to be found in what information  $L^*$  is truly giving.  $L^*$  is measured by reflectance in the visible range of the spectrum. So, it shows how much of the incident light has not entered the skin but has been reflected back to the detector. Accordingly, absorbing and forward scattering pigments will yield a low  $L^*$ -value whereas highly backscattering pigments result in high  $L^*$ -values. Besides, the  $L^*,a,b$ -color space covers the visible range of the spectrum. This has two consequences: first, it is not sensitive to pigments active in the ultraviolet and second, it is highly sensitive to pigments that are important in the visible though not necessarily in the ultraviolet. Haemoglobin for example strongly influences the skin color values. However, this chromophore is unimportant for the optical characterization of skin in the considered UV range as it is only found in the dermis whereas most UV interaction takes place in the epidermis above.

Unfortunately, we were not able to monitor the melanin index of the skin sites. It is obtained by taking the log of the inverse reflectance at each wavelength. Between 620 and 700 nm, this logarithm decreases in an approximately linear fashion with a slope



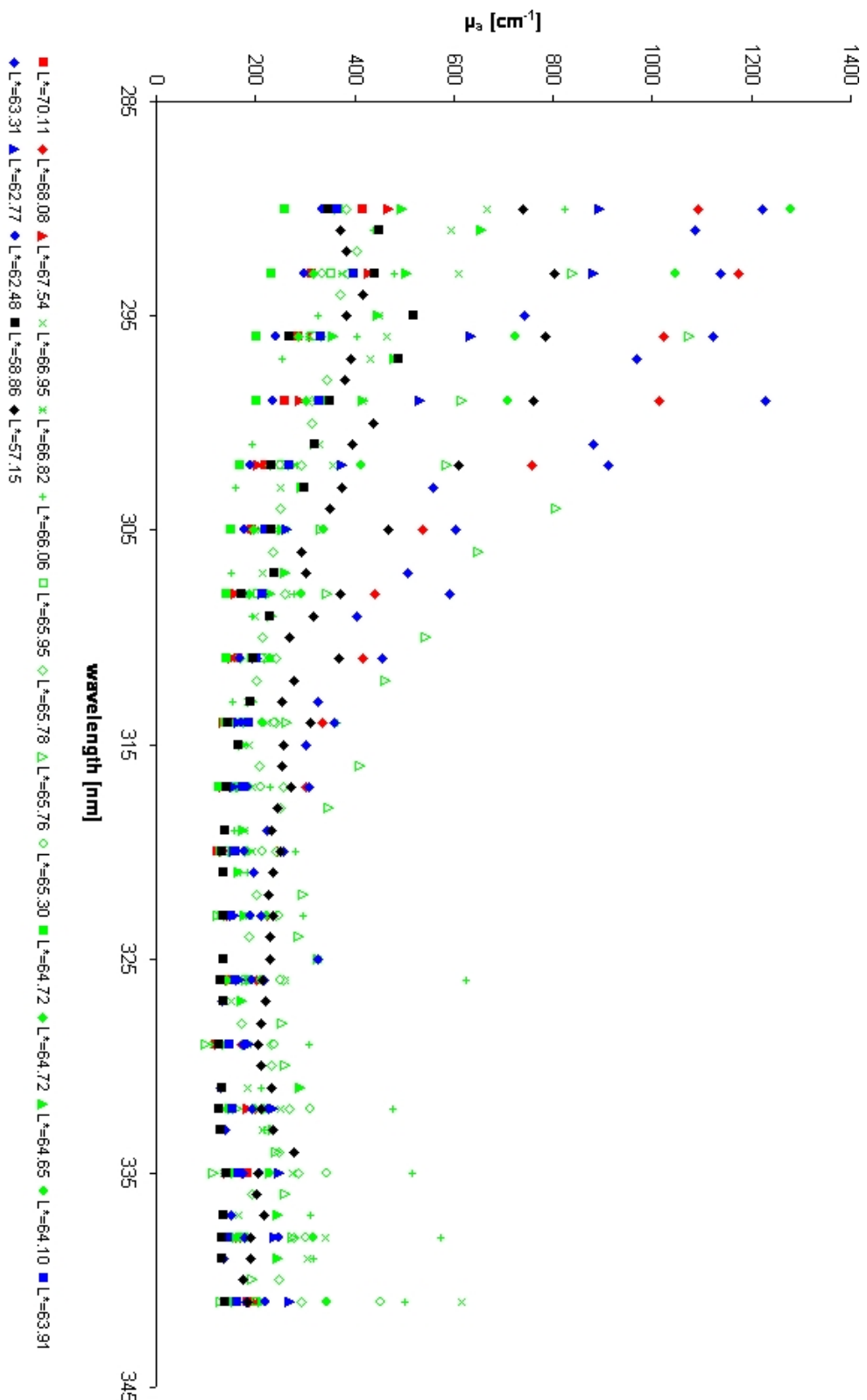


**Figure 8.26:** Mean spectra of the absorption coefficient  $\mu_a$  at the volar aspect of the forearm with reference to the chromameter  $L^*$ -values representing pigmentation. Spectra are grouped according to evenly spaced  $L^*$ -value ranges  $L^* > 67$ ,  $L^* = 67-64$ ,  $L^* = 64-61$ , and  $L^* < 61$  and colour marked accordingly.

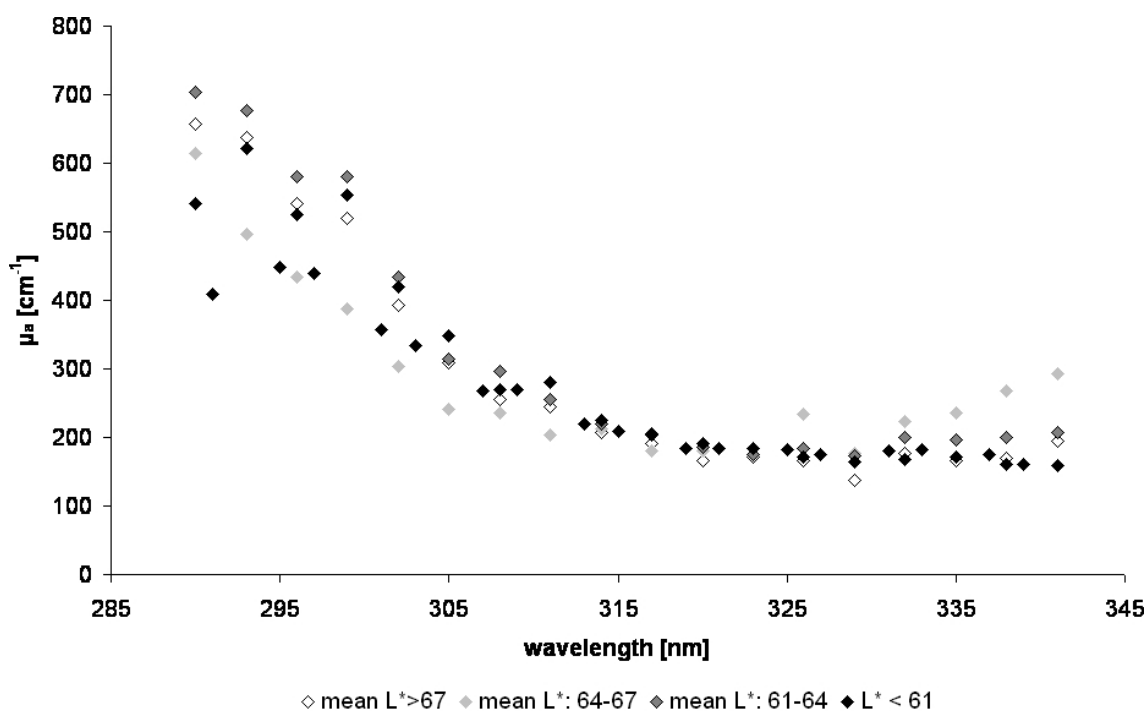


**Figure 8.27:** Mean spectra of the absorption coefficient  $\mu_a$  at the volar aspect of the forearm for four ranges of  $L^*$ .  $L^* > 67$  ( $n=3$ ) (very light skin),  $67 > L^* > 64$  ( $n=11$ ),  $64 > L^* > 61$  ( $n=4$ ),  $L^* < 61$  ( $n=2$ ) (very dark skin).

proportional to the concentration of melanin in the skin. This calculation is based on the idea that taking the log of the inverse reflectance transforms the remittance spectrum into a close approximation of the absorption spectrum. Its slope is defined as the Melanin Index, a unitless, continuous variable objectively quantifying skin color. This would have delivered a better indication of the individual melanin concentration as it is freed from the influences of haemoglobin for example.

In **conclusion of the interindividual comparison**, the fact that the  $L^*$ -values do not show any obvious correlation with the optoacoustic spectra can be read as a hint that melanin is at least not the only important chromophore in the ultraviolet range.

In anticipation of Sec. 8.3.4 it should be mentioned that the extreme penetration depths corresponding to the shown absorption spectra lie between ca.  $100 \mu\text{m}$  (UVA) and  $8 \mu\text{m}$  (UVB). The epidermis is relatively thin at this site of the skin, still it will probably be more than  $100 \mu\text{m}$  thick and the stratum corneum is reported to be  $10-20 \mu\text{m}$  thick here [68]. So, for low penetration depths - corresponding to absorption coefficients of  $500 \text{ cm}^{-1}$  or more for example - the chromophores in the stratum corneum are dominating the optical properties and probably, they will play a less pronounced but still considerable role also in the spectra with fairly low absorption coefficients.

Looking again at the  $\mu_a$  spectra of the different subjects and comparing them with the available spectra for the important chromophores (see Sec. 3.2.1), it seems as if (UVB-induced) melanin and constitutive epidermal melanin pigmentation would be responsible

for a baseline absorption in the epidermis. This pigment probably is dominant in the UVA where the spectra are fairly close together for all subjects. In the wavelength range around 325 nm most spectra are parallel and differ only in offset.

Comparing Fig. 8.24 in this Section with Fig. 3.7 in Sec. 3.2.2 shows that the theoretical spectrum of well-pigmented epidermis and the optoacoustically measured spectrum for phototype IV are very similar. However, the theoretical curves for light pigmented epidermis do not match the measured spectra of the UV sensitive phototypes. The epidermal spectra in Fig. 3.7 are primarily derived from assumed pigmentation. So melanin might be the dominant chromophore for the absorption spectra of skin with low UV sensitivity but not for skin with high UV sensitivity.

In the UVA, the absorption spectra show most divergence at the low wavelength end. A considerable part of the spectra is characterized by rising absorption coefficients towards 341 nm. This rise cannot be explained by the absorption spectrum of 'pure' melanin but there might be some correlation to the peak of constitutive epidermal melanin pigmentation around 335 nm (compare Fig. 3.4).

The keratin absorption may only play a considerable role in the UVB region of the spectra. Strong keratinization results in a steep increase of absorption towards the short wavelength end of the spectrum adding to the increasing melanin absorption. Judging by the absorption spectra of melanin and keratin and taking the characteristics of the measured skin spectra into account, the absorption coefficients in the wavelength region around 325 nm will allow the best estimation of pigmentation. Subject spectra with similar  $\mu_a$  in this range but strongly diverging absorption towards 290 nm can thus be read in the way that higher UVB absorption coefficients indicate stronger keratinization in the corresponding subject.

At 290 nm, absorption is maximal in nearly all subject spectra, but the mean absorption coefficient may range from  $257 \text{ cm}^{-1}$  for one subject (D.C.) up to  $1276 \text{ cm}^{-1}$  for another (Kr.G.).

For six subjects (L.K., K.K., Kr.G., P.R., Kn.G, and L.U.) the mean absorption coefficients in the range from 290-306 nm - which are most efficient for erythema induction - are well above  $500 \text{ cm}^{-1}$  corresponding to a penetration depth of less than  $20 \mu\text{m}$ , i.e. the maximal thickness of the horny layer in this area. L.K. and K.K are the subjects with the most divergence in their UVB spectra, so maybe keratinization is strongly changing from spot to spot here which would also explain why they are rather UV sensitive phototypes despite the partly high UVB absorption in the dead cell layers of the stratum corneum. L.K. as well as L.U. are regular solarium users which might have some extra keratinization by the UVB-parts of the solarium spectra or simply by dehydration [25]. P.R., Kn.G., and L.U. are all phototype IV. Interestingly, P.R. is a subject with very light skin which would normally be estimated skin type I or II by eye. In this subject, it could indeed be the highly absorbing keratin filter of the stratum corneum that causes the unexpected high MED.

These detailed observations and assumptions may be summarized and condensed in the following generalized statements:

- The absorption spectra at skin sites with low natural sun exposure show characteristics that can mainly be explained by the spectra of constitutive and UVB induced pigmentation as well as of keratin.
- The combination of these influences is probably different for different phototypes. For example, characteristics of constitutive melanin are mostly observed in rather light or UV sensitive phototypes whereas a strong influence of the keratin component is rather found in dark or UV insensitive phototypes.

### 8.3.2 UV-exposed skin

#### natural UV-exposure - dorsal forearm

Skin that is naturally exposed to sunlight should display optical properties different from those that are found in natural low exposure areas (such as the volar aspect of the forearm). The two major adaptation mechanisms presumably influencing the ultraviolet optical properties of skin are pigmentation and hyperkeratinization. A higher pigmentation, i.e. higher concentration of melanin in the epidermis, should show as a broadband increase in UV absorption (compare e.g. Fig. 8.1) whereas stronger keratinization should appear as an increase of absorption primarily in the UVB (compare Fig. 3.5).

The dorsal side of the forearm is a skin area that is naturally exposed to sunlight in the summer months. Of course, the face and the hands are exposed to sunlight over the whole year, but their skin is quite special and thus fairly hard to compare to the volar aspect of the forearm. Still, there are also some relevant differences between the two sides of the forearm. The dorsal aspect of the arm is of course more or less thickly covered with hair. Pigmentation is usually stronger here and might be more irregular than on the volar side. Besides, both epidermis and stratum corneum are thicker on the dorsal side than on the volar aspect - probably the stratum corneum is normally 20-30  $\mu\text{m}$  thick at the dorsal aspect. In order to avoid optoacoustic measurements on hair, the subjects were shaved at the measurement sites if necessary.

Figs. 8.28-8.47 show the mean absorption spectrum at the dorsal side of the forearm and its standard deviation as compared to the mean absorption spectrum at the volar side (see also Sec. 8.3.1) for each subject. The standard deviation of the volar spectrum is omitted for clarity reasons but may be looked up in the previous section (8.3.1). Figures are roughly ordered according to 'recent UV-exposure' groups as the study was conducted in late summer: the sunlight exposure conditions of the first three subjects (G.O., Kr.G., and W.K.) are unknown, but at least Kr.G. and W.K. indicated that they would not deliberately

seek the sun; the next 5 subjects (S.R., K.K., P.R., M.M., and K.H.) are indoor workers who did not report a marked preference for outdoor activities in their leisure time nor a recent holiday; M.H. reported a recent short holiday but is an indoor worker; the following 6 subjects (K.B., Kn.G., L.U., B.I., W.M., and L.K.) reported to have spent a considerable part of their leisure time outdoors in the previous weeks; E.R. and F.M. reported outdoor holidays that ended about four weeks before the study; and the last group of 3 subjects (D.C., K.I., and H.M.) just came back from their summer holidays when they entered the study. Within these groups, the subjects were sorted according to their difference in skin brightness  $L^*$  between volar and dorsal optoacoustic measurement site, as measured by a chromameter. Positive values of this difference  $\Delta L^* = L^*_{volar} - L^*_{dorsal}$  indicate darker skin.

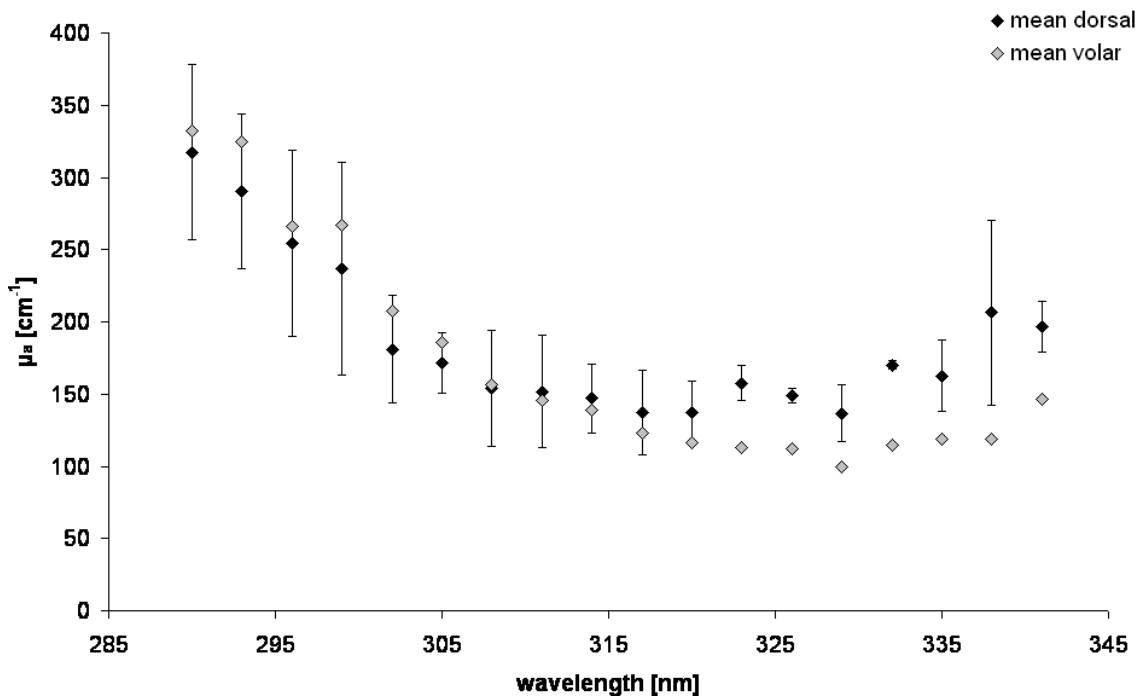


**Figure 8.28:** Spectra of  $\mu_a$  on the volar and dorsal aspect of the forearm. Subject G.O.: even (light) pigmentation. Phototype: I.  $L^*_{volar} - L^*_{dorsal} = -0.77$ .

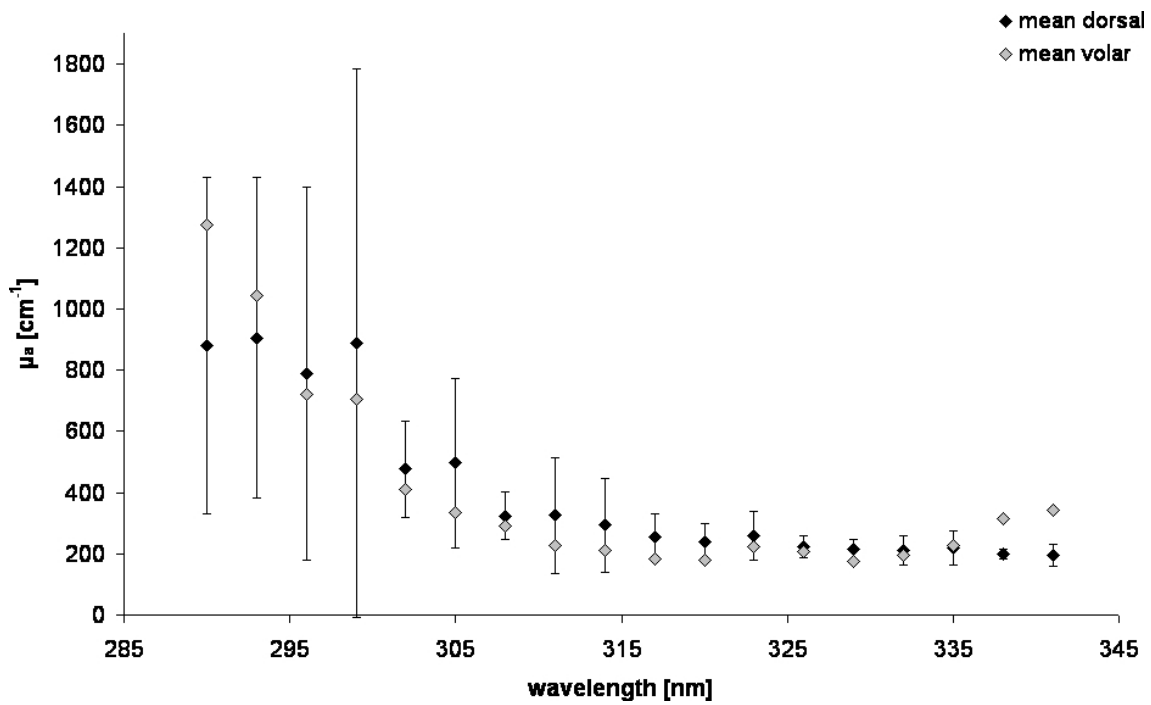


**Figure 8.29:** Spectra of  $\mu_a$  on the volar and dorsal aspect of the forearm. Subject Kr.G.: fairly inelastic skin. Phototype: II.  $L^*_{volar} - L^*_{dorsal} = 6.55$ .

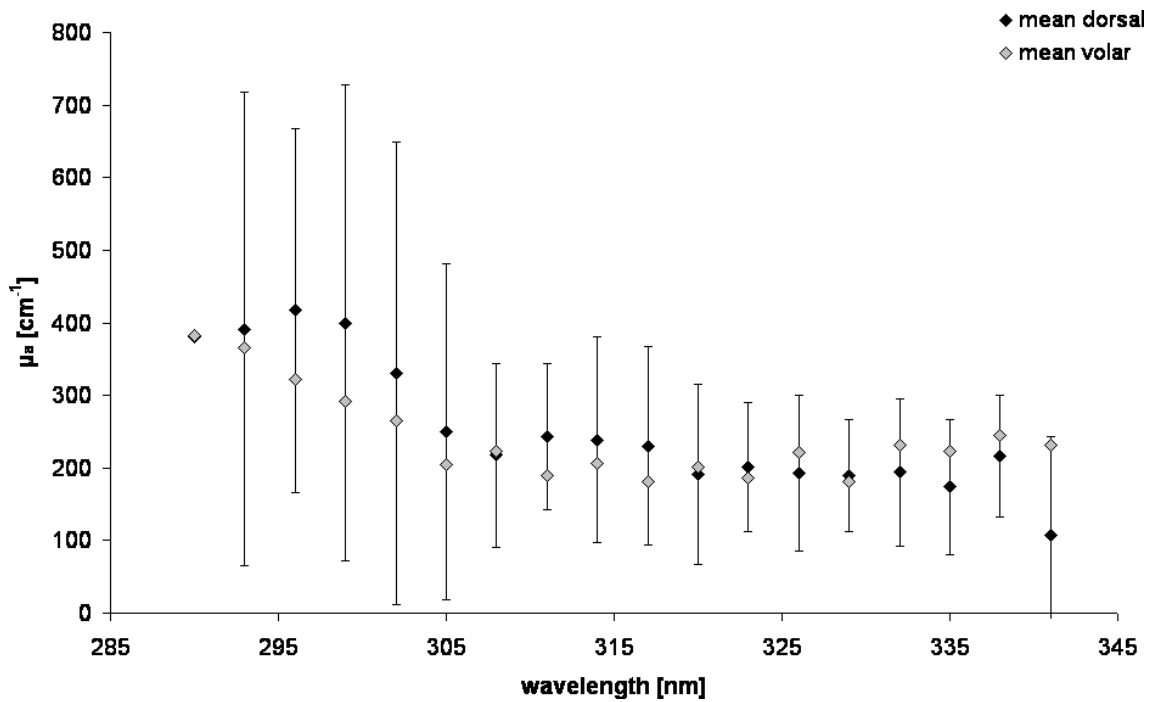


**Figure 8.30:** Spectra of  $\mu_a$  on the volar and dorsal aspect of the forearm. Subject W.K.: very dark hair. Phototype: II.  $L^*_{volar} - L^*_{dorsal} = 12.13$ .

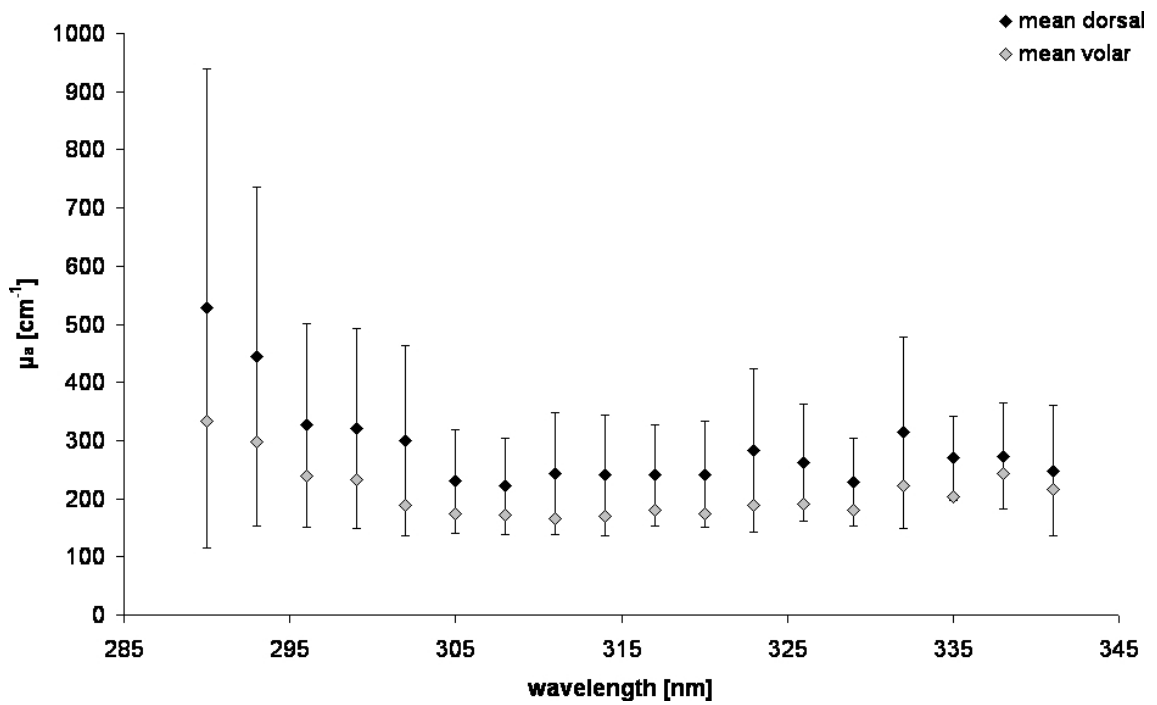


**Figure 8.31:** Spectra of  $\mu_a$  on the volar and dorsal aspect of the forearm. Subject S.R. Phototype: III.  $L^*_{volar} - L^*_{dorsal} = -1.32$ .

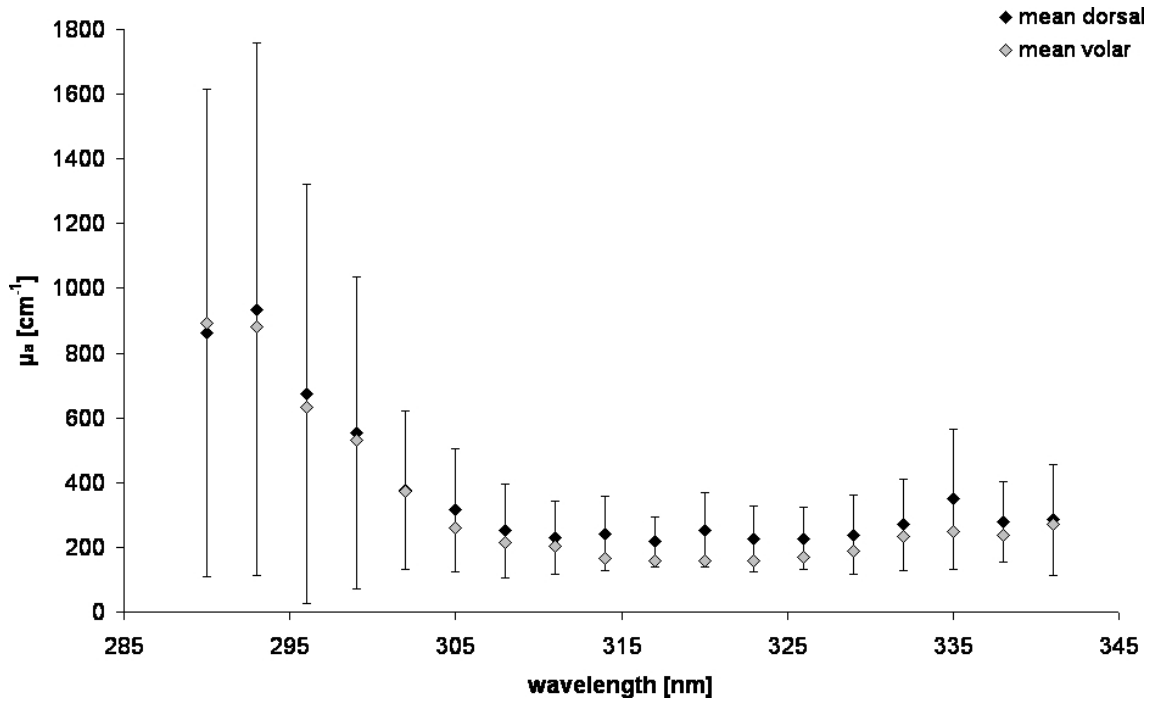


**Figure 8.32:** Spectra of  $\mu_a$  on the volar and dorsal aspect of the forearm. Subject K.K. Phototype: II.  $L^*_{volar} - L^*_{dorsal} = -0.69$ .

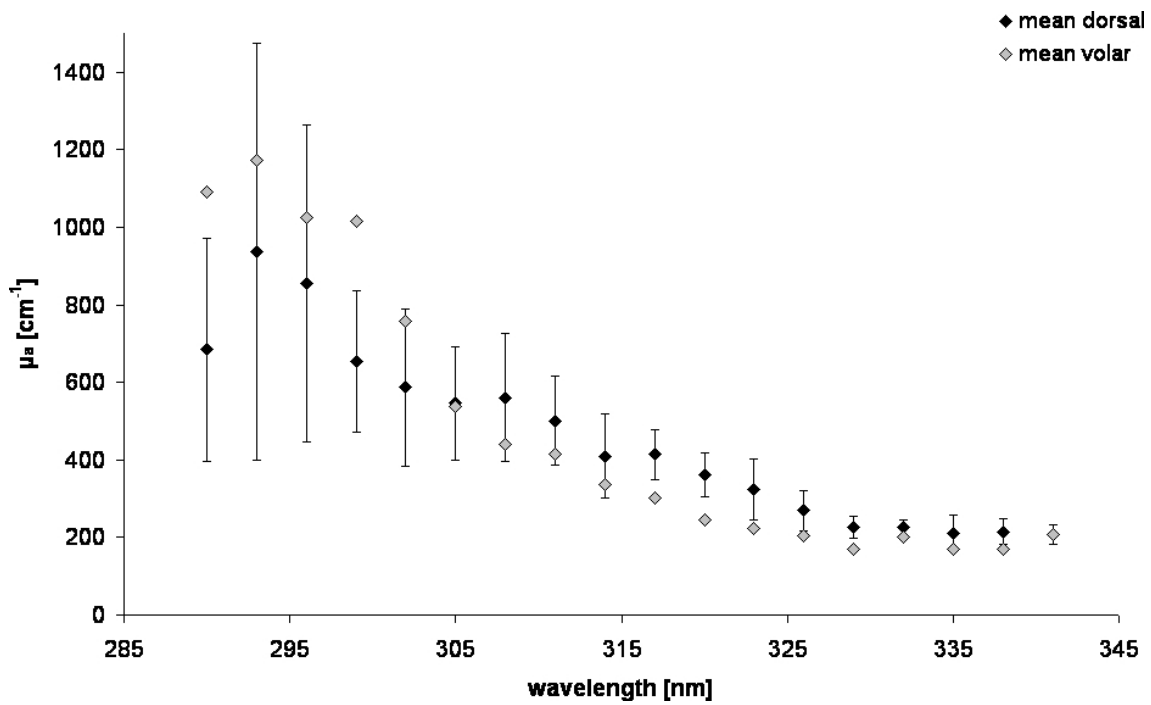


**Figure 8.33:** Spectra of  $\mu_a$  on the volar and dorsal aspect of the forearm. Subject P.R.: very light, ashen complexion. Phototype: IV.  $L^*_{volar}-L^*_{dorsal}=1.94$ .

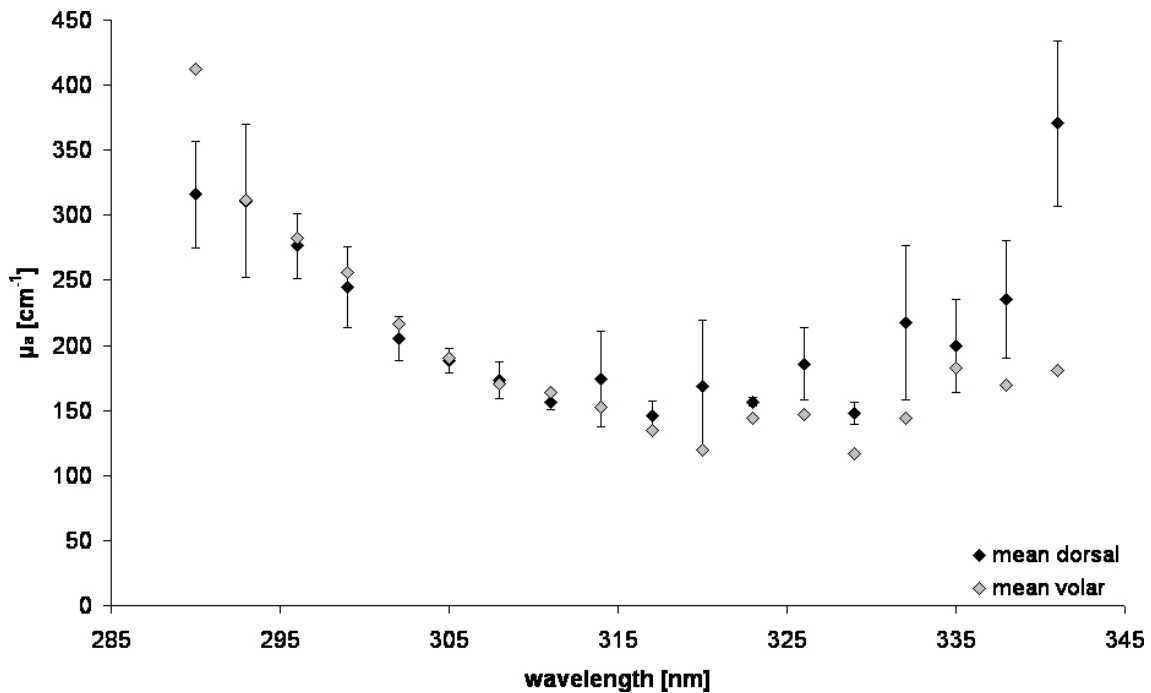


**Figure 8.34:** Spectra of  $\mu_a$  on the volar and dorsal aspect of the forearm. Subject M.M.: even (very light) pigmentation. Phototype I.  $L^*_{volar}-L^*_{dorsal}=2.07$ .



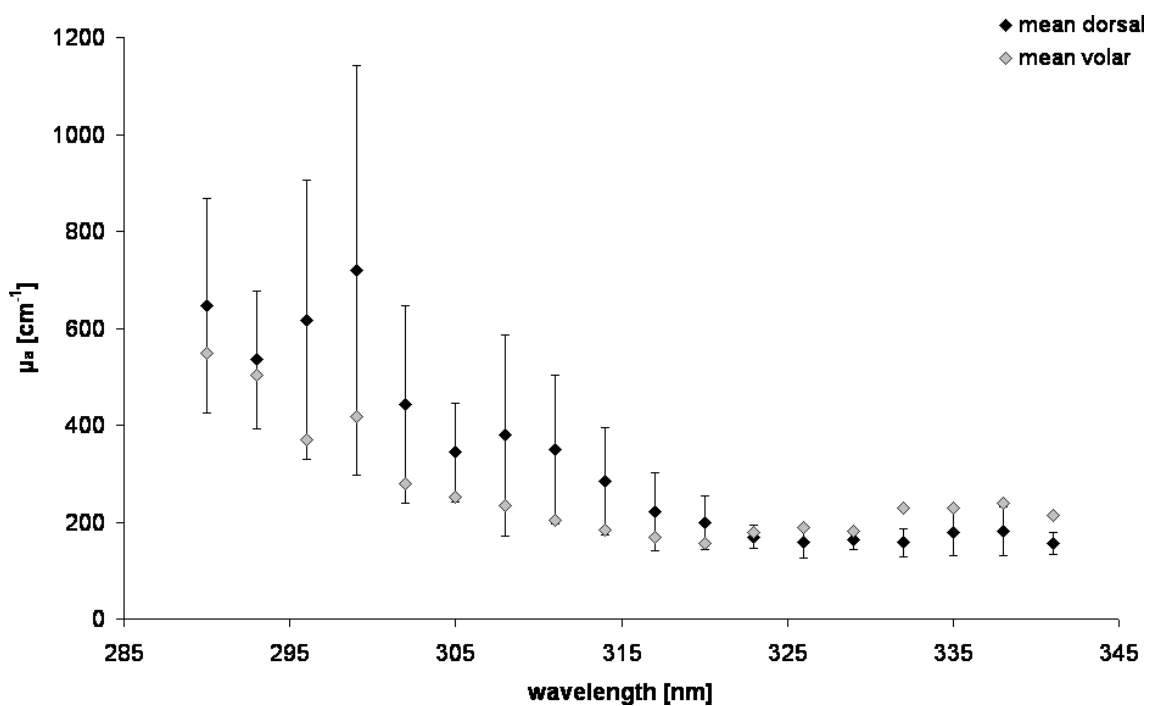


**Figure 8.35:** Spectra of  $\mu_a$  on the volar and dorsal aspect of the forearm. Subject K.H. Phototype: II.  $L^*_{volar}-L^*_{dorsal}= 4.96$ .

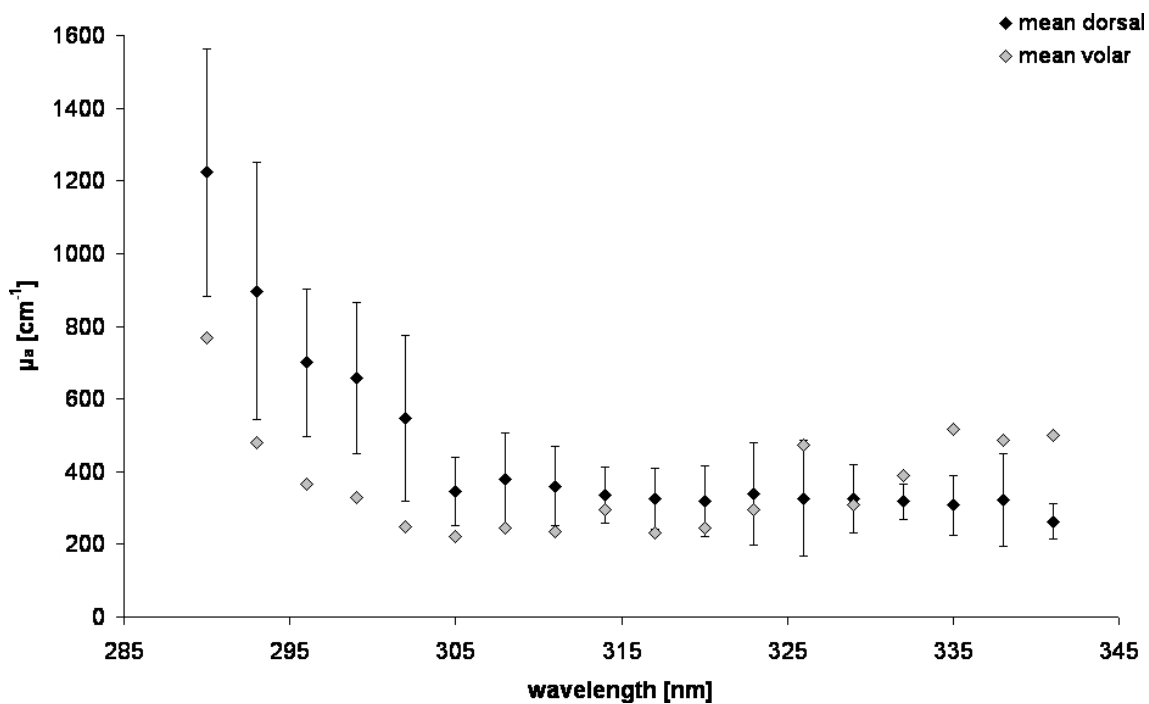


**Figure 8.36:** Spectra of  $\mu_a$  on the volar and dorsal aspect of the forearm. Subject M.H. Phototype II.  $L^*_{volar}-L^*_{dorsal}= 10.07$ .

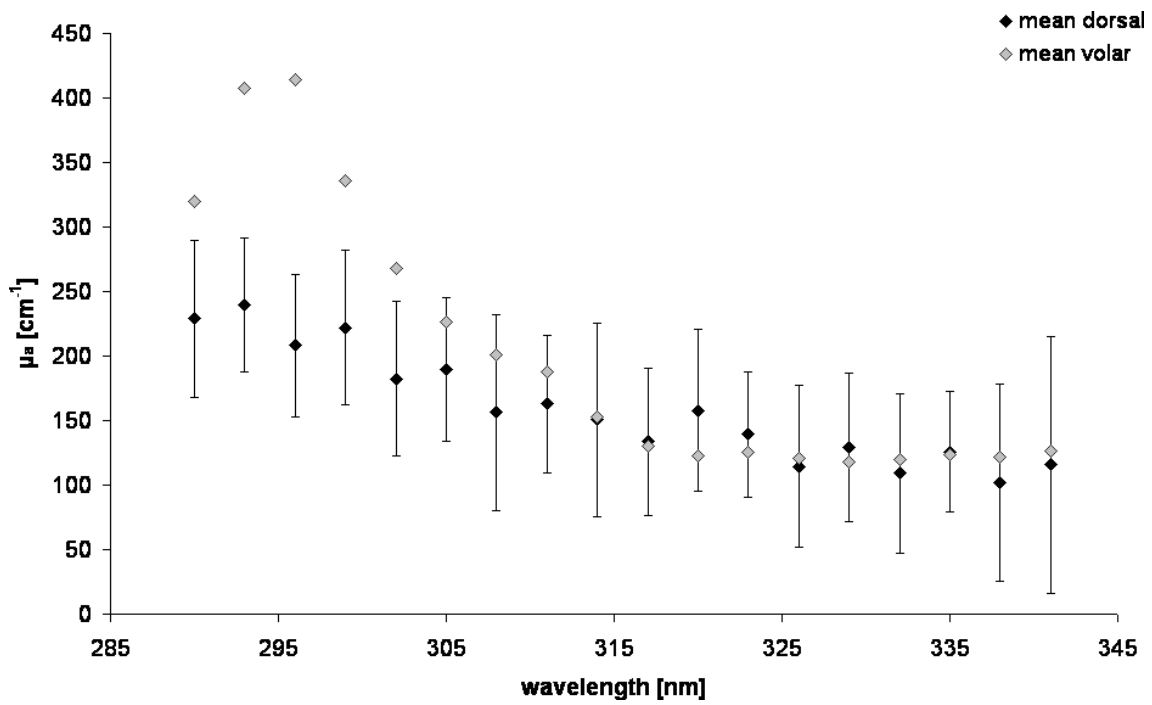


**Figure 8.37:** Spectra of  $\mu_a$  on the volar and dorsal aspect of the forearm. Subject K.B. Phototype: IV.  $L^*_{volar}-L^*_{dorsal}=6.57$ .

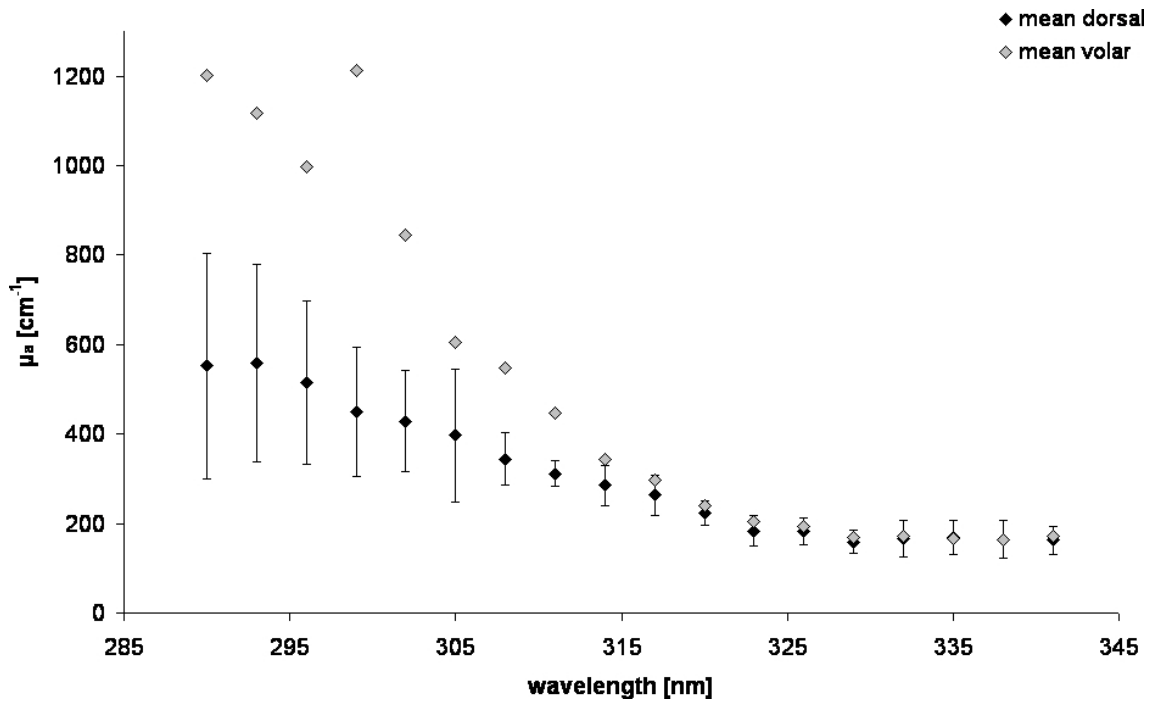


**Figure 8.38:** Spectra of  $\mu_a$  on the volar and dorsal aspect of the forearm. Subject Kn.G.: very dense freckled pigmentation. Phototype: IV.  $L^*_{volar}-L^*_{dorsal}=7.78$ .

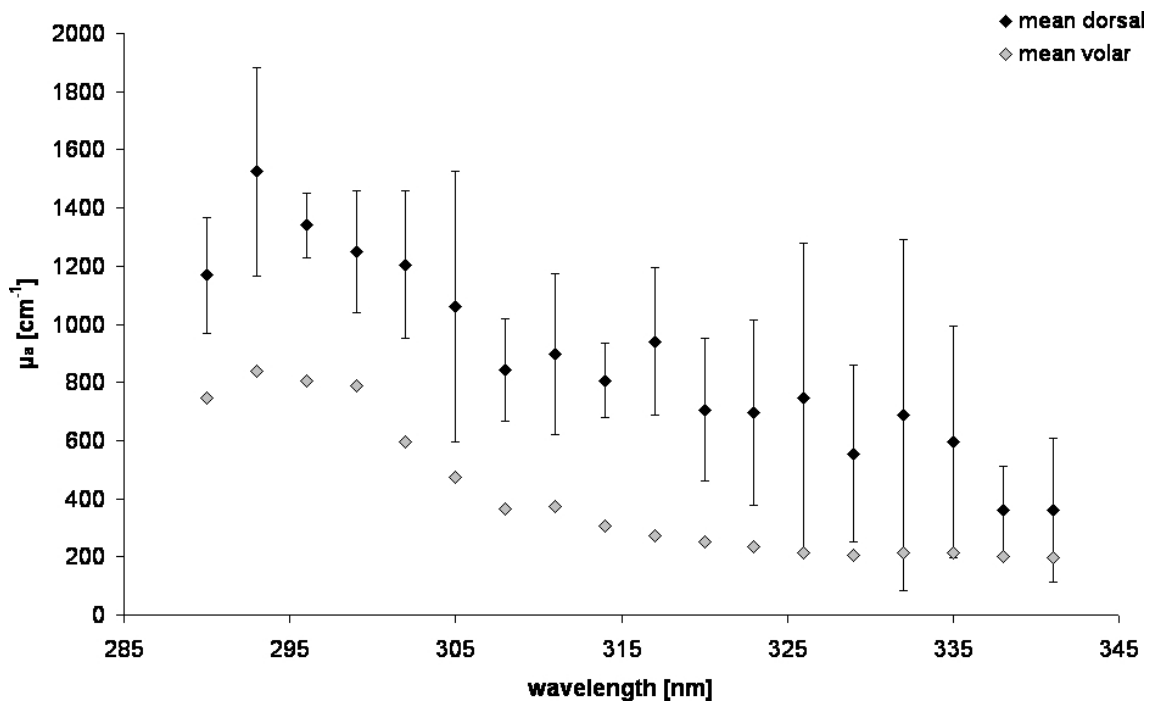


**Figure 8.39:** Spectra of  $\mu_a$  on the volar and dorsal aspect of the forearm. Subject L.U.: fairly inelastic skin, solarium user (very high weekly doses). Phototype: IV.  $L^*_{\text{volar}}-L^*_{\text{dorsal}}=6.67$ .

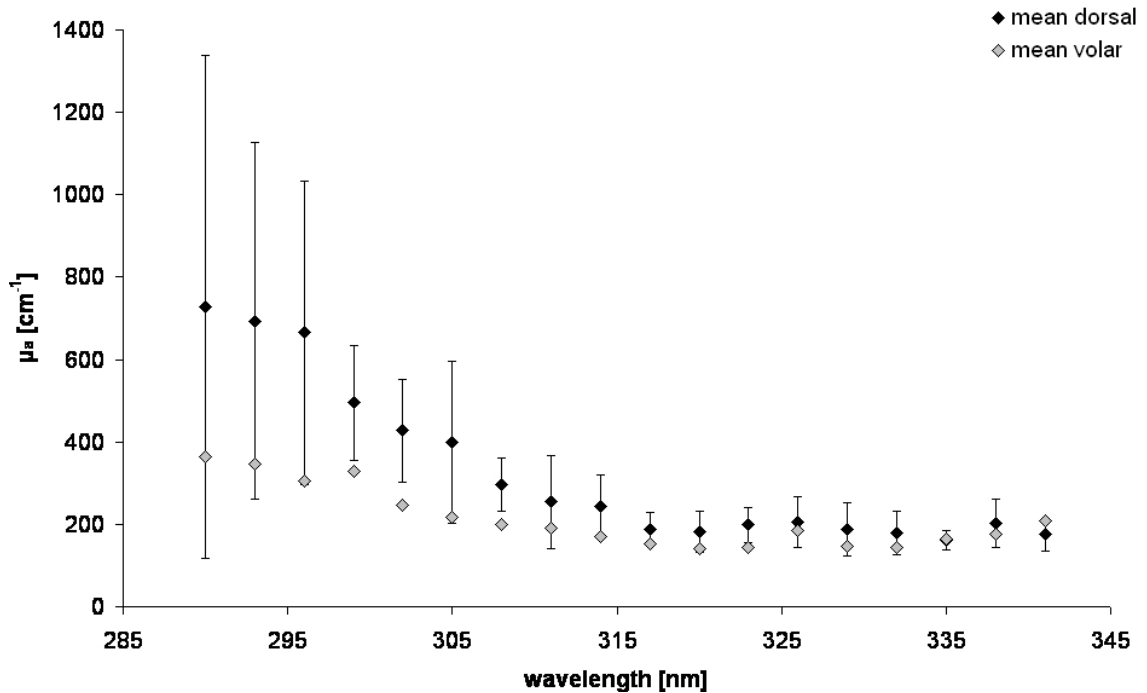


**Figure 8.40:** Spectra of  $\mu_a$  on the volar and dorsal aspect of the forearm. Subject B.I.: garden-worker, freckly, blotchy tan. Phototype: IV.  $L^*_{\text{volar}}-L^*_{\text{dorsal}}=8.03$ .

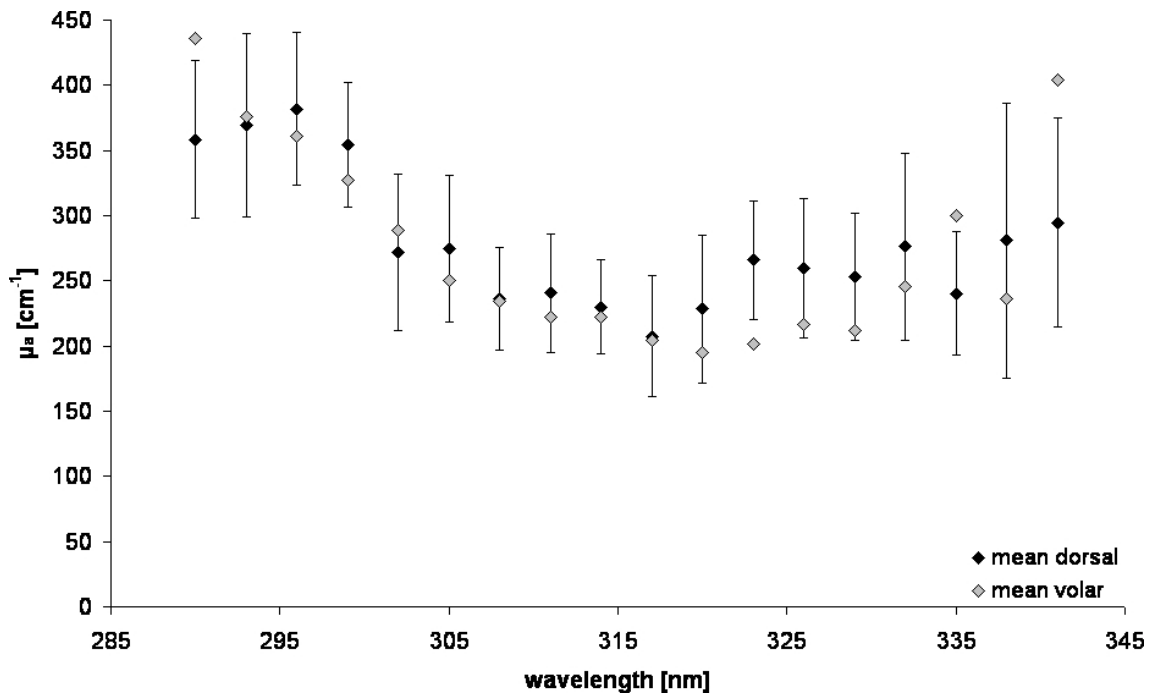


**Figure 8.41:** Spectra of  $\mu_a$  on the volar and dorsal aspect of the forearm. Subject W.M.: garden-worker, i.e. strong, even tan. Phototype: III.  $L^*_{volar}-L^*_{dorsal}=8.14$ .

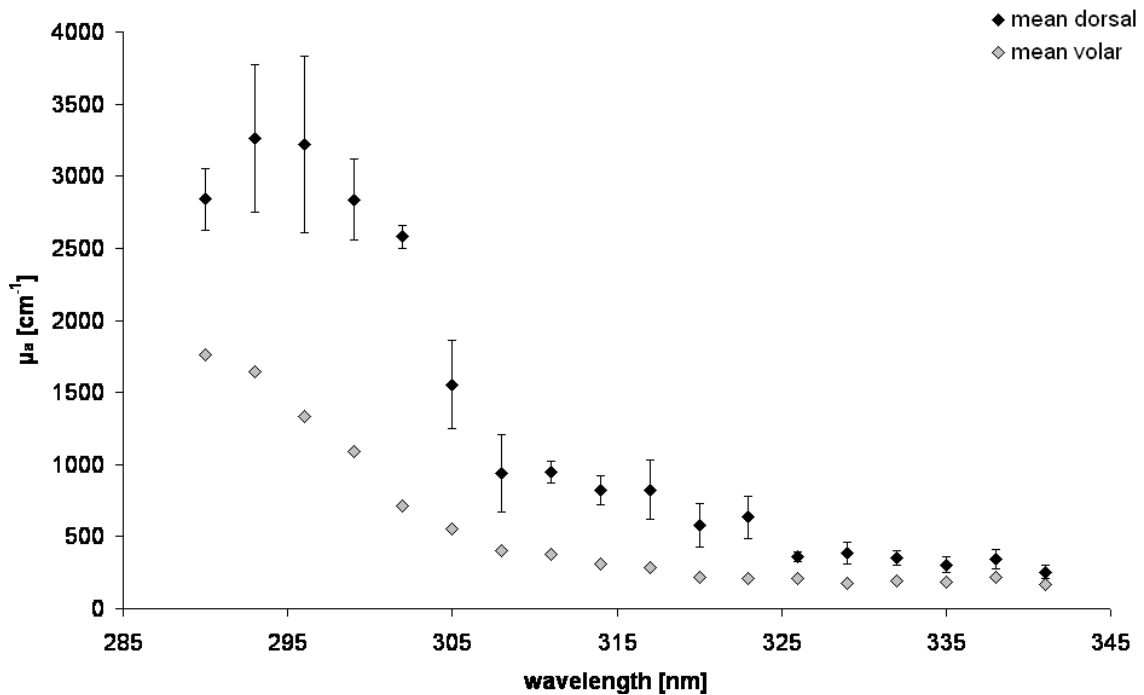


**Figure 8.42:** Spectra of  $\mu_a$  on the volar and dorsal aspect of the forearm. Subject L.K.: solarium user (weekly). Phototype I.  $L^*_{volar}-L^*_{dorsal}=10.08$ .

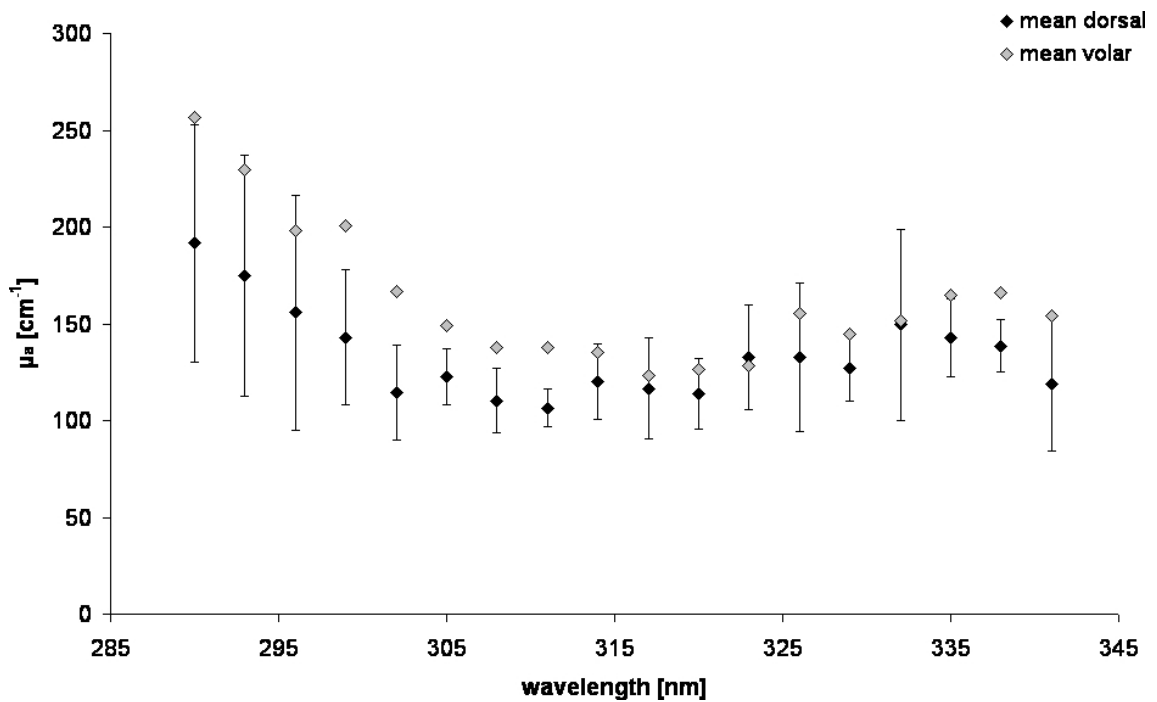


**Figure 8.43:** Spectra of  $\mu_a$  on the volar and dorsal aspect of the forearm. Subject E.R.: very soft, sensitive skin. Phototype: II.  $L^*_{volar}-L^*_{dorsal}=5.34$ .

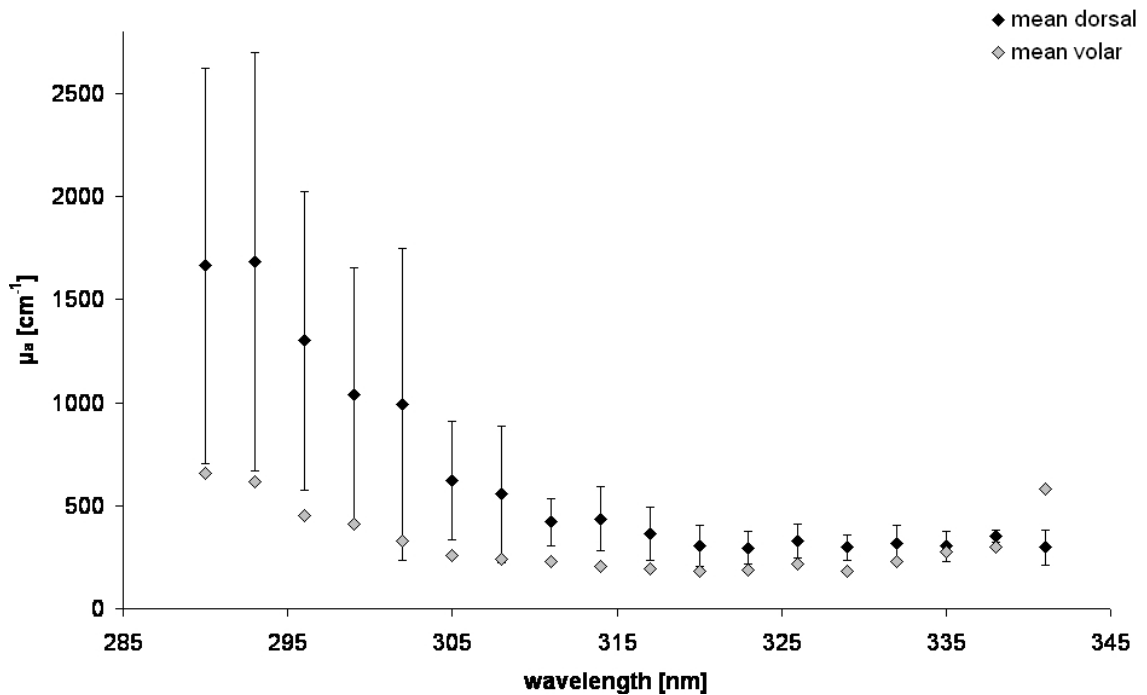


**Figure 8.44:** Spectra of  $\mu_a$  on the volar and dorsal aspect of the forearm. Subject F.M.: very densely freckled skin. Phototype: III.  $L^*_{volar}-L^*_{dorsal}=10.24$ .

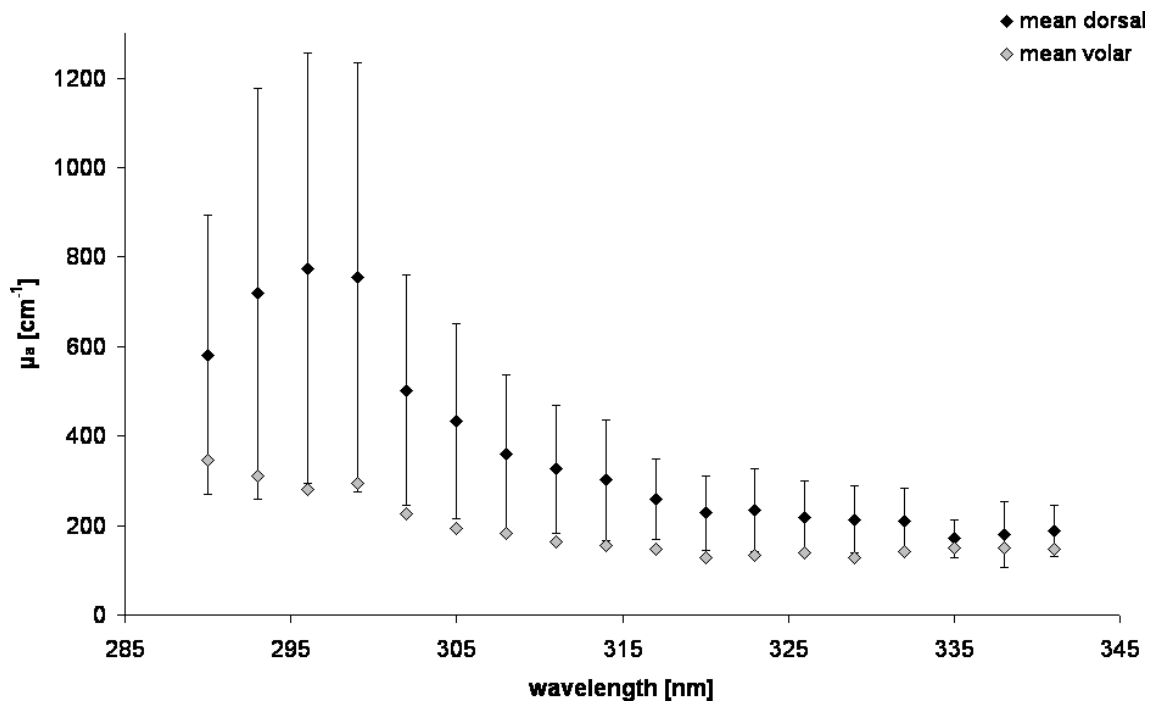


**Figure 8.45:** Spectra of  $\mu_a$  on the volar and dorsal aspect of the forearm. Subject D.C.: recent holiday, even mild tan. Phototype: III.  $L^*_{volar}-L^*_{dorsal}= 5.48$ .

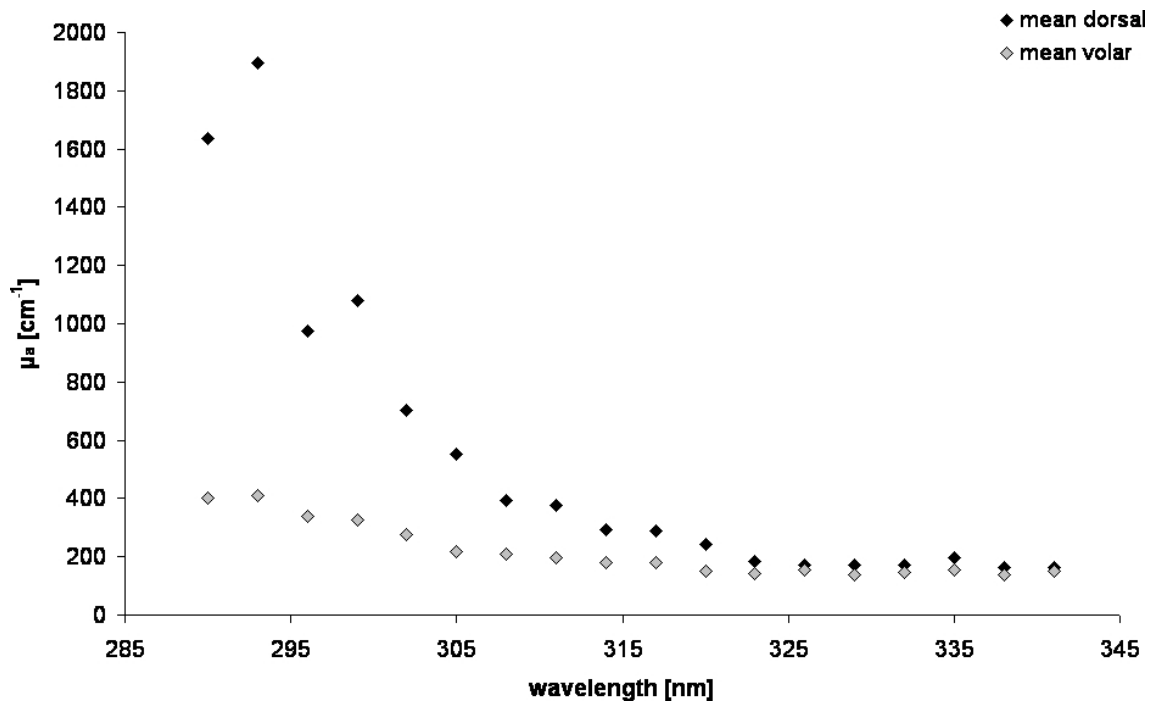


**Figure 8.46:** Spectra of  $\mu_a$  on the volar and dorsal aspect of the forearm. Subject K.I.: recent biking holiday. Phototype: III.  $L^*_{volar}-L^*_{dorsal}= 6.07$ .

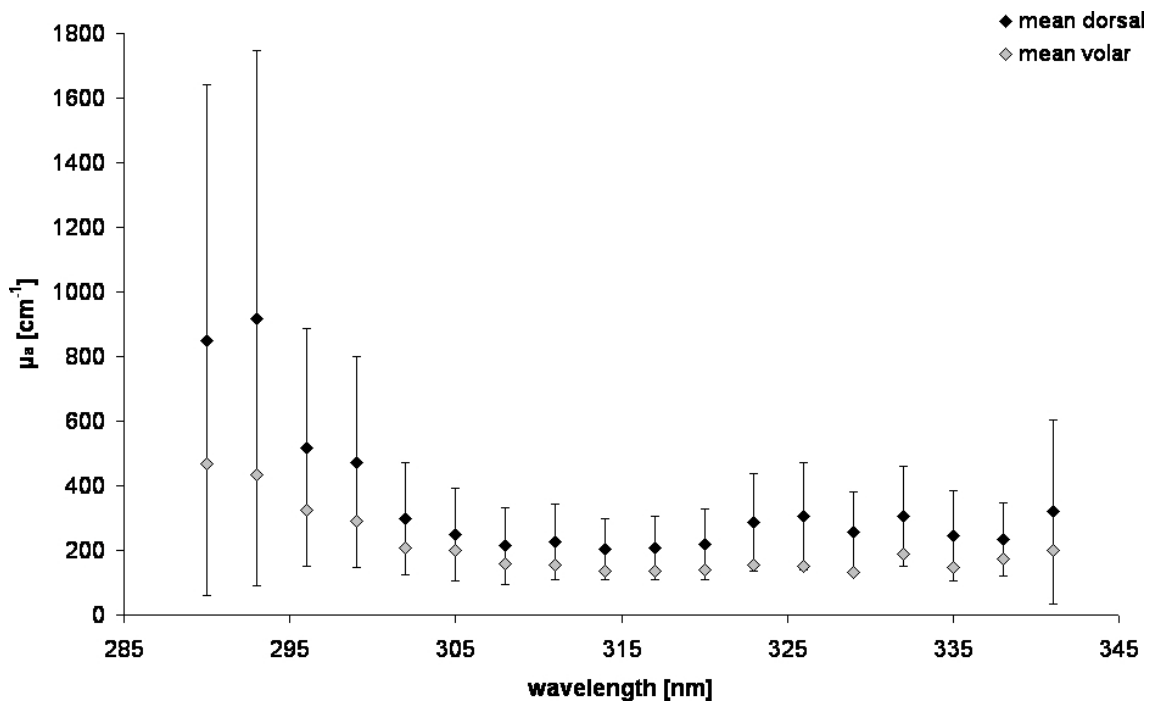


**Figure 8.47:** Spectra of  $\mu_a$  on the volar and dorsal aspect of the forearm. Subject H.M.: recent holiday/sun bathing. Phototype: II.  $L^*_{volar} - L^*_{dorsal} = 7.18$ .

Bearing in mind the similarities or differences among the spectra obtained at the volar aspect of the forearm, remarkable spectral differences between mean volar and mean dorsal spectra are found in some subjects.

One group of subjects does not show marked differences between the two mean absorption spectra. For 6 subjects (Kr.G., W.K., S.R., K.K., K.H., and H.M.) 90 % or more of the mean absorption coefficients for the volar aspect of the forearm lie within the standard deviation of the corresponding dorsal measurement. The impression of agreement is enhanced by the fact, that most corresponding  $\mu_a$  values lie fairly close to each other. For S.R. and H.M. the absorption coefficients of the dorsal aspect are higher than those at the volar throughout the spectrum, indicating maybe a slight increase in melanin pigmentation. Another three subjects' spectra do not fulfill the 90 % criterion but are still very similar: P.R., M.M., and W.M.. So, all the indoor workers and the two subjects with unknown but presumably non-sunseeking behaviour show only negligible differences in their volar and dorsal absorption spectra.

Looking at the other three subjects with similar dorsal and volar spectra, W.M. belongs to the 'outdoor' group and H.M. to the 'recent holiday' group. W.M. is an extreme case with respect to the ratio of UVB to UVA absorption at both skin sites. This subject shows the highest UVA absorption compared to the UVB absorption within the same subject. Only M.H. and M.M. show similar characteristics, but the former only on the volar aspect and the latter only on the dorsal aspect of the arm.

H.M. also belongs to another group with comparable spectral characteristics. This second

group includes all subjects with higher absorption coefficients on the dorsal than on the volar aspect throughout the spectrum (one outlier permitted): F.M., B.I., H.M., L.U., L.K., D.C., K.I., S.R., and K.K.. Interestingly, seven of them belong to the groups subject to rather high UV exposure (outdoor leisure time or holiday). Only the last two of this group belong to the 'indoor workers' again. However, these two cannot compete with the rest, as far as the difference between their volar and dorsal spectra are concerned. Especially for K.K., the difference between the respective volar and dorsal absorption is very small and for both, the difference does not show a pronounced spectral characteristic. Apart from L.U. and H.M., the rest of this group shows a strong increase of the difference between dorsal and volar absorption coefficients towards shorter wavelengths. In H.M., this characteristic is weaker and L.U. shows a noticeable difference between the two corresponding  $\mu_a$ -values throughout the spectrum with no remarkable spectral dependence.

So far, G.O., E.R., M.H., K.B. and Kn.G. have not been assigned to a special group. The spectra of G.O. and E.R. do not show a pronounced difference between dorsal and volar  $\mu_a$ -values. In G.O., UVA absorption is enhanced at the dorsal aspect whereas the E.R. spectra are characterized by the fact that they are the only pair where volar absorption is higher than dorsal absorption throughout the spectrum (one outlier permitted). The dorsal spectrum from M.H. again shows increased UVB absorption but weaker than that characteristic for the high UV exposure spectra and even a decrease of  $\mu_a$  at the long wavelength end. K.B. and Kn.G. again show similar but surprising spectral characteristics: the UVA absorption coefficients of both sites are very similar and the pronounced increase in UVB that was found on the volar side of the arm here is not present at the dorsal side.

Recapitulating, the overall picture developed by analyzing the natural pigmentation spectra shows the following tendencies:

- Spectra characteristic for subjects accumulating relatively high natural UV doses show increased  $\mu_a$  values at the dorsal aspect of the forearm compared to the volar aspect throughout the UVB and UVA-II spectrum. The difference of dorsal and volar absorption coefficients is (strongly) increasing towards shorter wavelengths.
- Subjects with low sun exposure, i.e. indoor workers, display small to negligible differences in the spectra of the volar and dorsal aspect of the forearm.

These characteristics can be explained by looking at the absorption spectra of the two chromophores most important in UV adaptation mechanisms: melanin and keratin (compare Sec. 3.2.1 again for the relevant spectra).

As already mentioned at different points throughout this chapter, stronger melanin pigmentation should result in an overall increase of  $\mu_a$  values. According to the constitutive pigmentation spectrum, the increase should be most prominent in the UVA-II. Hyperkeratinization, i.e. thickening of the horny layer, on the other hand will become primarily



noticeable as comparably steeply increasing UVB absorption. The indication of a strong increase of keratin content is only present in spectra of subjects belonging to the 'high UV exposure groups'. Judging by the subjects' spectra, the effect of hyperkeratinization is much stronger than the effect of melanogenesis. This observation is in accordance with the fact that the thickening of the horny layer is able to provide a much higher natural sun protection factor than melanogenesis.

The **change of skin brightness  $L^*$**  from the inner part to the outer part of the arm should provide an additional value for comparison of the UV exposure spectra. This value  $\Delta L^* = L^*_{volar} - L^*_{dorsal}$  is also indicated in the figure captions of Figs. 8.28-8.47. For comparison, the differences of the dorsal and volar absorption coefficients weighted by the absorption coefficient at 315 nm are shown for each subject in Figs. 8.48 and 8.49.

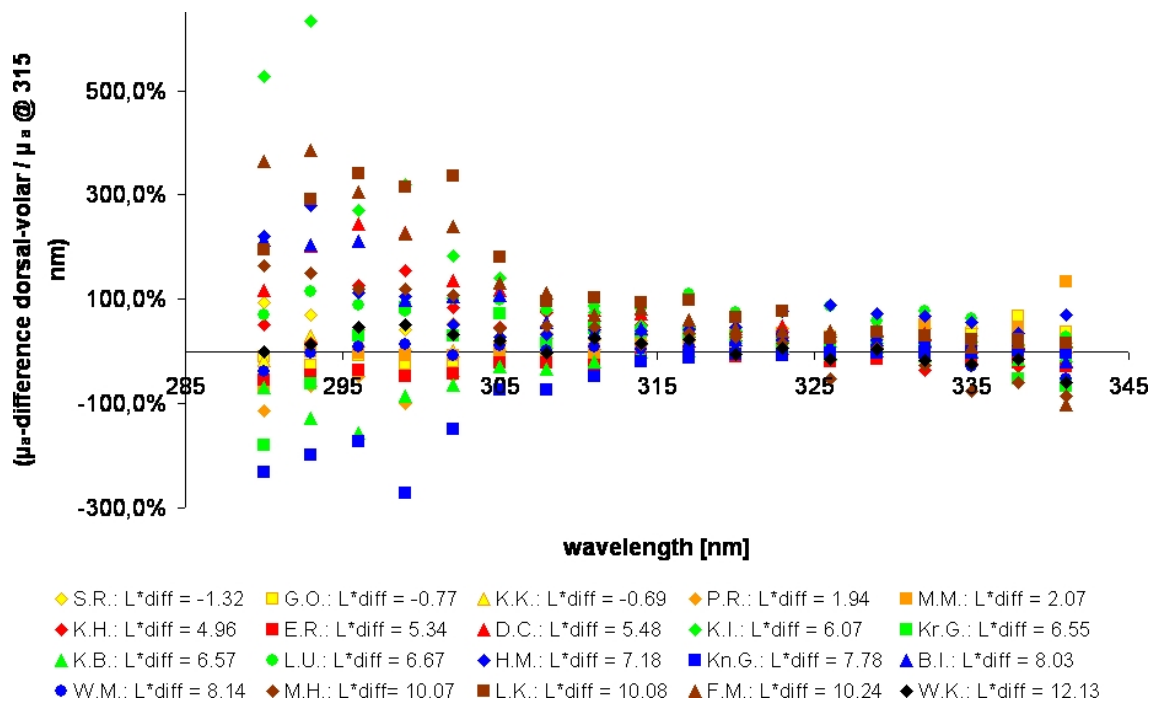


**Figure 8.48:** Spectra of the absorption coefficient differences of the dorsal and volar aspect of the forearm. Subjects are colour coded according to similar ranges in  $L^*$ -value difference  $\Delta L^*$  between volar and dorsal aspect.

Figure 8.48 shows the absorption difference spectra colour coded for  $L^*$  change. There is a tendency for small  $\Delta L^*$  (yellow and orange) to have spectra with comparably small  $\mu_a$  differences - as would have been expected. As well there is a tendency for difference spectra belonging to subjects with large  $\Delta L^*$  between volar and dorsal aspect (e.g. brown) to show large differences in the  $\mu_a$  difference spectra in the UVB. However, there are also outliers such as K.B., Kn.G. or W.K. who all are characterized by fairly high  $\Delta L^*$  between dorsal and volar aspect not matching the impression from the low  $\mu_a$  difference spectra. The former two are marked by lower  $\mu_a$  values on the dorsal aspect and correspondingly by negative values in the  $\mu_a$  difference spectrum. This was already discussed previously.

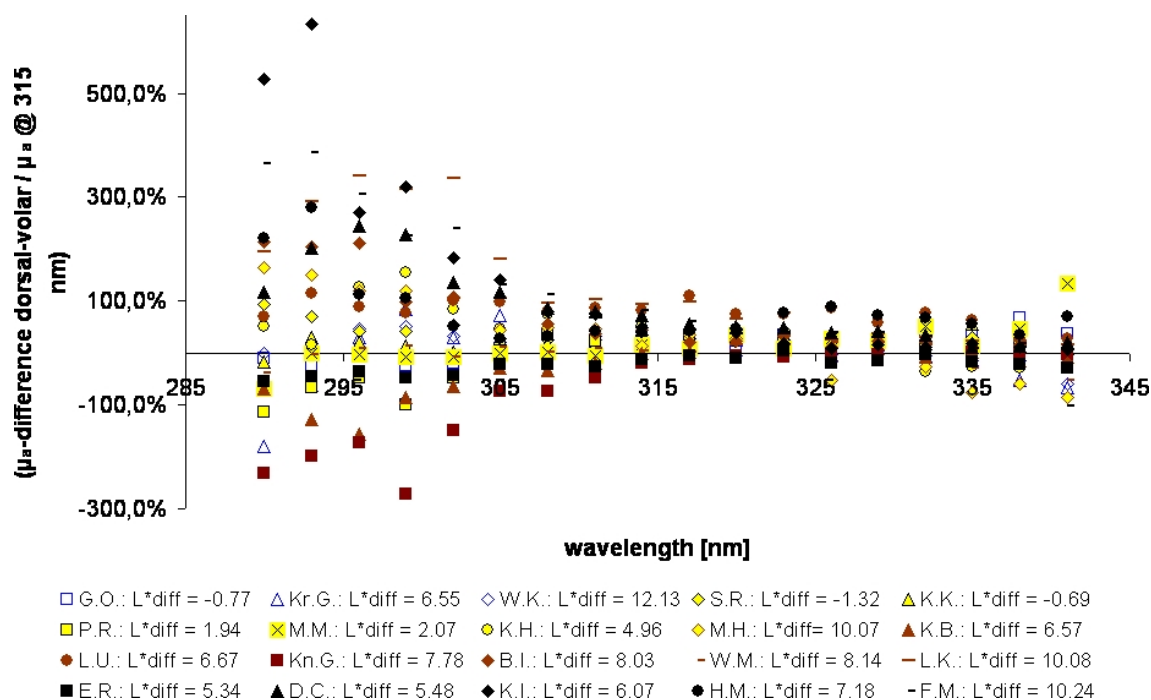


**Figure 8.49:** Spectra of the absorption coefficient differences of the dorsal and volar aspect of the forearm. Subjects are colour coded according to their UV exposure groups: blue outline - unknown/presumably low UV exposure; yellow/black outline - indoor workers; yellow/brown outline - indoor worker with recent short holiday trip; brown - outdoor leisure time; black - recent holiday.

Subject W.K. is contradictory in the way that the  $\Delta L^*$  is largest at this arm but still, the corresponding  $\mu_a$  spectrum pair is one of the closest in all subjects.

Fig. 8.49 shows the same spectra but this time colour coded according to the UV exposure groups. If Kn.G. and K.B. are considered to be outliers due to their extraordinary optical properties in the UVB (see Figs. 8.38 and 8.37), then only the difference spectrum of E.R. does not fit properly into the grouping of the subject spectra: people spending most of their time indoors display comparably low differences in the spectra of the volar and dorsal aspect of the forearm, whereas high  $\mu_a$  differences especially in the UVB part of the spectrum are features of people subject to fairly high UV doses.

Thus in summary, the change of optical properties and the change in skin brightness  $\Delta L^*$  agree fairly well for the comparison of the dorsal and the volar aspect of the forearm.

### 8.3.3 Intraindividual comparison of skin sites

In this section, the previous results are put into the context of all skin sites measured in the subject study. For this purpose, the previously shown absorption spectra of volar and dorsal forearm are completed by the spectra obtained by optoacoustic measurements at

the thenar and at the MED-site 72h after irradiation.

Measurements at the thenar were carried out to receive pure horny layer spectra as the stratum corneum is particularly thick at this site. These data will allow a more profound assessment of the question which characteristics of the human in vivo spectra are to be assigned to which chromophore: on the one hand the number of melanocytes is particularly low at the palm resulting in low pigmentation while on the other hand the thick stratum corneum's optical properties should be dominated by keratin.

The measurements at the MED-site 72h after irradiation were carried out to see whether one minimal erythema dose (MED) could induce a marked change in optical properties be it by thickening of the horny layer or melanogenesis. As persistent pigment darkening (PPD) peaks 72h after irradiation, this point in time was chosen for the additional determination of the optical properties at this site. Of course, the minimal melanogenic dose is normally higher than one MED, so only small effects if any are expected as far as pigmentation is concerned.

Figs. 8.50-8.69 show the mean spectra of all optoacoustic measurement sites: volar and dorsal aspect of forearm, site at volar aspect of forearm exposed to one MED 72h after irradiation, and the thenar. This time, the figures are sorted simply in the order of the subject's appearance in the laboratory so that measurements on the same day will usually appear next to each other. Standard deviations are omitted again in favor of a more concise presentation of the spectra. If desired, standard deviations for volar and dorsal forearm spectra from the previous sections may be consulted to get an impression of the typical order of magnitude of this value. Auxiliary lines are given to allow easier access to the absolute values of the data given in the diagrams. For maximal ranges of  $\mu_a$  up to  $1000\text{ cm}^{-1}$  auxiliary lines segment the diagram every  $100\text{ cm}^{-1}$ , for larger scales a segmentation of  $200\text{ cm}^{-1}$  is applied.

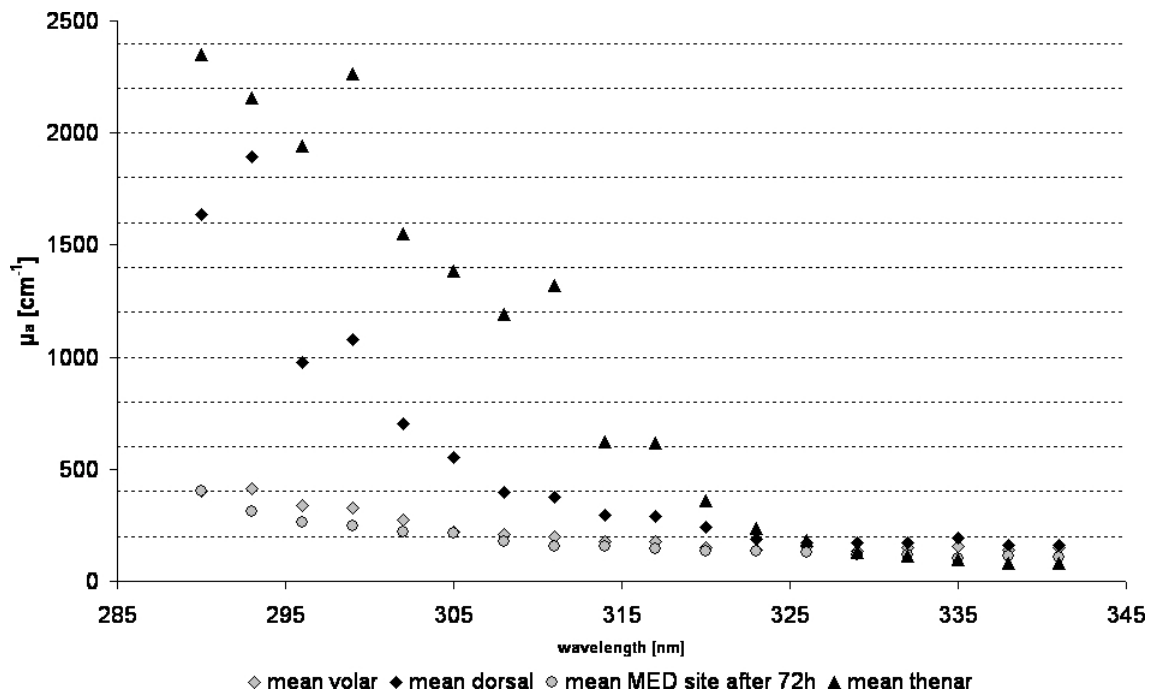


Figure 8.50: Overview of the mean, optoacoustically measured absorption spectra of subject K.I..

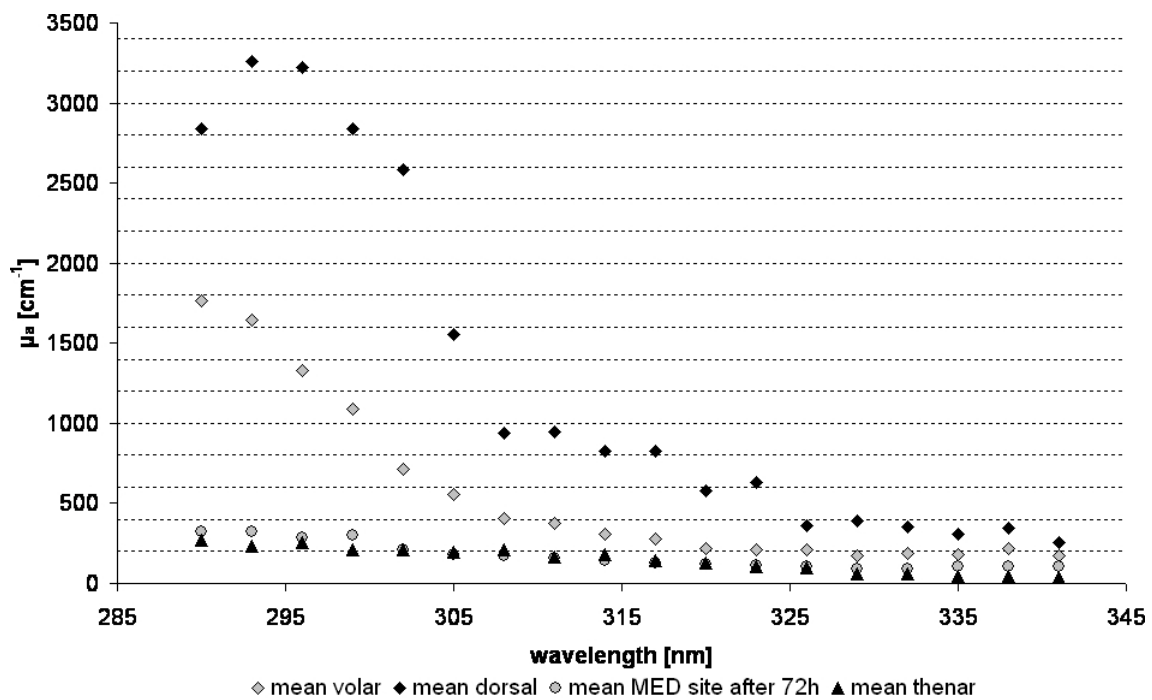


Figure 8.51: Overview of the mean, optoacoustically measured absorption spectra of subject L.K..

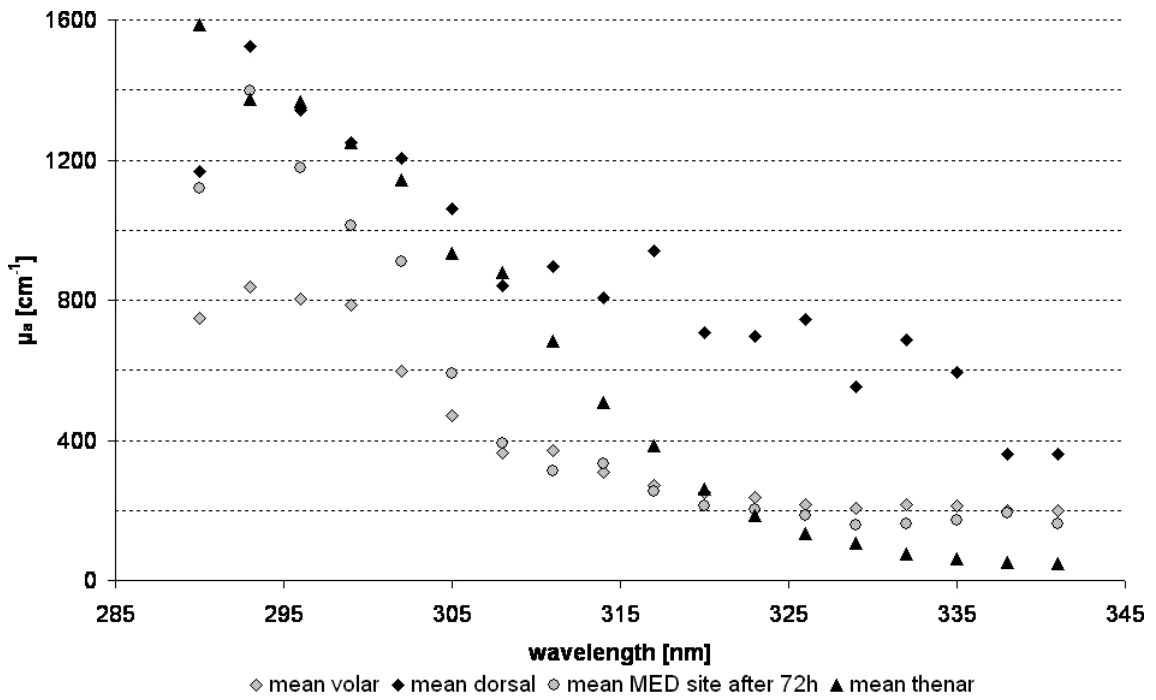


Figure 8.52: Overview of the mean, optoacoustically measured absorption spectra of subject L.U..

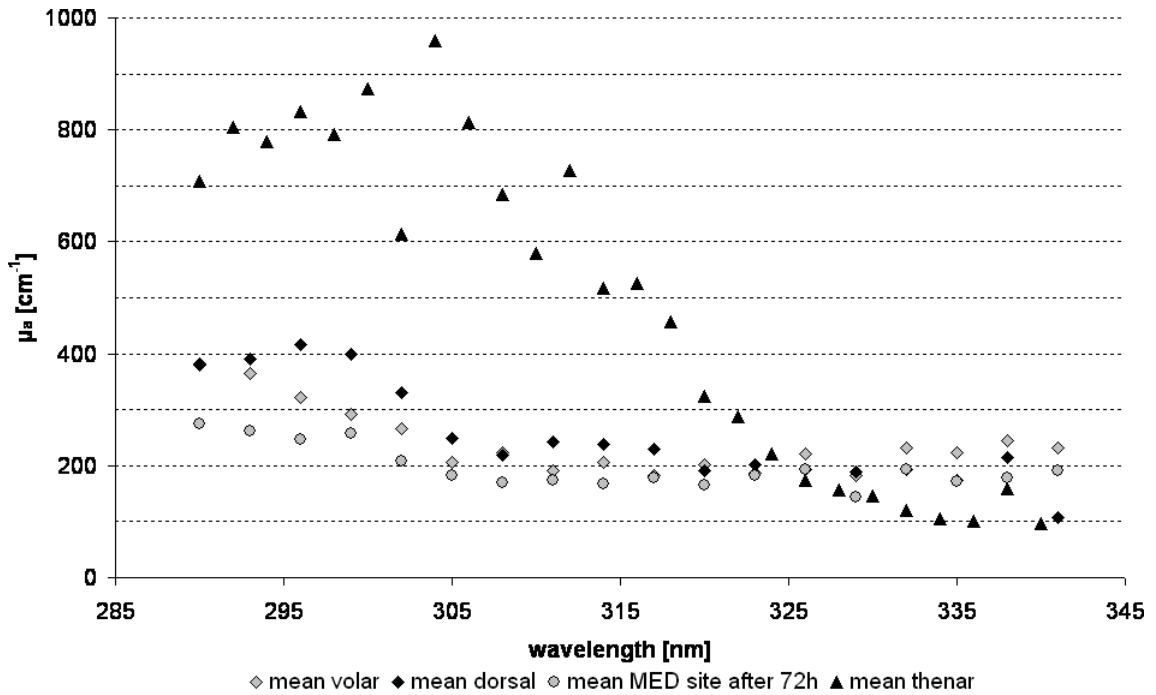


Figure 8.53: Overview of the mean, optoacoustically measured absorption spectra of subject W.K..

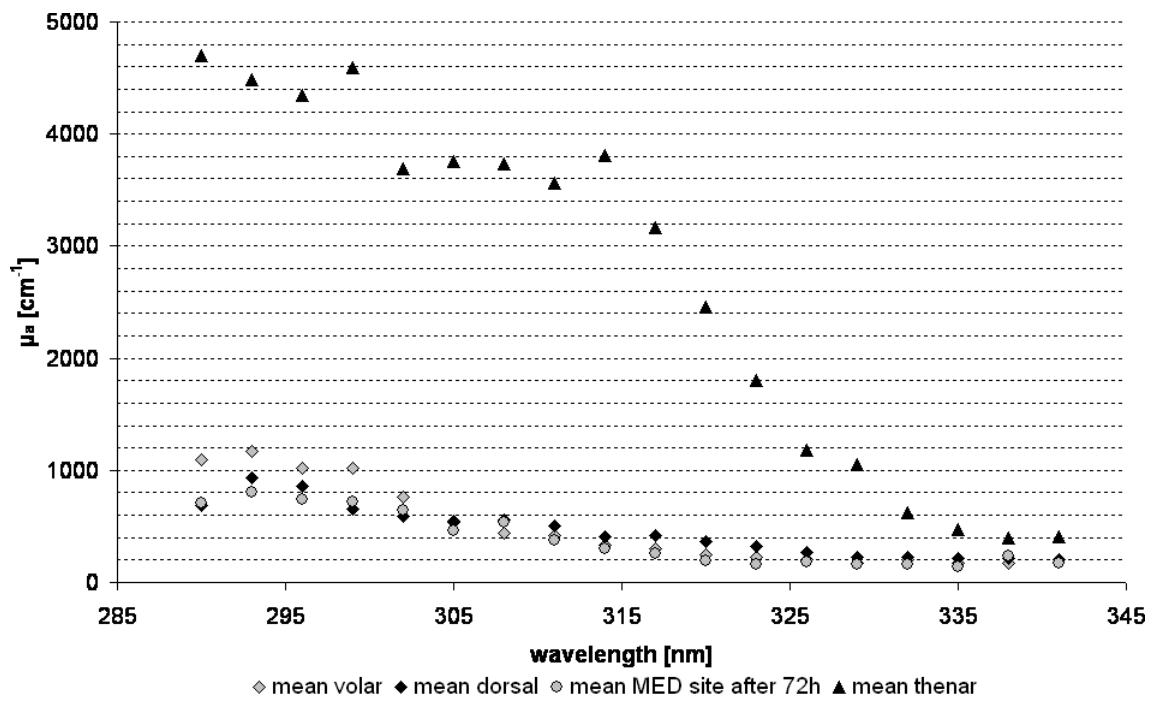


Figure 8.54: Overview of the mean, optoacoustically measured absorption spectra of subject P.R..

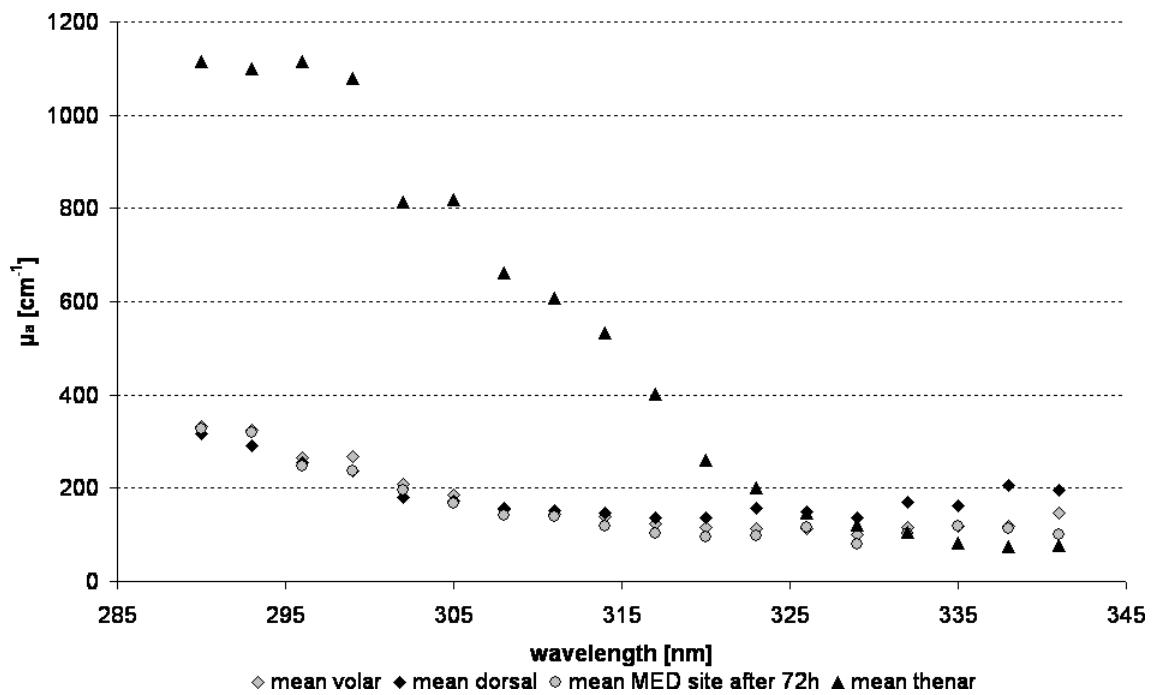
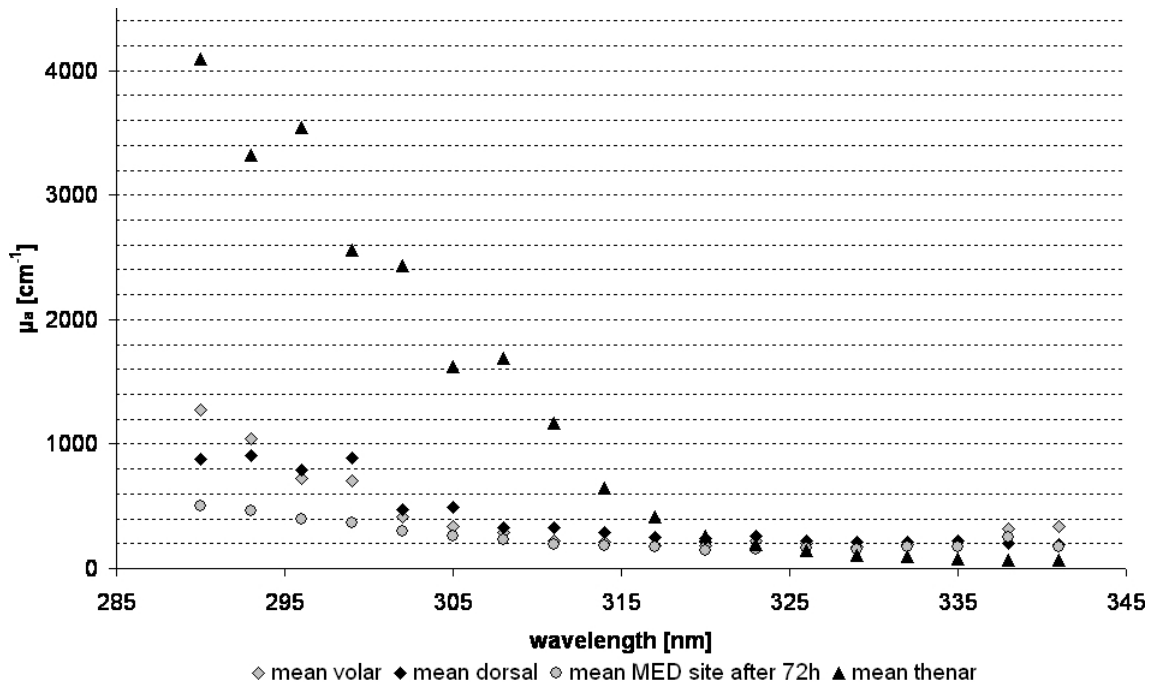
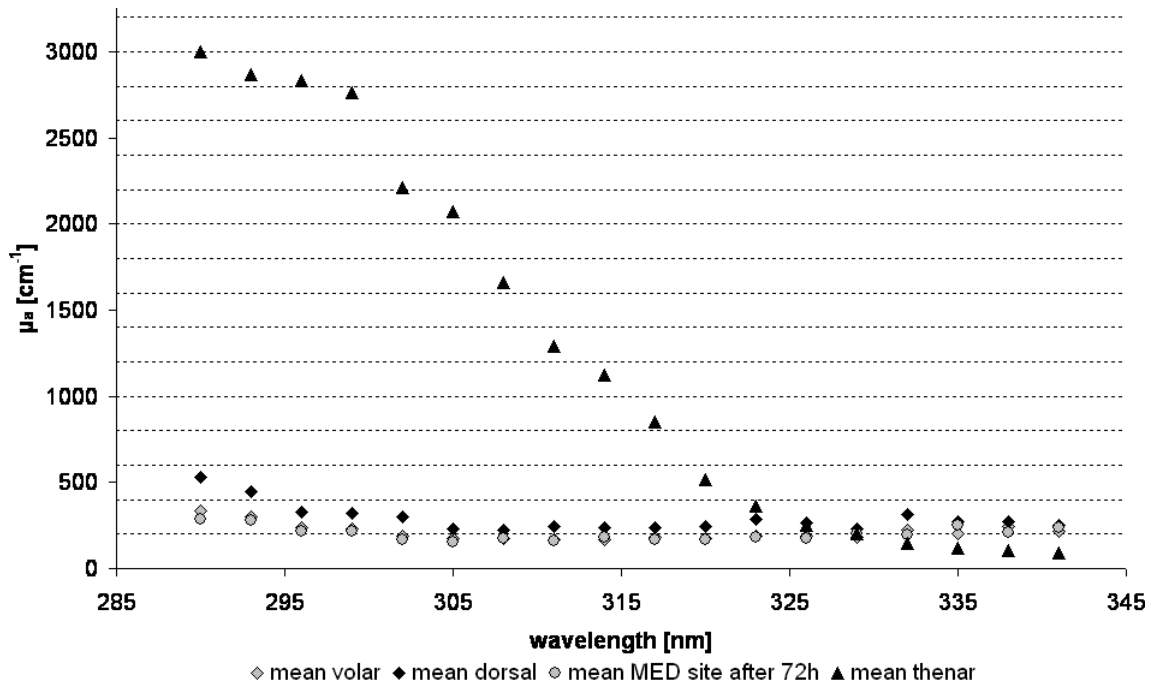


Figure 8.55: Overview of the mean, optoacoustically measured absorption spectra of subject G.O..



**Figure 8.56:** Overview of the mean, optoacoustically measured absorption spectra of subject Kr.G..



**Figure 8.57:** Overview of the mean, optoacoustically measured absorption spectra of subject S.R..

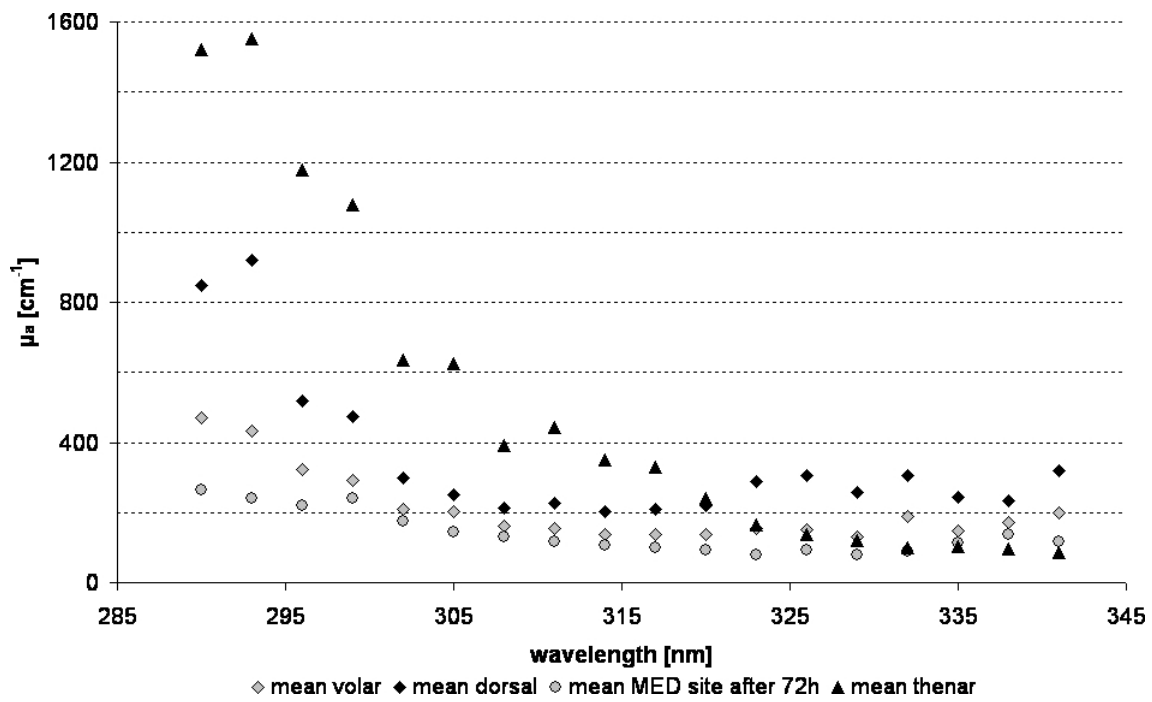


Figure 8.58: Overview of the mean, optoacoustically measured absorption spectra of subject H.M..

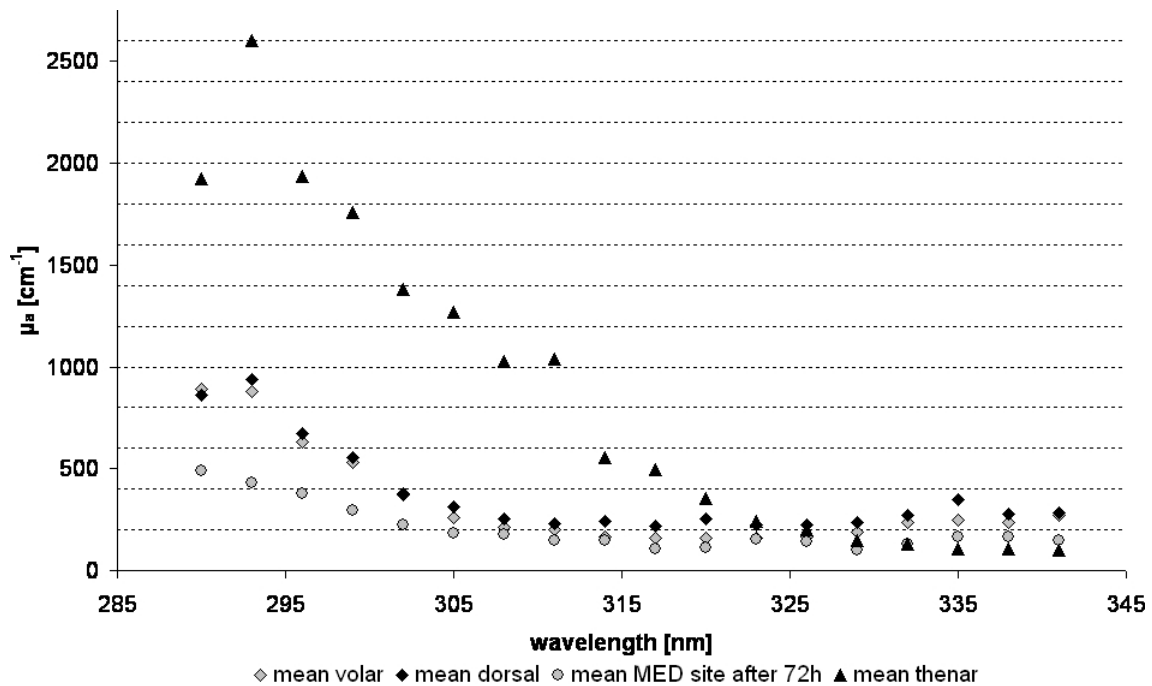


Figure 8.59: Overview of the mean, optoacoustically measured absorption spectra of subject K.K..



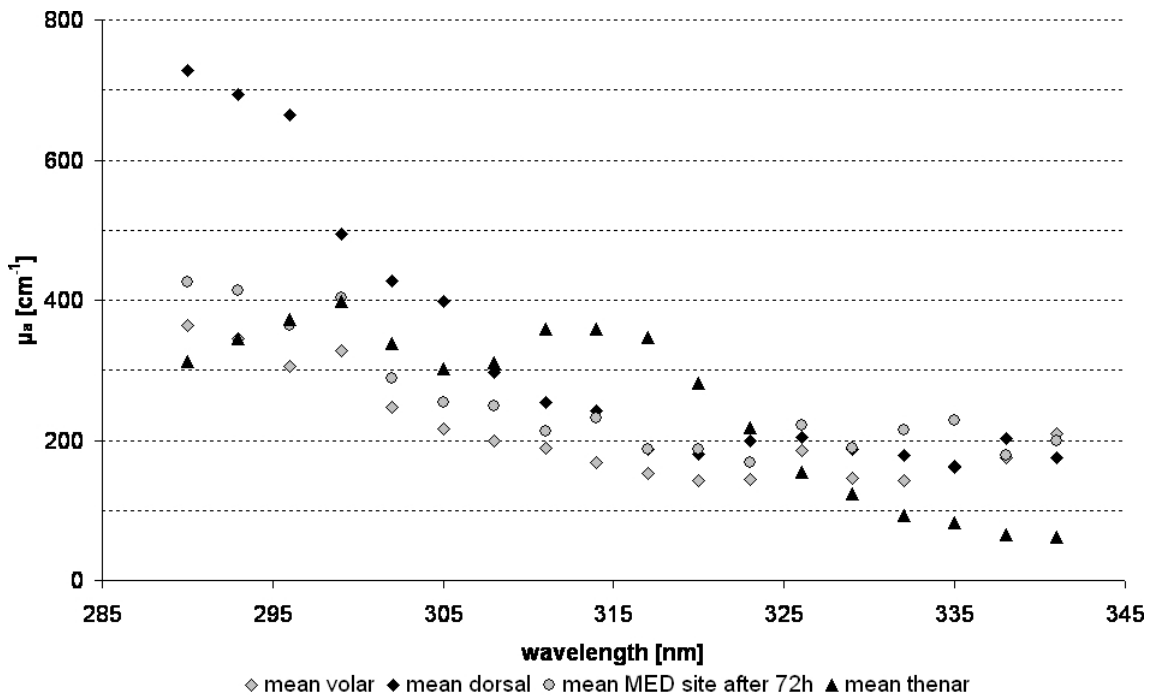


Figure 8.60: Overview of the mean, optoacoustically measured absorption spectra of subject B.I..

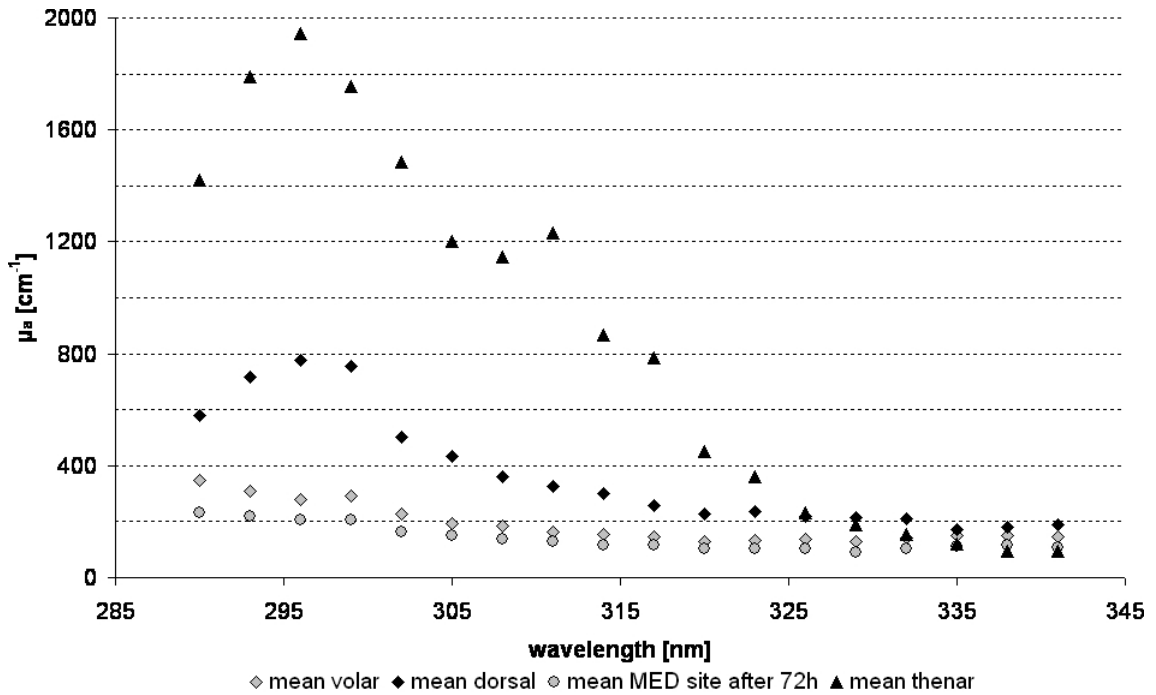
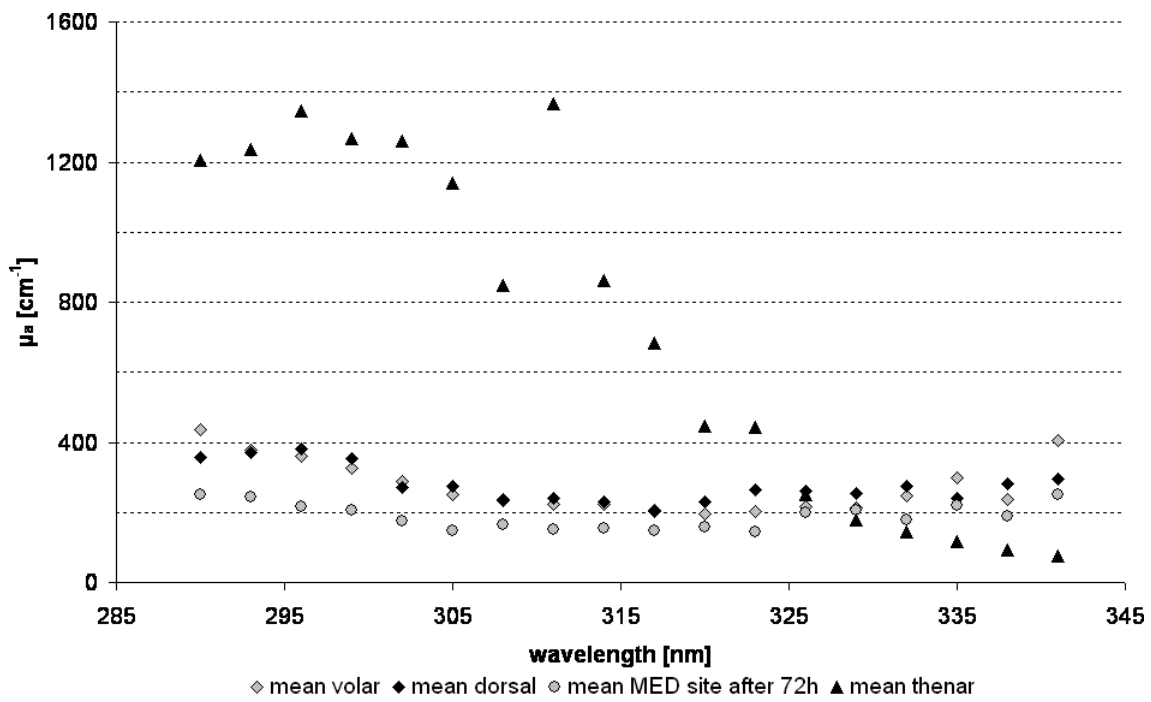
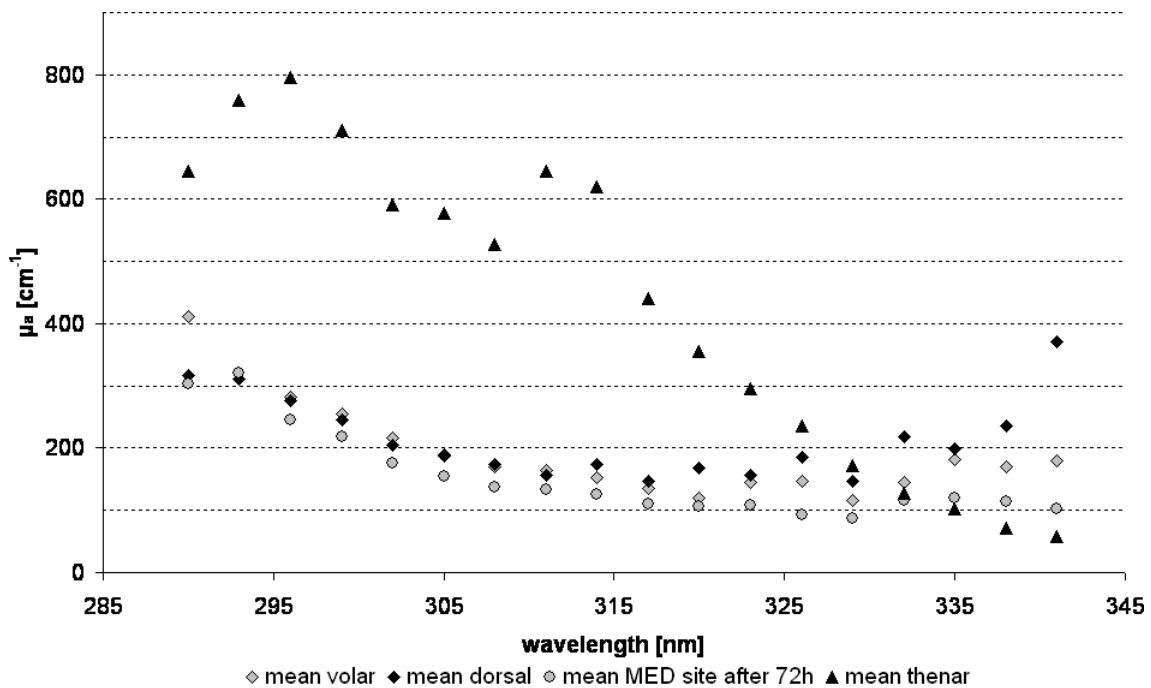


Figure 8.61: Overview of the mean, optoacoustically measured absorption spectra of subject D.C..



**Figure 8.62:** Overview of the mean, optoacoustically measured absorption spectra of subject W.M..



**Figure 8.63:** Overview of the mean, optoacoustically measured absorption spectra of subject M.M..

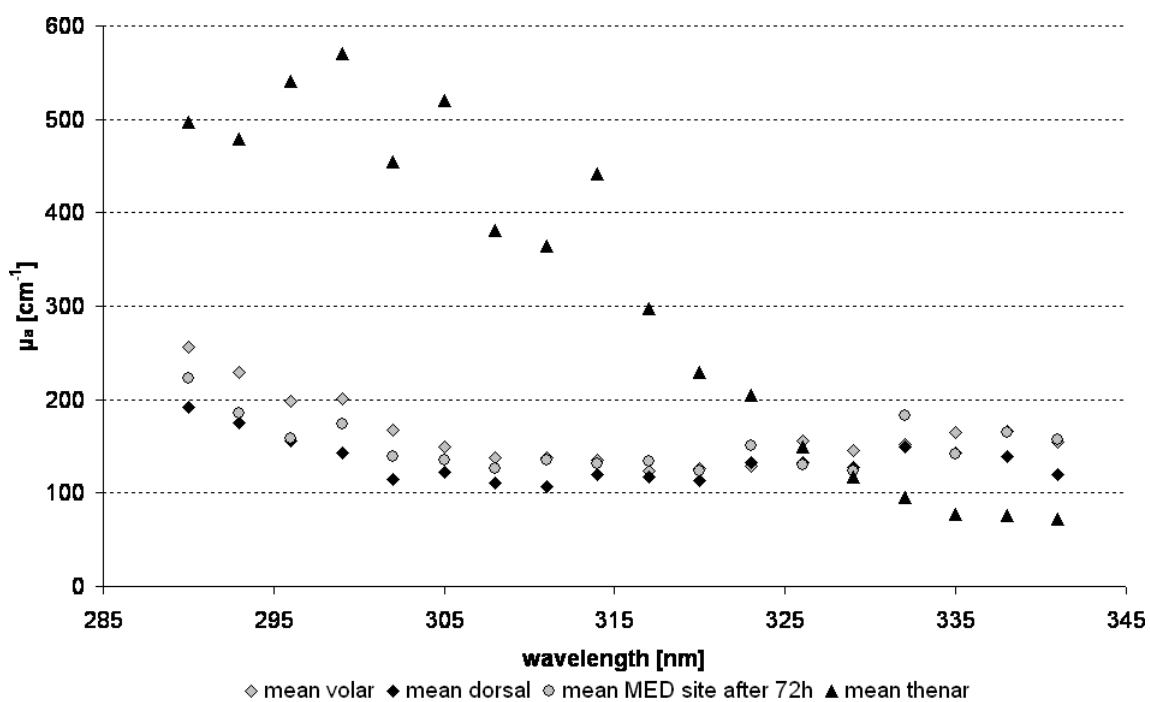


Figure 8.64: Overview of the mean, optoacoustically measured absorption spectra of subject E.R..

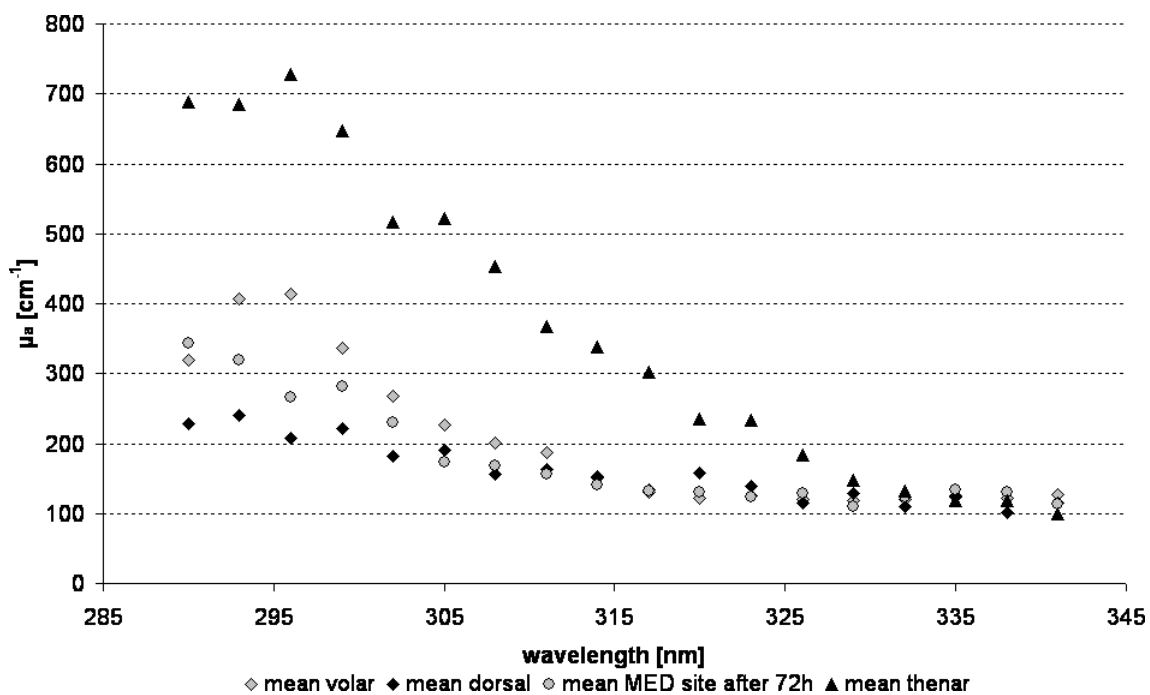


Figure 8.65: Overview of the mean, optoacoustically measured absorption spectra of subject K.B..

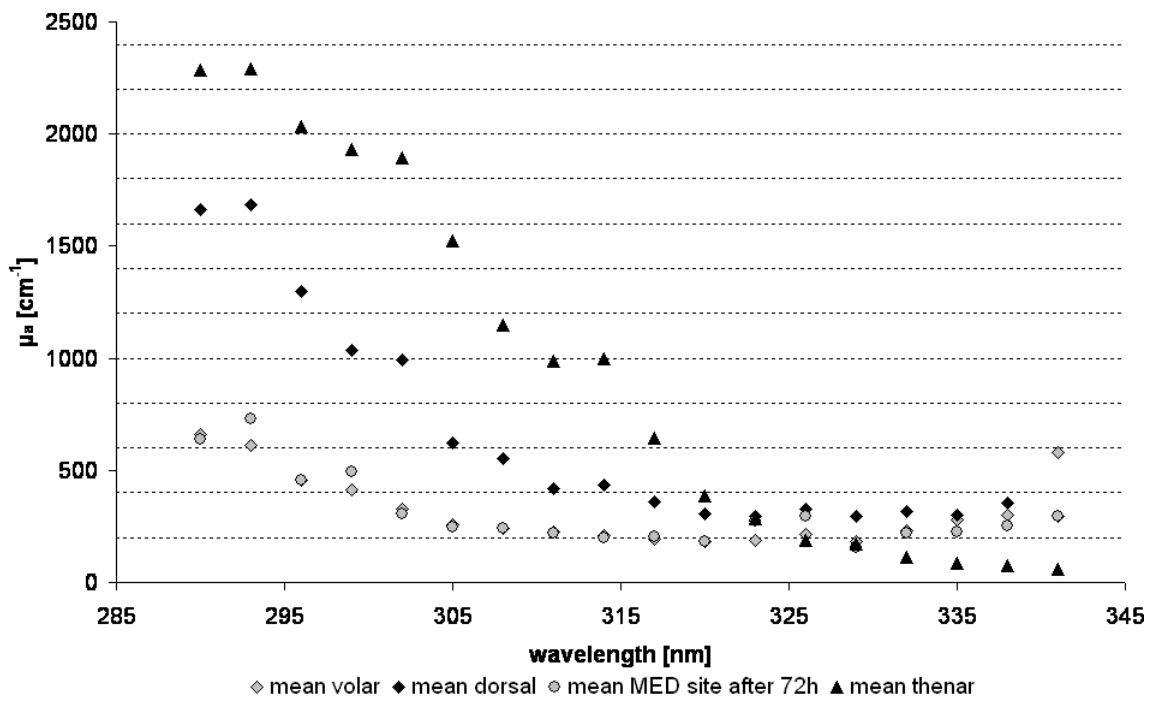


Figure 8.66: Overview of the mean, optoacoustically measured absorption spectra of subject F.M..

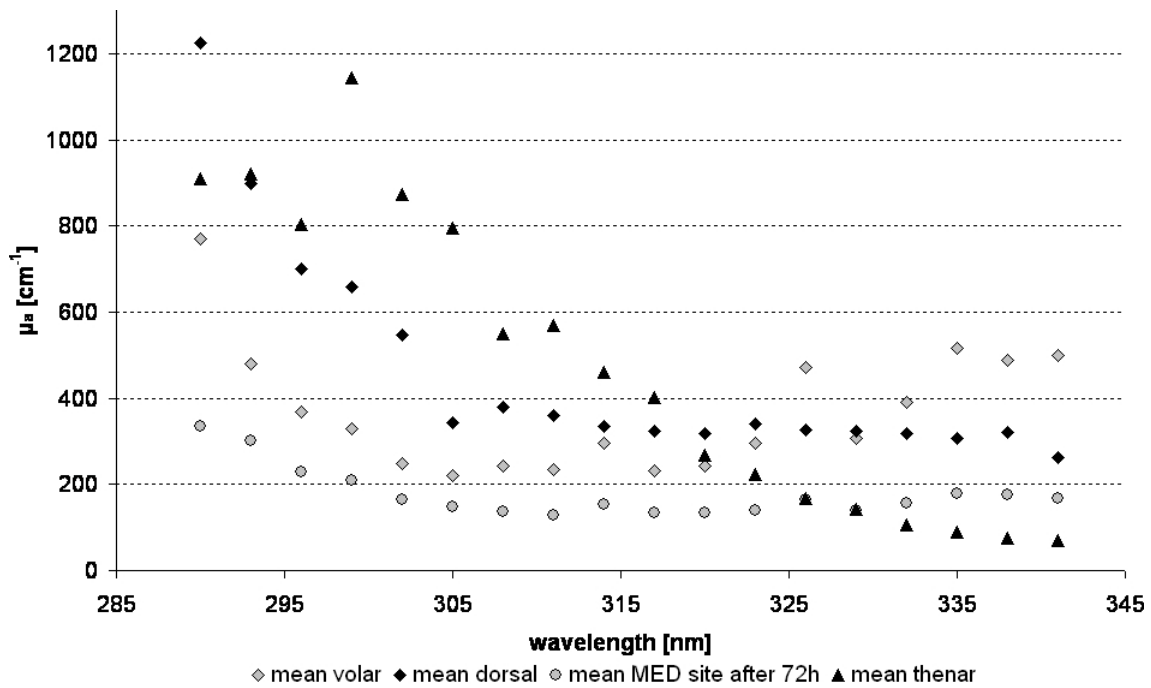


Figure 8.67: Overview of the mean, optoacoustically measured absorption spectra of subject M.H..

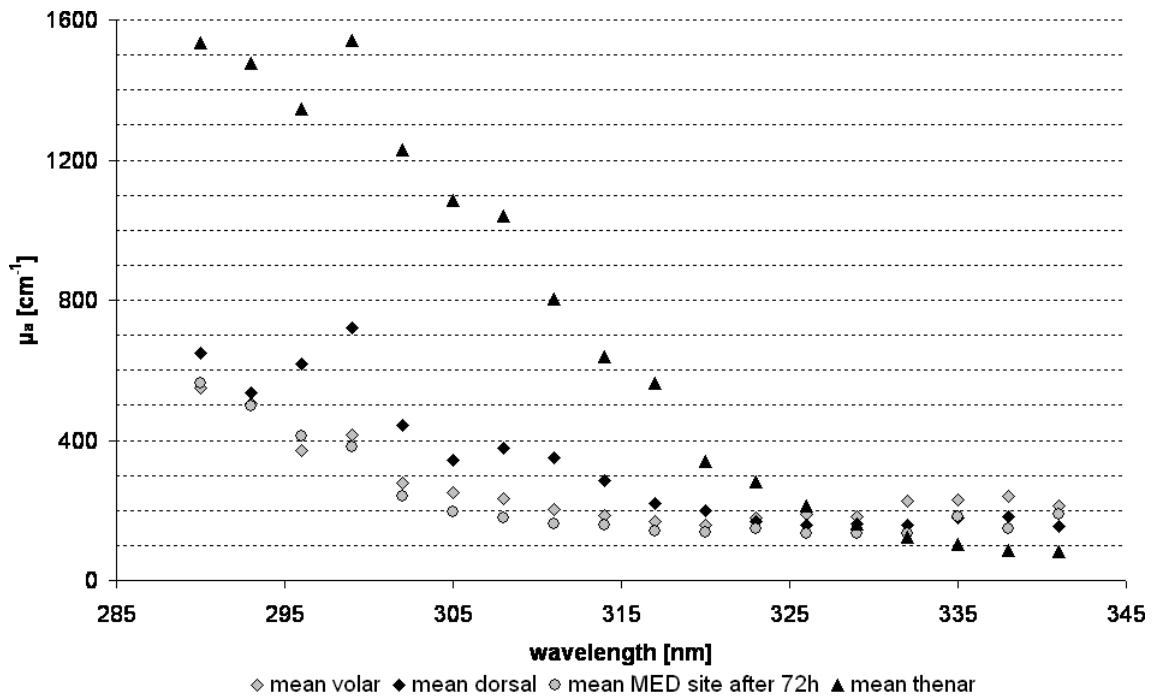


Figure 8.68: Overview of the mean, optoacoustically measured absorption spectra of subject K.H..

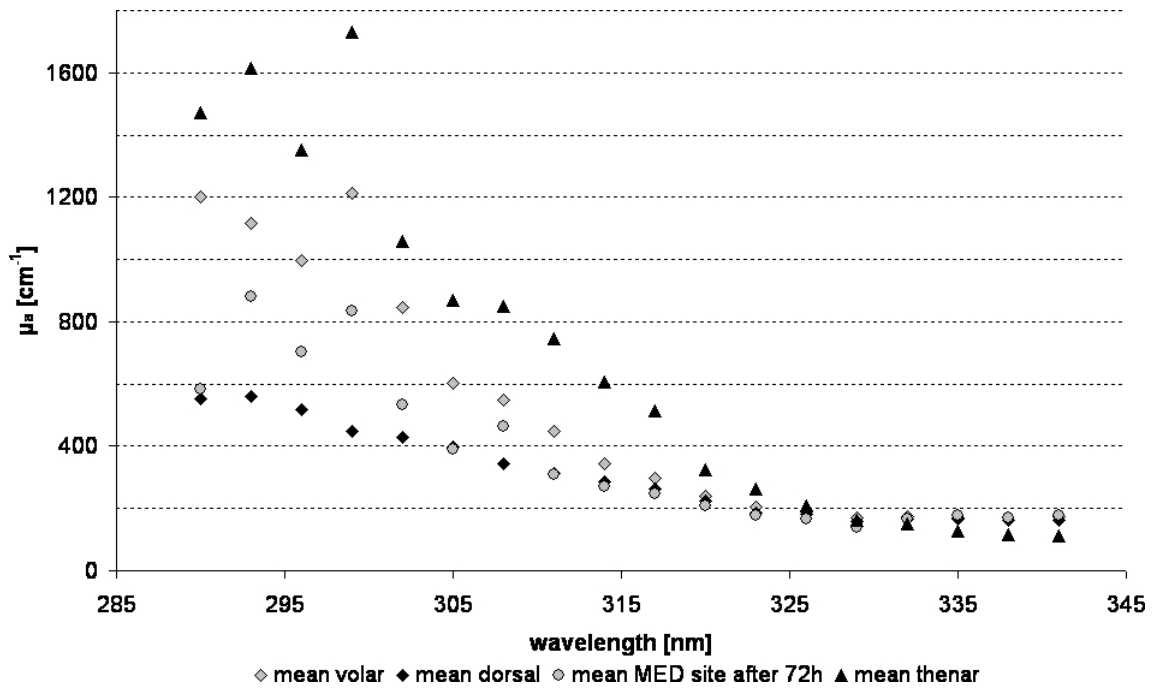


Figure 8.69: Overview of the mean, optoacoustically measured absorption spectra of subject Kn.G..

**thenar**

As pointed out already, optoacoustic signals are induced by pure stratum corneum at this skin site. Accordingly, the optical properties are expected to be dominated by keratin.

The most obvious characteristic of the absorption spectra measured at the thenar is the very high UVB absorption. As can be seen from Figs. 8.50-8.69 the highest values in the UVB absorption spectra of all different sites are found at the thenar of each subject with the exceptions of L.K., L.U., and B.I.. L.K. and L.U. are both regular solarium attendants and ingest carotenoid supplements throughout the year. So, their spectra may not be considered representative and will be excluded from the following analysis. The pronounced double peak structure in the thenar absorption spectrum of subject B.I. is seen in two of the three measurements used for averaging, indicating that this course of the spectrum is valid for this subject.

As mentioned before, the horny layer is particularly thick at this site. Assuming only 30  $\mu\text{m}$  for its thickness, wavelengths with absorption coefficients of approximately 350  $\text{cm}^{-1}$  or more would not reach the viable epidermis. Accordingly, no UVB light would penetrate the stratum corneum of almost all subjects.

The reasons for this high absorption in the dead cell layer may be twofold. As indicated in Sec. 3.2.1 keratin is the main constituent of the horny layer. Its optical properties will thus dominate the spectra. However, it is not clear, whether scattering or absorption dominates in the UV for this protein. If scattering was dominant or at least not negligible, the analysis of the optoacoustic data would have to be readjusted to this case and the spectra as shown may only be considered to reveal mere tendencies. However, the stratum corneum has been shown to be particularly strong forward scattering [13]. This condition reduces the influence of scattering on the light distribution and thus makes scattering more tolerable in an absorption focused theoretical approach of optoacoustic sound induction.

In any case the optoacoustic measurements at the thenar substantiate the speculations raised in the previous section claiming that the marked increase in UVB absorption coefficients seen in the spectra (dorsal aspect forearm) of most subjects belonging to the 'high UV exposure' groups is due to hyperkeratosis.

Because of the uncertainties concerning the reasons for the high UVB absorption in the stratum corneum of the thenar, it is difficult to speculate about the large differences between subjects. Maximal values for  $\mu_a$  at the thenar range from ca. 4700  $\text{cm}^{-1}$  (subject P.R., Fig. 8.54) to less than 600  $\text{cm}^{-1}$  (subject E.R., Fig 8.64).

This large range cannot be explained by point to point deviations and accidental selection of extreme measurement spots. Keratin as well as melanin may represent the cause for these strong deviations. Apart from the different thickness of horny layers, keratin may also occur in different concentrations or even packages. These parameters may vary between subjects but also from skin site to skin site. Keratin concentration will of course

influence both absorption and scattering coefficients whereas the keratin structure will probably have an effect only on the scattering properties of the skin layer. Melanin - despite its fairly low concentrations at the palm of the hand - may also account for some absorption variances. Melanin is produced at the inner layer of the epidermis. Consequently, the melanin supply becomes worse and worse towards the skin surface. The melanin contained in the keratinocytes pushed towards the surface is moreover subject to degradation. Thus the thicker the epidermis the less melanin will be contained in the surface layer of the skin. Furthermore, the initial melanin content of the keratinocytes will also vary between subjects analogous to the different constitutional pigmentation levels.

Three more intriguing spectral characteristics of the spectra from the horny layer compared to those from the other skin sites should be pointed at here.

Most strikingly 17 of the 18 spectra considered in this horny layer analysis cross the spectra of the other sites. This crossing is at or near 326/329 nm. In the longer wavelength range, the values for the absorption coefficients drop below those of areas with normal thin horny layer.

This is again a strong hint at keratin as the dominant chromophore in the stratum corneum in combination with only a minimal melanin concentration. Keratin absorption is drastically decreasing from its maximum at 280 nm towards longer wavelengths. The fact that the absorption coefficients of the horny layer drop considerably below all other spectra is a clear indication that the concentration of at least one other important UV chromophore is markedly lower at the thenar than elsewhere. If the melanin concentration in the horny layer was comparable to that of the other skin sites, the absorption coefficient could only have dropped to the normal baseline in the UVA as found in the other areas.

Less obvious but still worth considering are the absorption coefficients at 296/299 nm (and below) and at 311/314 nm. The optoacoustic measurements at the thenar have particularly large standard deviations especially in the UVB, so the following observations are stated with great reservation.

At least half of the considered subject's spectra show saturation characteristics below ca. 300 nm or even a maximum at 296/299 nm. K.B., G.O., P.R., and S.R. show a strongly reduced increase of the absorption coefficient whereas M.M., W.M., D.C. as well as E.R. even display a maximum at 296 nm or 299 nm respectively.

Besides, some spectra show an additional peak around 311/314 nm. In B.I. and M.M. the existence of this maximum is quite convincing, and it also seems to occur in some more spectra. However, in the other spectra it consists of one data point only, so it would clearly have been considered a measurement error if it was not for the repeated occurrence throughout the different measurement days: a relative maximum at 311/314 nm is seen in E.R., M.M., W.M., D.C., B.I., H.M., P.R., W.K., G.O., and very weakly in F.M. and K.K. - that is 11 out of 18 spectra considered.

It is difficult to find an explanation for these spectral features. The pure keratin absorption coefficients are steadily rising in the range from 341 nm to 290 nm. So are the  $\mu_a$  of

melanin. Carotenoids like  $\beta$ -carotene and lutein display weak absorption maxima around 310 nm and are found at relatively high concentrations in the skin of the palm. However, it is questionable whether these maxima are strong enough to induce the shift towards 300 nm and they are not sharp enough to serve as an explanation for the 311/314 nm maxima. So, these two spectral features of the absorption spectra of the horny layer cannot be solved here.

In conclusion, the most prominent characteristics of the absorption spectra from the thenar, i.e. pure horny layer are:

- The absorption spectra at the thenar are significantly different from those measured at skin sites with thin horny layer
- In general, absorption is strongly increasing towards shorter wavelengths. Maximal values of  $\mu_a$  in the UVB typically are about 16 times higher than the minimal values of  $\mu_a$  in the UVA
- Generally, the absorption coefficients of pure horny layer are higher than those of normal skin in the short wavelength range from 290 nm to about 326/329 nm. Towards longer wavelengths, the absorption coefficients at the thenar drop below those of normal skin.

#### **volar side of forearm - 72h after irradiation with 1 MED**

In contrast to the measurements at the thenar, the measurements at the volar side of the arm at the site where one MED had been applied 72h ago did not bring about new insights or further thought-provoking impulses.

For most subjects, these spectra lie within the standard deviation of the site before irradiation. This is in good agreement with the fact that the minimal melanogenic dose usually is lower than the minimal erythemal dose. Besides, no spectral features characteristic of an increased keratinization could be spotted.

The lack of significant change is paralleled in the  $L^*$ -value measurements of the site prior and 72h after irradiation with one MED. Table 8.1 lists some of the interesting  $\Delta L^*$  between two skin sites. Note again, that the difference between  $L^*$ -values at the volar aspect and the respective other sites are calculated. Thus positive  $\Delta L^*$  denote darker skin.

Probably,  $\Delta L^*$  of 2 or more before and 72h after irradiation - which is found in 9 subjects comparing pre and post irradiation - could already be expected to mark a fairly distinct difference in skin lightness, which optoacoustics should be able to spot. However,  $L^*$  values are not only related to pigmentation but show also a correlation to skin reddening. So, the remains of the erythema 72h after irradiation will add to the change in skin lightness. Even though no or hardly any erythema was perceived by eye.



subject	before - 72h after 1 MED	natural low - high UV exposure	thin (volar) - thick horny layer
K.I.	3.62	6.07	-3.07
L.K.	1.72	10.08	6.04
L.U.	0.95	6.67	-4.08
W.K.	0.84	12.13	1.91
P.R.	0.02	1.94	4.95
G.O.	2.72	-0.77	-0.77
Kr.G.	2.64	6.55	1.30
S.R.	1.14	-1.32	5.61
H.M.	1.62	7.18	7.37
K.K.	-0.93	-0.69	4.13
B.I.	3.00	8.03	2.80
D.C.	0.35	5.48	2.21
W.M.	4.22	8.14	-1.82
M.M.	3.38	2.07	7.41
E.R.	0.91	5.34	2.56
W.B.	4.22	8.14	-1.82
F.M.	3.01	10.24	4.11
M.H.	5.22	10.07	-0.76
K.H.	-0.06	4.96	0.72
Kn.G.	0.48	7.78	3.61

**Table 8.1:** Differences of skin lightness  $\Delta L^*$  between skin sites

### 8.3.4 wavelength dependent penetration depths

The results of the previous subsections can be reanalyzed in terms of the wavelength dependent penetration depths of the applied ultraviolet radiation.

Fig. 8.70 shows the **average wavelength dependent penetration depths** at the volar and dorsal aspect of the forearm and on the thenar together with their 90% confidence intervals. Each average spectrum was calculated from the 20 mean spectra of the subjects. The data shown in this figure are also given in Table 8.2.

As expected, the penetration depths at the volar and dorsal forearm show fairly similar characteristics. The ultraviolet light can penetrate deeper into the skin at the volar side throughout the spectrum. Minimal penetration depths of ca. 20  $\mu\text{m}$  are found at 290 nm for both sites. Towards longer wavelengths, the penetration depths are slowly increasing in both spectra. At the dorsal side, the penetration depths stay at a level of about 50  $\mu\text{m}$  from about 326 nm on. On the volar side, the increase is a bit steeper reaching a maximum of about 60  $\mu\text{m}$  at 320 nm and then slowly decreasing to the dorsal level of ca. 50  $\mu\text{m}$  at 341 nm.

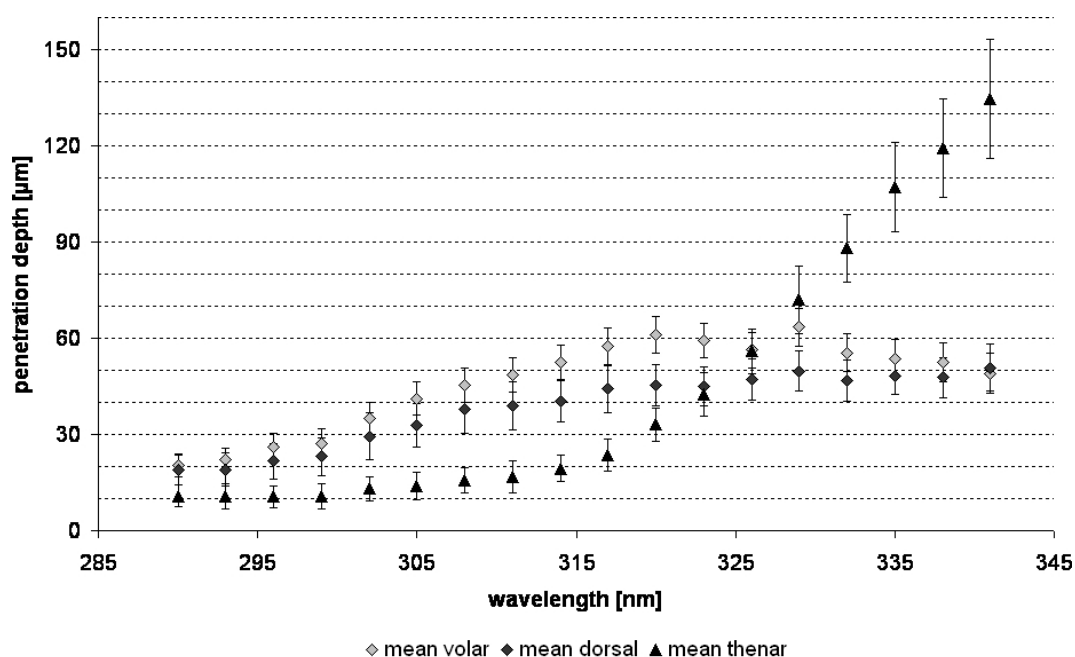


**Figure 8.70:** Average spectra for the penetration depths at the volar and dorsal aspect of the forearm and on the thenar. Error bars mark the 90% confidence interval of each spectrum.

wavelength [nm]	mean penetration depth [ $\mu\text{m}$ ] $\pm$ 90%-confidence interval		
	dorsal side of forearm	volar side of forearm	thenar/thick horny layer
341	51 $\pm$ 7	49 $\pm$ 6	135 $\pm$ 18
338	48 $\pm$ 6	53 $\pm$ 6	119 $\pm$ 15
335	48 $\pm$ 6	54 $\pm$ 6	107 $\pm$ 14
332	47 $\pm$ 6	56 $\pm$ 6	88 $\pm$ 11
329	50 $\pm$ 6	63 $\pm$ 6	72 $\pm$ 10
326	47 $\pm$ 6	56 $\pm$ 6	56 $\pm$ 7
323	45 $\pm$ 6	59 $\pm$ 5	42 $\pm$ 7
320	45 $\pm$ 6	61 $\pm$ 6	33 $\pm$ 5
317	44 $\pm$ 7	57 $\pm$ 6	24 $\pm$ 5
314	40 $\pm$ 7	53 $\pm$ 5	19 $\pm$ 4
311	39 $\pm$ 7	49 $\pm$ 5	17 $\pm$ 5
308	38 $\pm$ 7	45 $\pm$ 5	16 $\pm$ 4
305	33 $\pm$ 7	41 $\pm$ 5	14 $\pm$ 4
302	29 $\pm$ 7	35 $\pm$ 5	13 $\pm$ 4
299	23 $\pm$ 6	27 $\pm$ 4	11 $\pm$ 4
296	22 $\pm$ 6	26 $\pm$ 4	11 $\pm$ 3
293	19 $\pm$ 5	22 $\pm$ 4	11 $\pm$ 4
290	19 $\pm$ 5	20 $\pm$ 3	11 $\pm$ 3

**Table 8.2:** Wavelength dependent average values and their 90%-confidence interval for the penetration depths at the volar and dorsal aspect of the forearm as well as on the thenar with its thick horny layer.

The spectrum of penetration depths at the thenar differs significantly from those at the forearm. As pointed out already in the previous section, the viable cells of the epidermis are shielded from UVB radiation assuming a dead cell layer thickness of more than 20  $\mu\text{m}$  here. However, UV radiation at wavelengths longer than ca. 326 nm can penetrate deeper into the epidermis at the thenar than at the forearm sites. The reason for this behaviour probably is the rapidly decreasing efficiency of the keratin shielding towards longer wavelengths, which is not compensated for by melanin at the palm.

Figs. 8.71-8.73 take a closer look at the **phototype dependency of the penetration depths** at the three sites. This time the average penetration depth was calculated separately for

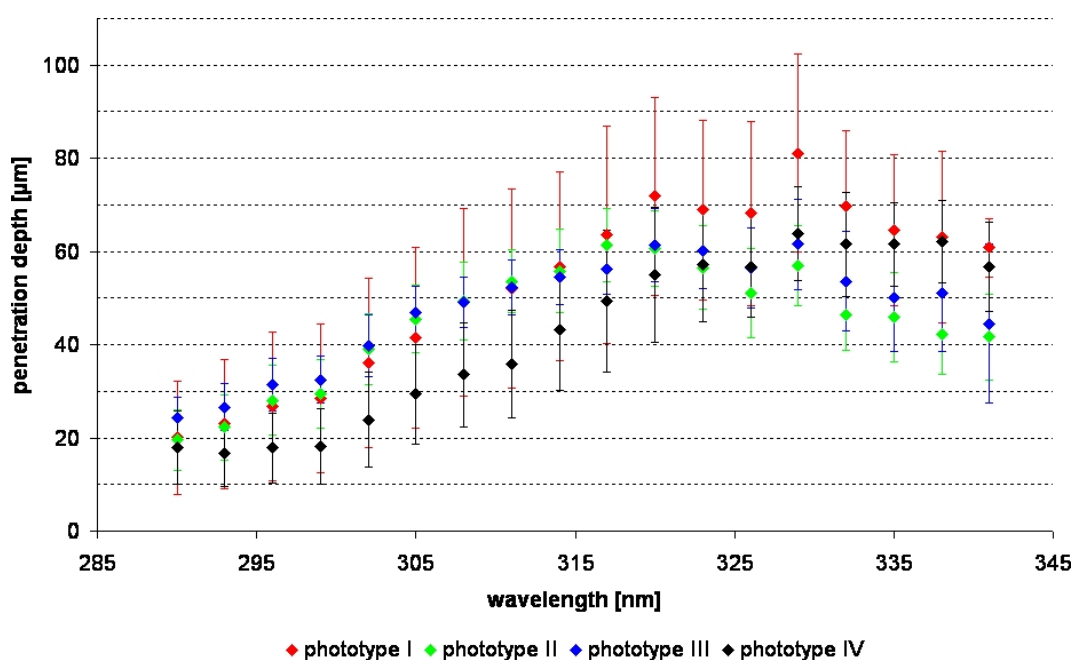


**Figure 8.71:** Average spectra of the penetration depths at the volar aspect of the forearm. Mean spectra and 90% confidence intervals are shown for phototypes I-IV.

the different phototypes. Of course, the 90% confidence intervals are fairly large here because of the small number of subjects:  $n=3$  for phototype I,  $n=7$  for phototype II,  $n=5$  for phototype III, and  $n=5$  for phototype IV. So, the following observations are only made under reserve - future measurements on a larger group of subjects may support or invalidate the conclusions.

At the volar side of the forearm (Fig. 8.71), penetration depths of phototype I-III are very close in the UVB. Penetration depth is minimal with a good 20  $\mu\text{m}$  at 290 nm and rises constantly up to about 55  $\mu\text{m}$  at 314 nm. It is maximal in the range from 317-329 nm and decreases again towards longer wavelengths. In the UVA the close agreement between the three phototypes is lost to some degree and the curves are less smooth. Penetration depths are now higher (approx. 60-80  $\mu\text{m}$ ) in phototypes I compared to phototypes II and III (well above 40  $\mu\text{m}$  to ca. 60  $\mu\text{m}$ ).

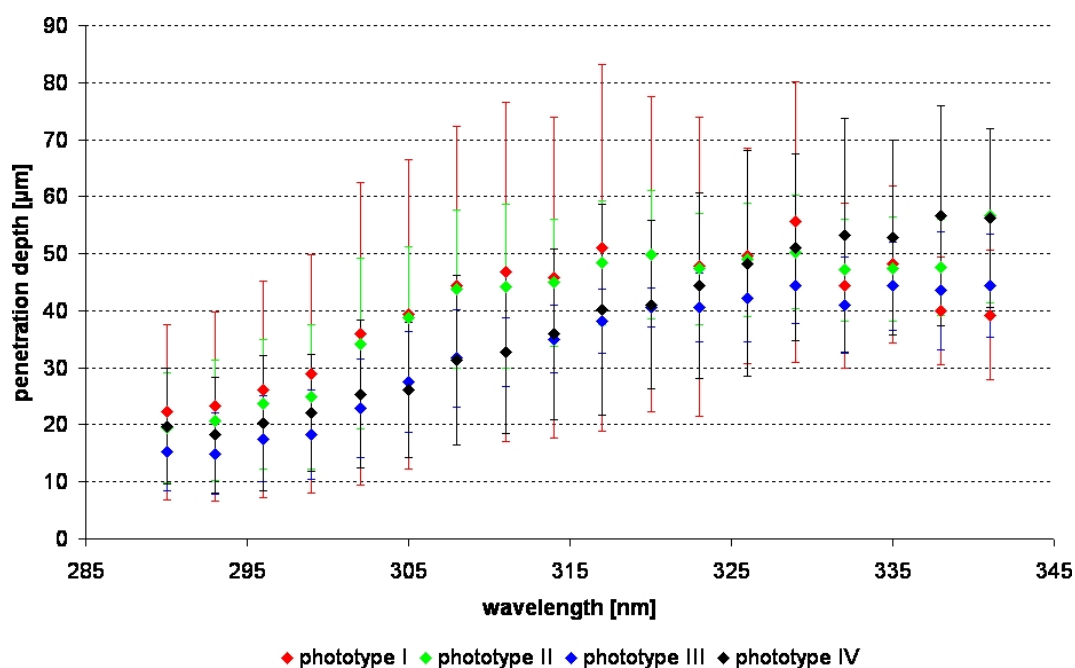


**Figure 8.72:** Average spectra of the penetration depths at the dorsal aspect of the forearm. Mean spectra and 90% confidence intervals are shown for phototypes I-IV.

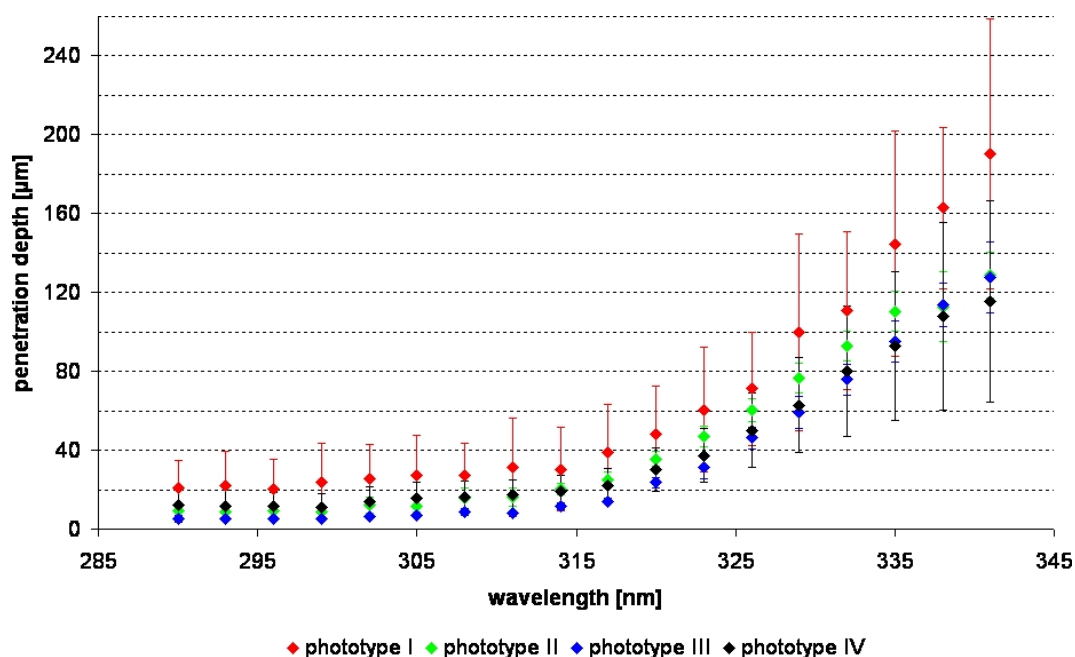


**Figure 8.73:** Average spectra of the penetration depths at the thenar. Mean spectra and 90% confidence intervals are shown for phototypes I-IV.

Phototype IV behaves a little different from the other three types. Penetration depth stays at a low level of less than  $20 \mu\text{m}$  from 290 nm up to 299 nm. Then it rises to another plateau at  $60 \pm 5 \mu\text{m}$  from 332 nm onwards. This implicates higher penetration depths in phototypes I and IV in the UVA range above ca. 330 nm than in phototypes II or III.

At the dorsal side of the forearm (Fig. 8.72), phototype I and II as well as III and IV seem to be grouped throughout the UVB and up to about 320 nm. However, this similarity is even less certain than the grouping at the volar site. Penetration depth is again rising from shorter to longer wavelengths and it is higher in the light skin types than in the darker ones. Phototypes behave differently towards lower wavelengths. In type IV, the penetration depth is constantly rising from about 20  $\mu\text{m}$  at 290 nm up to a good 45  $\mu\text{m}$  at 341 nm. Type III and II reach some kind of plateau in the UVA. However, this level is reached earlier in type II (at ca. 318 nm) than in type III (at ca. 326 nm) and it is as high as 50  $\mu\text{m}$  in skin type II and less than 45  $\mu\text{m}$  in type III. In Phototype I, penetration depths reach maximal levels of 50-55  $\mu\text{m}$  in the range of 318-329 nm and then decrease towards longer wavelengths down to 40  $\mu\text{m}$ .

It must be pointed out again that the phototype dependent characteristics described in the previous two paragraphs are unfortunately not much more than mere trends and have to be reviewed after further measurements.

The phototype dependent penetration depths calculated for the thenar (Fig. 8.73) show a quite intriguing trend that is more convincing judged by the confidence intervals: the penetration depths in the horny layer are considerably higher in skin type I than in the other skin types throughout the measured spectral range. Of course the confidence intervals of phototype I data are very large again, but on the other hand type I datapoints are not included in the confidence intervals of the other three types except at 332 nm.

If this trend can be confirmed in measurements on more subjects belonging to phototype I, it would give way to some interesting speculations: the measurements at the thenar are representative for pure horny layer data. The differences between phototypes I and II-IV indicate that the horny layer of type I is more transparent for UV radiation than that of the other three. There is no reason why this should be a characteristic unique to very thick horny layers. Consequently, a horny layer of the same thickness would provide much less UV shielding in type I than in the other three and this deficiency would represent an important cause for the high UV sensitivity of type I.

Subject P.R. can be taken as a real example and additional hint to these conclusions. Despite the very light, weakly pigmented skin, this subject is assigned to phototype IV. The spectra from this subject are dominated by keratin absorption which is best explained by a disproportionately high concentration of keratin. The spectral features in combination with the low UV sensitivity lead to the conclusion that a high concentration of keratin compensates for the low pigmentation apparent to the eye and confirmed by the chromameter measurements.

General assumptions for the penetration depths of ultraviolet light into human skin are usually globalized stating UVB penetrates the epidermis while UVA can even penetrate the dermis. Interestingly, the penetration depths calculated from the optoacoustic in vivo measurements draw quite a different picture at first sight showing penetration depths of less than 65  $\mu\text{m}$  for both normal skin sites over a wavelength range from 290 nm to 341

nm. This discrepancy can be interpreted in two ways. On the one hand, it must be pointed out that a penetration depth of  $x \mu\text{m}$  does not mean that no radiation of this wavelength will reach beyond this point. The penetration depth just marks the point where the incident radiation intensity has been attenuated to the  $1/e$ -level. So the presented measurements do not contradict the general assumptions about how far UV radiation may reach into the skin. However, they point to two facts: even the low radiation intensities still present behind the penetration depth border are capable of inducing photobiological action and indirect mechanisms induced in the upper layers of the epidermis also play a considerable role in the skin's photobiology.

General conclusions from the calculated penetration depths in the range from 290 nm - 341 nm may be summarized as follows:

- The spectra of the penetration depths are similar for the normal (thin horny layer) skin of the forearm but different at the thenar where the horny layer is particularly thick.
- Ultraviolet radiation can penetrate a little deeper into the skin at the volar side of the forearm (ca. 20-63  $\mu\text{m}$ ) than on the dorsal side (ca. 19-51  $\mu\text{m}$ ).
- The horny layer at the thenar completely shields the viable epidermis from UVB radiation. In the UVA-II, the penetration depth is strongly increasing up to ca. 135  $\mu\text{m}$  at 341 nm.
- Phototype dependent calculations of the penetration depth indicated a lower UV blocking capability for the keratin of the most UV sensitive phototype I.

### 8.3.5 sunscreens

Optoacoustic measurements on two skin sites at the volar aspect of the arm were conducted to assess the potential of UV-optoacoustics for the prediction of the sun protection factor of sun screen lotions *in vivo*.

The obtained spectra will not be shown here in detail. Two examples are given in Figs. 8.74 and 8.75. As can be seen from those two examples, the course of the spectra from the same sun protection lotion is similar on either subject. However, the absolute values of the calculated absorption coefficients are strongly differing from one subject to the other and as the large standard deviations indicate, they are also strongly diverging from spot to spot within the same subject.

This effect can be explained by the inhomogeneous distribution of the lotion on the skin. Even though the lotions were applied according to the recommendations of COLIPA, some inhomogeneity in the application cannot be avoided because it is only due to the structure of the skin. This is a well known problem in the assessment of sun protection lotions.

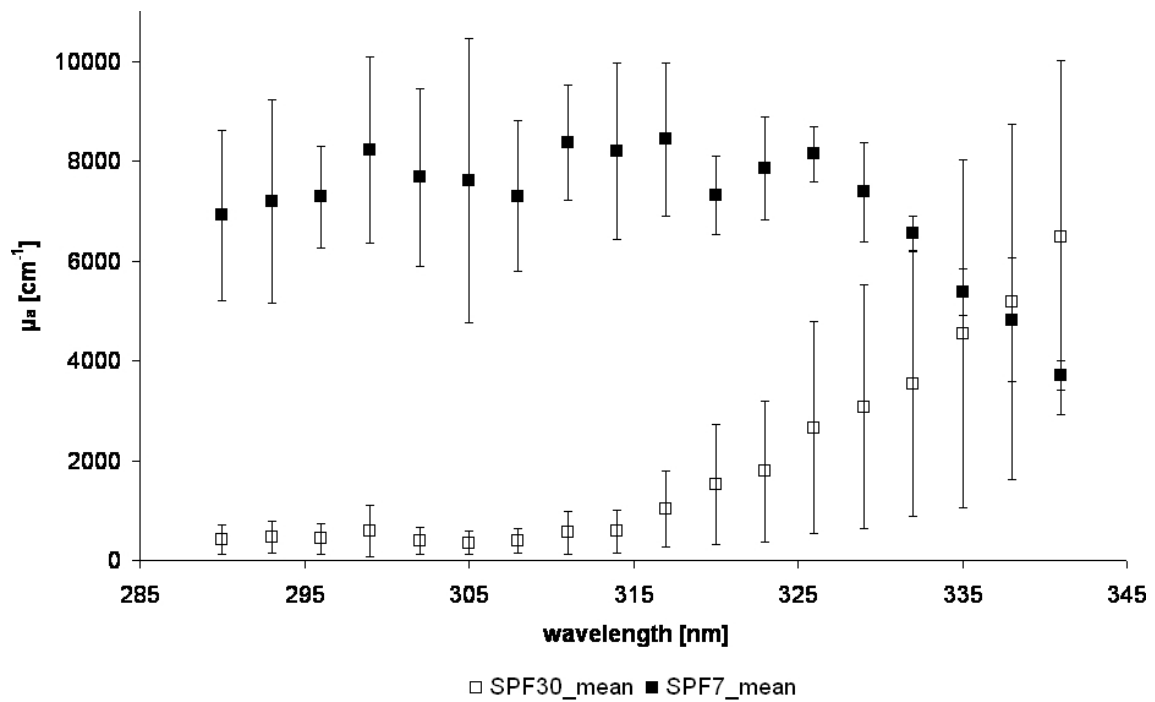


**Figure 8.74:** Average spectra and their standard deviation of two sunscreen lotions applied to the skin of subject S.R.. The sunscreen lotions were labeled sun protection factor 7 (SPF7) and 30 (SPF30) respectively.

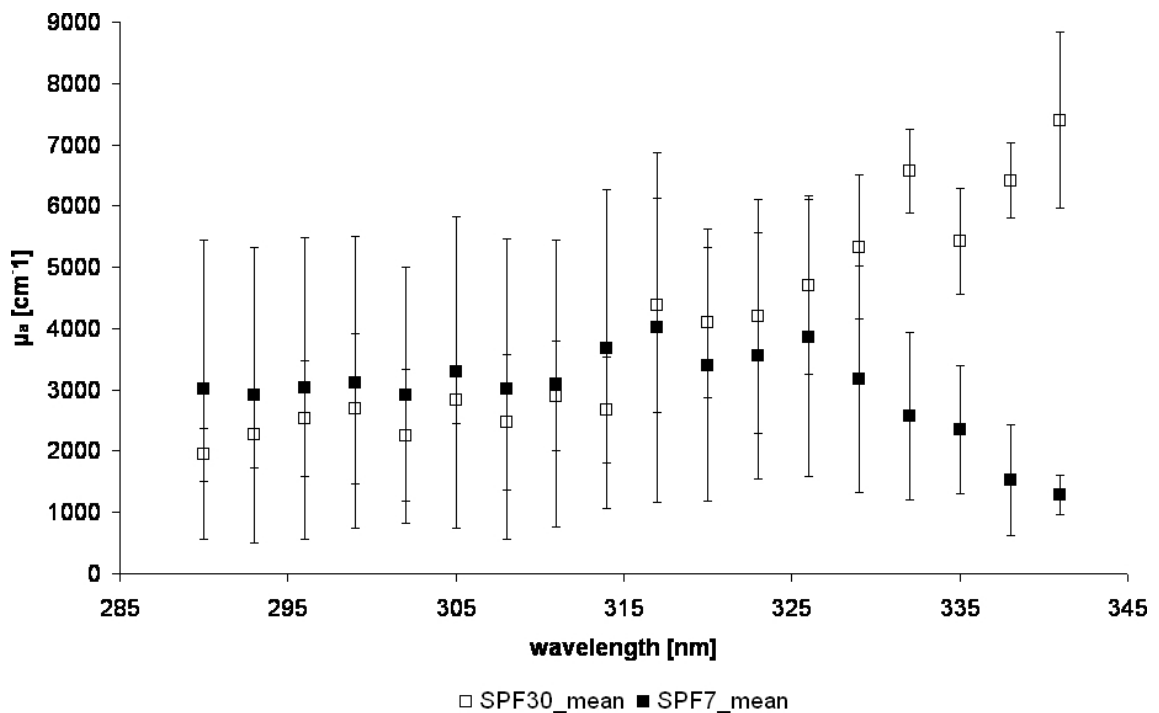


**Figure 8.75:** Average spectra and their standard deviation of two sunscreen lotions applied to the skin of subject G.O.. The sunscreen lotions were labeled protection factor 7 (SPF7) and 30 (SPF30) respectively.

Preliminary optoacoustic measurements on sun screens had indicated that the inhomogeneous distribution of the lotion on the skin can be compensated by averaging over several spots. The more elaborate data obtained from this subject study show that a reliable assessment is probably only reasonable using an optoacoustic detector with a larger detection area (as outlined already in Sec. 8.3.1).

In addition, sun protection lotions may contain UV filters that are highly scattering. So, scattering should be included in the simulation analysis to allow a thorough evaluation of the spectra.

It must be pointed out again however, that the spectra of the same lotion display similar characteristics, despite the adversary conditions of the measurements. This underscores the potential of UV optoacoustics to assess sun protection lotions, even though some technical advancements are prerequisite before optoacoustic evaluation of sun protection lotions *in vivo* can be truly beneficial.



## 9 Conclusions and Outlook

The ambition of this dissertation project was the development and application of an experimental setup to determine the optical properties of human skin *in vivo* in the ultraviolet wavelength range. As outlined in the introduction to this thesis, it was motivated by the fairly poor data about these fundamental properties found in the literature. This aim was successfully accomplished. The necessary experimental and analytical tools were developed and finally applied in a study on 20 subjects plumbing the potentials of optoacoustics, the method of choice, in this scientific context.

Optoacoustics is a very promising technique for *in vivo* measurements of optical properties. Its advantages are particularly convincing dealing with human skin in the ultraviolet range. In the UV, human skin is characterized by very high absorption and of course the applied UV doses have to be minimized and sharply limited not to pose a risk to the subject's health.

In optoacoustics the radiation only has to get into the sample and not out again in contrast to purely optical techniques such as optical coherence tomography (OCT), reflection, fluorescence, Raman scattering etc.. The information is transported by ultrasound, which travels through skin unhamperedly. This significantly reduces the radiation exposure necessary to obtain information about the optical properties in a certain depth, as the light energy is attenuated exponentially with the pathlength it has to travel in an absorbing medium.

Besides, the optoacoustic signal allows straightforward access to the depths dependency of the optical properties which are simply coded by the runtime of the acoustic signal. In reflection spectroscopy for example - which is one of the rather gentle optical techniques - calculating the depths dependency of the absorption and scattering coefficients is quite elaborate and restricted to the superficial part of the sample (for details, compare the Introduction again).

Any technique which should be applied for the investigation of optical properties of human skin in the UV must furthermore be operable in reflection mode - illuminating and detecting the response from the same side of the sample. This demand poses an additional severe constraint especially on the techniques working with scattered light as only the very limited part backscattered to the detector can be used for investigations.

In summary, there is no other technique that combines such a lot of advantages for this particular application.

To achieve the aim of determining the optical properties of human skin *in vivo*, a diverse lot of preparatory developmental work had to be carried out in the first place. This work was divided among two dissertation projects. Dipl.-Phys. Ronald Krebs was responsible for the electronic and software development (transducer, automated measurement procedure, signal processing, and optoacoustic simulation program) and proof of principle investigations.

As set out in this dissertation at hand, my primary responsibility was the advancement of the optoacoustic detector according to the demands of *in vivo* measurements, the development and construction of a suitable UV laser system tunable over the terrestrial ultraviolet range, which was achieved in a diploma work, as well as the adjustment of optoacoustic theory to the particular experimental conditions of this project providing the theoretical basis for the optoacoustic simulation program. All these diverse prerequisite requirements were successfully achieved in the first phase of this dissertation project as outlined in chapters 2, 4, and 5.

Of course, the final goal of my dissertation work was to design and conduct the subject study after consultation and in agreement with our cooperation partner, the Institut für experimentelle Dermatologie/DermaTronnier at the Universität Witten-Herdecke as well as the analysis of the data and their discussion. Chapters 6, 7, and most importantly 8 deal with this main focus of my thesis.

Recapitulating, it was shown that the optical properties of human skin *in vivo* can be measured using optoacoustics. The achievement of this investigation were UV absorption spectra of *in vivo* human skin that are unequalled in the literature as shown in Chap. 3. To our knowledge, so far the best and most cited data about the optical properties of human skin in the UV came from *ex vivo* data ([20, 26, 33, 34] and references therein) or were extrapolated from theoretical considerations (esp. [34]). This thesis now provides data on the optical properties of human skin in the ultraviolet wavelength range from 290 nm to 341 nm (UVB and UVA-II) with a spectral resolution of 3 nm. In detail and answering the questions posed at the beginning of the core Section 8.3, the following results were achieved:

- The wavelength dependent absorption coefficients of human skin were determined at the volar and dorsal aspect of the forearm and on the thenar.
- At the volar forearm, different UV sensitivity (phototype/minimal erythema dose) of the subjects appeared also as a trend in the spectral characteristics, which was however not significant compared to the standard deviations of the average data: type IV shows higher absorption than type I in the UVB whereas it is vice versa in the UVA-II range; the mean spectra of the absorption coefficients of phototype I and IV cross at about 315 nm.

- Subjects with high natural sun exposure could in most cases be discriminated from low exposure subjects by their absorption spectra at the dorsal side of the forearm. The markedly increased UVB absorption in people subject to rather high UV exposure is probably the result of thickening of the horny layer - a well known UV adaptation mechanism - and thus due to keratin.
- The optoacoustic absorption spectra from the thenar provide additional proof for the theory of keratin as a major UVB shielding factor.
- Based on the obtained absorption spectra, the penetration depths of UV light into human skin were reevaluated and showed penetration depths of up to about 60  $\mu\text{m}$  for forearm skin. At the thenar, the penetration spectrum is different. For UV radiation from 290-300 nm a penetration depth of only about 10  $\mu\text{m}$  was calculated whereas it rises up to ca. 135  $\mu\text{m}$  at 341 nm.
- Grouping and averaging of the thenar spectra according to the phototypes provoked the idea that the shielding ability of natural keratin could be less effective in phototype I compared to the other less sensitive types. This hint could add new arguments to the discussion about the reasons for high UV sensitivity.
- Optoacoustic investigations on topically applied sunscreens cannot be conducted satisfactorily with the present detector. Despite the adversary measurement conditions, spectra from the same lotion are similar in their spectral course. This indicates considerable potential of UV optoacoustics to assess sun protection lotions, even though some technical advancements are prerequisite before optoacoustic evaluation of sun protection lotions in vivo can be truly beneficial.

In future subject studies, these results will have to be substantiated by further data of course - especially as far as differences according to UV sensitivity are concerned - and the wavelength range should be extended to the UVA-I.

Besides, the significance and clarity of the results should be enhanced especially because any biological sample involves large natural deviations.

The fact that some of the results from the analysis of the subject study can only be presented as trends here and not as significant facts is caused and accepted by the design of the study. The aim of this study was primarily to get a basis for reasonable assumptions about the potential of UV optoacoustics in the investigation of human skin in vivo. This called for as much variety of objectives as possible. On the other hand, we were conducting an in vivo study. So, UV doses had to be limited and minimized not to put the subject's health at risk and to keep experimental time within reasonable limits for the subjects. Accordingly, the number of measurements and the covered wavelength range had to be adjusted to these demands. Remarkably, the chosen compromise still allowed a lot of interesting insights in the UV optical properties of human skin in vivo and is a good basis for follow up scientific work.

The thesis at hand already suggests concrete plans for further developments and improvements. Unfortunately, these tasks are too extensive to be dealt with within the limits of this thesis.

Accuracy can be enhanced by diminishing technical error sources. The energy measurement of the single laser pulses, acoustic matching of sample and detector by the ultrasound gel and signal to noise ratio of the transducer are promising targets for future work.

Especially the measurements on sunscreen promoted the idea of a complementary large area optoacoustic detector. Building an acoustic detector with a larger area is not a problem but finding a solution for a homogeneous illumination of an area large compared to the area of the acoustic detector is challenging. A high ratio of illumination to detection area allows considerable simplification of the optoacoustic theory and should definitely be kept if possible. Probably a fiber array would be the best approach to start with. The present high lateral resolution detector and a new integral detector could provide a reasonable combination dealing with the inhomogeneity of human skin.

Furthermore, it could be beneficial to include scattering in the analysis of the optoacoustic signals. This is of special importance if the investigation of sunscreens in vivo is to be carried on, as there are important sunscreen filters (such as titanium dioxide) which are highly scattering. The theoretical description outlined in Chap. 2 already paves the way for this extension. However, this should be taken one step further. Based on light distribution theory, an approach should be found and followed that incorporates the refeed of fluence due to the unisotropic scattering profile.

# APPENDIX

# A Physical properties of relevant materials

The following Table shows a list of physical properties for relevant materials collected from [20].

Material	$c_l [\frac{cm}{\mu s}]$	$\rho [\frac{g}{cm^3}]$	$\chi [\frac{cm^2}{s}]$	$\beta [C^{\circ-1} * 10^{-4}]$	$c_p [\frac{kJ}{kgK}]$
water	0.148	0.998	1440	2.1/2.07 (20 C°) 3.0/3.03 (30 C°) 3.9/0.385 (40 C°)	4.182
skin	0.158	1.01	1190 (blood) -1470 (muscle) 400 (skin)	9.2 (15-37 C°) (fat) 3.5 (blood cells)	3.15-3.28 (dermis, pig) 3.470 (J/kgK)
epidermis					3.53-3.71 (pig)
ultrasound gel	0.15	1.04			
gelatine					3.84 (18.7%) 4.03 (9%)
PVDF	0.22	1.78			1.21417

## **B Documentation - study subjects**

### **B.1 Measurement sites at subjects' arms - photographs**

DigiCam pictures were taken from each subject's arms for documentation (see also Chap. 6). Lighting conditions changed from subject to subject allowing only restricted comparability. Still, the photographs give a first impression of the different skin phototypes of the subjects as they appear to the eye. Measurement sites are usually marked by white labels, sometimes by pen markings or shaving. Pictures on the left hand side show the volar aspect of both arms, on the right hand side, the dorsal aspect of the subject's arm is shown.

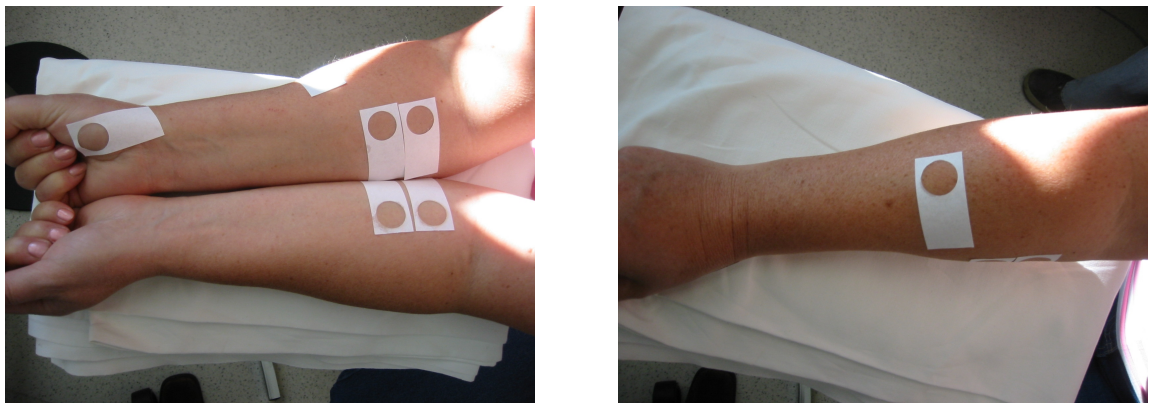


**Figure B.1:** subject B.I.

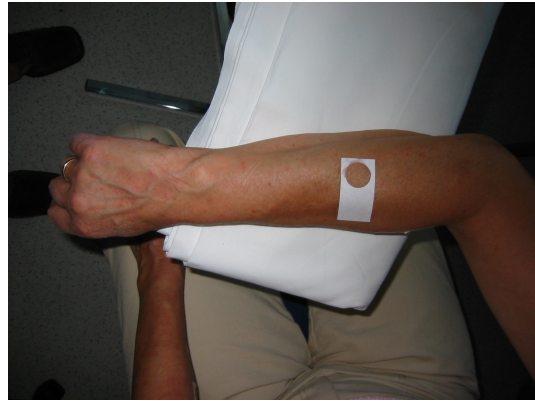
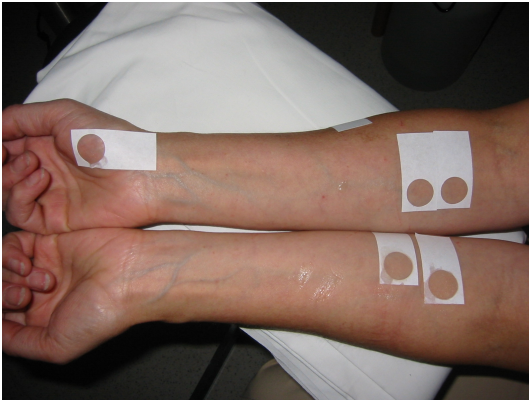


**Figure B.2:** subject E.R.

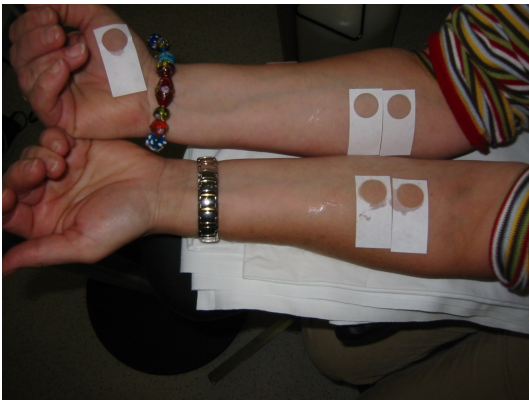


**Figure B.3:** subject F.M.

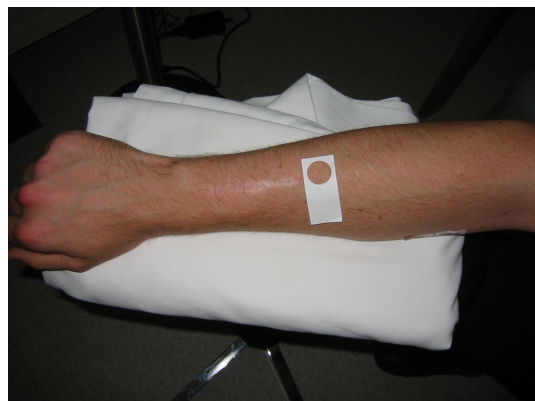
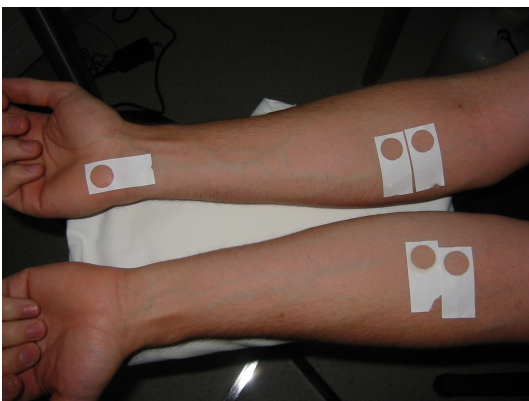


**Figure B.4:** subject G.O.



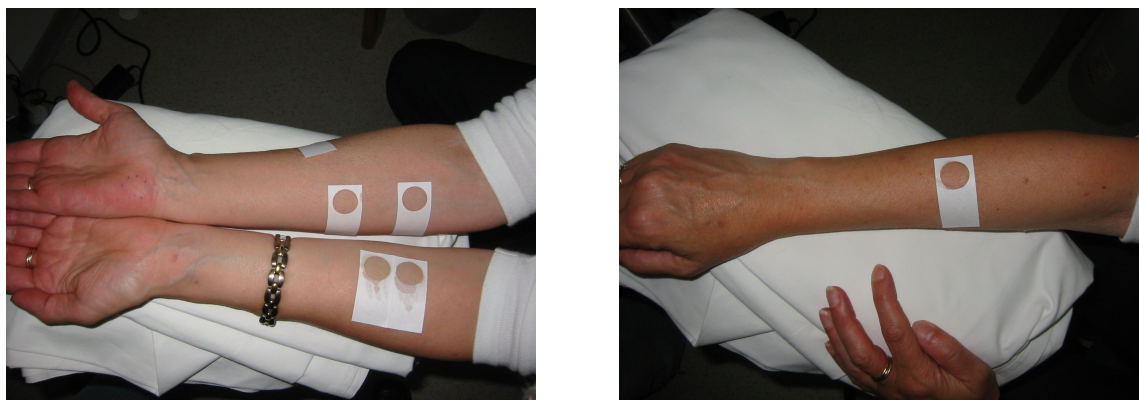


**Figure B.5:** subject H.M.

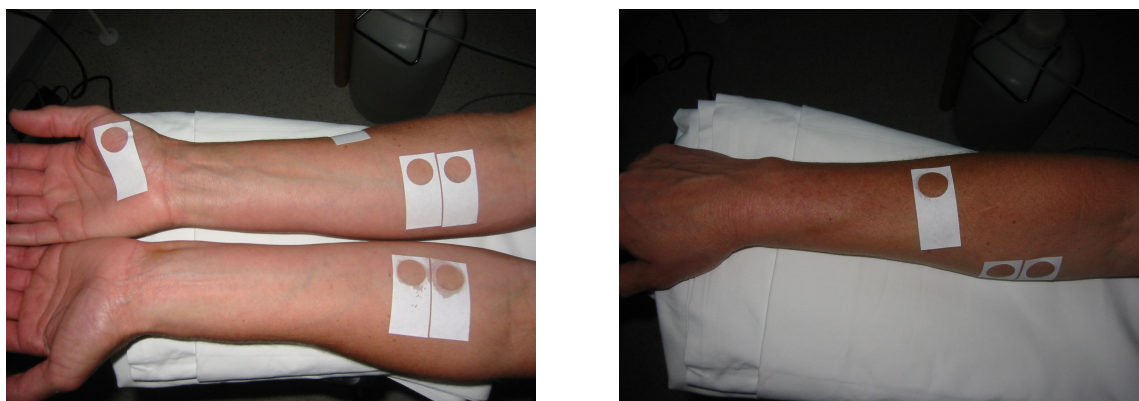


**Figure B.6:** subject Kn.G.

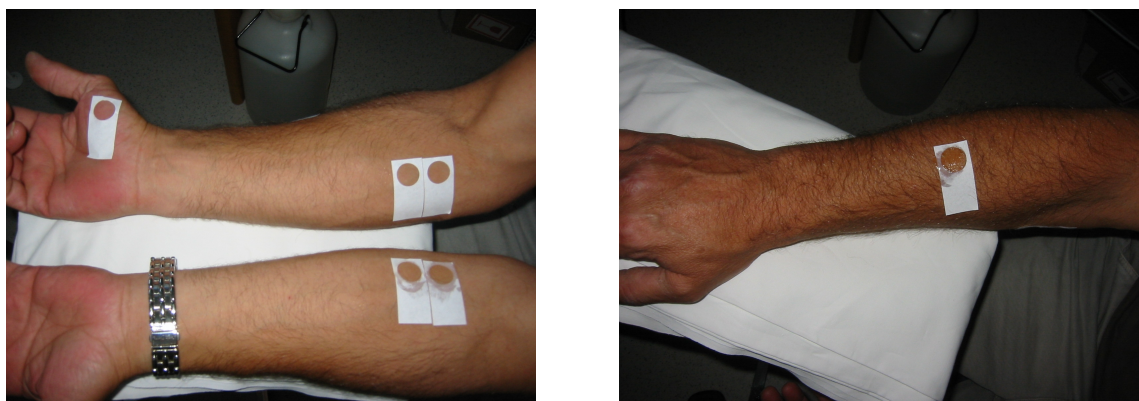


**Figure B.7:** subject K.B.

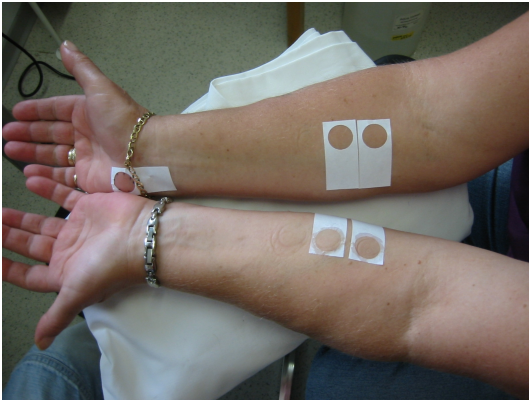


Figure B.8: subject Kr.G.

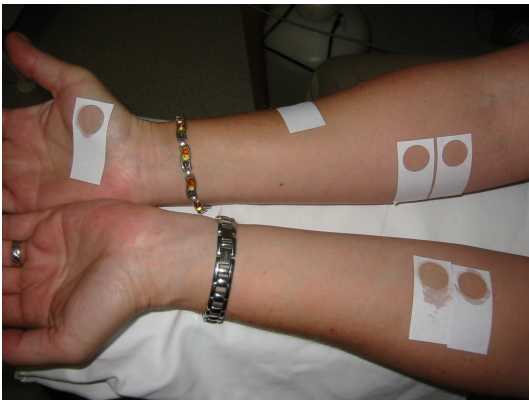


Figure B.9: subject K.H.

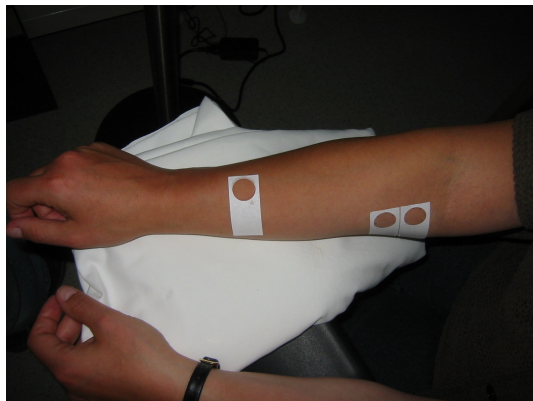
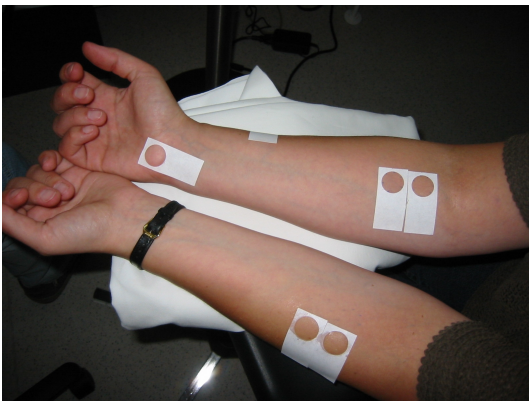


Figure B.10: subject K.I.

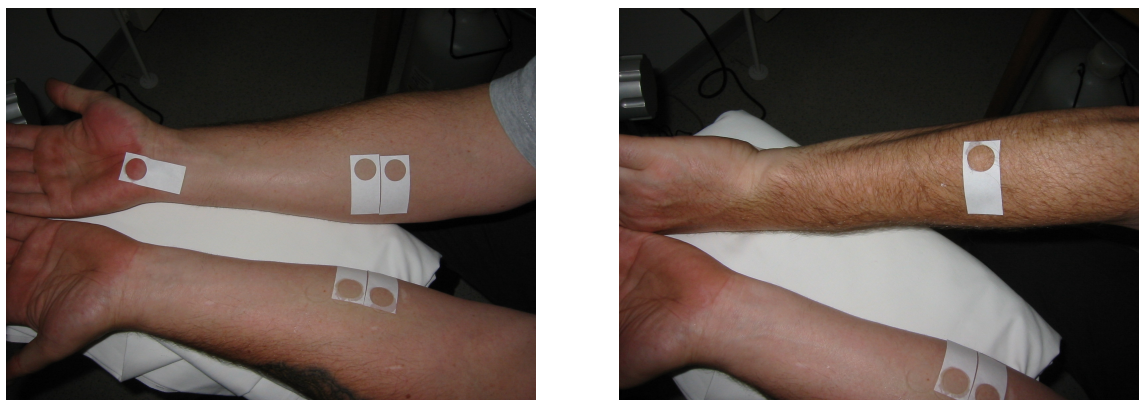


Figure B.11: subject K.K.

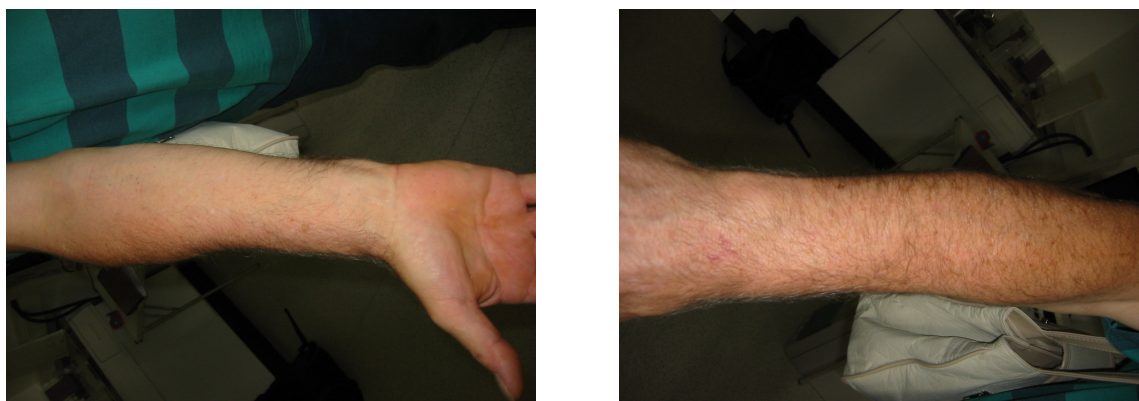
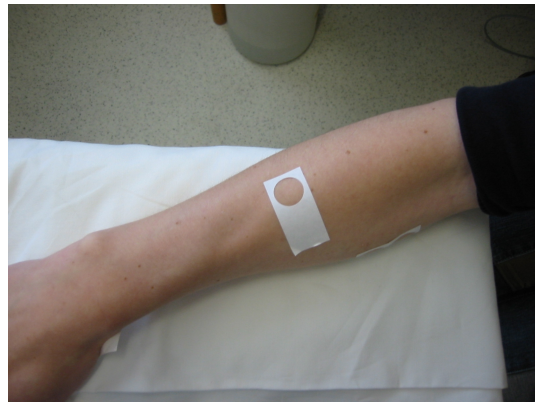
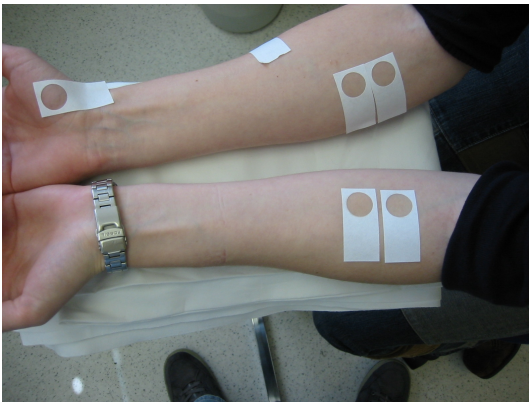


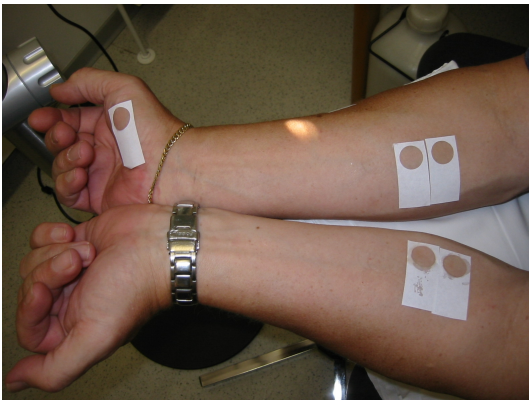
Figure B.12: subject L.K.



Figure B.13: subject L.U.



**Figure B.14:** subject M.M.



**Figure B.15:** subject M.H.

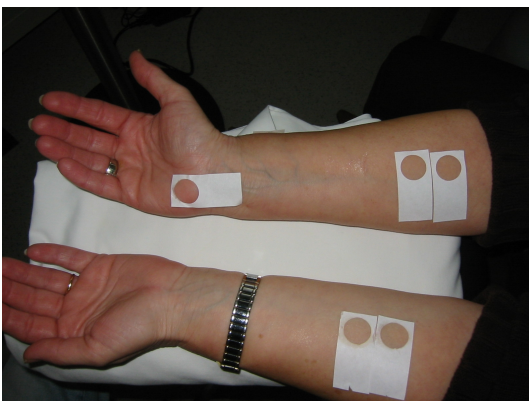


**Figure B.16:** subject P.R.

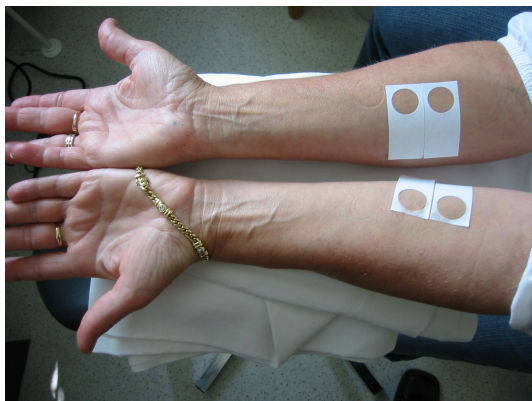


**Figure B.17:** subject S.R.

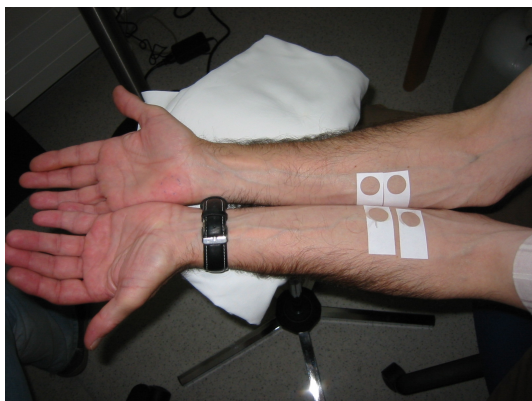


**Figure B.18:** subject W.K.

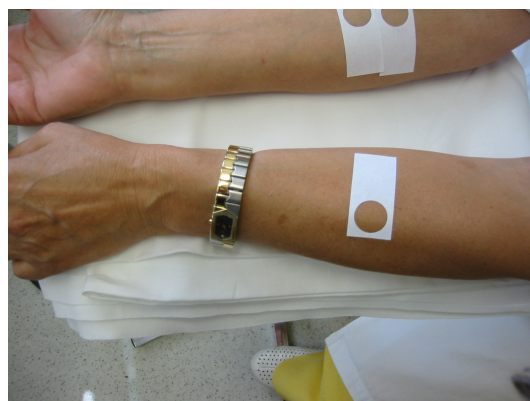
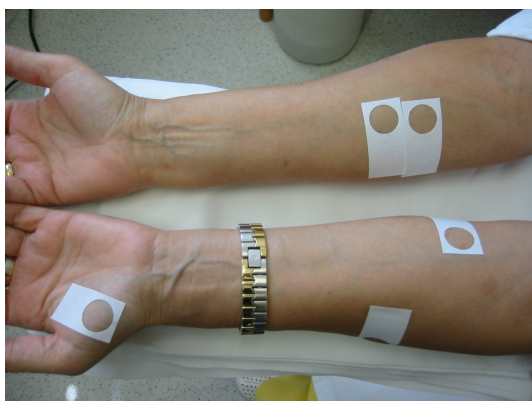


**Figure B.19:** subject W.M.

## B.2 SELS pictures

SELS pictures (see also Chap. 6) were taken to document the skin structure of the subjects and spot sizes of erythema and pigmentation due to optoacoustic measurements - or their non-existence. Both erythema and pigmentation appear as a darkening in the SELS pictures. However, pigmentation spots usually appear to have sharper edges. SELS software allows automatic image optimization for higher contrast.

On the following pages a selection of SELS pictures are shown to give an idea of the information obtained. Of course, pictures from all subjects may be inquired from the author.

Pictures in the top row show the skin after 24 hours on the sites of optoacoustic measurements. At this time, erythema had appeared in some of the subjects due to the UV doses applied by optoacoustic measurements which show as darker spots in the SELS pictures. Up to three measurement spots - according to the three optoacoustic scans on nearby areas for averaging - can be seen.

In the bottom row, SELS pictures taken 72h after oa-irradiation are shown. Erythema had disappeared in most subjects at that time and pigmentation had become the dominant colour change.

Pictures on the left are original, pictures on the right are optimized for contrast by SELS software. Picture orientation is rotated in some cases for the picture after 72h compared to that taken after 24h (e.g. in the last shown subject H.M.).

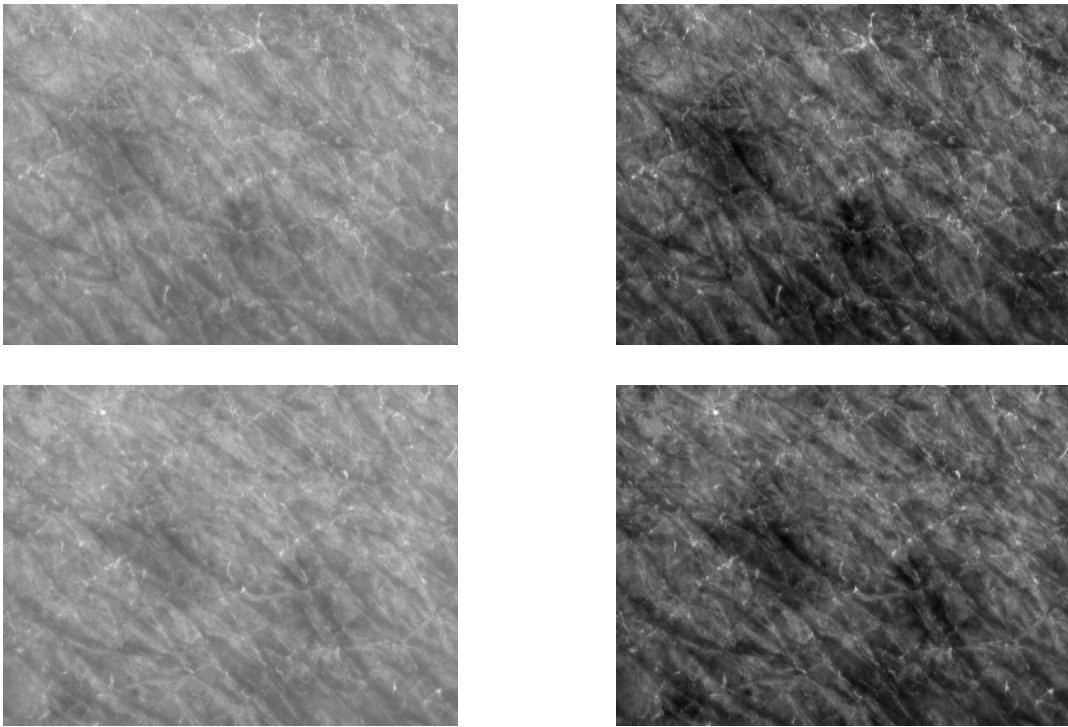


**Figure B.20:** Subject B.I.

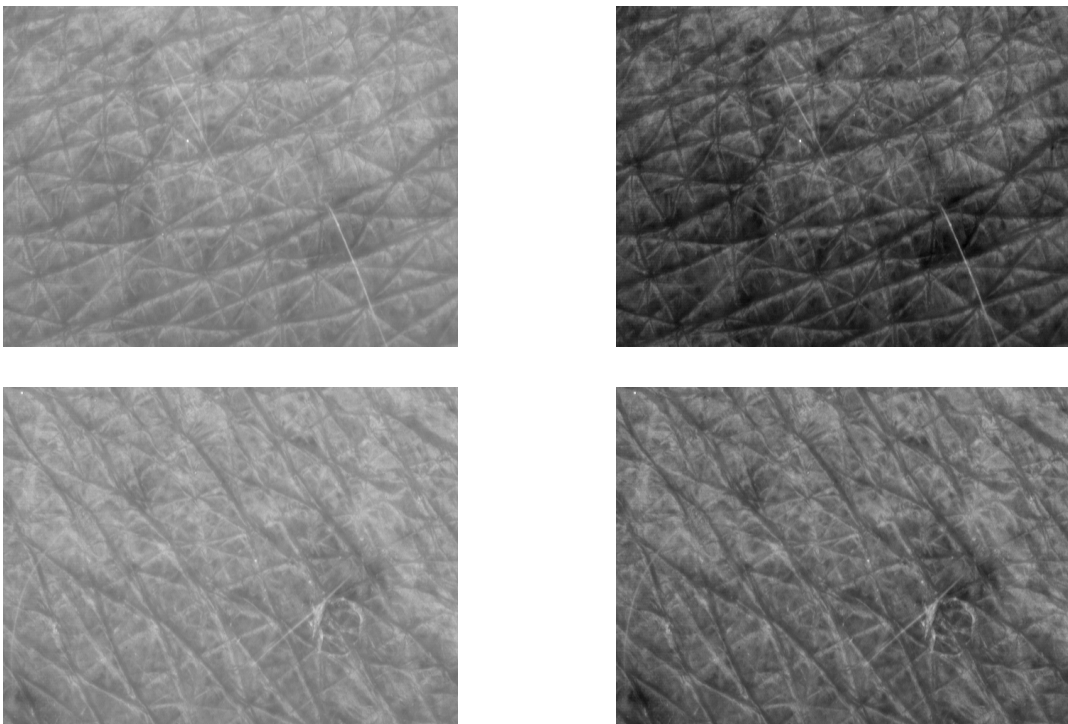


**Figure B.21:** Subject D.C.

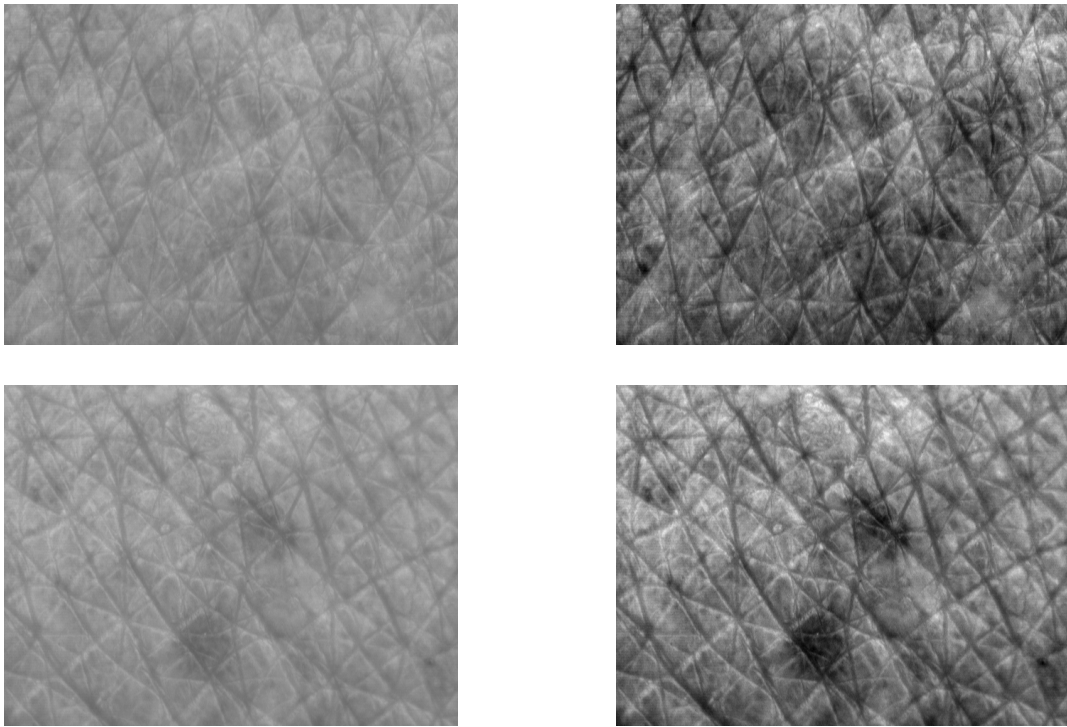


**Figure B.22:** Subject E.R.

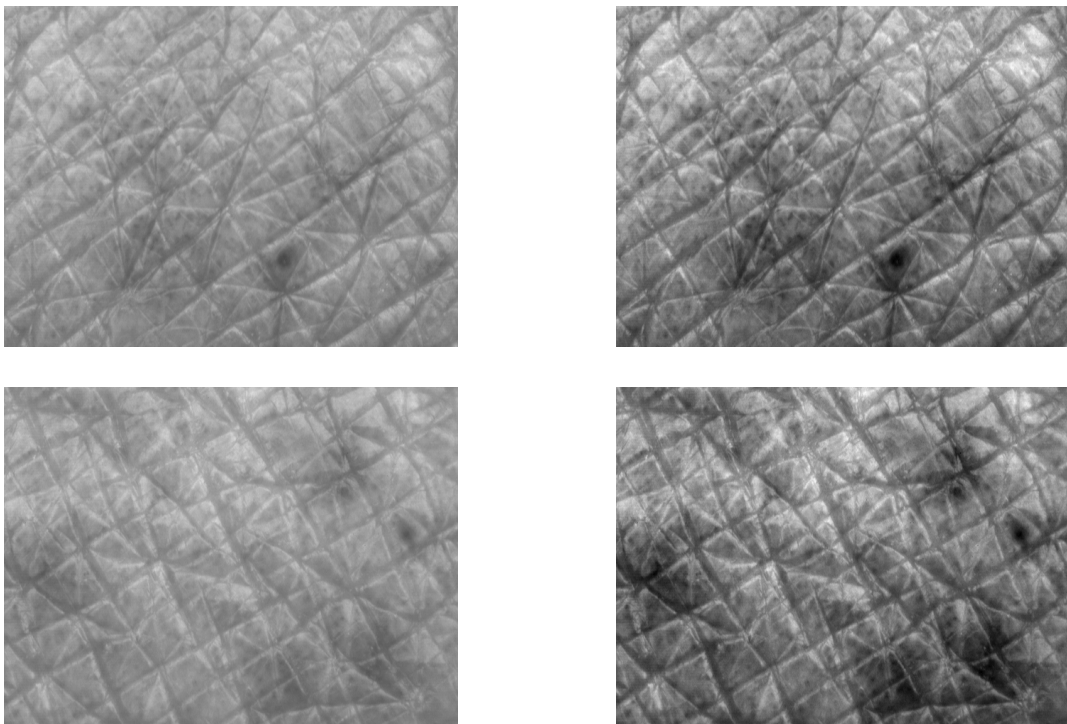


**Figure B.23:** Subject H.M.



## B.3 FotoFinder pictures

Fotofinder (see also Chap. 6) allows overview pictures of the relevant body part as well as skin microscopy in 20x, 40x, and 80x magnification. In this case, the volar side of each subject's forearm were photographed. Pictures were taken 24h ours after the first experimental session - that is one day after irradiation with M.U.T. solar simulator for determination of MED and first optoacoustic measurements.

The overview shows MED spots (ca. 1 cm diameter) and optoacoustic spots (much smaller) if they appeared one day after irradiation. Magnified pictures were taken from the spots induced by the optoacoustic measurements - or where they should have appeared - 24h (erythema) and 72h (pigmentation) after the measurements. Only a selection of pictures are shown here - a comprehensive documentation may of course be inquired from the author.

In the first three examples, the MED irradiation site(s) can be fairly clearly recognized. Optoacoustic measurement spots in contrast are much weaker which is the normal case. In the last example (H.M.), the spots from the solar simulator irradiation cannot be seen as the UV dose was too low to induce erythema at this first try. However, this subject was most sensitive to the optoacoustic measurements which induced pronounced erythema.



**Figure B.24:** subject B.I.; top: overview 24h after optoacoustic measurements/solar simulator irradiation, middle left: 24h oa skin area (20x), middle right: 24h oa skin area (40x), bottom left: 72h oa skin area (20x), bottom right: 72h oa skin area (40x)



**Figure B.25:** subject D.C.; top: overview 24h after optoacoustic measurements/solar simulator irradiation, middle left: 24h oa skin area (20x), middle right: 24h oa skin area (40x) bottom left: 72h oa skin area (20x), bottom right: 72h oa skin area (80x)

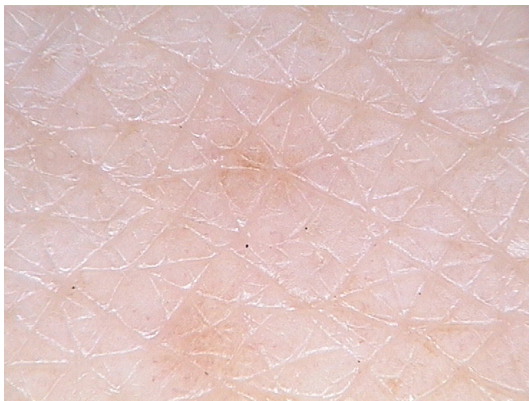
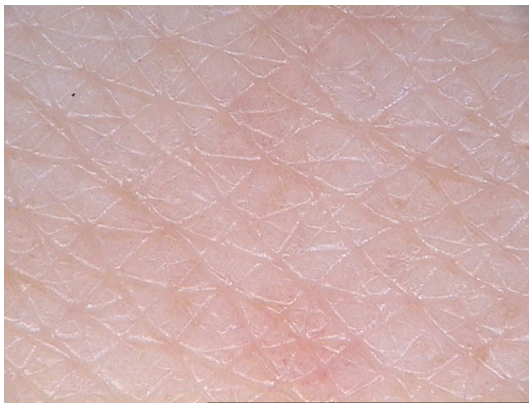


**Figure B.26:** subject E.R.; top: overview 24h after optoacoustic measurements/solar simulator irradiation, middle left: 24h oa skin area (20x), middle right: 24h oa skin area (40x), bottom left: 72h oa skin area (20x), bottom right: 72h oa skin area (80x)



**Figure B.27:** subject H.M.; top: overview 24h after optoacoustic measurements/solar simulator irradiation, middle left: 24h oa skin area (20x), middle right: 24h oa skin area (40x) bottom left: 72h oa skin area (40x), bottom right: 72h oa skin area (80x)



# Bibliography

- [1] S. AKHMANOV, V. GUSEV and A. KARABUTOV: *Pulsed laser optoacoustics: achievements and perspective*. Infrared Physics, 29(2-4):815–838, 1989.
- [2] A. ANDERS, H.-J. ALTHEIDE, M. KNÄLMANN and H. TRONNIER: *Action Spectrum for erythema in humans investigated with dye lasers*. Photochemistry and Photobiology, 61:200–205, 1995.
- [3] A. ANDERS, H.-J. ALTHEIDE and H. TRONNIER: *Erythema and action spectra in humans*. CIE Collection in Photobiology and Photochemistry Div. 6 reportship, 2001.
- [4] A. ANDERS: *Action Spectroscopy of Skin with Tunable Lasers*. research note CIE 148:2002, CIE - Commission internationale de l'éclairage, 2002.
- [5] *Beta Barium Borate*. <http://www.aotk.com/html-pro/bbo-002.htm>, 2005.
- [6] P. ASAWANONDA, R. ANDERSON, Y. CHANG and C. TAYLOR: *308-nm excimer laser for the treatment of psoriasis, A Dose-Response Study*. Arch Dermatol., 136:619–624, 2000.
- [7] S. ASTNER and R. R. ANDERSON: *Skin Phototypes 2003*. J Invest Dermatol, 122:xxx–xxxi, 2004.
- [8] M. BARTELS, M. MEINHARDT, R. KREBS, H. PETERING, T. WERFEL and A. ANDERS: *Optoacoustics, laserinduced fluorescence (LIF), and photometry for investigation of different skin types in vitro and in vivo*. In Proc. SPIE Vol. 4143: *Novel Optical Instrumentations for Biomedical Applications*, pages 50–58, 2003.
- [9] M. BARTELS: *Optische Eigenschaften von humanen Hautzellen und Hautgewebe mittels lasergestützter Strukturcharakterisierung - Untersuchungen in vivo und in vitro*. Master's thesis, University of Hannover, January 2003.
- [10] E. BENDIT and D. ROSS: *A Technique for Obtaining the Ultraviolet Absorption Spectrum of Solid Keratin*. Applied Spectroscopy, 15(4):103–105, 1961.

- [11] J. BOROVSANÝ and M. ELLEDER: *Melanosome Degradation: Fact or Fiction*. *Pigment Cell Research*, 16:280–286, 2003.
- [12] L. U. BRACKMANN: *Lambdachrome Laser Dyes*. [http://bcp.phys.strath.ac.uk/ultrafast/Blue\\_book/Lamdachrome-laser-dyes.pdf](http://bcp.phys.strath.ac.uk/ultrafast/Blue_book/Lamdachrome-laser-dyes.pdf).
- [13] W. BRULS and J. VAN DER LEUN: *Forward scattering properties of human epidermal layers*. *Photochem Photobiol*, 40:231–242, 1984.
- [14] L. BURMISTROVA, A. KARABUTOV, A. PORTNYAGIN, O. RUDENKO and E. CHEREPETSKAYA: *Method of transfer functions in problems of thermo-optical sound generation*. *Sov. Phys. Acoust.*, 24(5):369–374, 1978.
- [15] V. J. BYKOV, J. A. MARCUSON and K. HEMMINKI: *Effect of constitutional pigmentation on ultraviolet-B induced DNA-damage in fair-skinned people*. *Journal of Investigative Dermatology*, 114(1):40–43, 2000.
- [16] A. CADER and J. JANKOWSKI: *Reflection of ultraviolet radiation from different skin types*. *Health Phys*, 74:169–172, 1998.
- [17] C. CHEN, B. WU, A. JIANG and G. YOU: . *Sci. Sin. B*, 1985.
- [18] C. M. R. CLANCY and J. D. SIMON: *Ultrastructural Organization of Eumelanin from Sepia officinalis Measured by Atomic Force Microscopy*. *Biochemistry*, 40:13353–13360, 2001.
- [19] S. DORNELLES, J. GOLDIM and T. CESTARI: *Determination of the Minimal Erythema Dose and Colorimetric Measurements as Indicators of Skin Sensitivity to UV-B Radiation*. *Photochemistry and Photobiology*, 79(6):540–544, 2004.
- [20] F. A. DUCK: *Physical Properties of Tissue*. Academic Press, 1990.
- [21] C. DUVAL, N. P. SMIT, A. M. KOLB, M. RÉGNIER, S. PAVEL and R. SCHMIDT: *Keratinocytes Control the Pheo/Eumelanin Ratio in Cultured Normal Human Melanocytes*. *Pigment Cell Res*, 15:440–446, 2002.
- [22] EKSPLA: *Optical Parametric Oscillator - PG122/UV, general sytem information*, 2005.
- [23] M. A. EVERETT, E. YEARGERS, R. M. SAYRE and R. L. OLSEN: *Penetration of epidermis by ultraviolet rays*. *Photochemistry and Photobiology*, 5:533–542, 1966.
- [24] T. B. FITZPATRICK: *The validity and practicality of sun-reactive skin types I through VI*. *Arch Dermatol*, 124:869–871, 1988.



- [25] T. GAMBICHLER, K. SAUERMAN, M. ALTINTAS, V. PAECH, A. KREUTER, P. ALTMAYER and K. HOFFMANN: *Effects of repeated sunbed exposures on the human skin. In vivo measurements with confocal microscopy*. *Photodermatology, Photoimmunology and Photomedicine*, 20(1):27, 2004.
- [26] M. J. C. VAN GEMERT, S. L. JACQUES, H. J. C. M. STERENBORG and W. M. STAR: *Skin Optics*. *IEEE Transactions on Biomedical Engineering*, 36(12):1146–1154, 1989.
- [27] V. E. GUSEV and A. A. KARABUTOV: *Laser Optoacoustics*. AIP Press, 1993.
- [28] T. HA, H. JAVEDAN, K. WATERSTON, L. NAYSMITH and J. L. REES: *The Relationship Between Constitutive Pigmentation and Sensitivity to Ultraviolet Radiation Induced Erythema is Dose Dependent*. *Pigment Cell Research*, 16:477–479, 2003.
- [29] M. HENRIKSEN, R. NA, M. S. ÅGREN and H. C. WULF: *Minimal erythema dose after multiple UV exposures depends on pre-exposure skin pigmentation*. *Photodermatology Photoimmunology Photomedicine*, 20:163–169, 2004.
- [30] W. HOGERVORST, J. M. BOON-ENGERING, W. E. VAN DER VEER and J. W. GERRITSEN: *Bandwidth studies of an injection-seeded beta-barium borate optical parametric oscillator*. *Optics Letters*, 20:380–382, 1995.
- [31] M. F. HOLICK and M. JENKINS: *The UV Advantage*. Simon & Schuster, 2004.
- [32] S. ITO and K. WAKAMATSU: *Quantitative Analysis of Eumelanin and Pheomelanin in Humans, Mice, and Other Animals: a Comparative Review*. *Pigment Cell Res*, 16:523–531, 2003.
- [33] S. L. JACQUES. <http://omlc.ogi.edu/news/jan98/skinoptics.html>, Januar 1998.
- [34] S. L. JACQUES. <http://omlc.ogi.edu/spectra/melanin/extcoeff.html>, 2005.
- [35] A. L. KADEKARO, R. J. KAVANAGH, K. WAKAMATSU, S. ITO, M. A. PIPITONE and Z. A. ABDEL-MALEK: *Cutaneous Photobiology. Melanocyte vs. the Sun: Who Will Win the Final Round?* *Pigment Cell Research*, 16:4334–447, 2003.
- [36] M. N. KAMEL: *The Electronic Textbook of Dermatology, Anatomy of the Skin*. <http://telemedicine.org/anatomy/anatomy.htm#keratin>, May 2006.
- [37] A. KARABUTOV, N. PODYMOVA and V. LETOKHOV: *Time-resolved laser optoacoustic tomography of inhomogeneous media*. *Applied Physics B: Lasers and Optics*, 63:545–563, 1996.
- [38] A. A. KARABUTOV, N. B. PODYMOVA, I. M. PELIVANOW, S. E. SKIPETROV and A. A. ORAEVSKY: *Direct measurement of axial distribution of absorbed energy in turbid media by time-resolved optoacoustic method*. In A. ORAEVSKY (editor):

- Biomedical Optoacoustics*, volume 3916 of *Proceedings of SPIE*, pages 112–121, 2000.
- [39] A. A. KARABUTOV, E. V. SAVATEEVA and A. A. ORAEVSKY: *Imaging of layered structures in biological tissues with opto-acoustic front surface transducer*. In *Laser-Tissue Interaction X: Photochemical, Photothermal, and Photomechanical*, volume 3601 of *Proceedings of SPIE*, pages 284–295, 1999.
- [40] A. A. KARABUTOV, E. V. SAVATEEVA, N. B. PODYMOVA and A. A. ORAEVSKY: *Backward mode detection of laser-induced wide-band ultrasonic transients with optoacoustic transducer*. *Applied Physics*, 87(4):2003–2014, 2000.
- [41] A. KHARINE, S. MANOHAR, R. SEETON, R. G. M. KOLKMAN, R. A. B. W. STEENBERGEN and F. F. M. DE MUL: *Poly(vinyl alcohol) gels for use as tissue phantoms in photoacoustic mammography*. *Phys. Med. Biol.*, 48:357–370, 2003.
- [42] A.-K. KNIGGENDORF: *Entwicklung einer durchstimmbaren Laserquelle im UV-A Bereich - 266 nm OPO*. Master's thesis, Institut für Biophysik, Universität Hannover, 2004.
- [43] N. KOLLIAS: *The spectroscopy of human melanin pigmentation*. In *Melanin: Its Role in Human Photoprotection*, March 1994.
- [44] R. KREBS, M. BARTELS, M. MEINHARDT, H. LUBATSCHOWSKI and A. ANDERS: *Characterization of optical structures in biological tissue by means of UV-optoacoustics*. *Laser Physics*, 13:1–6, 2003.
- [45] R. KREBS, M. MEINHARDT, U. OBERHEIDE, H. LUBATSCHOWSKI and A. ANDERS: *Investigations of optical properties of human skin in the UV*. *Proceedings of SPIE*, Vol. 4618, pages 22–30, 2002.
- [46] R. KREBS. PhD thesis, Institut für Biophysik, Universität Hannover. in preparation.
- [47] J. KRUTMANN and H. HÖNIGSMANN: *Handbuch der dermatologischen Phototherapie und Photodiagnostik*. Springer Verlag, 1997.
- [48] M. MEINHARDT: *Aufbau einer optoakustischen Messapparatur zur Analyse der optischen Eigenschaften von Humanhaut in vivo*. Master's thesis, Institut für Biophysik, Universität Hannover, November 2001.
- [49] C. MICHEELSEN: *Sun simulator operating manual*. M.U.T. GmbH, 2001.
- [50] D. MOYAL, A. CHARDON and N. KOLLIAS: *Determination of UVA protection factors using the persistent pigment darkening (PPD) as the end point*. *Photodermatol Photoimmunol Photomed*, 16:245–249 und 250–255, 2000.
- [51] OPOTEK INC.: *Vibrant - Tunable UV*. [http://www.opotek.com/tunable\\_uv.htm](http://www.opotek.com/tunable_uv.htm).

- [52] A. A. ORAEVSKY, S. L. JACQUES and F. K. TITTEL: *Determination of tissue optical properties by piezoelectric detection of laser-induced stress waves*. In S. L. JACQUES (editor): *Laser-Tissue Interaction IV*, volume 1882 of *Proceedings of SPIE*, pages 86–101, 1993.
- [53] H. OU-YANG, G. STAMATAS and N. KOLLIAS: *Spectral Responses of Melanin to Ultraviolet A Irradiation*. *J Invest Dermatol*, 122:492–496, 2004.
- [54] M. A. PATHAK: *Functions of Melanin and Protection by Melanin*. In *Melanin: Its Role in Human Photoprotection*, pages 125–135, March 1994.
- [55] Q. PENG: *Basis for selective porphyrin formation in skin lesions*. <http://www.photocure.com/professionals/display.asp?xmlID=165>, May 2006.
- [56] A. V. RAWLINGS, I. R. SCOTT, C. R. HARDING and P. A. BOWSER: *Stratum Corneum Moisturization at the Molecular Level*. *J Invest Dermatol*, (5):731–740, 1994.
- [57] SKINETHIC. <http://www.skinethic.com/>, November 2005.
- [58] A. V. SMITH: *SNLO*. <http://www.sandia.gov/imrl/XWEB1128/xxtal.htm>.
- [59] SONOTECH INC.: *Couplant feature comparison chart*. [http://www.sonotech-inc.com/PDF/NDT\\_Couplant\\_Feature\\_Comparison\\_Chart.pdf](http://www.sonotech-inc.com/PDF/NDT_Couplant_Feature_Comparison_Chart.pdf), 2005.
- [60] G. N. STAMATAS, B. Z. ZMUDZKA, N. KOLLIAS and J. Z. BEER: *Non-Invasive Measurements of Skin Pigmentation In Situ*. *Pigment Cell Research*, 17:618–626, 2004.
- [61] R. SUTHERLAND: *Handbook of Nonlinear Optics*. Marcel Dekker Inc., New York, 1996.
- [62] H. TAKIWAKI: *Measurement of skin color: practical application and theoretical considerations*. *The Journal of Medical Investigation*, 44:121–126, 1998.
- [63] V. V. TUCHIN, S. R. UTZ and I. YAROSLAVSKY: *Tissue optics, light distribution, and spectroscopy*. *Optical Engineering*, 33(10):3178–3188, 1994.
- [64] S. WAN, R. ROX and J. A. PARRISH: *Analytical modeling for the optical properties of the skin with in vitro and in vivo applications*. *Photochemistry and Photobiology*, 34:493–499, 1981.
- [65] A. WELCH and M. MOTAMEDI: *Interaction of laser light with biological tissue*. In S. MARTELLUCCI and A. CHESTER (editors): *Laser photobiology and photomedicine*. Plenum Press, New York and London, 1985.

- [66] WORLD HEALTH ORGANIZATION: *Fact sheets: ultraviolet radiation*. <http://www.who.int/mediacentre/factsheets/who271/en/>, <http://www.who.int/mediacentre/factsheets/fs287/en/index.html>, <http://www.who.int/mediacentre/factsheets/fs261/en/index.html>, <http://www.who.int/mediacentre/factsheets/fs287/en/index.html>, 2005.
- [67] S. WU, G. A. BLAKE, S. SUN and H. YU: *Two-photon absorption inside beta-BBO crystal during UV nonlinear optical conversion*. In J. W. PIERCE (editor): *Nonlinear Materials, Devices, and Applications*, volume 3928 of *Proceedings of SPIE*, pages 221–227, March 2000.
- [68] P. XIAO and R. E. IMHOF: *Opto-thermal measurement of stratum corneum thickness and hydration depth profile*. In *SPIE Proc 2970: Lasers in Surgery: Advanced Characterization, Therapeutics, and Systems VII*, pages 276–86, May 1997.
- [69] A. R. YOUNG: *Chromophores in human skin*. *Phys. Med. Biol.*, 42:789–802, 1997.

# Curriculum Vitae

<b>name</b>	Merve Meinhardt
<b>place, date of birth</b>	Hannover, Germany, 10. November 1976
<b>school career</b>	<i>08/1983 - 07/1987: primary school in Hannover</i> <i>08/1987 - 07/1989: Orientierungsstufe in Hannover</i> <i>08/1989 - 07/1996: Käthe-Kollwitz-Gymnasium Hannover</i>
<b>school qualifications</b>	Abitur (German equivalent of A-levels)
<b>university career</b>	<i>10/1996 - 02/2002: studies of physics at the Universität Hannover</i> <i>10/1996 - 05/2002: studies of "Lehramt an Gymnasien"</i> at the Universität Hannover (teachers training for the German equivalent of grammar-/highschool) subjects: English, physics <i>06/2002 - 11/2002: preparation of dissertation project /</i> application for funding <i>12/2002-05/2006: doctorate studies,</i> funded by a doctorate scholarship from the Studienstiftung des deutschen Volkes (German National Academic Foundation) from 12/2002 to 12/2005
<b>university qualifications</b>	diploma in physics 1. Staatsexamen in Lehramt/Gymnasien



# Danksagung

Prof. Dr. Angelika Anders danke ich für die Betreuung dieser Arbeit, für die Anstiftung zur biophysikalischen Forschung an menschlicher Haut und für all die Unterstützung und Freiheiten während der Arbeit.

Ich danke Ronald für die Zusammenarbeit in den letzten Jahren. Ich werde unsere Teamarbeit sehr vermissen.

Dem Insitut für experimentelle Dermatologie der Universität Witten/Herdecke (Derma-Tronnier) und seinen Mitarbeitern gilt mein besonderer Dank. Ohne die finanzielle, personelle und wissenschaftliche Unterstützung wäre keine solche Probandenstudie möglich gewesen.

PD Dr. Holger Lubatschowski und der Lasermedizin-Gruppe am Laser Zentrum Hannover e.V. danke ich für viel Anschubhilfe und fruchtbare Diskussionen.

Ann, Myriam und Inés danke ich für die wissenschaftliche Auseinandersetzung und viel Spaß während ihrer Diplomarbeiten.

Ein besonderer Dank gebührt dem gesamten Werkstatt-Team und insbesondere Michael Senft. Vom Laserbau bis zum Umzug des Messsystems nach Witten - wo wären wir ohne Euch geblieben?

Ein großer Dank geht auch an jeden einzelnen aus der LASER-AG am Institut für Biophysik im speziellen und an alle Mitglieder des Institus im allgemeinen.

Dank an Carsten Reinhardt für die Idee mit dem 266nm-OPO und für das Verschweigen der potentiellen Probleme.

Ich danke meinen Eltern dafür, dass sie immer Interesse für die Dinge zeigen, die mich begeistern und Rückhalt bieten, wann immer ich ihn brauche.

Amadeus danke ich dafür, dass er schlicht der beste Bruder der Welt ist (mit allen möglichen Auswirkungen auf meine Arbeit).

Dir, Andy, möchte ich für die Motivation und Aufmunterung danken, dafür, dass Du alle Zeiten, wo die Doktorarbeit meinen Lebensrhythmus bestimmt hast, hingenommen hast und mir die Möglichkeit gegeben hast in diesen Zeiten aus wenig Freizeit mit Dir die optimale Erholung zu ziehen.

Meine Gedanken sind bei Matthias.